University of Reading

Cortical and subcortical contributions to human cognitive flexibility

PhD Neuroscience

School of Psychology and Clinical Language Sciences,

Centre for Integrative Neuroscience and Neurodynamics

Brendan Williams

October 2021

Declaration

I confirm that this is my own work and the use of all material from other sources

has been properly and fully acknowledged.

Brendan Williams

Acknowledgements

To describe studying for a PhD as “it takes a village”, would not oversell this process in the slightest. There are more people than one page can hold who have enabled me to be where I am today, and though wholly disproportionate to their input, I hope these words will go some way as a fitting tribute to them.

Firstly, to Anastasia Christakou. Thank you for your ever-present support. For your wise words of wisdom. Thank you for your encouragement and allowing me to be creative, yet never letting me fall when I have a crazy and impractical idea. Thanks also for the constant stream of biscuits that have got us through many a meeting. Without you, I would not be half the academic I am today. To the CINN community, thank you for the sense of camaraderie and belonging that I have felt since joining. I am especially indebted to Nico Biagi, Wiebke Gandhi, Shan Shen, Jess Eastwood, Etienne Roesch, and Carolyn McNabb for your help and support with this work. This truly is a friendly place to work, and a joy to be a part of. I look forward to our upcoming years together. Thank you to the friends I have made on this journey. To Nico, who I have always been able to rely on – thank you for your companionship; to Rich Harrison and Zola Dean, the most welcoming and generous couple – I hope you shall always have a tequila close at hand; to the Australian King and Queen Tim and Tara Rossow, thank you for endless laughs; to Michael Lindner, a kindred spirit who had an indelible impact on me; and to Jess Eastwood, Anthony Haffey, Thalia Theodoraki, Michal Korenar, Toms Voits, Gabriella Rossetti, Wiebke, and Aamir Sohail, among others. Special thanks must also go to my right-hand man, Iwan Rowlands – I don’t know how I’d have got through this without you or our “virtual office”. And lastly, to friends old for the many good times both virtually and in person over these past years.

To my parents, Ian and Miriam. I could write a whole other thesis on all that you have done for me. Thank you for your enduring love. You made the impossible, possible, and your continual support in all aspects is simply more than words can describe. And to the rest of my family. Thank you for being the caring, supportive, crazy, funny, loving bunch that you are. Thank you, Auntie Naomi, for welcoming me into your home while I was studying for my masters – I would not be here today if it weren’t for your generosity. To Mr G, I wish you could be here with us to see this day. Lastly, and by no means least, to Iz. My northern star. Thank you for nonconditional love, unwavering support, graciousness, generosity, ever-present fun, and time. Here’s to the future. I am excited for what it holds.

Table of Contents

Abstract

Cognitive flexibility enables individuals to respond adaptively to an ever-changing world. Neurally, flexibility is underpinned by involvement from across the cerebrum, and there is evidence from animal and human neuroscience suggesting that integration of cortical and thalamic signals in the striatum is necessary for appropriate behavioural control. A commonly used assay of flexibility is reversal learning, an associative learning task with high inter-species translatability. Evidence from animal literature has clearly defined the importance of the striatal cholinergic system in regulating striatal activity and output from the basal ganglia, and there is nascent evidence suggesting this system operates in a similar way in humans. However, there is a need to further disentangle the role of cortical, striatal, and thalamic regions during reversal learning in humans to better understand how the system works, and whether it has heterogeneous functionality in different contexts. Furthermore, as studying these processes is not trivial, further methodological work is required to enable us to understand the system.

In chapter two we systematically assess an automated parcellation technique for identifying specific thalamic nuclei. Despite generally being treated as a homologous structure in neuroimaging work, nuclei within the thalamus have dissociable roles, and have diverse contributions to cognitive functioning, including reversal learning. We found mixed efficacy for segmentations across the thalamus, with some regions being more accurately defined relative to a "gold standard" atlas than others. Crucially, we find that the centromedian and parafascicular nuclei, which have an important role in reversal learning, are clearly defined and have little overlap with contiguous regions. These results show we can use this automated parcellation technique to identify specific thalamic nuclei that are relevant for cognitive flexibility and use these parcellations to study functionally relevant processes.

Recent work has demonstrated that the functional relevance of the striatal cholinergic system can be studied *in vivo* using magnetic resonance spectroscopy by separating the peaks of different metabolites. But this non-conventional approach has not yet been widely adopted, and work is needed to determine its reliability. Chapter three presents test-retest reliability data on the use of magnetic resonance spectroscopy to study cholinergic activity in the striatum and cortex. We find measures of choline containing compounds are highly correlated when peaks are separated and when they are not. Across time we find that choline concentrations are relatively inconsistent, and that this was due to changes in the functionally relevant metabolite choline. Conversely, metabolites that we think are not functionally relevant were stable over time. We believe these

differences may underly differences in acetylcholine function over time and may explain some intra-individual behavioural variability.

In chapter four we use functional magnetic resonance imaging and psychophysiological interaction analysis to study corticostriatal and thalamostriatal connectivity during serial reversal learning. Functional connectivity between the centromedian-parafascicular nuclei of the thalamus and the associative dorsal striatum, and between the lateral-orbitofrontal cortex and the associative dorsal striatum was related to processing feedback during reversal learning. Specifically, thalamostriatal connectivity was found across the task, and may reflect a general error signal used to identify potential changes in context. Conversely, corticostriatal connectivity was found to be specific to when behaviour changed and suggests this may be a mechanism for the implementing adaptive change. We also show findings from exploratory work that may explain further how the cortex supports flexibility during reversal learning.

Lastly, we used magnetic resonance spectroscopy to investigate whether the state of the cholinergic system at rest is related to reversal learning performance and latent measures of behaviour using computational modelling. Choline concentrations at rest showed significant functional relevance to our measures of reversal learning. More specifically, we found that errors during reversal learning, and learning rates for positive and negative prediction errors, explained significant variance in choline. However, the relationship between choline levels and task performance presented here differ from previous work which instead used a multi-alternative reversal learning task, and suggests that the striatal cholinergic system may have dissociable roles in different contexts.

Overall, we show that the striatum, its cholinergic interneuron system, and its afferent projections from the cortex and thalamus, are associated with performance during serial reversal learning. Moreover, these findings suggest that the system may operate in separable ways in different contexts which may be dependent on internal representations of task structure.

Introduction

Cognitive flexibility

Flexibility is essential for goal-directed behaviour, as it enables an individual to adjust and respond to a non-stationary environment. This ability is an emergent property of executive function and enables an individual to maintain a given goal whilst altering the necessary actions to reach that goal (Dajani & Uddin, 2015). Furthermore, flexibility is not merely whether an individual is more disposed to switching or not, but is argued to encompass an ability to identify, choose, and execute an optimal response strategy (Yu et al., 2019). The production of this flexible response requires two overlapping yet distinct processes, namely cognitive flexibility and behavioural flexibility. Broadly defined, cognitive flexibility is the mental capacity required to produce flexible computations, while behavioural flexibility is the phenotypic response of an individual to a changing environment (Uddin, 2021). Thus, cognitive flexibility without behavioural flexibility is intractable, whilst behavioural flexibility without cognition is impossible. Within this thesis the term cognitive flexibility will be used interchangeably to describe both the underlying computation, and the behaviour that arises from it.

Executive function and flexibility

The main features of executive functioning underlying cognitive flexibility are working memory, attention and salience detection, inhibition, and switching (Dajani & Uddin, 2015). Working memory is important for caching information in mind that is not perceptually accessible and for performing mental operations on it. This storage and processing of relevant information is like the central processing unit of a computer, which stores and performs calculations on relatively small chunks of information and generates output that can be acted upon, discarded, or stored in longer term memory. The processes underlying working memory in the brain are thought to rely on the dorsolateral prefrontal cortex (D'Esposito et al., 1999). Working memory also reciprocally supports inhibitory control (Diamond, 2013). Inhibitory control is the ability for an individual to voluntarily manage sensory, cognitive, and behavioural information and responses that are irrelevant for goal directed behaviour (Tiego et al., 2018). This includes the suppression of prepotent habitual or reflexive thoughts and responses in favour of more relevant goal-directed actions or assigning attentional control to process only relevant sensory stimuli. Inhibitory control is important for cognitive flexibility, as changes in an environment require the reorientation of behaviour to maintain goal-directed action. Response inhibition is thought to be supported by the ventrolateral prefrontal cortex and subthalamic nucleus for motor inhibition and the inferior frontal junction for the detection of behaviourally relevant stimuli (Aron & Poldrack, 2006; Levy & Wagner, 2011; Verbruggen & Logan, 2008). Insular activity is associated with both inhibition and

salience detection, and forms part of the salience network alongside the anterior cingulate cortex (Menon & Uddin, 2010). The salience of a stimulus is dependent on its importance, intensity, and detectability (APA, 2020). Salience is important for flexibility, as stimuli signalling a change in context need to be identified and processed to determine whether a change in response is needed to maintain goal-directed action (Dajani & Uddin, 2015). If salient information is not correctly identified, then behaviour can quickly become maladaptive following a change in environment if an individual does not correctly identify that they need a switch in behaviour. Two types of switching paradigms are frequently used for measuring cognitive flexibility. In set shifting paradigms participants learn a set of rules that are relevant in different contexts and can be used to achieve a specific goal. Task switching involves participants switching between completing more than one type of task. In set shifting tasks participants learn through feedback how to flexibly respond in different contexts, while task switching involves flexibly using different explicit rules to guide behaviour (Kehagia et al., 2010).

Disorders of flexibility

Numerous neurological and mental health conditions are characterised by impaired executive functioning and aberrant cognitive flexibility. These disorders include neurodegenerative diseases such as Parkinson's and Huntington's disease, neurodevelopmental disorders such as Attention Deficit Hyperactivity Disorder and Autism Spectrum Disorder, trait anxiety and depression, schizophrenia and Obsessive Compulsive Disorder (Itami & Uno, 2002; Nickchen et al., 2017; Peterson et al., 2009; Remijnse et al., 2009; Schlagenhauf et al., 2014; South et al., 2012; C. G. Wilson et al., 2018). Impaired flexibility in these disorders is related to inattentiveness, cognitive rigidity, restrictive and recurrent thoughts and behaviours, and negative thinking (Uddin, 2021).

Individuals with Autism Spectrum Disorder show a general impairment across several domains of executive functioning throughout childhood, adolescence and adulthood (Demetriou et al., 2018). Individuals with Autism Spectrum Disorder are able to set-shift in cognitive flexibility tasks, but show impairments in the maintenance of set shifting, relative to non-autistic individuals (Miller et al., 2015). Moreover, this impairment in set-shifting maintenance is positively associated with the severity of repetitive and restrictive behaviour, a hallmark of Autism Spectrum Disorder (Lopez et al., 2005; Miller et al., 2015). Impaired cognitive flexibility is also seen in Obsessive Compulsive Disorder. Obsessive Compulsive Disorder is characterised by intrusive and compulsive thoughts or feelings to repetitively perform actions that are maladaptive (Uddin, 2021). Executive functioning is impaired in Obsessive Compulsive Disorder (Penadés et al., 2005) and is associated

with increased distractibility, excessive error monitoring and elevated inflexibility in tests of executive function, and cognitive flexibility (Veale et al., 1996).

Neurodegeneration in Parkinson's and Huntington's disease is accompanied by deficits in cognition, including impaired flexibility (Brown & Tait, 2016). Parkinson's disease is characterised by neuronal loss in the dopaminergic midbrain and substantia nigra, which results in stereotypical Parkinsonian tremor, muscle rigidity and reduced movement (Alexi et al., 2000). Parkinson's is also associated with reduced cognitive and executive functioning independent from dementia (Watson & Leverenz, 2010), with a loss of dopaminergic input to the prefrontal cortex and striatum thought to reduce the balance between stability and flexibility, resulting in increased inflexibility in Parkinson's disease (Cools & D'Esposito, 2011). Huntington's disease is a genetic neurodegenerative disease caused by an increased number of CAG nucleotide repeats in the DNA sequence of the gene encoding the Huntingtin protein (MacDonald et al., 1993). This expanded CAG repeat region causes aggregation of the Huntingtin protein, and leads to degeneration in the striatum and cortex of affected individuals (DiFiglia et al., 1997), which is positively associated with impairments in cognitive flexibility (Lawrence et al., 1999; Nickchen et al., 2017).

Development and flexibility

Executive functioning develops as children transition into adolescence and then adulthood. These changes show a general trend where executive functioning improves, and is accompanied by the maturation of the cerebral cortex into an individual's early twenties (Gogtay et al., 2004; Thompson-Schill et al., 2009). However, unlike executive functions which show an increase over development, there is some evidence suggesting cognitive flexibility does not follow the same developmental trajectory (Gopnik et al., 2015; Johnson & Wilbrecht, 2011; Lucas et al., 2014). For instance, Gopnik et al. (2017) tested how pre-schoolers (4 years old (y/o)), younger school aged children (6-7 y/o), older pre-adolescent children (9-11 y/o), young adolescents (12-14 y/o) and adults use evidence to guide decision making and whether prior knowledge can be flexibly used in novel situations. Participants were told that "Blickets" are required to make a machine work (Figure 1). Participants then received training showing Blickets have 1. a conjunctive relationship, meaning two objects are required to activate the machine, 2. A disjunctive relationship, meaning one was required to activate the machine, or 3. received no training (Figure 1). Participants who received conjunctive training were more likely to correctly identify a Blicket from a novel set as conjunctive than those who received disjunctive or no training. However, of those who received conjunctive

training, pre-schoolers were significantly more likely to correctly label a novel object with a conjunctive relationship as a Blicket than school age pre-adolescents (6-7 & 9-11 y/o), and school age pre-adolescents were significantly more likely to label this object as a Blicket than young adolescents and adults. The proportion of adolescents judging the object as a Blicket did not differ significantly when compared to adults. Pre-schoolers were also more likely to use multiple objects than young school aged children when asked to activate the machine themselves, suggesting the use of the conjunctive rule to activate the machine. School age pre-adolescents, young adolescents and adults did not significantly differ with respect to the number of objects they used to activate the machine. The findings of Gopnik et al. (2017) show that the flexible implementation of the more unusual, yet correct, conjunctive rule decreases across development, with transitionary periods seen in middle childhood and adolescence. Further, these findings illustrate how changes in flexibility are related to changes in experience, executive function and plasticity. Younger individuals lack life experience and mature executive function but can rely on plasticity to use what they have learned to infer the conjunctive rule. Conversely, increases in life experience and executive function plus decreases in plasticity across development result in the conjunctive rule being used more infrequently, with an increased reliance on prior knowledge.

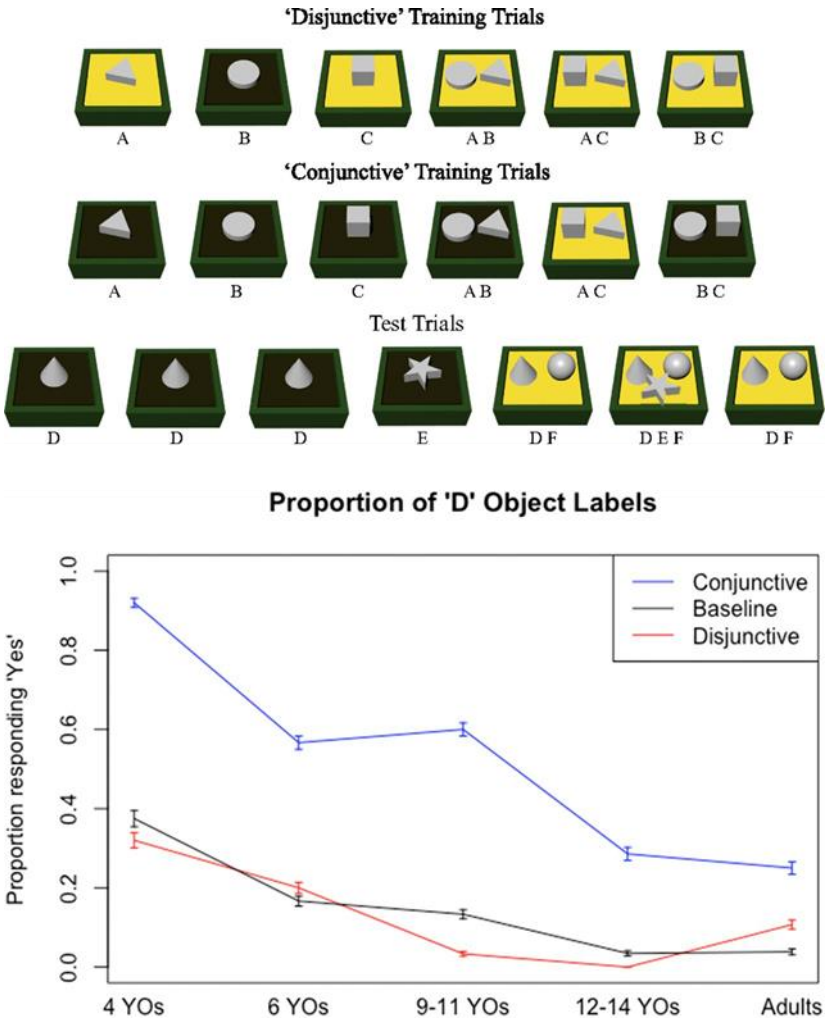

Figure 1 (Upper) Overview of disjunctive and conjunctive training. Disjunctive training taught participants that whether an object is a Blicket, and therefore will activate the machine, is not dependent on other Blickets. Conjunctive training taught that two Blickets are required to activate the machine. During the test phase object D was a Blicket, and participants were asked whether they thought object D was a Blicket or not. (Lower) Proportion of participants in each age group across conditions defining object D as a Blicket. Figure reproduced from Gopnik et al. (2017).

The development of the human brain from childhood to adulthood is characterised by regional variation in maturational trajectories, with phylogenetically older and lower-order areas reaching maturity before newer and high-order regions (Gogtay et al., 2004). Development is also characterised by changes in connectivity when learning from experience (van den Bos et al., 2012), with regions involved in reward and punishment processing (e.g. ventral striatum, medial and dorsolateral prefrontal cortices, and insula) showing age-related differences across development (Bolenz et al., 2017). These developmental trajectories are associated with changes in risk taking

behaviour (Christakou et al., 2013), and tolerance for ambiguity (van den Bos & Hertwig, 2017) during adolescence. However, although adolescents do not appear to be different from adults in adapting their rate of learning to environmental change, they appear to make decisions with less certainty than adults (Javadi et al., 2014), and overestimate environmental volatility (Jepma et al., 2020). This may explain why adolescents learn at different rates to adults (Hauser et al., 2015; Palminteri et al., 2016) and make choices that are based less on expected value (Christakou et al., 2013). By contrast, adults appear more strategic in their exploration (Somerville et al., 2017), and better able to maximise reward than adolescents or children (Burnett et al., 2010; Plate et al., 2018). These differences may be underpinned by changes in reward-processing mechanisms across development.

One way to examine this possibility is through computational modelling. For instance, Crawley et al. (2020) assessed how mechanisms underlying cognitive flexibility change across development. Children (6-11 y/o), adolescents (12-17 y/o) and adults (18-30 y/o) completed a probabilistic reversal learning task, and three computational models were fit to their behaviour. All three models varied in how information was used to update expected values. A counterfactual update model updated expected values for both the chosen and unchosen choice on each trial using a single learning rate, and the inverse outcome was used to update expected value of the unchosen option. A dual-learning rate model had separate learning rates for positive and negative prediction errors but did not update the expected value for unchosen options. Lastly, an experience-weighted attraction-dynamic learning rate model was used; this model enables dynamic updating of expected values, based on prior knowledge. In children, adolescents, and adults, behaviour in the task was best explained by the counterfactual, dual-learning rate, and experience-weighted models, respectively. These results suggest changes in value computation exist across development, with mechanisms becoming more elaborate with age. Furthermore, changes in cognitive flexibility and its underlying computations are likely to be related to biological changes across an individual's journey to adulthood, which means that operationalising appropriate tests of these competences becomes very important in developmental work.

Operationalising cognitive flexibility - the reversal learning task

The reversal learning task is a commonly used set-shifting paradigm for measuring cognitive flexibility (Izquierdo et al., 2017). In the standard version of the reversal learning task (for example in Fellows & Farah, (2003)) a participant is trained to discriminate between two visual stimuli. One of these stimuli is the correct choice and is consistently associated with a positive or rewarding outcome, whilst the other is incorrect and is associated with a negative or non-rewarding outcome.

The aim of the task is to select the correct choice to maximise positive outcomes. Stimulus-outcome associations are learned through experience, and after selecting the correct choice a predetermined number of times the participant reaches the learning criterion and the outcomes associated with each stimulus are switched. Therefore, the stimulus that was correct is now incorrect and vice versa. Following reversal, the participant needs to switch from selecting the previously correct response in order to maintain task performance. This type of reversal learning task is known as deterministic reversal learning, since a stimulus is always either correct or incorrect. A major benefit of this paradigm is that its relative simplicity means that is can be easily translated across species. For instance, rodent studies of reversal learning adapt the task by using mazes and lever press tasks (e.g. Palencia & Ragozzino, 2004; Panayi & Killcross, 2018), while primate and human studies often use visual object discrimination (e.g. Cools et al., 2002; Rygula et al., 2010). This translational viability means techniques from across animal and human neuroscience can be used to understand how flexible behaviour is supported by neural activation, and how aberrant functioning at the biological level leads to disorders of flexibility.

In the standard reversal learning task described above, the contingencies between stimuli and outcome are deterministic, meaning they faithfully predict whether a stimulus is the correct choice or not. However deterministic reversal learning is relatively straightforward for humans to complete because there is no ambiguity between the mapping of stimulus-outcome contingencies (Einhorn & Hogarth, 1985; Frisch & Baron, 1988). Probabilistic reversal learning tasks can be used to minimise the use of simple strategies to achieve reversal learning (Izquierdo et al., 2017). In probabilistic reversal learning, outcomes only partially predict whether a stimulus is the correct choice or not; for instance, selection of the correct choice may only be rewarded 80% of the time. Distinct neural responses during outcome processing, especially in the case of negative outcomes, are seen between deterministic and probabilistic reversal learning (Habiby Alaoui et al., 2021), and suggests differences in task complexity means the brain processes deterministic and probabilistic learning in separable ways. Habiby Alaoui et al. (2021) show negative prediction errors during deterministic but not probabilistic reversal learning produce an early frontal event related potential that is predictive of behaviour. Furthermore, event related potentials were generally associated with prediction error and surprise in both tasks, but only with behaviour during deterministic reversal learning. Lastly they show using source localisation, that the absence of expected outcomes generated differential, and more extensive activation for probabilistic than deterministic reversal learning.

Using probabilistic feedback is also interesting because it means reversal learning can be used to study how people respond to unexpected errors. Because feedback is only probabilistic, sometimes

people will make a choice and receive feedback that is incongruent, i.e. negative feedback for correct choices, and vice versa; these are known as probabilistic errors. Probabilistic errors could lead to a change in behaviour even though contingencies have not changed (Yaple & Yu, 2019). Probabilistic reversal learning can also be used to study perseverative and regressive errors (Hill et al., 2015), which can be informative about the processes involved in reversal behaviours. Following the reversal of outcome contingencies, the continued use of the previously correct response strategy is known as response perseveration, referring to the number of times the previously correct choice is selected before a switch in behaviour, namely the number of perseverative errors. Conversely, regressive errors are made when an individual returns to using the previously, but no longer, correct response after they had identified the reversal of reward contingencies and changed to the newly correct rule.

Another way the reversal learning task can vary is the number of options that are included in the task. Increasing choices from two to three or four options makes it easier to distinguish between perseverative and regressive errors, and for investigating variability in exploratory and exploitative choice strategies (Izquierdo et al., 2017). Activation when feedback was unexpectedly omitted was found to be significantly greater in several regions including the ventral striatum, cingulate cortex, thalamus and midbrain in four choice reversal learning compared to two choice reversal learning (D'Cruz et al., 2011), and suggests that increased uncertainty in the four choice task increases computational demand. This, demand may, in part, be provided by the orbitofrontal cortex. For example, Kim & Ragozzino, (2005) found that chemical inactivation of the rat orbitofrontal cortex impairs reversal learning; increased perseveration following inactivation was observed in two choice reversal learning, however four choice reversal learning saw increases in both perseverative and regressive errors.

The neural computations underpinning reversal learning in humans require the recruitment of several regions across the brain. Studies of patients with damage to the frontal lobe have found that this damage is associated with impaired performance during reversal learning, that may be associated with a loss of cognitive function (Daum et al., 1991; Rolls et al., 1994; Verin et al., 1993). In particular, lesions to the orbitofrontal cortex in humans appear to have a negative effect on reversal learning performance, where an increased number of errors following the reversal of outcome contingencies is seen, relative to individuals with lesions of the dorsolateral prefrontal cortex and also control participants (Bechara et al., 1994; Fellows & Farah, 2003, 2005). The effects of orbitofrontal and dorsolateral prefrontal lesions on reversal learning were further studied by Hornak et al. (2004), who found performance during reversal learning to be impaired for patients with bilateral orbitofrontal lesions, but not those with unilateral lesions. Moreover, lesions to the

dorsolateral prefrontal cortex negatively impaired performance, but only in participants who did not attend to feedback; all patients with lesions to the orbitofrontal cortex paid attention to feedback, but this did not ameliorate the effect of lesions on reversal learning performance. This suggests the orbitofrontal cortex is important for monitoring changes in reward value and using these values to guide adaptive behaviour, while the dorsolateral prefrontal cortex is important for identifying the relevance of information for guiding behaviour. This perspective is supported by more recent lesion work, with Tsuchida et al. (2010) finding lesions to the orbitofrontal cortex increased both the number of errors made during initial and reversal learning, and that participants chose alternative options after receiving positive feedback more frequently than the control subjects.

Lesions of the basal ganglia have also been associated with impaired reversal learning performance. For instance, Bellebaum et al. (2008) found patients with basal ganglia lesion were not impaired during initial learning, but did show reduced performance during reversal relative to control participants; in particular, the most impaired reversal learning performance was observed in patients who had lesions of the dorsal striatum. The reversal learning performance of patients with bilateral lesions of the amygdala, caused by Urbach–Wiethe disease, has also been studied by Hampton et al. (2007). Hampton and colleagues found that patients with amygdala lesions showed an increased tendency to switch to the alternative option, regardless of whether they received a reward. However, both amygdala lesion participants performed better than chance, suggesting these lesions only made them more insensitive to using reward to guide behaviour. Furthermore, patients with amygdala lesions did not show impairments in other metrics of performance, such as initial learning and response perseveration. When comparing switch with stay trials, Hampton et al. (2007) also showed amygdala lesion patients had clusters in the bilateral anterior insula/lateral orbitofrontal cortex, and anterior cingulate cortex where activation was significantly reduced, relative to control participants. Amygdala lesion participants also had significantly reduced activation relating to the estimation of expected value in the medial prefrontal cortex. Lastly, amygdala lesion patients showed no difference in responses to positive and negative outcomes in comparison to controls. These results suggest amygdala lesions may impair the calculation of expected value, and the use of these values to guide adaptive behaviour during reversal learning, leading to behaviour that is increasingly stochastic. This is in line with proposals by Schoenbaum et al. (2007), who suggest the role of the orbitofrontal cortex in flexibility is to encode expected value and facilitate changes in associative encoding in downstream regions such as the striatum and amygdala when expected and actual outcomes are incongruent. This is likely to include the striatal cholinergic system, where orbitofrontal cortex neurons are reported to be necessary for the

representation of the current environmental state by cholinergic interneurons (Stalnaker et al., 2016).

However, although lesion studies are important for understanding structure-function relationships in humans, they are nonetheless restricted. Firstly, patients with lesions are relatively rare. Lesions may be due to genetic or environmental factors leading to tissue atrophy, or a clinical condition requiring the ablation of problematic brain tissue, such as in epilepsy. The scarcity of lesion patients makes it relatively impractical to conduct research within these populations, and comorbid conditions may make the interpretation of results difficult. Secondly, the heterogeneity of lesion location is also problematic, and this also makes interpreting findings difficult. Furthermore, lesion studies generally make the implicit assumption that functional losses due to lesions mean that function must be localised within the region that is lost. However, it is more likely that lesions affect not only the site of the lesion but also other interconnected parts of the brain, given the brain is not a modular organ, with specific cognitive functions restricted to discrete regions.

Functional magnetic resonance imaging overcomes the limitations of lesions studies, by enabling the non-invasive study of structure-function relationships in both normative and clinical populations. In line with findings from lesion studies, functional magnetic resonance imaging work has consistently shown orbitofrontal cortex activation during reversal learning (Ghahremani et al., 2010; Hampshire et al., 2012; Kringelbach & Rolls, 2003; Morris et al., 2016; O'Doherty et al., 2001; Remijnse et al., 2005; Ruge & Wolfensteller, 2016). Wilson et al. (2014) propose that the role of the orbitofrontal cortex is to produce representations of task space, that act as an internal model of an individual's environment. These representations are particularly useful in uncertain and volatile environments, where the orbitofrontal cortex can integrate information about task state with information from other cortical and subcortical regions to generate expectations to guide adaptive behaviour (Howard & Kahnt, 2018). For instance, if sensory information violates expectations in the orbitofrontal cortex then flexible change in downstream regions, including the frontal pole, insula, striatum, amygdala, hippocampus, and thalamus can be produced (Heather Hsu et al., 2020; Wilson et al., 2014). The medial and lateral divisions of the orbitofrontal cortex have purportedly distinct yet complementary roles that may be important for flexibility in downstream regions. The medial orbitofrontal cortex is thought to be involved in the evaluation of outcomes, while the lateral orbitofrontal cortex is associated with the representation of the current state which includes the associated contingencies for action-outcome associations (Hampshire et al., 2012; Hervig et al., 2020; Noonan et al., 2017; Ruge & Wolfensteller, 2016). If evaluated outcomes are incongruent with expectations for the current state, then this may lead to preparation for a change in behaviour. This perspective that the orbitofrontal cortex produces a map of task space is

consistent with the idea of "model-based" reinforcement learning. In "model-based" learning, goal-directed behaviour arises from the use of internal representations of state to make predictions about future value and guide behaviour in environments that are only partially observable (Daw et al., 2005; Dayan & Berridge, 2014).

The anterior cingulate and insular cortices are the cortical hubs for the salience network, a group of brain regions that are involved in the identification and filtering of behaviourally relevant stimuli (Seeley, 2019). The identification of behaviourally relevant stimuli determines how attentional and processing resources are allocated and is important for cognitive flexibility (Dajani & Uddin, 2015). A recent meta-analysis of the reversal learning paradigm found consistent activity in the salience network during reversal learning and suggests the function of the salience network to provide long term stable performance, maintaining cognitive control during error processing and the formation of new associations (Yaple & Yu, 2019). In particular, the anterior cingulate is thought to be important for using information about reward to sustain choice behaviour, and to switch behaviour when the outcome of an action suggests that change is favourable (Behrens et al., 2007; Chudasama et al., 2013; Liu et al., 2015; Waegeman et al., 2014). Furthermore, the anterior cingulate is thought to encode multiple distinct representations of value across the region that are relevant over different time intervals, and that the distribution of these representations can change depending on the volatility of the environment (Mohr et al., 2018). Concurrent shorter- and longer-term representations of expected value supports flexible behaviour because multiple expected values can be used and weighted to make decisions. Additionally, being able to adjust the distribution of these representations in response to volatility supports flexibility as in more volatile environments it is better to dedicate resources to shorter term evidence, while optimal behaviour in more stable environments is more likely to be guided by long term estimates of expected value.

Studies have also reported activation within the striatum during reversal learning (Cools et al., 2002; Meder et al., 2016; Remijnse et al., 2005). Activity in the ventral striatum is associated with the encoding of prediction errors (Li et al., 2011; Meder et al., 2016). Prediction error signals are thought to originate from midbrain dopaminergic neurons within the ventral tegmental area and the substantia nigra which project to both the dorsal and ventral striatum (Schultz, 1998; Schultz et al., 1997). Dopaminergic activity and reward prediction errors are commonly associated with "model-free" reinforcement learning, where the expected value for an action is based on its reward history and behaviour is driven by actions with the highest cached value; following action cached values are updated using prediction errors (Averbeck & O'Doherty, 2021). However, evidence suggests that prediction error signals are reflective of both "model-free" and "model-based" learning (Daw et al., 2011; Deserno et al., 2015), with Deserno et al. (2015) finding presynaptic dopamine levels

in the ventral striatal dopamine are positively correlated with the "model-based" learning signals in the lateral prefrontal cortex. Therefore, prediction error signals in the ventral striatum during reversal learning appear to balance innervation from cortical and subcortical inputs, and between "model-based" and "model-free" like learning signals to guide behaviour.

Previous findings have also shown that the dorsal striatum is involved in reversal learning in humans (D'Cruz et al., 2016; Gläscher et al., 2009; Hampshire et al., 2012; Mitchell et al., 2008; Morris et al., 2016; Robinson et al., 2010; Waegeman et al., 2014), though not all studies consistently find dorsal striatal activity (Yaple & Yu, 2019). One proposed role for the dorsal striatum during reversal learning is the expression of stimulus-outcome associations. Xue et al. (2008) trained participants to learn whether novel Japanese Hiragana symbols were associated with male or female names, and whether either a left of a right key press was the appropriate response to categorise the symbols as male and female; because of this design the authors could distinguish between stimulus-outcome and stimulus-response learning processes, respectively. After a period of initial learning, either stimulus-outcome (correct gender) and/or stimulus-response (correct keypress) associations could change, or both associations could stay the same. Participants were not informed about the reversal of these associations, and so they had to learn the new associations through trial and error. During reversal learning, striatal activation was significantly increased when participants correctly responded to symbols with reversed stimulus-outcome associations, relative to symbols where was no change in associations. Moreover, striatal activity was also significantly greater when participants correctly responded to symbols with reversed stimulus-outcome associations than symbols with reversed stimulus-response associations. Dorsal striatum activation was also reported by Ruge & Wolfensteller, (2016), who found that activity within the caudate nucleus was associated with the encoding of rules during instructed reversal learning. Furthermore, caudate nucleus activity was negatively associated with the cost of reversal, indexed as the difference in reaction time between initial and reversal learning. Together, these results suggest that flexible encoding of stimulus-outcome associations in the dorsal striatum is important for promoting adaptive goal-directed behaviour and flexibility that is required for reversal learning. This function may also explain why not all reversal learning studies report dorsal striatal activity, as its dynamic activity may not be appropriately described by simple contrasts (Waegeman et al., 2014).

Summary

Cognitive flexibility is an emergent property of executive functioning that is important for adaptive goal-directed behaviour in environments that are non-stationary or volatile. It is supported by

several executive functions including working memory, inhibition, attention and salience detection, and switching. However, unlike executive functions that show a general increase across development, flexibility may not follow the same trend, with adults relatively less flexible due to an increased reliability on prior knowledge instead of learning to guide behaviour. Impairments in cognitive flexibility are seen in developmental, mood, and mental disorders and in neurodegeneration. The reversal learning task is a commonly used paradigm for studying cognitive flexibility, and neuroimaging studies suggest the involvement of multiple brain regions in flexibility. This includes the orbitofrontal cortex which is thought to generate internal representations of task state based on cortical and subcortical input and uses this information to guide flexibility via its efferent connectivity. The anterior cingulate cortex is associated with the representation of value across multiple timescales and using reward information to determine whether to switch or sustain current choice behaviour. The ventral striatum is associated with prediction error which signals the difference in expected and actual outcomes. The dorsal striatum is thought to be important for the encoding of stimulus-outcome associations, and the flexible encoding of these associations are important for cognitive flexibility.

Reversal learning, the striatum, and acetylcholine

Acetylcholine is a chemical messenger found throughout the nervous system. Within the peripheral nervous system acetylcholine acts as a neurotransmitter controlling the action of muscles and autonomic ganglia; in the central nervous system acetylcholine acts primarily as a neuromodulator, meaning acetylcholine is not directly involved in excitatory or inhibitory neurotransmission, but instead changes the responsivity of other neurons to stimulation (Picciotto et al., 2012). Two regions of the brain have cholinergic neurons that project to the cerebral cortex and thalamus, namely the basal forebrain, and the pedunculopontine nucleus (Perry et al., 1999). The primary source of cholinergic input to the cerebral cortex are the nucleus basalis and the medial septal nucleus in the basal forebrain, which have efferent projections that innervate all of cerebral cortex (Mesulam, 2004). Aside from projection neurons, cholinergic interneurons are also found in the striatum. These neurons are tonically active, are identifiable by their expression of the enzyme choline acetyltransferase, and are responsive to conditioned sensory stimuli (Aosaki et al., 1995). The following sections will describe the structural characteristics of basal ganglia circuitry and its role in cognitive flexibility, with a focus on the relevance of striatal cholinergic interneurons for flexibility.

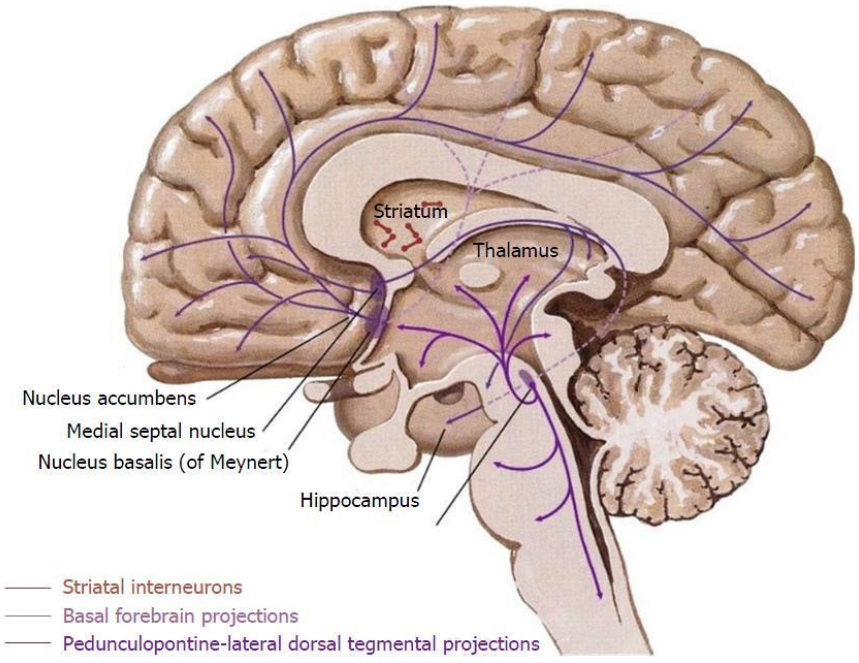

Figure 2 Cholinergic projection and interneuron systems in the brain. Figure reproduced from (Hopper et al., 2016)

Striatal architecture

The striatum, acting as in the input to the basal ganglia, is involved in sensory, motor, associative, and limbic processes. Glutamatergic and dopaminergic neurons provide the main input to the striatum; glutamatergic inputs originate from the cortex, thalamus and limbic regions, while dopaminergic inputs are received from the ventral tegmental area and the substantia nigra (Burke et al., 2017). Most of these inputs synapse onto medium spiny neurons, which are the primary cell type of the striatum. In rodents, medium spiny neurons account for approximately 95% of all neuronal cells within the striatum while in primates and humans it is thought that around 75% of striatal neurons are medium spiny neurons (Bernácer et al., 2007; Graveland & Difiglia, 1985). Striatal medium spiny neurons have projections to the rest of the basal ganglia and are defined as direct or indirect pathway neurons based on neuropeptide and gene expression. Striatonigral medium spiny neurons are part of the direct pathway and express the dopamine D1a receptor, the genes *Tac1*, *Pdyn*, and *Isl1*, and the neuropeptides dynorphin and substance P; the direct pathway of the striatum projects directly to the globus pallidus interna and the substantia nigra pars reticulata from the striatum (Ehrman et al., 2013; Heiman et al., 2008; Williams, 2018; Yager et al., 2015). Striatopallidal medium spiny neurons form part of the indirect pathway, and express the dopamine receptor D2, the genes *Adora2a*¸and *Penk*, and the neuropeptide enkephalin; they have indirect connectivity from the striatum to the globus pallidus interna and the substantia nigra pars reticulata via the globus pallidus externa and the subthalamic nucleus, which itself receives input from the globus pallidus externa (Heiman et al., 2008; Williams, 2018; Yager et al., 2015)[1].

[1] A subset of medium spiny neurons in rodents and primates express D1-D2 heteromers, but at a lower level than D1 or D2 expressing neurons (Hasbi et al., 2020)

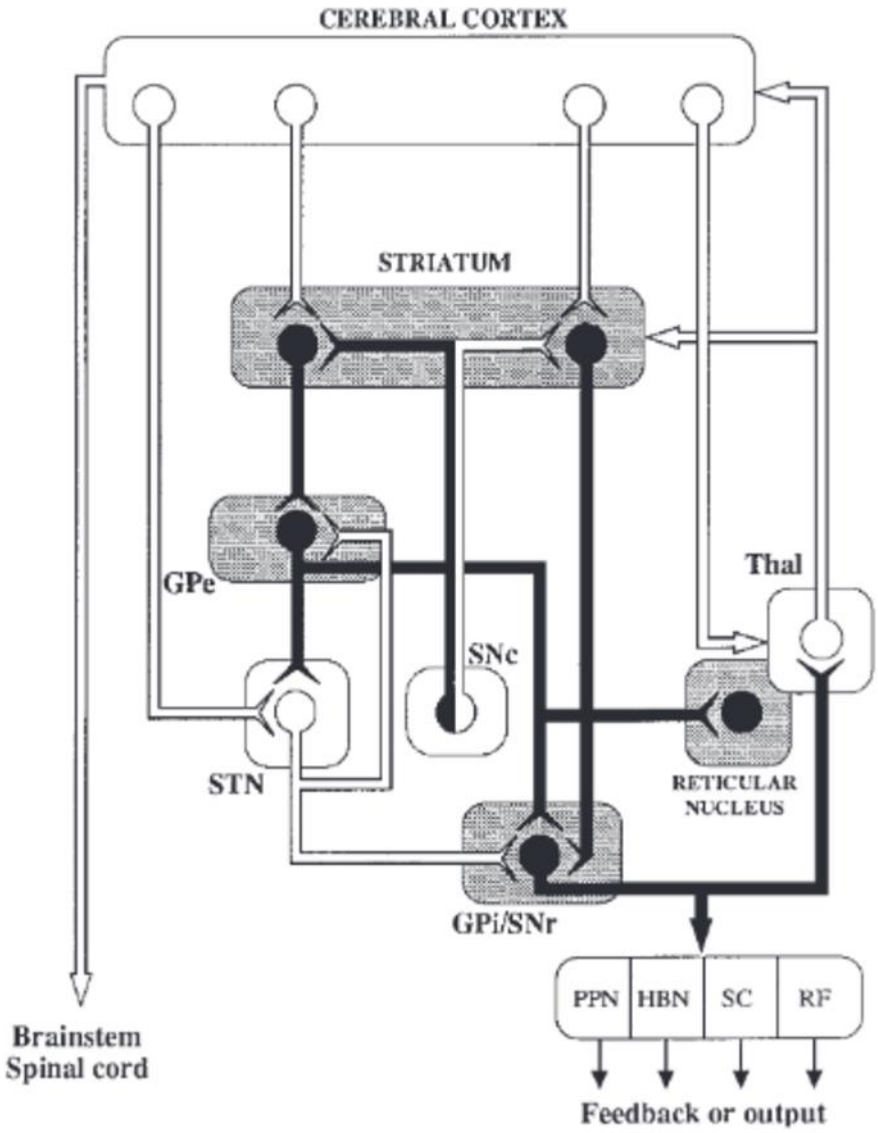

Figure 3 Connectivity in the basal ganglia with projection neurons from the cerebral cortex and thalamus. Excitatory glutamatergic connections are clear, inhibitory GABAergic connections are black. GPe: globus pallidus externa, GPi: globus pallidus interna, HBN: lateral habenular nucleus, PPN: pedunculopontine nucleus, RF: parvicellular reticular formation, SC: superior colliculus, SNc: substantia nigra pars compacta, SNr: substantia nigra pars reticulata, STN: subthalamic nucleus, Thal: thalamus. Figure reproduced from (Smith et al., 1998)

The remaining neuronal cells in the striatum are interneurons that have a modulatory effect on the output of the striatum. These interneurons are gamma-Aminobutyric acid (GABAergic) and acetylcholine (cholinergic) releasing interneurons and are identifiable based on protein expression. The three canonical subgroups of GABAergic interneurons are fast-spiking, low threshold spiking, and calretinin expressing interneurons, which express either parvalbumin, or somatostatin & nitric

oxide synthase & neuropeptide Y, or calretinin, respectively (Burke et al., 2017). Cholinergic interneurons are identifiable based on the expression of choline acetyltransferase, and estimates suggest they account for between 1-2% to up to 20% of the striatal neuronal population in humans (Bernácer et al., 2007; Prado et al., 2017). Cholinergic interneurons primarily receive input via glutamatergic projections from the thalamus, and have broad dendritic arborisations allowing them to innervate much of the striatum (Kawaguchi et al., 1995).

Cholinergic interneurons are tonically active, with an irregular firing rate of 3-10Hz on average in anaesthetised rats (Wilson et al., 1990). This tonic activation is intrinsically driven and independent of synaptic input (Bennett et al., 2000), and is important for modulating ion channels on medium spiny neurons, plasticity of glutamatergic afferents, GABA release from GABAergic interneurons, and the tonic release of dopamine from dopaminergic neurons (Wilson, 2005). Cholinergic interneurons also show a transient pause in firing followed by a rebound in activity to conditioned stimuli associated with reward, which reduces as the conditioned association is extinguished (Aosaki et al., 1994; Kimura et al., 1984). This pause and rebound response was initially thought to be important for associating conditioned stimuli and responses, however more recent evidence suggests cholinergic interneurons respond not only to conditioned stimuli, but that they integrate contextual information from cortical, thalamic and midbrain dopaminergic inputs to flexibly generate appropriate actions for a given context (Apicella, 2007, 2017). For instance Deffains et al. (2010) recorded the response of striatal cholinergic interneurons in monkeys while they completed a reaching task. The monkeys are presented with three illuminating buttons and at the start of each trial the central button is illuminated, signalling the start of the trial. This button is then extinguished, and one of the three buttons is illuminated; this button is the trigger, and correctly pressing the trigger button leads to the delivery of reward. In one condition triggers are illuminated in a repeating pattern from left to right across trials, while in another the illuminated trigger is pseudorandom. In the repeating condition, cholinergic interneurons either responded to both the cue and the trigger, selectively to either the cue or trigger or showed no response. Following a change from the repeated to the random condition, 51% of cholinergic interneurons changed their response pattern to the cue and trigger, which was accompanied by a change in the level of activation of a subset of medium spiny neurons between conditions. These results suggest cholinergic interneurons are sensitive to changes in task context requiring a change in behavioural response, and that this may be achieved by modulating the level of activation in a sub-population of medium spiny neurons.

The direct effect of acetylcholine on medium spiny neurons in the striatum are mainly driven by the activation of muscarinic M1 and M4 receptor subtypes (Kljakic et al., 2017). Cholinergic

interneurons primarily synapse onto the dendritic spines of medium spiny neurons (Abudukeyoumu et al., 2019), where muscarinic M1 receptors are expressed by direct (D1) and indirect (D2) pathway medium spiny neurons and have an excitatory effect on medium spiny neurons (Assous, 2021). M4 muscarinic receptors are also expressed by medium spiny neurons, but at a much higher level in direct pathway than indirect pathway neurons; M4 muscarinic receptors decrease the activity of medium spiny neurons (Assous, 2021; Kreitzer, 2009). Cholinergic interneurons express M2 and M4 muscarinic receptors, which are thought to function as autoreceptors inhibiting their own activation (Kljakic et al., 2017; Kreitzer, 2009). Acetylcholine can also have an indirect effect on medium spiny neurons via the expression of acetylcholine receptors on glutamatergic inputs from the cortex and thalamus, dopaminergic inputs from the midbrain and substantia nigra, and local GABAergic interneurons in the striatum (Kljakic et al., 2017). For instance, cholinergic interneurons can indirectly inhibit medium spiny neuron activity via nicotinic acetylcholine receptor activation of GABAergic interneurons (English et al., 2012) and reducing input from glutamatergic projection neurons via activation of M2 muscarinic receptors (Ding et al., 2010). Cholinergic interneurons can also facilitate the activation of medium spiny neurons by activating M1 receptors on projection neurons (Ding et al., 2010), and nicotinic receptors on dopaminergic neurons (Threlfell et al., 2012). In addition to releasing acetylcholine, cholinergic interneurons also express the vesicular glutamate transporter 3 which enables cholinergic interneurons to co-release glutamate and produces a glutamatergic-dependent response in striatal medium spiny neurons (Higley et al., 2011).[2]

[2] This section provides an overview of the important interactions of cholinergic interneurons with glutamatergic and dopaminergic projection neurons, GABAergic interneurons, and medium spiny neurons. A comprehensive review of these interactions is beyond the scope of this section but has been produced by Abudukeyoumu et al. (2019).

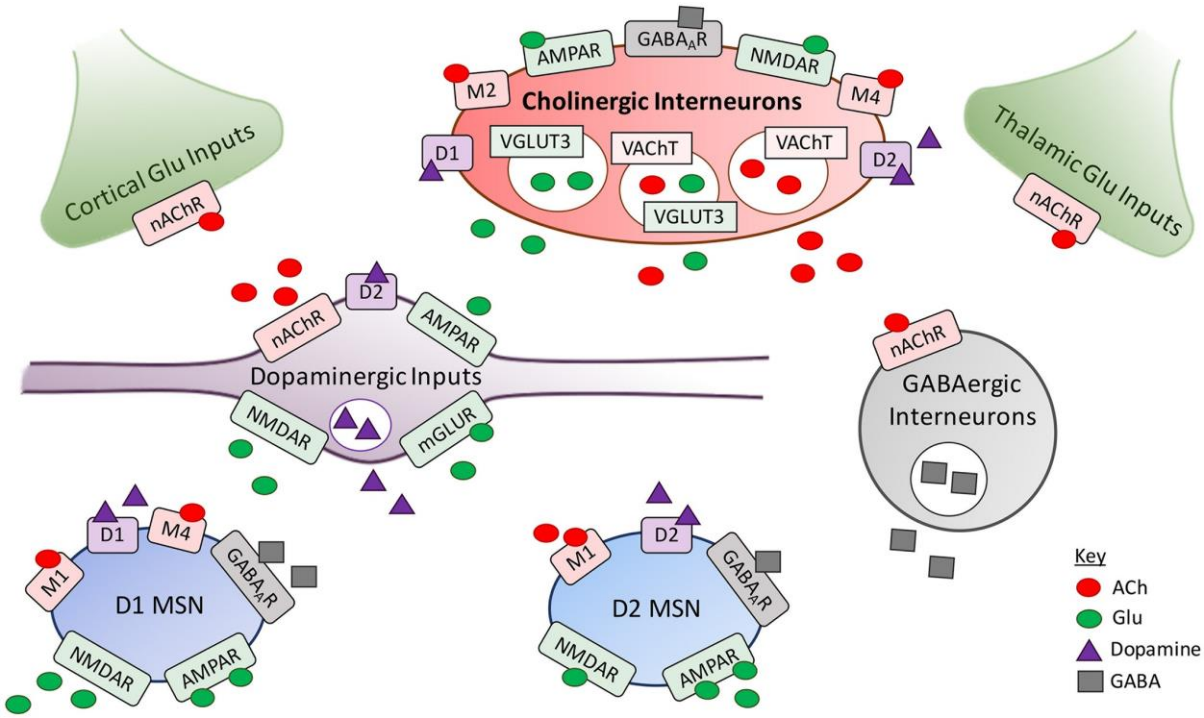

Figure 4 Cholinergic, glutamatergic, dopaminergic and GABAergic receptor expression by the major cell types found in the striatum. Figure reproduced from Kljakic et al. (2017)

Striatal acetylcholine and reversal learning in rodents

Numerous experiments studying the role of the striatum in flexible behaviour have used the reversal learning task as a behavioural assay due to its high translational value across rodents, non-human primates and humans. In particular, chemical inactivation and lesion studies in rodents have shown the importance of the striatal cholinergic system in the dorsomedial striatum for cognitive flexibility. For instance, inactivation of the rodent dorsomedial striatum using anaesthetic has been found to impair reversal learning, and increase regressive errors relative to control animals (Ragozzino et al., 2002; Ragozzino & Choi, 2004). To localise the effects of chemical inactivation to cholinergic interneurons Ragozzino et al. (2009) used the M2 receptor agonist oxotremorine sesquifumurate and the M2 antagonist AF-DX-116 to investigate their effects reversal learning. Chemical inactivation of cholinergic interneurons via M2 auto-receptor agonism did not impair initial learning but did significantly impair reversal learning performance relative to control animals. Furthermore, reductions in reversal learning performance were accompanied with significant decreases in acetylcholine efflux from cholinergic interneurons. Co-administration of the M2 receptor agonist and antagonist recovered cholinergic interneuron activity and ameliorated the effects of inactivation on reversal learning performance and acetylcholine efflux, such that there

were no differences with controls. These results replicate the findings of chemical inactivation of the whole dorsomedial striatum and support the functional involvement of cholinergic interneurons for reversal learning.

The effects of striatal acetylcholine on reversal learning may be specific to the modulation of medium spiny neurons. In the striatum nicotinic acetylcholine receptors are mainly expressed by glutamatergic inputs from the cortex and thalamus, dopaminergic inputs, and GABAergic interneurons, while muscarinic receptors are mainly expressed by medium spiny neurons (Kljakic et al., 2017). Tzavos et al. (2004), for example, demonstrated that M1 muscarinic, but not nicotinic receptor inactivation in the dorsomedial striatum impaired reversal but not initial learning, and increased the number of regressive errors that animals made. Furthermore, the role of muscarinic receptors in reversal learning is thought to be specific to M1, rather than M4 receptors, with McCool et al. (2008) showing that the antagonism of M1 but not M4 muscarinic receptors produces the same impairments in reversal learning as other previous inactivation studies. Yet, despite the apparent causative role of acetylcholine for flexible behaviour, these effects may themselves be dependent on glutamate, which is co-released with acetylcholine by cholinergic interneurons (Higley et al., 2011). Palencia & Ragozzino, (2004) used the glutamatergic NMDA receptor antagonist AP-5 to impair glutamatergic activity in the dorsomedial striatum. Similar to the inactivation of cholinergic interneurons and M1 receptors, the blockade of NMDA receptors led to impairments in reversal learning, but not initial learning, and increased the number of regressive errors that rodents made. This blockade of NMDA receptors was shown to reduce the release of acetylcholine from cholinergic interneurons both at rest and during reversal learning.

Although cholinergic interneurons appear to have a modulatory effect that precipitates flexible output from the striatum, the effects of cholinergic interneurons are themselves dependent on afferent connectivity. The primary source of thalamostriatal connections are the intralaminar nuclei of the thalamus, which provide glutamatergic input to the striatum from the centromedian-parafascicular nuclei in primates, and the homologous parafascicular nucleus[3] in rodents (Girasole & Nelson, 2015). Anterograde tracing of neurons from the centromedian-parafascicular of rodents and primates have shown these neurons have projections that preferentially terminate in the striatum (Deschênes et al., 1996; Sadikot, Parent, & François, 1992), and these terminations are in regions of the striatum coincide with high co-expression of choline acetyltransferase (Lapper & Bolam, 1992; Sadikot, Parent, Smith, et al., 1992). These thalamostriatal connections also appear to mediate the expression of flexible behaviour. For instance, Brown et al. (2010) showed that

[3] Herein, description and discussion of rodent parafascicular nucleus with the primate centromedian-parafascicular shall refer to these analogous regions as the centromedian-parafascicular nuclei for clarity.

inactivation of the rodent parafascicular nucleus using GABA agonists leads to impairments in reversal, but not initial learning, and increases regressive errors. These behavioural changes are paralleled by changes in acetylcholine efflux in the dorsomedial striatum, with GABAergic inactivation of the parafascicular nucleus preventing an increase in acetylcholine efflux following the reversal of contingencies. These findings are consistent cholinergic interneuron inactivation studies (Ragozzino et al., 2009) and suggest that the output of cholinergic inputs are at least partially mediated by connectivity with the thalamus.

In a series of experiments Bradfield et al. (2013) also investigated the role of thalamostriatal connections between the centromedian-parafascicular nucleus and the striatal cholinergic system in goal directed, flexible behaviour. First, rats received either excitotoxic lesions of the parafascicular nucleus of the thalamus, or sham lesions. These rats then underwent training to learn to associate pressing one of two leavers with the receipt of either food pellets or sucrose as an outcome. A devaluation procedure was then used to reduce the subjective value of one outcome relative to the other by providing the rats with unrestricted access to either the food pellets or the sucrose, allowing them to become sated in the absence of the test levers. Following outcome devaluation, the rats were presented with the same two leavers they had learned were associated with either food or sucrose, but now their lever presses did not result in the delivery of either of the outcomes. During this period, both the rats with excitotoxic and sham lesions of the parafascicular nucleus responded preferentially to the leaver associated with the outcome that had not been devalued, showing the parafascicular nucleus was not necessary for initial discrimination learning. After this test of initial learning, one of the outcome contingencies was degraded by making it equally likely that one outcome would be delivered whether the lever was pressed or not pressed. During outcome degradation, rats with sham lesions showed a decrease in lever presses for the lever associated with the degraded outcome, however, rats with lesions of the parafascicular did not show a decrease in responsivity to the degraded lever. Following degradation, the associations between levers and food pellets or sucrose were reversed, such that the lever that was initially associated with food pellets was now associated with sucrose, and vice versa. Rats were then given time to learn these new contingencies, before another devaluation test was used to see whether the rats had learned the new action-outcome associations. Additionally, a reinstatement test was used to test outcome-related changes in behaviour. During reinstatement, at first neither lever leads to the delivery of outcome. Then, one lever press leads to the delivery of the associated outcome. Lever presses for the associated or not-associated lever before and after outcome delivery are then measured. Rats who received excitotoxic lesions of the parafascicular nucleus showed non-specific responsivity to both levers following outcome devaluation and showed equal responsivity to both

levers following outcome delivery during the reinstatement test. Sham lesioned rats preferentially responded to the non-devalued leaver during outcome devaluation, and to the lever specifically associated with the delivered outcome during outcome devaluation. These results show that lesions of the parafascicular nucleus of the thalamus impairs the learning of outcome contingencies during reversal learning, but that the initial learning of outcome contingencies are spared.

To confirm the specificity of these results to connectivity between the parafascicular nucleus and cholinergic interneurons in the posterior dorsomedial striatum, the previously described experiments were repeated by Bradfield et al. (2013). The first repetition set included rats who received lesions in the parafascicular nucleus of the thalamus and the posterior dorsomedial striatum. These lesions were either sham lesions, ipsilateral lesions which one set of thalamostriatal connections, or contralateral which spared no thalamostriatal connections. As parafascicular neurons project to the ipsilateral hemisphere of the brain, this lesion approach enabled the authors to study the effects of partial or complete abolition of thalamostriatal connections on reversal learning. In the second repetition, rats received unilateral lesions of the of the parafascicular nucleus, and had either the M2 receptor agonist oxotremorine sesquifumurate, or a control infusion in the dorsomedial striatum contralateral to the parafascicular lesion. Like the previous contralateral lesion approach, this strategy enabled the study of partial or complete disconnection of connections, but with specificity for the striatal cholinergic system. Rats who received contralateral lesions of the parafascicular nucleus and the posterior dorsomedial striatum, and those who received unilateral parafascicular lesions with contralateral oxotremorine sesquifumurate infusion showed deficits in learning that were in line with rats who received the previously described bilateral parafascicular lesions. More specifically, these animals did not show impairments in initial learning, but did show impairments during reversal learning, with non-discriminant selection of the devalued and non-devalued leavers during outcome devaluation, and of the associated and non-associated lever during contingency reinstatement following the reversal of outcome contingencies. Conversely, ipsilateral and sham lesions, and unilateral parafascicular lesions with contralateral control infusions showed no impairments during initial or reversal learning, as was seen in rats with bilateral sham lesions of the parafascicular nucleus. These results again show the importance of thalamostriatal connections for reversal learning, and specifically implicate the striatal cholinergic system in flexible behaviour. Moreover, they suggest the striatal cholinergic system may have a modulatory effect on the striatum whereby cholinergic neurons reduce interference between existing and new learning, thereby enabling flexible behaviour, and that this modulation is driven by input from the parafascicular nucleus of the thalamus.

Striatal acetylcholine and reversal learning in humans

It is likely the dynamic role played by the dorsal striatum during reversal learning in humans is at least partially modulated by the activity of the striatal cholinergic system as in animal studies (Bradfield et al., 2013; Brown et al., 2010; Ragozzino et al., 2009), with several studies from Bell and colleagues suggesting this is the case. Magnetic resonance spectroscopy is a non-invasive neuroimaging technique for studying neurochemistry *in-vivo*[4], and has been used by Bell, Lindner, et al. (2018) to study the functional relevance of the dorsal striatal cholinergic system for reversal learning. In this study participants completed a four choice multi-alternative probabilistic reversal learning task while quantitative measures of choline containing metabolites were acquired in the dorsal striatum. The multi-alternative reversal learning task closely mimics the setup of animal studies of reversal learning. It has a protracted period of initial and reversal learning, with an uninstructed reversal of outcome contingencies. Therefore, participants learn contingencies for the initial and reversal contexts through trial and error, with no prior knowledge of the task outline. This is distinct from serial reversal learning tasks, where internal representations of task context are readily acquired. During serial reversal learning, once an "if not A, then B" heuristic for correct and incorrect choices exists, no additional information is relevant for representing task structure. Therefore, task representation in serial reversal learning may be considered as "saturated". However, task representations for the multi-alternative task can be considered as "unsaturated", since participants are not instructed on the structure of the task and only compile mature task representations following both the protracted initial and reversal learning periods.

In the multi-alternative task used by Bell, Lindner, et al. (2018), two choices were initially assigned as the correct choices, and the other two were initially incorrect. Reward probabilities for correct choices were 75% and 60%, and 40% and 25% for the incorrect choices. Participants had to reach a learning criterion which was the selection of the correct choice on 80% of 20 consecutive trials. After reaching criterion, a stability phase equal to 60% of trials to criterion preceded the unsigned reversal of contingencies. Participants then had to re-reach criterion during the reversal learning phase, which was followed by a second stability phase.

Functional changes in choline are thought to be a viable indirect measure of acetylcholine activity (Lindner et al., 2017), therefore Bell, Lindner, et al. (2018) aimed to use this approach to study the functional relevance of the human striatal cholinergic system for adaptive behaviour. No change in dorsal striatal choline concentrations were seen during initial learning yet following the reversal of

[4] A methodological overview of magnetic resonance spectroscopy is presented in "Proton magnetic resonance spectroscopy"

reward contingencies a significant decrease in choline was seen, relative to initial learning. This decrease in choline is in line with previous descriptions of choline kinetics during the stimulation of cholinergic interneurons (Löffelholz, 1998), and suggests a significant increase in the activity of dorsal striatal cholinergic interneurons following the reversal of reward contingencies. Additionally, no functional changes in the concentrations of other choline containing compounds (glycerophosphocholine and phosphocholine) were observed, suggesting this result is specific to choline, which is the precursor and rate limiting factor in acetylcholine synthesis (Taylor & Brown, 1999). Lower levels of striatal choline at rest were also seen in participants who learned and reached criterion during initial and reversal learning than in participants who only reached criterion during initial learning.

The state of the striatal cholinergic system and its association with reversal learning performance was further investigated by Bell et al. (2019). In this study, participants completed the same multi-alternative reversal learning task as in Bell, Lindner, et al. (2018)[5], and metabolite spectra were then acquired in the dorsal and ventral striatum, and also in the cerebellum while at rest. Incorrect choices during reversal learning were classified as perseverative errors, while incorrect choices during the stability phase following reversal were classified as regressive errors. Choices during initial learning, reversal learning, and both stability phases were separately fitted to a temporal difference reinforcement learning model with separate learning rates for positive and negative prediction errors. Spectroscopy data were fitted, quantifying separate concentrations of choline, and glycerophosphocholine plus phosphocholine.

Choline concentrations in the dorsal striatum were associated with performance during reversal but not initial learning. Dorsal striatal choline concentrations were negatively correlated with the learning rate for negative prediction errors during reversal learning and positively correlated with the number of perseverative errors. Moreover, dorsal striatal choline concentrations significantly increased the explained variance in perseveration compared to negative prediction errors during reversal and trait impulsivity. Cerebellum, and ventral striatal choline concentrations were not associated with reversal learning performance, demonstrating the specificity of these results to the dorsal striatal choline. These findings suggest that the efficiency of reversal learning performance is associated with levels of dorsal striatal choline at rest, enabling participants to adapt to a change in outcome contingencies more quickly than those with higher levels of dorsal striatal choline. Bell et al. (2019) suggest choline concentrations at rest may influence reversal learning efficiency by increasing the contrast in acetylcholine concentration between rest and reversal learning, or may

[5] Except the learning criterion was set as the correct choice 80% of the time over 10 consecutive trials.

reflect a more efficient re-uptake of choline and conversion into acetylcholine by cholinergic interneurons.

Centromedian-parafascicular nuclei of the thalamus and flexibility in humans

Animal studies suggest that striatal cholinergic system involvement in flexibility is at least partially driven by input from the centromedian-parafascicular nuclei (Bradfield et al., 2013; Brown et al., 2010). Furthermore, there is also research pointing to the importance of this system for goal-direct behaviour in humans. Schepers et al. (2017) used deep brain stimulation electrodes to record activity in the centromedian-parafascicular nuclei of six individuals being treated for chronic pain while they completed a three-class auditory oddball task, and a multi-speaker paradigm. In the auditory oddball task participants were presented with three different tones. One task was frequently presented, while two were infrequently presented. One of the infrequent tones was a target tone that participants needed to respond, while the other was a deviant tone requiring no response. The frequently presented tone also did not require a response. In the multi-speaker paradigm participants were concurrently presented with two streams of speech. Each stream contained a target word (name) that indicated which voice they had to pay attention to, and two task words (a colour and number) which they had to listen out for. Each trial began with participants being told the target word and ended with a target image indicating they needed to report the task words from the target stream. Centromedian-parafascicular nuclei neurons showed a transient increase in activity for target tones compared to frequent and deviant tones in the auditory oddball task, and the target word compared to task words in the multi-speaker paradigm. Additionally, increased activity for the target tone in the auditory oddball task was seen regardless of whether a motor response was made. In the multi-speaker paradigm, a transient response in centromedian-parafascicular activity to the target image was also seen in two of the six participants. These results show that task-relevant sensory stimuli requiring either a covert or overt change in behaviour for goal-directed action cause a transient increase in centromedian-parafascicular nuclei activity, and suggest this region is as important for promoting flexibility in humans as in non-human animals.

Thalamic stroke is reported to account for 2.8% and 3.1% of haemorrhagic and ischemic stroke cases respectively (del Mar Sáez de Ocariz et al., 1996), and are useful cases for assessing the importance of the thalamus in cognitive processes. In a study recent study by Liebermann et al. (2013), the cognitive functioning of nineteen patients with thalamic stroke lesions was assessed. A subset of eight patients showed particularly impaired performance on the Wisconsin Card Sorting Test, commonly used as an assay for cognitive flexibility. All eight patients had scores at least two

standard deviations away from the group mean on one measure of performance, and five were impaired on three of the four performance measures. Comparing the localisation of thalamic lesions in the impaired versus non-impaired groups showed that impairment in the Wisconsin Card Sorting Test was associated with lesions in the ventro-medial thalamus mainly encompassing the centromedian-parafascicular nuclei, while focal lesions of the centromedian-parafascicular were not found in patients with unimpaired task performance.

Preliminary evidence also suggests connectivity between the centromedian-parafascicular nuclei and the dorsal striatum is involved in reversal learning in humans. Using functional magnetic resonance imaging Bell, Langdon, et al. (2019) concurrently acquired whole-brain imaging data while participants completed the same multi-alternative reversal learning task as in Bell et al. (2018) and Bell, Lindner, et al. (2019). Functional connectivity between the centromedian-parafascicular nuclei orbitofrontal cortex with the striatum was assess using psychophysiological interaction analysis, and a reinforcement learning model was fit to behaviour to infer latent variables describing behaviour. Functional connectivity between the centromedian-parafascicular nuclei and the dorsal striatum was significantly greater during reversal learning than initial learning, and the strength of functional connectivity was inversely correlated with the number of regressive errors after the reversal of reward contingencies. Moreover, the relationship between thalamostriatal connectivity and regressive errors was found to be significantly mediated by the inverse temperature parameter from the reinforcement learning model. This parameter weighs how much choice behaviour is driven by expected value, and suggests thalamostriatal connectivity reduces regressive errors by promoting new learning during the reversal period and forming stable task representations. This is in line with findings from animal literature suggesting this thalamostriatal connectivity is important for combining new and existing learning (Bradfield et al., 2013), and that lesions result in increased regressive errors in reversal learning following the loss of centromedian-parafascicular input to the dorsal striatum (Brown et al., 2010). Similarly, Bell, Langdon, et al. (2019) found functional connectivity between the lateral orbitofrontal cortex and the dorsal striatum was significantly increased during reversal learning compared to initial learning. Corticostriatal functional connectivity was found to negatively correlate with the number of the number of trials taken to research criterion during. This relationship was significantly mediated by the learning rate for positive prediction errors during reversal learning, and suggests corticostriatal connectivity may be important for instigating a change in behaviour, reducing the number of trials taken to reach criterion during the reversal phase by promoting learning from unexpected positive outcomes which reduces response perseveration by continuing with previously correct choices.

Summary

As the input node to the basal ganglia the striatum receives many afferent projections including glutamatergic inputs from the cerebral cortex and thalamus, and dopaminergic inputs from the ventral tegmental area and substantia nigra. The striatum contains two sets of interneurons, namely GABAergic and cholinergic interneurons which modulate local activity within the striatum. The modulation of local striatal systems by dorsal striatal cholinergic interneurons is important for flexibility, with chemical inactivation studies in rodents demonstrating the loss of cholinergic activity impairs reversal learning. Cholinergic involvement in reversal learning is supported by input from the centromedian-parafascicular nuclei of the thalamus to cholinergic interneurons. The functional role of the striatal cholinergic system and centromedian-parafascicular nuclei in cognitive flexibility is also supported by evidence from human neuroscience using a combination of stroke studies, functional magnetic resonance imaging, and magnetic resonance spectroscopy. It is thought the thalamostriatal system is important for promoting new learning and forming stable task representations during reversal learning and reducing regressive errors following a change in behaviour. Corticostriatal connectivity between the lateral orbitofrontal cortex and the dorsal striatum is also thought to be important for reversal learning, but this system is thought to be important in promoting a change in behaviour following the reversal of reward contingencies and reducing response perseveration.

Neuroimaging techniques for studying flexibility

Proton magnetic resonance spectroscopy

Magnetic resonance spectroscopy is an analytical tool that uses the principles of magnetic resonance to non-invasively study biochemistry *in vivo*. It can be used to measure metabolites and macromolecules in biological tissue, including in the brain. Proton magnetic resonance spectroscopy (^{1}H-MRS) is the most used application of magnetic resonance spectroscopy in human neuroimaging research. In ^{1}H-MRS metabolites and macromolecules are characterised by the chemical shifts and spin-spin coupling of protons.

The most common isotope of hydrogen is formed from a single proton, electron, and no neutrons. Its nucleus is equivalent to a positively charged hydrogen ion, also known as a proton. This proton has a natural spin, and the spin of this proton (also known as procession) generates a magnetic moment; this means a proton can behave like a magnet. When placed in an induced magnetic field this proton can either processes parallel (a lower energy state) or anti-parallel (a higher energy state) to the magnetic field. These states are known as α- and β-spin states, respectively. Most protons will process in the α-spin state as it is a lower energy state. The frequency of procession is known as the Larmour frequency, and is proportional to the strength of the magnetic field; given this, chemical shift is used to make measures comparable across field strengths and is expressed in parts per million. When a proton is exposed to a radiofrequency pulse that matches its Larmour frequency, it can flip from the lower energy α-spin state to the higher energy β-spin state. This Larmour frequency is equal to the energy difference between the α-spin and β-spin state. Excitation using radiofrequency pulses causes net magnetisation to shift away from the induced magnetic field due to more protons entering the β-spin state. As protons return to the lower energy α-spin state, net magnetisation realigns with the induced magnetic field and energy is released; this is called relaxation.

Organic compounds are chemical molecules containing covalently bonded hydrogen and carbon atoms. When a hydrocarbon (an organic compound formed only of carbon and hydrogen atoms) is placed in an induced magnetic field, the valence electrons of carbon (electrons in the outer shell of an atom) also generate an electric field, which slightly shields protons from the induced magnetic field. This effect, known as local diamagnetic shielding, reduces effect of the magnetic field on the proton, and the more shielded a proton is the less energy is required to shift the net magnetisation. The actual strength of the magnetic field for a proton after accounting for diamagnetic shielding is called the effective field. However, not all organic molecules are hydrocarbons, and the presence

of other elements can influence the shielding of protons in a compound. Elements that are more electronegative than carbon have a deshielding effect on protons as they attract the valence electrons of carbon, decreasing its electron density. In a static magnetic field, a proton with more deshielding has a higher chemical shift value because a higher radiofrequency pulse is required to flip it proton into a higher energy state.

As the structure of a given organic compound is immutable, known information about the shielding of protons can be used to determine the readout of a given molecule on a metabolite spectrum. The number of peaks for a given compound is dependent upon two factors. Firstly, the number of peaks is equal to the number of unique proton shielding configurations, with the amount of shielding determining where on the spectrum this peak will appear. Secondly each peak could be split into sub-peaks depending on spin-spin coupling. Neighbouring protons that have non-equivalent shielding will cause a peak to be separated into N+1 sub-peaks. The example in Figure 5 below explains this relationship. H_a and H_b are not equivalently shielded, since the carbon that H_a has covalent bonds with is also bonded to one chlorine atom, which is more electronegative than carbon. The carbon that H_b is bonded to has two bonded to two choline atoms, therefore, H_b is more deshielded than H_a and appears at a higher chemical shift value. The two H_a protons have spin-spin coupling with one H_b proton, therefore the peak for the two H_a protons is split into a doublet. Conversely, the one H_b proton has spin-spin coupling with two H_a protons, therefore, its peak is a triplet (Libretexts, 2014a).

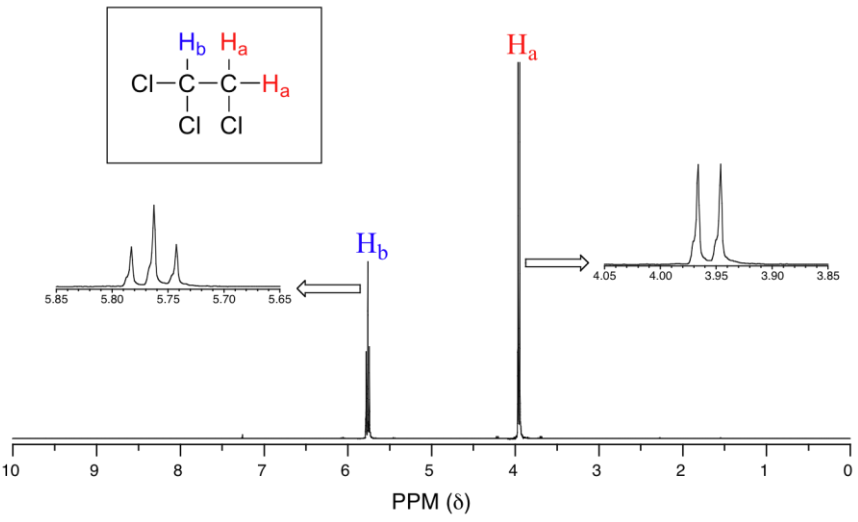

Figure 5 An example of protons producing two different peaks on the metabolite spectra. These peaks appear at different ppm due to differences in shielding, and have a different number of sub-peaks due to differences in spin-spin coupling. (Libretexts, 2014b)

Unlike other neuroimaging approaches that typically acquire data from the whole brain, magnetic resonance spectroscopy is often used for studying a single area of the brain (although magnetic resonance spectroscopic imaging can be used for whole brain acquisition) (Juchem & Rothman, 2014). Point RESolved Spetroscopy (PRESS) is a popular sequence used for acquiring single-voxel spectroscopy data. Data acquisition using PRESS uses three slice selective pulses to acquire data from a given voxel. Firstly, acquisition is localised to a given slice using a single 90 degree radiofrequency pulse in one plane, followed by two slice selective 180 degree refocusing pulses in the other two planes. Only spins that are excited by all three pulses should echo during acquisition; spoiler gradients can be used to suppress unwanted signal (Lei et al., 2014). Water is the most abundant molecules found in many types of biological tissue, including the brain. Water concentrations in the brain are approximately 10^3-10^4 times greater than other metabolites in the brain that are detectable using ^{1}H-MRS, and water suppression methods are useful for aiding the detection of these more sparsely concentrated compounds (Juchem & Rothman, 2014). CHEmical Shift-Selective water suppression is commonly used to suppress water signals by using a radiofrequency pulse to excite then dephase water to minimise its effect on net magnetisation (Lei et al., 2014). Nevertheless, acquiring water-unsuppressed spectra alongside water suppressed spectra has the additional benefit that the water suppressed spectrum can be used to calculate absolute metabolite concentrations from the metabolite spectrum, rather than calculating the ratios of one metabolite against another (Barker & Lin, 2006).

The synthesis of acetylcholine from acetylcholine coenzyme A and choline is catalysed by the enzyme choline acetyltransferase. To produce acetylcholine the body is required to source choline, and this is done in two ways. Firstly, choline can be obtained via dietary intake, with both choline and its esterified forms (phosphocholine, glycerophosphocholine, phosphatidylcholine, and sphingomyelin) found in foods with cell membranes; secondly, choline is synthesised *de novo* by phosphatidylethanolamine N-methyltransferase in the liver, which converts phosphatidylethanolamine to phosphatidylcholine (Zeisel, 2006). After synthesis, acetylcholine is packaged into vesicles near synaptic boutons. The propagation of an action potentials causes cholinergic neurons to release acetylcholine into the synaptic cleft, where it can bind to muscarinic and nicotinic acetylcholine receptors and be broken down into choline by acetylcholinesterase. Cholinergic neurons contain high-affinity proteins for the reuptake of choline, and the reuptake of choline is thought to be the rate-limiting factor in acetylcholine synthesis (Taylor & Brown, 1999). Most intracellular choline is phosphorylated into phosphocholine by choline kinase (Li & Vance, 2008), and phosphocholine is then either converted back to choline, or is converted into cytidine diphosphocholine. Cytidine diphosphocholine is then converted into the phospholipid

phosphatidylcholine by diacylglycerol cholinephosphotransferase, and is a key component of cell membranes. Phosphatidylcholine can be broken down into lyso-phosphatidylcholine and then into glycerophosphocholine by phospholipase and lysophospholipase, respectively. Finally, glycerophosphocholine is converted into phosphocholine by glycerophosphocholine lipase.

The use of magnetic resonance spectroscopy to quantify choline containing compounds show they have a peak at around 3.2ppm on the metabolite spectrum. This peak is thought to be due to choline containing compounds freely available in the cytoplasm, as membrane bound choline metabolites are thought to not visible on the metabolite spectrum (Lin & Gant, 2014). Indeed, concentrations of choline, glycerophosphocholine, and phosphocholine are associated with the concentrations measured using magnetic resonance spectroscopy, while phosphatidylcholine concentrations are not (Miller et al., 1996). The choline containing compounds, namely choline, phosphocholine, and glycerophosphocholine resonate at 3.19ppm, 3.22ppm, and 3.23ppm respectively; acetylcholine is also identifiable using magnetic resonance spectroscopy, however its concentrations are much lower than the other choline containing metabolites, and therefore its signal is masked (Katz-Brull et al., 2005). Choline containing compounds are often quantified as a single peak on the metabolite spectra due to their proximity to each other, however doing so masks the relationship between choline and acetylcholine. For instance, synthesis of acetylcholine is limited by choline concentrations (Taylor & Brown, 1999) and concentrations of choline are associated with cholinergic interneuron activity (Löffelholz, 1998).

In a series of experiments Lindner et al., (2017) provided evidence that suggested that choline could be measured and quantified separately from the other choline containing compounds, and that functional changes in choline concentration were in line with previous findings describing the role of acetylcholine in visuospatial attention. By simulating a series of metabolite spectra at three tesla with varying concentrations of choline, and a combined peak for phosphocholine and glycerophosphocholine, Lindner et al., (2017) demonstrated that spectral quantitation could recapture the initial concentrations for each peak independently from the concentration of the other peak. Additionally, Lindner et al., (2017) showed that changes in choline concentration in the parieto-occipital cortex were related to changes in visuospatial attention, and that these functional changes were in line with the expected role of acetylcholine. This same approach quantifying a separate peak for choline to phosphocholine and glycerophosphocholine was also used by (Bell et al., 2018; Bell, Lindner, et al., 2019) to study the role of the striatal cholinergic system in reversal learning[6]. This quantitation approach thus provides a method for using magnetic resonance

[6] See "Striatal acetylcholine and reversal learning in humans" for further details.

spectroscopy to non-invasively study acetylcholine indirectly *in vivo* by using choline concentration as a proxy for acetylcholine action.

Automated segmentation

The thalamus is a grey matter structure located in the diencephalon and has a vast number of afferent and efferent projections across the cerebral cortex and subcortical regions of the brain. Traditionally, the thalamus is thought of as an information relay for sensory-motor signals – however, the thalamus also has an integral role in cognitive processes, and this includes cognitive flexibility (Wolff & Vann, 2019). Moreover, there is an increasing appreciation for the role of the thalamus in cognition within the human neuroimaging literature (Geier et al., 2020; Huang et al., 2019; Schepers et al., 2017). However, a major hurdle for studying the role of individual thalamic nuclei in cognitive processes using magnetic resonance imaging is the delineation of nuclei boundaries. Pulse sequences that are commonly used in human neuroimaging studies to produce high-resolution structural images of the brain have low image contrast in the thalamus, meaning the thalamus appears as a largely homogeneous structure. Therefore, the delineation of functional and anatomical subdivisions of the thalamus can be problematic, given that structural boundaries are not visually present, and because a high level of anatomical knowledge would be required to produce manual segmentations by inferring the location of individual nuclei.

An issue related to the parcellation of individual thalamic nuclei is the nomenclature used for nuclei. Variability in neuroanatomy across the lifespan and individuals, and a lack of consensus on organisation between experts means inconsistencies are seen between thalamic atlases (Buren & Borke, 1972; Ding et al., 2016; Feremutsch & Simma, 1971; Hassler, 1977; Hassler et al., 1979; Ilinsky et al., 2018; Mai & Majtanik, 2017; Morel, 2007; Percheron, 2004), and recent efforts have aimed to harmonise these perspectives (Donkelaar et al., 2017; Mai & Majtanik, 2019). One commonly used definition for the thalamus is the Morel atlas (Morel, 2007; Morel et al., 1997) and is defined based on the cyto- and myeloarchitecture, and functional significance of the thalamus. The Morel atlas is also considered a "gold-standard" definition of the thalamus (Hale et al., 2015), and has also been digitised in MNI space (Krauth et al., 2010), meaning it is also useful for neuroimaging research. However, given this atlas is in MNI space, it cannot be used to infer individual variability in thalamic architecture based on underlying neuroanatomy.

To address the previously described limitations in thalamic contrast, a number of different approaches have been taken. For example, increasing the contrast within the thalamus on anatomical images can be achieved by using specially developed sequences such as cortex

attenuated inversion recovery and white-matter nulled magnetization-prepared rapid gradient-echo (WMn MPRAGE) sequence, or by combining 3D gradient echo phase data with optimised MPRAGE images (Bender et al., 2017; Magnotta et al., 2000; Tourdias et al., 2014). These images can then be used to more accurately define nuclei because there is an increased number of visible anatomical boundaries. However, unless automated supplementary segmentation algorithms are developed (as is the case for WMn MPRAGE, see Su et al. (2019)), specialist expertise in neuroanatomy and neuroradiology are also required to accurately identify thalamic nuclei. Therefore, automated parcellation routines using diffusion weighted, resting state, and anatomical images have been developed for segmenting thalamic nuclei.

Early attempts to provide automated segmentations of the thalamus used diffusion weighted imaging. For instance, Behrens et al. (2003) demonstrated that probabilistic tractography between the thalamus and seven cortical grey matter regions, defined based on their connectivity with the thalamus in non-human primates, could segment the thalamus into seven regions that corresponded with boundaries in the Morel atlas (Morel, 2007; Morel et al., 1997). Diffusion imaging has also been used by Wiegell et al. (2003), who used the local diffusion properties of the thalamus to produce parcellations for fourteen distinct nuclei. These local diffusion properties were most likely resultant from myelinated connections between the thalamus and the cortex, rather than unmyelinated connectivity with the striatum and brainstem or local connectivity in the thalamus. More recently, combining local diffusion properties and machine learning for segmenting the thalamus has been shown to produce segmentations of the thalamus that more faithfully correspond with histological atlases and are more reproducible (Battistella et al., 2017). Nevertheless, diffusion-based methods are limited in that the connectivity patterns are likely reflective of only connectivity between the thalamus and cortex as other thalamic connections are unmyelinated (Wiegell et al., 2003). Further limitations of using diffusion imaging for thalamic segmentation include spatial resolution and trade-offs between signal-noise and b-value in diffusion imaging (Sotiropoulos et al., 2013).

Resting state functional magnetic resonance imaging has also been used for producing segmentations of the thalamus. Like early reports using diffusion-weighted imaging, initial investigations using resting state data quantified functional connectivity between regions of the cortex and the thalamus. For instance, Zhang et al. (2008) used bilateral prefrontal, parietal and occipital, temporal, motor and premotor, and somatosensory regions as cortical seed regions for resting stated-based segmentation with voxels being classified based on the cortical seed they had the strongest positive correlation with. Independent component analysis has also been used to produce segmentations of the thalamus. The main tenet of this approach is that identifying distinct

patterns of spontaneous activity should reveal clusters of voxels that can be structurally decomposed from one-another based on differences in functionally relevant signal. This independent component analysis was used by Kim et al. (2013) to identify thirty-one components in the basal ganglia and thalamus. Instantaneous connectivity parcellation, developed by van Oort et al. (2018) is an extension of the independent component approach that uses temporal unfolding to improve the signal to noise ratio of transient events. This improves the identification of components, relative to standard independent component analysis. Using their extended independent component analysis, van Oort et al. (2018) segmented thirty thalamic nuclei. Yet, thalamus segmentation using resting state data is restricted by some of the same limitations as using diffusion data. For instance, spatial resolution using high field, relative to ultra-high field magnetic resonance imaging is somewhat restrictive for identifying smaller thalamic nuclei. An additional issue using resting state data for segmentation is that inferences about structure are made based upon functional relationships. Moreover, resting state data uses blood-oxygen level dependent signal as an imaging contrast, which is only an indirect measure of neuronal activity. Inter-individual variability in haemodynamic response function shape across individuals and regions of the thalamus may result in spurious correlations. Furthermore, because the relationships used to produce segmentations using resting state analyses and independent component analysis are purely statistical in nature, significant relationships may be identified that are not reflective of the underlying anatomy; indeed Zhang et al. (2008) found that using only unilateral seed regions produced segmentations in the contralateral thalamus despite connectivity between the cortex and thalamus being mostly ipsilateral.

Thalamic parcellation using structural imaging overcomes several issues using diffusion weighted and resting state data for segmentation, including imaging resolution and limitations in inferring the underlying biological structure. As seen in diffusion weighted approaches, machine learning has also been used for segmenting the thalamus (Amini et al., 2004) and its nuclei (Deoni et al., 2007; Yovel & Assaf, 2007) from structural images. For instance Yovel & Assaf (2007) propose a multi-contrast approach using T1 and T2-weighted, magnetisation transfer, T2*, and proton density imaging to segment the thalamus into seven nuclei, while (Deoni et al., 2007) describe the segmentation of the thalamus into fifteen nuclei using differences between T1 and T2-weighted images. WMn MPRAGE imaging improves the intra-thalamic contrast during image acquisition and juxtaposes intra-nuclei myelination with surrounding grey matter regions to improve the delineation of individual nuclei (Tourdias et al., 2014). An automated parcellation routines has been developed for WMn MPRAGE (Su et al., 2019). However, the WMn MPRAGE imaging is not conventionally used in neuroimaging studies, and furthermore the usefulness of this approach is

restrictive when analysing existing datasets that do not contain WMn MPRAGE data. A recent approach for parcellating the thalamus using T1 weighted is described by Iglesias et al. (2018). This method uses Bayesian inference to fit a probabilistic atlas of the thalamus to T1-weighted images. The boundary between the mediodorsal and pulvinar nuclei with the other nuclei of the thalamus[7], and the shape of the whole thalamus are used during fitting of the probabilistic atlas. This probabilistic atlas is generated from high-resolution *ex-vivo* magnetic resonance imaging with a voxel size of 0.25mm isotropic and histological analysis using Nissl staining. Individual nuclei were segmented using the Nissl-stained sections, and blockface photos were used to merge magnetic resonance and histology data. Thalamic nuclei were digitally reconstructed, and the probabilistic atlas was formed as a tetrahedral mesh which is adaptable to individual variability in anatomy. This parcellation method is advantageous as it combines histological methods used to define thalamic architecture at the cellular level with magnetic resonance imaging at the macro level and means inferences are based on underlying neuroanatomy. Furthermore, this approach does not require the use of non-conventional imaging sequences such as WMn MPRAGE imaging and is therefore more readily applicable. Lastly, structural images have a higher spatial resolution than diffusion or functional images and therefore smaller thalamic nuclei can be delineated using structural approaches.

[7] The boundary between the mediodorsal and pulvinar nuclei with other thalamic nuclei is faint, but visible on T1-weighted images.

Aims and hypotheses

In this thesis I have three main goals. Firstly, I aim to systematically assess the segmentations of thalamic nuclei produced by the approach described by Iglesias et al. (2018). Secondly, I aim to assess variability in choline containing compound concentrations when using magnetic resonance spectroscopy. Lastly, I aim to extend our understanding of the involvement of the cortical, striatal, and thalamic regions in flexible behaviour during serial reversal learning. To do this I use a combination of magnetic resonance spectroscopy to study the striatal cholinergic system, and functional magnetic resonance imaging to study corticostriatal and thalamostriatal functional connectivity.

This thesis aims to answer the following questions:

1. Can we use automated segmentation to faithfully delineate thalamic nuclei?

In chapter two we use T1-weighted anatomical data from the Human Connectome Project (Van Essen et al., 2013) to generate subject-space segmentations of thalamic nuclei using the approach described by Iglesias et al. (2018). We then compare these segmentations to a digitised version of the Morel stereotaxic atlas (Krauth et al., 2010; Morel, 2007; Morel et al., 1997) to assess the effectiveness of this automated segmentation approach for delineating individual thalamic nuclei using quantitative measures of dissimilarity and overlap. We do this to determine whether the automated segmentation approach described by Iglesias et al. (2018) produces segmentations of the centromedian and parafascicular nuclei of the thalamus that faithfully correspond to the Morel stereotaxic atlas, given the importance of their specification in our working model of the system.

2. How variable are choline containing compound concentrations over time?

We have previously demonstrated that quantifying choline containing compound concentrations using magnetic resonance spectroscopy can be used as an indirect and non-invasive method for studying acetylcholine *in vivo* (Bell, Lindner, et al., 2019; Lindner et al., 2017), and that functional changes in choline appear in line with the underlying dynamics of acetylcholine (Bell et al., 2018; Lindner et al., 2017). However, we do not know how quantified concentrations of choline containing compounds vary with the number of transients averaged in a single session (i.e. with the density of the acquired data), nor how these concentrations vary across time. Yet, variability due to different measurement approaches is important to understand if we wish to use choline as a proxy for studying acetylcholine. Furthermore, it is useful to know how concentrations may vary over time, since this may explain some variance in differences in flexibility within individuals. This

variability in choline containing compounds will be explored in chapter three and informs the future development of the study of the system's functional neurochemistry.

3. Is corticostriatal and thalamostriatal functional connectivity observed during serial reversal learning?

Functional magnetic resonance imaging data acquired during serial reversal learning is presented in chapter four. Here, we use psychophysiological interaction analysis to investigate corticostriatal, and thalamostriatal functional connectivity during serial reversal learning. Furthermore, the functional relevance of connectivity is contrasted with previous findings from Bell, Langdon, et al. (2019) which described the importance of these connections for flexibility during multi-alternative reversal learning. We explain how contrasting these behavioural contexts provides insight about the way in which these systems engage in separable aspects of flexible behaviour.

4. Is variability in choline associated with serial reversal learning performance?

Lastly, we use magnetic resonance spectroscopy to measure choline in the dorsal striatum and examine how variability in choline is associated with reversal learning behaviour. Previous work has shown that choline concentrations at rest are related to performance during multi-alternative reversal learning (Bell, Lindner, et al., 2019), and here we ask whether this is also the case during serial reversal learning. We quantify reversal learning performance by the number of reversals participants complete and the errors they make. We also quantify latent variables describing behaviour using computational modelling and relate this to choline concentrations.

References:

Abudukeyoumu, N., Hernandez-Flores, T., Garcia-Munoz, M., & Arbuthnott, G. W. (2019). Cholinergic modulation of striatal microcircuits. *European Journal of Neuroscience*, *49*(5), 604–622. https://doi.org/10.1111/ejn.13949

Alexi, T., Borlongan, C. V., Faull, R. L. M., Williams, C. E., Clark, R. G., Gluckman, P. D., & Hughes, P. E. (2000). Neuroprotective strategies for basal ganglia degeneration: Parkinson's and Huntington's diseases. *Progress in Neurobiology*, *60*(5), 409–470. https://doi.org/10.1016/S0301-0082(99)00032-5

Amini, L., Soltanian-Zadeh, H., Lucas, C., & Gity, M. (2004). Automatic segmentation of thalamus from brain MRI integrating fuzzy clustering and dynamic contours. *IEEE Transactions on Biomedical Engineering*, *51*(5), 800–811. https://doi.org/10.1109/TBME.2004.826654

Aosaki, T., Kimura, M., & Graybiel, A. M. (1995). Temporal and spatial characteristics of tonically active neurons of the primate's striatum. *Journal of Neurophysiology*, *73*(3), 1234–1252. https://doi.org/10.1152/jn.1995.73.3.1234

Aosaki, T., Tsubokawa, H., Ishida, A., Watanabe, K., Graybiel, A. M., & Kimura, M. (1994). Responses of tonically active neurons in the primate's striatum undergo systematic changes during behavioral sensorimotor conditioning. *Journal of Neuroscience*, *14*(6), 3969–3984. https://doi.org/10.1523/JNEUROSCI.14-06-03969.1994

APA. (2020). *Stimulus salience – APA Dictionary of Psychology*. https://dictionary.apa.org/stimulus-salience

Apicella, P. (2007). Leading tonically active neurons of the striatum from reward detection to context recognition. *Trends in Neurosciences*, *30*(6), 299–306. https://doi.org/10.1016/j.tins.2007.03.011

Apicella, P. (2017). The role of the intrinsic cholinergic system of the striatum: What have we learned from TAN recordings in behaving animals? *Neuroscience*, *360*, 81–94. https://doi.org/10.1016/j.neuroscience.2017.07.060

Aron, A. R., & Poldrack, R. A. (2006). Cortical and Subcortical Contributions to Stop Signal Response Inhibition: Role of the Subthalamic Nucleus. *Journal of Neuroscience*, *26*(9), 2424–2433. https://doi.org/10.1523/JNEUROSCI.4682-05.2006

Assous, M. (2021). Striatal cholinergic transmission. Focus on nicotinic receptors' influence in striatal circuits. *European Journal of Neuroscience*, *53*(8), 2421–2442. https://doi.org/10.1111/ejn.15135

Averbeck, B., & O'Doherty, J. P. (2021). Reinforcement-learning in fronto-striatal circuits. *Neuropsychopharmacology*, 1–16. https://doi.org/10.1038/s41386-021-01108-0

Barker, P. B., & Lin, D. D. M. (2006). In vivo proton MR spectroscopy of the human brain. *Progress in Nuclear Magnetic Resonance Spectroscopy*, *49*(2), 99–128. https://doi.org/10.1016/j.pnmrs.2006.06.002

Battistella, G., Najdenovska, E., Maeder, P., Ghazaleh, N., Daducci, A., Thiran, J.-P., Jacquemont, S., Tuleasca, C., Levivier, M., Bach Cuadra, M., & Fornari, E. (2017). Robust thalamic

nuclei segmentation method based on local diffusion magnetic resonance properties. *Brain Structure and Function*, *222*(5), 2203–2216. https://doi.org/10.1007/s00429-016-1336-4

Bechara, A., Damasio, A. R., Damasio, H., & Anderson, S. W. (1994). Insensitivity to future consequences following damage to human prefrontal cortex. *Cognition*, *50*(1), 7–15. https://doi.org/10.1016/0010-0277(94)90018-3

Behrens, T. E. J., Johansen-Berg, H., Woolrich, M. W., Smith, S. M., Wheeler-Kingshott, C. a. M., Boulby, P. A., Barker, G. J., Sillery, E. L., Sheehan, K., Ciccarelli, O., Thompson, A. J., Brady, J. M., & Matthews, P. M. (2003). Non-invasive mapping of connections between human thalamus and cortex using diffusion imaging. *Nature Neuroscience*, *6*(7), 750–757. https://doi.org/10.1038/nn1075

Behrens, T. E. J., Woolrich, M. W., Walton, M. E., & Rushworth, M. F. S. (2007). Learning the value of information in an uncertain world. *Nature Neuroscience*, *10*(9), 1214–1221. https://doi.org/10.1038/nn1954

Bell, T., Langdon, A., Lindner, M., Lloyd, W., & Christakou, A. (2019). *Orbitofrontal and Thalamic Influences on Striatal Involvement in Human Reversal Learning* (p. 246371). https://doi.org/10.1101/246371

Bell, T., Lindner, M., Langdon, A., Mullins, P. G., & Christakou, A. (2019). Regional Striatal Cholinergic Involvement in Human Behavioral Flexibility. *The Journal of Neuroscience*, *39*(29), 5740–5749. https://doi.org/10.1523/JNEUROSCI.2110-18.2019

Bell, T., Lindner, M., Mullins, P. G., & Christakou, A. (2018). Functional neurochemical imaging of the human striatal cholinergic system during reversal learning. *The European Journal of Neuroscience*, *47*(10), 1184–1193. https://doi.org/10.1111/ejn.13803

Bellebaum, C., Koch, B., Schwarz, M., & Daum, I. (2008). Focal basal ganglia lesions are associated with impairments in reward-based reversal learning. *Brain: A Journal of Neurology*, *131*(Pt 3), 829–841. https://doi.org/10.1093/brain/awn011

Bender, B., Wagner, S., & Klose, U. (2017). Optimized depiction of thalamic substructures with a combination of T1-MPRAGE and phase: MPRAGE*. *Clinical Neuroradiology*, *27*(4), 511–518. https://doi.org/10.1007/s00062-016-0513-4

Bennett, B. D., Callaway, J. C., & Wilson, C. J. (2000). Intrinsic Membrane Properties Underlying Spontaneous Tonic Firing in Neostriatal Cholinergic Interneurons. *Journal of Neuroscience*, *20*(22), 8493–8503. https://doi.org/10.1523/JNEUROSCI.20-22-08493.2000

Bernácer, J., Prensa, L., & Giménez-Amaya, J. M. (2007). Cholinergic Interneurons Are Differentially Distributed in the Human Striatum. *PLOS ONE*, *2*(11), e1174. https://doi.org/10.1371/journal.pone.0001174

Bolenz, F., Reiter, A. M. F., & Eppinger, B. (2017). Developmental Changes in Learning: Computational Mechanisms and Social Influences. *Frontiers in Psychology*, *8*, 2048. https://doi.org/10.3389/fpsyg.2017.02048

Bradfield, L. A., Bertran-Gonzalez, J., Chieng, B., & Balleine, B. W. (2013). The Thalamostriatal Pathway and Cholinergic Control of Goal-Directed Action: Interlacing New with Existing

Learning in the Striatum. *Neuron*, *79*(1), 153–166. https://doi.org/10.1016/j.neuron.2013.04.039

Brown, H. D., Baker, P. M., & Ragozzino, M. E. (2010). The Parafascicular Thalamic Nucleus Concomitantly Influences Behavioral Flexibility and Dorsomedial Striatal Acetylcholine Output in Rats. *Journal of Neuroscience*, *30*(43), 14390–14398. https://doi.org/10.1523/JNEUROSCI.2167-10.2010

Brown, V. J., & Tait, D. S. (2016). Attentional Set-Shifting Across Species. In T. W. Robbins & B. J. Sahakian (Eds.), *Translational Neuropsychopharmacology* (pp. 363–395). Springer International Publishing. https://doi.org/10.1007/7854_2015_5002

Buren, J. M. van, & Borke, R. (1972). *Variations and Connections of the Human Thalamus: 1 The Nuclei and Cerebral Connections of the Human Thalamus. 2 Variations of the Human Diencephalon*. Springer-Verlag. https://doi.org/10.1007/978-3-642-88594-5

Burke, D. A., Rotstein, H. G., & Alvarez, V. A. (2017). Striatal Local Circuitry: A New Framework for Lateral Inhibition. *Neuron*, *96*(2), 267–284. https://doi.org/10.1016/j.neuron.2017.09.019

Burnett, S., Bault, N., Coricelli, G., & Blakemore, S.-J. (2010). Adolescents' heightened risk-seeking in a probabilistic gambling task. *Cognitive Development*, *25*(2), 183–196. https://doi.org/10.1016/j.cogdev.2009.11.003

Christakou, A., Gershman, S. J., Niv, Y., Simmons, A., Brammer, M., & Rubia, K. (2013). Neural and psychological maturation of decision-making in adolescence and young adulthood. *Journal of Cognitive Neuroscience*, *25*(11), 1807–1823.

Chudasama, Y., Daniels, T. E., Gorrin, D. P., Rhodes, S. E. V., Rudebeck, P. H., & Murray, E. A. (2013). The Role of the Anterior Cingulate Cortex in Choices based on Reward Value and Reward Contingency. *Cerebral Cortex (New York, NY)*, *23*(12), 2884–2898. https://doi.org/10.1093/cercor/bhs266

Cools, R., Clark, L., Owen, A. M., & Robbins, T. W. (2002). Defining the neural mechanisms of probabilistic reversal learning using event-related functional magnetic resonance imaging. *The Journal of Neuroscience: The Official Journal of the Society for Neuroscience*, *22*(11), 4563–4567. https://doi.org/20026435

Cools, R., & D'Esposito, M. (2011). Inverted-U–Shaped Dopamine Actions on Human Working Memory and Cognitive Control. *Biological Psychiatry*, *69*(12), e113–e125. https://doi.org/10.1016/j.biopsych.2011.03.028

Crawley, D., Zhang, L., Jones, E. J. H., Ahmad, J., Oakley, B., Cáceres, A. S. J., Charman, T., Buitelaar, J. K., Murphy, D. G. M., Chatham, C., Ouden, H. den, Loth, E., & Group, the E.-A. L. (2020). Modeling flexible behavior in childhood to adulthood shows age-dependent learning mechanisms and less optimal learning in autism in each age group. *PLOS Biology*, *18*(10), e3000908. https://doi.org/10.1371/journal.pbio.3000908

Dajani, D. R., & Uddin, L. Q. (2015). Demystifying cognitive flexibility: Implications for clinical and developmental neuroscience. *Trends in Neurosciences*, *38*(9), 571–578. https://doi.org/10.1016/j.tins.2015.07.003

Daum, I., Schugens, M. M., Channon, S., Polkey, C. E., & Gray, J. A. (1991). T-Maze Discrimination and Reversal Learning After Unilateral Temporal or Frontal Lobe Lesions in Man. *Cortex*, *27*(4), 613–622. https://doi.org/10.1016/S0010-9452(13)80010-X

Daw, N. D., Gershman, S. J., Seymour, B., Dayan, P., & Dolan, R. J. (2011). Model-Based Influences on Humans' Choices and Striatal Prediction Errors. *Neuron*, *69*(6), 1204–1215. https://doi.org/10.1016/j.neuron.2011.02.027

Daw, N. D., Niv, Y., & Dayan, P. (2005). Uncertainty-based competition between prefrontal and dorsolateral striatal systems for behavioral control. *Nature Neuroscience*, *8*(12), 1704–1711. https://doi.org/10.1038/nn1560

Dayan, P., & Berridge, K. C. (2014). Model-based and model-free Pavlovian reward learning: Revaluation, revision, and revelation. *Cognitive, Affective, & Behavioral Neuroscience*, *14*(2), 473–492. https://doi.org/10.3758/s13415-014-0277-8

D'Cruz, A.-M., Mosconi, M. W., Ragozzino, M. E., Cook, E. H., & Sweeney, J. A. (2016). Alterations in the functional neural circuitry supporting flexible choice behavior in autism spectrum disorders. *Translational Psychiatry*, *6*(10), e916. https://doi.org/10.1038/tp.2016.161

D'Cruz, A.-M., Ragozzino, M. E., Mosconi, M. W., Pavuluri, M. N., & Sweeney, J. A. (2011). Human reversal learning under conditions of certain versus uncertain outcomes. *NeuroImage*, *56*(1), 315–322. https://doi.org/10.1016/j.neuroimage.2011.01.068

Deffains, M., Legallet, E., & Apicella, P. (2010). Modulation of Neuronal Activity in the Monkey Putamen Associated With Changes in the Habitual Order of Sequential Movements. *Journal of Neurophysiology*, *104*(3), 1355–1369. https://doi.org/10.1152/jn.00355.2010

del Mar Sáez de Ocariz, M., Nader, J. A., Santos, J. A., & Bautista, M. (1996). Thalamic Vascular Lesions. *Stroke*, *27*(9), 1530–1536. https://doi.org/10.1161/01.STR.27.9.1530

Demetriou, E. A., Lampit, A., Quintana, D. S., Naismith, S. L., Song, Y. J. C., Pye, J. E., Hickie, I., & Guastella, A. J. (2018). Autism spectrum disorders: A meta-analysis of executive function. *Molecular Psychiatry*, *23*(5), 1198–1204. https://doi.org/10.1038/mp.2017.75

Deoni, S. C. L., Rutt, B. K., Parrent, A. G., & Peters, T. M. (2007). Segmentation of thalamic nuclei using a modified k-means clustering algorithm and high-resolution quantitative magnetic resonance imaging at 1.5 T. *NeuroImage*, *34*(1), 117–126. https://doi.org/10.1016/j.neuroimage.2006.09.016

Deschênes, M., Bourassa, J., Doan, V. D., & Parent, A. (1996). A Single-cell Study of the Axonal Projections Arising from the Posterior Intralaminar Thalamic Nuclei in the Rat. *European Journal of Neuroscience*, *8*(2), 329–343. https://doi.org/10.1111/j.1460-9568.1996.tb01217.x

Deserno, L., Huys, Q. J. M., Boehme, R., Buchert, R., Heinze, H.-J., Grace, A. A., Dolan, R. J., Heinz, A., & Schlagenhauf, F. (2015). Ventral striatal dopamine reflects behavioral and neural signatures of model-based control during sequential decision making. *Proceedings of the National Academy of Sciences*, *112*(5), 1595–1600. https://doi.org/10.1073/pnas.1417219112

D'Esposito, M., Postle, B. R., Ballard, D., & Lease, J. (1999). Maintenance versus Manipulation of Information Held in Working Memory: An Event-Related fMRI Study. *Brain and Cognition*, *41*(1), 66–86. https://doi.org/10.1006/brcg.1999.1096

Diamond, A. (2013). Executive Functions. *Annual Review of Psychology*, *64*(1), 135–168. https://doi.org/10.1146/annurev-psych-113011-143750

DiFiglia, M., Sapp, E., Chase, K. O., Davies, S. W., Bates, G. P., Vonsattel, J. P., & Aronin, N. (1997). Aggregation of Huntingtin in Neuronal Intranuclear Inclusions and Dystrophic Neurites in Brain. *Science*, *277*(5334), 1990–1993. https://doi.org/10.1126/science.277.5334.1990

Ding, J. B., Guzman, J. N., Peterson, J. D., Goldberg, J. A., & Surmeier, D. J. (2010). Thalamic Gating of Corticostriatal Signaling by Cholinergic Interneurons. *Neuron*, *67*(2), 294–307. https://doi.org/10.1016/j.neuron.2010.06.017

Ding, S.-L., Royall, J. J., Sunkin, S. M., Ng, L., Facer, B. A. C., Lesnar, P., Guillozet-Bongaarts, A., McMurray, B., Szafer, A., Dolbeare, T. A., Stevens, A., Tirrell, L., Benner, T., Caldejon, S., Dalley, R. A., Dee, N., Lau, C., Nyhus, J., Reding, M., … Lein, E. S. (2016). Comprehensive cellular-resolution atlas of the adult human brain. *Journal of Comparative Neurology*, *524*(16), 3127–3481. https://doi.org/10.1002/cne.24080

Donkelaar, H. J. T., Broman, J., Neumann, P. E., Puelles, L., Riva, A., Tubbs, R. S., & Kachlik, D. (2017). Towards a Terminologia Neuroanatomica. *Clinical Anatomy*, *30*(2), 145–155. https://doi.org/10.1002/ca.22809

Ehrman, L. A., Mu, X., Waclaw, R. R., Yoshida, Y., Vorhees, C. V., Klein, W. H., & Campbell, K. (2013). The LIM homeobox gene Isl1 is required for the correct development of the striatonigral pathway in the mouse. *Proceedings of the National Academy of Sciences*, *110*(42), E4026–E4035. https://doi.org/10.1073/pnas.1308275110

Einhorn, H. J., & Hogarth, R. M. (1985). Ambiguity and uncertainty in probabilistic inference. *Psychological Review*, *92*(4), 433–461. https://doi.org/10.1037/0033-295X.92.4.433

English, D. F., Ibanez-Sandoval, O., Stark, E., Tecuapetla, F., Buzsáki, G., Deisseroth, K., Tepper, J. M., & Koos, T. (2012). GABAergic circuits mediate the reinforcement-related signals of striatal cholinergic interneurons. *Nature Neuroscience*, *15*(1), 123–130. https://doi.org/10.1038/nn.2984

Fellows, L. K., & Farah, M. J. (2003). Ventromedial frontal cortex mediates affective shifting in humans: Evidence from a reversal learning paradigm. *Brain*, *126*(8), 1830–1837. https://doi.org/10.1093/brain/awg180

Fellows, L. K., & Farah, M. J. (2005). Different Underlying Impairments in Decision-making Following Ventromedial and Dorsolateral Frontal Lobe Damage in Humans. *Cerebral Cortex*, *15*(1), 58–63. https://doi.org/10.1093/cercor/bhh108

Feremutsch, K., & Simma, K. (1971). Anatomy of the normal human thalamus. In A. Dewulf (Ed.), *Anatomy of the Normal Human Thalamus*. Elsevier Science Ltd.

Frisch, D., & Baron, J. (1988). Ambiguity and rationality. *Journal of Behavioral Decision Making*, *1*(3), 149–157. https://doi.org/10.1002/bdm.3960010303

Geier, K. T., Buchsbaum, B. R., Parimoo, S., & Olsen, R. K. (2020). The role of anterior and medial dorsal thalamus in associative memory encoding and retrieval. *Neuropsychologia*, *148*, 107623. https://doi.org/10.1016/j.neuropsychologia.2020.107623

Ghahremani, D. G., Monterosso, J., Jentsch, J. D., Bilder, R. M., & Poldrack, R. A. (2010). Neural components underlying behavioral flexibility in human reversal learning. *Cerebral Cortex (New York, N.Y.: 1991)*, *20*(8), 1843–1852. https://doi.org/10.1093/cercor/bhp247

Girasole, A. E., & Nelson, A. B. (2015). Probing striatal microcircuitry to understand the functional role of cholinergic interneurons. *Movement Disorders*, *30*(10), 1306–1318. https://doi.org/10.1002/mds.26340

Gläscher, J., Hampton, A. N., & O'Doherty, J. P. (2009). Determining a role for ventromedial prefrontal cortex in encoding action-based value signals during reward-related decision making. *Cerebral Cortex (New York, N.Y.: 1991)*, *19*(2), 483–495. https://doi.org/10.1093/cercor/bhn098

Gogtay, N., Giedd, J. N., Lusk, L., Hayashi, K. M., Greenstein, D., Vaituzis, A. C., Nugent, T. F., Herman, D. H., Clasen, L. S., Toga, A. W., Rapoport, J. L., & Thompson, P. M. (2004). Dynamic mapping of human cortical development during childhood through early adulthood. *Proceedings of the National Academy of Sciences*, *101*(21), 8174–8179. https://doi.org/10.1073/pnas.0402680101

Gopnik, A., Griffiths, T. L., & Lucas, C. G. (2015). When Younger Learners Can Be Better (or at Least More Open-Minded) Than Older Ones. *Current Directions in Psychological Science*, *24*(2), 87–92. https://doi.org/10.1177/0963721414556653

Gopnik, A., O'Grady, S., Lucas, C. G., Griffiths, T. L., Wente, A., Bridgers, S., Aboody, R., Fung, H., & Dahl, R. E. (2017). Changes in cognitive flexibility and hypothesis search across human life history from childhood to adolescence to adulthood. *Proceedings of the National Academy of Sciences*, *114*(30), 7892–7899. https://doi.org/10.1073/pnas.1700811114

Graveland, G. A., & Difiglia, M. (1985). The frequency and distribution of medium-sized neurons with indented nuclei in the primate and rodent neostriatum. *Brain Research*, *327*(1), 307–311. https://doi.org/10.1016/0006-8993(85)91524-0

Habiby Alaoui, S., Adam-Darqué, A., Ptak, R., & Schnider, A. (2021). Distinct outcome processing in deterministic and probabilistic reversal learning. *Cortex*, *141*, 224–239. https://doi.org/10.1016/j.cortex.2021.04.008

Hale, J. R., Mayhew, S. D., Mullinger, K. J., Wilson, R. S., Arvanitis, T. N., Francis, S. T., & Bagshaw, A. P. (2015). Comparison of functional thalamic segmentation from seed-based analysis and ICA. *NeuroImage*, *114*, 448–465. https://doi.org/10.1016/j.neuroimage.2015.04.027

Hampshire, A., Chaudhry, A. M., Owen, A. M., & Roberts, A. C. (2012). Dissociable roles for lateral orbitofrontal cortex and lateral prefrontal cortex during preference driven reversal learning. *NeuroImage*, *59*(4), 4102–4112. https://doi.org/10.1016/j.neuroimage.2011.10.072

Hampton, A. N., Adolphs, R., Tyszka, M. J., & O'Doherty, J. P. (2007). Contributions of the amygdala to reward expectancy and choice signals in human prefrontal cortex. *Neuron*, *55*(4), 545–555. https://doi.org/10.1016/j.neuron.2007.07.022

Hasbi, A., Sivasubramanian, M., Milenkovic, M., Komarek, K., Madras, B. K., & George, S. R. (2020). Dopamine D1-D2 receptor heteromer expression in key brain regions of rat and higher species: Upregulation in rat striatum after cocaine administration. *Neurobiology of Disease*, *143*, 105017. https://doi.org/10.1016/j.nbd.2020.105017

Hassler, R. (1977). Architectonic organization of the thalamic nuclei. In G. Schaltenbrand & W. Wahren (Eds.), *Atlas for stereotaxy of the human brain*. Thieme.

Hassler, R., Mundinger, F., & Riechert, T. (1979). *Stereotaxis in Parkinson Syndrome: Clinical-Anatomical Contributions to Its Pathophysiology*. Springer-Verlag. https://doi.org/10.1007/978-3-642-66521-9

Hauser, T. U., Iannaccone, R., Walitza, S., Brandeis, D., & Brem, S. (2015). Cognitive flexibility in adolescence: Neural and behavioral mechanisms of reward prediction error processing in adaptive decision making during development. *NeuroImage*, *104*, 347–354. https://doi.org/10.1016/j.neuroimage.2014.09.018

Heather Hsu, C.-C., Rolls, E. T., Huang, C.-C., Chong, S. T., Zac Lo, C.-Y., Feng, J., & Lin, C.-P. (2020). Connections of the Human Orbitofrontal Cortex and Inferior Frontal Gyrus. *Cerebral Cortex*, *30*(11), 5830–5843. https://doi.org/10.1093/cercor/bhaa160

Heiman, M., Schaefer, A., Gong, S., Peterson, J., Day, M., Ramsey, K. E., Suárez-Fariñas, M., Schwarz, C., Stephan, D. A., Surmeier, D. J., Greengard, P., & Heintz, N. (2008). Development of a BACarray translational profiling approach for the molecular characterization of CNS cell types. *Cell*, *135*(4), 738–748. https://doi.org/10.1016/j.cell.2008.10.028

Hervig, M. E., Fiddian, L., Piilgaard, L., Božič, T., Blanco-Pozo, M., Knudsen, C., Olesen, S. F., Alsiö, J., & Robbins, T. W. (2020). Dissociable and Paradoxical Roles of Rat Medial and Lateral Orbitofrontal Cortex in Visual Serial Reversal Learning. *Cerebral Cortex*, *30*(3), 1016–1029. https://doi.org/10.1093/cercor/bhz144

Higley, M. J., Gittis, A. H., Oldenburg, I. A., Balthasar, N., Seal, R. P., Edwards, R. H., Lowell, B. B., Kreitzer, A. C., & Sabatini, B. L. (2011). Cholinergic Interneurons Mediate Fast VGluT3-Dependent Glutamatergic Transmission in the Striatum. *PLOS ONE*, *6*(4), e19155. https://doi.org/10.1371/journal.pone.0019155

Hill, S. K., Reilly, J. L., Ragozzino, M. E., Rubin, L. H., Bishop, J. R., Gur, R. C., Gershon, E. S., Tamminga, C. A., Pearlson, G. D., Keshavan, M. S., Keefe, R. S. E., & Sweeney, J. A. (2015). Regressing to Prior Response Preference After Set Switching Implicates Striatal Dysfunction Across Psychotic Disorders: Findings From the B-SNIP Study. *Schizophrenia Bulletin*, *41*(4), 940–950. https://doi.org/10.1093/schbul/sbu130

Hopper, S., Udawela, M., Scarr, E., & Dean, B. (2016). Allosteric modulation of cholinergic system: Potential approach to treating cognitive deficits of schizophrenia. *World Journal of Pharmacology*, *5*(1), 32–43. https://doi.org/10.5497/wjp.v5.i1.32

Hornak, J., O'Doherty, J., Bramham, J., Rolls, E. T., Morris, R. G., Bullock, P. R., & Polkey, C. E. (2004). Reward-related reversal learning after surgical excisions in orbito-frontal or

dorsolateral prefrontal cortex in humans. *Journal of Cognitive Neuroscience*, *16*(3), 463–478. https://doi.org/10.1162/089892904322926791

Howard, J. D., & Kahnt, T. (2018). Identity prediction errors in the human midbrain update reward-identity expectations in the orbitofrontal cortex. *Nature Communications*, *9*(1), 1611. https://doi.org/10.1038/s41467-018-04055-5

Huang, A. S., Rogers, B. P., & Woodward, N. D. (2019). Disrupted modulation of thalamus activation and thalamocortical connectivity during dual task performance in schizophrenia. *Schizophrenia Research*, *210*, 270–277. https://doi.org/10.1016/j.schres.2018.12.022

Iglesias, J. E., Insausti, R., Lerma-Usabiaga, G., Bocchetta, M., Van Leemput, K., Greve, D. N., van der Kouwe, A., Fischl, B., Caballero-Gaudes, C., & Paz-Alonso, P. M. (2018). A probabilistic atlas of the human thalamic nuclei combining ex vivo MRI and histology. *NeuroImage*, *183*, 314–326. https://doi.org/10.1016/j.neuroimage.2018.08.012

Ilinsky, I., Horn, A., Paul-Gilloteaux, P., Gressens, P., Verney, C., & Kultas-Ilinsky, K. (2018). Human Motor Thalamus Reconstructed in 3D from Continuous Sagittal Sections with Identified Subcortical Afferent Territories. *ENeuro*, *5*(3). https://doi.org/10.1523/ENEURO.0060-18.2018

Itami, S., & Uno, H. (2002). Orbitofrontal cortex dysfunction in attention-deficit hyperactivity disorder revealed by reversal and extinction tasks. *NeuroReport*, *13*(18), 2453–2457.

Izquierdo, A., Brigman, J. L., Radke, A. K., Rudebeck, P. H., & Holmes, A. (2017). The neural basis of reversal learning: An updated perspective. *Neuroscience*, *345*, 12–26. https://doi.org/10.1016/j.neuroscience.2016.03.021

Javadi, A. H., Schmidt, D. H. K., & Smolka, M. N. (2014). Adolescents adapt more slowly than adults to varying reward contingencies. *Journal of Cognitive Neuroscience*, *26*(12), 2670–2681. https://doi.org/10.1162/jocn_a_00677

Jepma, M., Schaaf, J. V., Visser, I., & Huizenga, H. M. (2020). Uncertainty-driven regulation of learning and exploration in adolescents: A computational account. *PLOS Computational Biology*, *16*(9), e1008276. https://doi.org/10.1371/journal.pcbi.1008276

Johnson, C., & Wilbrecht, L. (2011). Juvenile mice show greater flexibility in multiple choice reversal learning than adults. *Developmental Cognitive Neuroscience*, *1*(4), 540–551. https://doi.org/10.1016/j.dcn.2011.05.008

Juchem, C., & Rothman, D. L. (2014). Chapter 1.1—Basis of Magnetic Resonance. In C. Stagg & D. Rothman (Eds.), *Magnetic Resonance Spectroscopy* (pp. 3–14). Academic Press. https://doi.org/10.1016/B978-0-12-401688-0.00001-X

Katz-Brull, R., Koudinov, A. R., & Degani, H. (2005). Direct detection of brain acetylcholine synthesis by magnetic resonance spectroscopy. *Brain Research*, *1048*(1), 202–210. https://doi.org/10.1016/j.brainres.2005.04.080

Kawaguchi, Y., Wilson, C. J., Augood, S. J., & Emson, P. C. (1995). Striatal interneurones: Chemical, physiological and morphological characterization. *Trends in Neurosciences*, *18*(12), 527–535. https://doi.org/10.1016/0166-2236(95)98374-8

Kehagia, A. A., Murray, G. K., & Robbins, T. W. (2010). Learning and cognitive flexibility: Frontostriatal function and monoaminergic modulation. *Current Opinion in Neurobiology*, *20*(2), 199–204. https://doi.org/10.1016/j.conb.2010.01.007

Kim, D.-J., Park, B., & Park, H.-J. (2013). Functional connectivity-based identification of subdivisions of the basal ganglia and thalamus using multilevel independent component analysis of resting state fMRI. *Human Brain Mapping*, *34*(6), 1371–1385. https://doi.org/10.1002/hbm.21517

Kim, J., & Ragozzino, M. E. (2005). The involvement of the orbitofrontal cortex in learning under changing task contingencies. *Neurobiology of Learning and Memory*, *83*(2), 125–133. https://doi.org/10.1016/j.nlm.2004.10.003

Kimura, M., Rajkowski, J., & Evarts, E. (1984). Tonically discharging putamen neurons exhibit set-dependent responses. *Proceedings of the National Academy of Sciences*, *81*(15), 4998–5001. https://doi.org/10.1073/pnas.81.15.4998

Kljakic, O., Janickova, H., Prado, V. F., & Prado, M. A. M. (2017). Cholinergic/glutamatergic co-transmission in striatal cholinergic interneurons: New mechanisms regulating striatal computation. *Journal of Neurochemistry*, *142*(S2), 90–102. https://doi.org/10.1111/jnc.14003

Krauth, A., Blanc, R., Poveda, A., Jeanmonod, D., Morel, A., & Székely, G. (2010). A mean three-dimensional atlas of the human thalamus: Generation from multiple histological data. *NeuroImage*, *49*(3), 2053–2062. https://doi.org/10.1016/j.neuroimage.2009.10.042

Kreitzer, A. C. (2009). Physiology and Pharmacology of Striatal Neurons. *Annual Review of Neuroscience*, *32*(1), 127–147. https://doi.org/10.1146/annurev.neuro.051508.135422

Kringelbach, M. L., & Rolls, E. T. (2003). Neural correlates of rapid reversal learning in a simple model of human social interaction. *NeuroImage*, *20*(2), 1371–1383. https://doi.org/10.1016/S1053-8119(03)00393-8

Lapper, S. R., & Bolam, J. P. (1992). Input from the frontal cortex and the parafascicular nucleus to cholinergic interneurons in the dorsal striatum of the rat. *Neuroscience*, *51*(3), 533–545. https://doi.org/10.1016/0306-4522(92)90293-B

Lawrence, A. D., Sahakian, B. J., Rogers, R. D., Hodges, J. R., & Robbins, T. W. (1999). Discrimination, reversal, and shift learning in Huntington's disease: Mechanisms of impaired response selection. *Neuropsychologia*, *37*(12), 1359–1374. https://doi.org/10.1016/S0028-3932(99)00035-4

Lei, H., Xin, L., Gruetter, R., & Mlynárik, V. (2014). Chapter 1.2—Localized Single-Voxel Magnetic Resonance Spectroscopy, Water Suppression, and Novel Approaches for Ultrashort Echo-Time Measurements. In C. Stagg & D. Rothman (Eds.), *Magnetic Resonance Spectroscopy* (pp. 15–30). Academic Press. https://doi.org/10.1016/B978-0-12-401688-0.00002-1

Levy, B. J., & Wagner, A. D. (2011). Cognitive control and right ventrolateral prefrontal cortex: Reflexive reorienting, motor inhibition, and action updating. *Annals of the New York Academy of Sciences*, *1224*(1), 40–62. https://doi.org/10.1111/j.1749-6632.2011.05958.x

Li, J., Schiller, D., Schoenbaum, G., Phelps, E. A., & Daw, N. D. (2011). Differential roles of human striatum and amygdala in associative learning. *Nature Neuroscience*, *14*(10), 1250–1252. https://doi.org/10.1038/nn.2904

Li, Z., & Vance, D. E. (2008). Thematic Review Series: Glycerolipids. Phosphatidylcholine and choline homeostasis. *Journal of Lipid Research*, *49*(6), 1187–1194. https://doi.org/10.1194/jlr.R700019-JLR200

Libretexts. (2014a, June 19). *14: NMR Spectroscopy*. Libretexts. https://chem.libretexts.org/Bookshelves/Organic_Chemistry/Map%3A_Organic_Chemistry_(Bruice)/14%3A_NMR_Spectroscopy

Libretexts. (2014b, June 19). *14.10: The Splitting of the Signals is Described by the N + 1 Rule*. Chemistry LibreTexts. https://chem.libretexts.org/Bookshelves/Organic_Chemistry/Map%3A_Organic_Chemistry_(Bruice)/14%3A_NMR_Spectroscopy/14.10%3A_The_Splitting_of_the_Signals_is_Described_by_the_N__1_Rule

Liebermann, D., Ploner, C. J., Kraft, A., Kopp, U. A., & Ostendorf, F. (2013). A dysexecutive syndrome of the medial thalamus. *Cortex*, *49*(1), 40–49. https://doi.org/10.1016/j.cortex.2011.11.005

Lin, J. C., & Gant, N. (2014). Chapter 2.3—The Biochemistry of Choline. In C. Stagg & D. Rothman (Eds.), *Magnetic Resonance Spectroscopy* (pp. 104–110). Academic Press. https://doi.org/10.1016/B978-0-12-401688-0.00008-2

Lindner, M., Bell, T., Iqbal, S., Mullins, P. G., & Christakou, A. (2017). In vivo functional neurochemistry of human cortical cholinergic function during visuospatial attention. *PLOS ONE*, *12*(2), e0171338. https://doi.org/10.1371/journal.pone.0171338

Liu, Z., Braunlich, K., Wehe, H. S., & Seger, C. A. (2015). Neural networks supporting switching, hypothesis testing, and rule application. *Neuropsychologia*, *77*, 19–34. https://doi.org/10.1016/j.neuropsychologia.2015.07.019

Löffelholz, K. (1998). Brain choline has a typical precursor profile. *Journal of Physiology Paris*, *92*(3–4), 235–239. https://doi.org/10.1016/S0928-4257(98)80025-9

Lopez, B. R., Lincoln, A. J., Ozonoff, S., & Lai, Z. (2005). Examining the Relationship between Executive Functions and Restricted, Repetitive Symptoms of Autistic Disorder. *Journal of Autism and Developmental Disorders*, *35*(4), 445–460. https://doi.org/10.1007/s10803-005-5035-x

Lucas, C. G., Bridgers, S., Griffiths, T. L., & Gopnik, A. (2014). When children are better (or at least more open-minded) learners than adults: Developmental differences in learning the forms of causal relationships. *Cognition*, *131*(2), 284–299. https://doi.org/10.1016/j.cognition.2013.12.010

MacDonald, M. E., Ambrose, C. M., Duyao, M. P., Myers, R. H., Lin, C., Srinidhi, L., Barnes, G., Taylor, S. A., James, M., Groot, N., MacFarlane, H., Jenkins, B., Anderson, M. A., Wexler, N. S., Gusella, J. F., Bates, G. P., Baxendale, S., Hummerich, H., Kirby, S., … Harper, P. S. (1993). A novel gene containing a trinucleotide repeat that is expanded and unstable on Huntington's disease chromosomes. *Cell*, *72*(6), 971–983. https://doi.org/10.1016/0092-8674(93)90585-E

Magnotta, V. A., Gold, S., Andreasen, N. C., Ehrhardt, J. C., & Yuh, W. T. C. (2000). Visualization of Subthalamic Nuclei with Cortex Attenuated Inversion Recovery MR Imaging. *NeuroImage*, *11*(4), 341–346. https://doi.org/10.1006/nimg.2000.0552

Mai, J. K., & Majtanik, M. (2017). *Human brain in standard MNI space: Structure and function: a comprehensive pocket atlas*. Academic Press, an imprint of Elsevier.

Mai, J. K., & Majtanik, M. (2019). Toward a Common Terminology for the Thalamus. *Frontiers in Neuroanatomy*, *12*, 114. https://doi.org/10.3389/fnana.2018.00114

McCool, M. F., Patel, S., Talati, R., & Ragozzino, M. E. (2008). Differential involvement of M1-type and M4-type muscarinic cholinergic receptors in the dorsomedial striatum in task switching. *Neurobiology of Learning and Memory*, *89*(2), 114–124. https://doi.org/10.1016/j.nlm.2007.06.005

Meder, D., Madsen, K. H., Hulme, O., & Siebner, H. R. (2016). Chasing probabilities—Signaling negative and positive prediction errors across domains. *NeuroImage*, *134*, 180–191. https://doi.org/10.1016/j.neuroimage.2016.04.019

Menon, V., & Uddin, L. Q. (2010). Saliency, switching, attention and control: A network model of insula function. *Brain Structure and Function*, *214*(5), 655–667. https://doi.org/10.1007/s00429-010-0262-0

Mesulam, M.-M. (2004). The cholinergic innervation of the human cerebral cortex. In *Progress in Brain Research* (Vol. 145, pp. 67–78). Elsevier. https://doi.org/10.1016/S0079-6123(03)45004-8

Miller, B. L., Changl, L., Booth, R., Ernst, T., Cornford, M., Nikas, D., McBride, D., & Jenden, D. J. (1996). In vivo 1H MRS choline: Correlation with in vitro chemistry/histology. *Life Sciences*, *58*(22), 1929–1935. https://doi.org/10.1016/0024-3205(96)00182-8

Miller, H. L., Ragozzino, M. E., Cook, E. H., Sweeney, J. A., & Mosconi, M. W. (2015). Cognitive Set Shifting Deficits and Their Relationship to Repetitive Behaviors in Autism Spectrum Disorder. *Journal of Autism and Developmental Disorders*, *45*(3), 805–815. https://doi.org/10.1007/s10803-014-2244-1

Mitchell, D. G. V., Rhodes, R. A., Pine, D. S., & Blair, R. J. R. (2008). The contribution of ventrolateral and dorsolateral prefrontal cortex to response reversal. *Behavioural Brain Research*, *187*(1), 80–87. https://doi.org/10.1016/j.bbr.2007.08.034

Mohr, H., Wolfensteller, U., & Ruge, H. (2018). Large-scale coupling dynamics of instructed reversal learning. *NeuroImage*, *167*, 237–246. https://doi.org/10.1016/j.neuroimage.2017.11.049

Morel, A. (2007). *Stereotactic Atlas of the Human Thalamus and Basal Ganglia*. CRC Press.

Morel, A., Magnin, M., & Jeanmonod, D. (1997). Multiarchitectonic and stereotactic atlas of the human thalamus. *Journal of Comparative Neurology*, *387*(4), 588–630. https://doi.org/10.1002/(SICI)1096-9861(19971103)387:4<588::AID-CNE8>3.0.CO;2-Z

Morris, L. S., Kundu, P., Dowell, N., Mechelmans, D. J., Favre, P., Irvine, M. A., Robbins, T. W., Daw, N., Bullmore, E. T., Harrison, N. A., & Voon, V. (2016). Fronto-striatal organization: Defining functional and microstructural substrates of behavioural flexibility. *Cortex; a*

Journal Devoted to the Study of the Nervous System and Behavior, *74*, 118–133. https://doi.org/10.1016/j.cortex.2015.11.004

Nickchen, K., Boehme, R., Del Mar Amador, M., Hälbig, T. D., Dehnicke, K., Panneck, P., Behr, J., Prass, K., Heinz, A., Deserno, L., Schlagenhauf, F., & Priller, J. (2017). Reversal learning reveals cognitive deficits and altered prediction error encoding in the ventral striatum in Huntington's disease. *Brain Imaging and Behavior*, *11*(6), 1862–1872. https://doi.org/10.1007/s11682-016-9660-0

Noonan, M. P., Chau, B. K. H., Rushworth, M. F. S., & Fellows, L. K. (2017). Contrasting effects of medial and lateral orbitofrontal cortex lesions on credit assignment and decision-making in humans. *Journal of Neuroscience*, *37*(29), 7023–7035. https://doi.org/10.1523/JNEUROSCI.0692-17.2017

O'Doherty, J., Kringelbach, M. L., Rolls, E. T., Hornak, J., & Andrews, C. (2001). Abstract reward and punishment representations in the human orbitofrontal cortex. *Nature Neuroscience*, *4*(1), 95–102. https://doi.org/10.1038/82959

Palencia, C. A., & Ragozzino, M. E. (2004). The influence of NMDA receptors in the dorsomedial striatum on response reversal learning. *Neurobiology of Learning and Memory*, *82*(2), 81–89. https://doi.org/10.1016/j.nlm.2004.04.004

Palminteri, S., Kilford, E. J., Coricelli, G., & Blakemore, S.-J. (2016). The Computational Development of Reinforcement Learning during Adolescence. *PLOS Computational Biology*, *12*(6), e1004953. https://doi.org/10.1371/journal.pcbi.1004953

Panayi, M. C., & Killcross, S. (2018). Functional heterogeneity within the rodent lateral orbitofrontal cortex dissociates outcome devaluation and reversal learning deficits. *ELife*, *7*, e37357. https://doi.org/10.7554/eLife.37357

Penadés, R., Catalán, R., Andrés, S., Salamero, M., & Gastó, C. (2005). Executive function and nonverbal memory in obsessive-compulsive disorder. *Psychiatry Research*, *133*(1), 81–90. https://doi.org/10.1016/j.psychres.2004.09.005

Percheron, G. (2004). Thalamus. In G. Paxinos & J. K. Mai (Eds.), *The Human Nervous System (Second Edition)* (pp. 592–675). Academic Press. https://doi.org/10.1016/B978-012547626-3/50021-1

Perry, E., Walker, M., Grace, J., & Perry, R. (1999). Acetylcholine in mind: A neurotransmitter correlate of consciousness? *Trends in Neurosciences*, *22*(6), 273–280. https://doi.org/10.1016/S0166-2236(98)01361-7

Peterson, D. A., Elliott, C., Song, D. D., Makeig, S., Sejnowski, T. J., & Poizner, H. (2009). Probabilistic reversal learning is impaired in Parkinson's disease. *Neuroscience*, *163*(4), 1092–1101. https://doi.org/10.1016/j.neuroscience.2009.07.033

Picciotto, M. R., Higley, M. J., & Mineur, Y. S. (2012). Acetylcholine as a Neuromodulator: Cholinergic Signaling Shapes Nervous System Function and Behavior. *Neuron*, *76*(1), 116–129. https://doi.org/10.1016/j.neuron.2012.08.036

Plate, R. C., Fulvio, J. M., Shutts, K., Green, C. S., & Pollak, S. D. (2018). Probability Learning: Changes in Behavior Across Time and Development. *Child Development*, *89*(1), 205–218. https://doi.org/10.1111/cdev.12718

Prado, V. F., Janickova, H., Al-Onaizi, M. A., & Prado, M. A. M. M. (2017). Cholinergic circuits in cognitive flexibility. *Neuroscience*, *345*, 130–141. https://doi.org/10.1016/j.neuroscience.2016.09.013

Ragozzino, M. E., & Choi, D. (2004). Dynamic Changes in Acetylcholine Output in the Medial Striatum During Place Reversal Learning. *Learning & Memory*, *11*(1), 70–77. https://doi.org/10.1101/lm.65404

Ragozzino, M. E., Jih, J., & Tzavos, A. (2002). Involvement of the dorsomedial striatum in behavioral flexibility: Role of muscarinic cholinergic receptors. *Brain Research*, *953*(1–2), 205–214. https://doi.org/10.1016/S0006-8993(02)03287-0

Ragozzino, M. E., Mohler, E. G., Prior, M., Palencia, C. A., & Rozman, S. (2009). Acetylcholine activity in selective striatal regions supports behavioral flexibility. *Neurobiology of Learning and Memory*, *91*(1), 13–22. https://doi.org/10.1016/j.nlm.2008.09.008

Remijnse, P. L., Nielen, M. M. A., Uylings, H. B. M., & Veltman, D. J. (2005). Neural correlates of a reversal learning task with an affectively neutral baseline: An event-related fMRI study. *NeuroImage*, *26*(2), 609–618. https://doi.org/10.1016/j.neuroimage.2005.02.009

Remijnse, P. L., Nielen, M. M. A., van Balkom, A. J. L. M., Hendriks, G.-J., Hoogendijk, W. J., Uylings, H. B. M., & Veltman, D. J. (2009). Differential frontal-striatal and paralimbic activity during reversal learning in major depressive disorder and obsessive-compulsive disorder. *Psychological Medicine*, *39*(9), 1503–1518. https://doi.org/10.1017/S0033291708005072

Robinson, O. J., Frank, M. J., Sahakian, B. J., & Cools, R. (2010). Dissociable responses to punishment in distinct striatal regions during reversal learning. *NeuroImage*, *51*(4), 1459–1467. https://doi.org/10.1016/j.neuroimage.2010.03.036

Rolls, E. T., Hornak, J., Wade, D., & McGrath, J. (1994). Emotion-related learning in patients with social and emotional changes associated with frontal lobe damage. *Journal of Neurology, Neurosurgery & Psychiatry*, *57*(12), 1518–1524. https://doi.org/10.1136/jnnp.57.12.1518

Ruge, H., & Wolfensteller, U. (2016). Distinct contributions of lateral orbito-frontal cortex, striatum, and fronto-parietal network regions for rule encoding and control of memory-based implementation during instructed reversal learning. *NeuroImage*, *125*, 1–12. https://doi.org/10.1016/j.neuroimage.2015.10.005

Rygula, R., Walker, S. C., Clarke, H. F., Robbins, T. W., & Roberts, A. C. (2010). Differential Contributions of the Primate Ventrolateral Prefrontal and Orbitofrontal Cortex to Serial Reversal Learning. *Journal of Neuroscience*, *30*(43), 14552–14559. https://doi.org/10.1523/JNEUROSCI.2631-10.2010

Sadikot, A. F., Parent, A., & François, C. (1992). Efferent connections of the centromedian and parafascicular thalamic nuclei in the squirrel monkey: A PHA-L study of subcortical projections. *Journal of Comparative Neurology*, *315*(2), 137–159. https://doi.org/10.1002/cne.903150203

Sadikot, A. F., Parent, A., Smith, Y., & Bolam, J. P. (1992). Efferent connections of the centromedian and parafascicular thalamic nuclei in the squirrel monkey: A light and electron microscopic study of the thalamostriatal projection in relation to striatal

heterogeneity. *Journal of Comparative Neurology*, *320*(2), 228–242. https://doi.org/10.1002/cne.903200207

Schepers, I. M., Beck, A. K., Bräuer, S., Schwabe, K., Abdallat, M., Sandmann, P., Dengler, R., Rieger, J. W., & Krauss, J. K. (2017). Human centromedian-parafascicular complex signals sensory cues for goal-oriented behavior selection. *NeuroImage*, *152*, 390–399. https://doi.org/10.1016/j.neuroimage.2017.03.019

Schlagenhauf, F., Huys, Q. J. M., Deserno, L., Rapp, M. A., Beck, A., Heinze, H.-J., Dolan, R., & Heinz, A. (2014). Striatal dysfunction during reversal learning in unmedicated schizophrenia patients. *NeuroImage*, *89*, 171–180. https://doi.org/10.1016/j.neuroimage.2013.11.034

Schoenbaum, G., Saddoris, M. P., & Stalnaker, T. A. (2007). Reconciling the Roles of Orbitofrontal Cortex in Reversal Learning and the Encoding of Outcome Expectancies. *Annals of the New York Academy of Sciences*, *1121*(1), 320–335. https://doi.org/10.1196/annals.1401.001

Schultz, W. (1998). Predictive Reward Signal of Dopamine Neurons. *Journal of Neurophysiology*, *80*(1), 1–27. https://doi.org/10.1152/jn.1998.80.1.1

Schultz, W., Dayan, P., & Montague, P. R. (1997). A Neural Substrate of Prediction and Reward. *Science*, *275*(5306), 1593–1599. https://doi.org/10.1126/science.275.5306.1593

Seeley, W. W. (2019). The Salience Network: A Neural System for Perceiving and Responding to Homeostatic Demands. *Journal of Neuroscience*, *39*(50), 9878–9882. https://doi.org/10.1523/JNEUROSCI.1138-17.2019

Smith, Y., Bevan, M. D., Shink, E., & Bolam, J. P. (1998). Microcircuitry of the direct and indirect pathways of the basal ganglia. *Neuroscience*, *86*(2), 353–387. https://doi.org/10.1016/s0306-4522(98)00004-9

Somerville, L. H., Sasse, S. F., Garrad, M. C., Drysdale, A. T., Abi Akar, N., Insel, C., & Wilson, R. C. (2017). Charting the expansion of strategic exploratory behavior during adolescence. *Journal of Experimental Psychology: General*, *146*(2), 155–164. https://doi.org/10.1037/xge0000250

Sotiropoulos, S. N., Jbabdi, S., Xu, J., Andersson, J. L., Moeller, S., Auerbach, E. J., Glasser, M. F., Hernandez, M., Sapiro, G., Jenkinson, M., Feinberg, D. A., Yacoub, E., Lenglet, C., Van Essen, D. C., Ugurbil, K., & Behrens, T. E. J. (2013). Advances in diffusion MRI acquisition and processing in the Human Connectome Project. *NeuroImage*, *80*, 125–143. https://doi.org/10.1016/j.neuroimage.2013.05.057

South, M., Newton, T., & Chamberlain, P. D. (2012). Delayed Reversal Learning and Association With Repetitive Behavior in Autism Spectrum Disorders. *Autism Research*, *5*(6), 398–406. https://doi.org/10.1002/aur.1255

Stalnaker, T. A., Berg, B., Aujla, N., & Schoenbaum, G. (2016). Cholinergic Interneurons Use Orbitofrontal Input to Track Beliefs about Current State. *The Journal of Neuroscience : The Official Journal of the Society for Neuroscience*, *36*(23), 6242–6257. https://doi.org/10.1523/JNEUROSCI.0157-16.2016

Su, J. H., Thomas, F. T., Kasoff, W. S., Tourdias, T., Choi, E. Y., Rutt, B. K., & Saranathan, M. (2019). Thalamus Optimized Multi Atlas Segmentation (THOMAS): Fast, fully automated segmentation of thalamic nuclei from structural MRI. *NeuroImage*, *194*, 272–282. https://doi.org/10.1016/j.neuroimage.2019.03.021

Taylor, P., & Brown, J. H. (1999). Synthesis, Storage and Release of Acetylcholine. *Basic Neurochemistry: Molecular, Cellular and Medical Aspects. 6th Edition*. https://www.ncbi.nlm.nih.gov/books/NBK28051/

Thompson-Schill, S. L., Ramscar, M., & Chrysikou, E. G. (2009). Cognition Without Control: When a Little Frontal Lobe Goes a Long Way. *Current Directions in Psychological Science*, *18*(5), 259–263. https://doi.org/10.1111/j.1467-8721.2009.01648.x

Threlfell, S., Lalic, T., Platt, N. J., Jennings, K. A., Deisseroth, K., & Cragg, S. J. (2012). Striatal Dopamine Release Is Triggered by Synchronized Activity in Cholinergic Interneurons. *Neuron*, *75*(1), 58–64. https://doi.org/10.1016/j.neuron.2012.04.038

Tiego, J., Testa, R., Bellgrove, M. A., Pantelis, C., & Whittle, S. (2018). A Hierarchical Model of Inhibitory Control. *Frontiers in Psychology*, *9*, 1339. https://doi.org/10.3389/fpsyg.2018.01339

Tourdias, T., Saranathan, M., Levesque, I. R., Su, J., & Rutt, B. K. (2014). Visualization of intra-thalamic nuclei with optimized white-matter-nulled MPRAGE at 7T. *NeuroImage*, *84*, 534–545. https://doi.org/10.1016/j.neuroimage.2013.08.069

Tsuchida, A., Doll, B. B., & Fellows, L. K. (2010). Beyond reversal: A critical role for human orbitofrontal cortex in flexible learning from probabilistic feedback. *The Journal of Neuroscience: The Official Journal of the Society for Neuroscience*, *30*(50), 16868–16875. https://doi.org/10.1523/JNEUROSCI.1958-10.2010

Tzavos, A., Jih, J., & Ragozzino, M. E. (2004). Differential effects of M1 muscarinic receptor blockade and nicotinic receptor blockade in the dorsomedial striatum on response reversal learning. *Behavioural Brain Research*, *154*(1), 245–253. https://doi.org/10.1016/j.bbr.2004.02.011

Uddin, L. Q. (2021). Cognitive and behavioural flexibility: Neural mechanisms and clinical considerations. *Nature Reviews Neuroscience*, *22*(3), 167–179. https://doi.org/10.1038/s41583-021-00428-w

van den Bos, W., Cohen, M. X., Kahnt, T., & Crone, E. A. (2012). Striatum–Medial Prefrontal Cortex Connectivity Predicts Developmental Changes in Reinforcement Learning. *Cerebral Cortex*, *22*(6), 1247–1255. https://doi.org/10.1093/cercor/bhr198

van den Bos, W., & Hertwig, R. (2017). Adolescents display distinctive tolerance to ambiguity and to uncertainty during risky decision making. *Scientific Reports*, *7*(1), 40962. https://doi.org/10.1038/srep40962

Van Essen, D. C., Smith, S. M., Barch, D. M., Behrens, T. E. J., Yacoub, E., & Ugurbil, K. (2013). The WU-Minn Human Connectome Project: An overview. *NeuroImage*, *80*, 62–79. https://doi.org/10.1016/j.neuroimage.2013.05.041

van Oort, E. S. B., Mennes, M., Navarro Schröder, T., Kumar, V. J., Zaragoza Jimenez, N. I., Grodd, W., Doeller, C. F., & Beckmann, C. F. (2018). Functional parcellation using time

courses of instantaneous connectivity. *NeuroImage*, *170*, 31–40. https://doi.org/10.1016/j.neuroimage.2017.07.027

Veale, D. M., Sahakian, B. J., Owen, A. M., & Marks, I. M. (1996). Specific cognitive deficits in tests sensitive to frontal lobe dysfunction in obsessive–compulsive disorder. *Psychological Medicine*, *26*(6), 1261–1269. https://doi.org/10.1017/S0033291700035984

Verbruggen, F., & Logan, G. D. (2008). Response inhibition in the stop-signal paradigm. *Trends in Cognitive Sciences*, *12*(11), 418–424. https://doi.org/10.1016/j.tics.2008.07.005

Verin, M., Partiot, A., Pillon, B., Malapani, C., Agid, Y., & Dubois, B. (1993). Delayed response tasks and prefrontal lesions in man—Evidence for self generated patterns of behaviour with poor environmental modulation. *Neuropsychologia*, *31*(12), 1379–1396. https://doi.org/10.1016/0028-3932(93)90105-9

Waegeman, A., Declerck, C. H., Boone, C., Seurinck, R., & Parizel, P. M. (2014). Individual differences in behavioral flexibility in a probabilistic reversal learning task: An fMRI study. *Journal of Neuroscience, Psychology, and Economics*, *7*(4), 203–218. https://doi.org/10.1037/npe0000026

Watson, G. S., & Leverenz, J. B. (2010). Profile of Cognitive Impairment in Parkinson's Disease. *Brain Pathology*, *20*(3), 640–645. https://doi.org/10.1111/j.1750-3639.2010.00373.x

Wiegell, M. R., Tuch, D. S., Larsson, H. B. W., & Wedeen, V. J. (2003). Automatic segmentation of thalamic nuclei from diffusion tensor magnetic resonance imaging. *NeuroImage*, *19*(2), 391–401. https://doi.org/10.1016/S1053-8119(03)00044-2

Williams, B. (2018). *Investigating the expression of dopamine receptors in mouse striatum*. King's College London.

Wilson, C. G., Nusbaum, A. T., Whitney, P., & Hinson, J. M. (2018). Trait anxiety impairs cognitive flexibility when overcoming a task acquired response and a preexisting bias. *PLOS ONE*, *13*(9), e0204694. https://doi.org/10.1371/journal.pone.0204694

Wilson, C. J. (2005). The Mechanism of Intrinsic Amplification of Hyperpolarizations and Spontaneous Bursting in Striatal Cholinergic Interneurons. *Neuron*, *45*(4), 575–585. https://doi.org/10.1016/j.neuron.2004.12.053

Wilson, C. J., Chang, H. T., & Kitai, S. T. (1990). Firing patterns and synaptic potentials of identified giant aspiny interneurons in the rat neostriatum. *Journal of Neuroscience*, *10*(2), 508–519. https://doi.org/10.1523/JNEUROSCI.10-02-00508.1990

Wilson, R. C., Takahashi, Y. K., Schoenbaum, G., & Niv, Y. (2014). Orbitofrontal Cortex as a Cognitive Map of Task Space. *Neuron*, *81*(2), 267–279. https://doi.org/10.1016/j.neuron.2013.11.005

Wolff, M., & Vann, S. D. (2019). The Cognitive Thalamus as a Gateway to Mental Representations. *Journal of Neuroscience*, *39*(1), 3–14. https://doi.org/10.1523/JNEUROSCI.0479-18.2018

Xue, G., Ghahremani, D. G., & Poldrack, R. A. (2008). Neural substrates for reversing stimulus-outcome and stimulus-response associations. *The Journal of Neuroscience: The Official*

Journal of the Society for Neuroscience, *28*(44), 11196–11204. https://doi.org/10.1523/JNEUROSCI.4001-08.2008

Yager, L. M., Garcia, A. F., Wunsch, A. M., & Ferguson, S. M. (2015). The ins and outs of the striatum: Role in drug addiction. *Neuroscience*, *301*, 529–541. https://doi.org/10.1016/j.neuroscience.2015.06.033

Yaple, Z. A., & Yu, R. (2019). Fractionating adaptive learning: A meta-analysis of the reversal learning paradigm. *Neuroscience and Biobehavioral Reviews*, *102*, 85–94. https://doi.org/10.1016/j.neubiorev.2019.04.006

Yovel, Y., & Assaf, Y. (2007). Virtual definition of neuronal tissue by cluster analysis of multi-parametric imaging (virtual-dot-com imaging). *NeuroImage*, *35*(1), 58–69. https://doi.org/10.1016/j.neuroimage.2006.08.055

Yu, C., Beckmann, J. F., & Birney, D. P. (2019). Cognitive flexibility as a meta-competency / Flexibilidad cognitiva como meta-competencia. *Estudios de Psicología*, *40*(3), 563–584. https://doi.org/10.1080/02109395.2019.1656463

Zeisel, S. H. (2006). Choline: Critical Role During Fetal Development and Dietary Requirements in Adults. *Annual Review of Nutrition*, *26*(1), 229–250. https://doi.org/10.1146/annurev.nutr.26.061505.111156

Zhang, D., Snyder, A. Z., Fox, M. D., Sansbury, M. W., Shimony, J. S., & Raichle, M. E. (2008). Intrinsic Functional Relations Between Human Cerebral Cortex and Thalamus. *Journal of Neurophysiology*, *100*(4), 1740–1748. https://doi.org/10.1152/jn.90463.2008

Systematic validation of an automated thalamic parcellation technique using anatomical data at 3T

Brendan Williams[1,2], Etienne Roesch[1,2], Anastasia Christakou[1,2]

1. Centre for Integrative Neuroscience and Neurodynamics, University of Reading, UK
2. School of Psychology and Clinical Language Sciences, University of Reading, UK

Abstract

The thalamus is a brain region formed from functionally distinct nuclei, which contribute in important ways to various cognitive processes. Yet, much of the human neuroscience literature treats the thalamus as homologous region, and consequently the unique contribution of specific nuclei to behaviour remains underappreciated. This is likely due in part to the technical challenge of dissociating nuclei using conventional structural imaging approaches. Yet, multiple algorithms exist in the neuroimaging literature for the automated segmentation of thalamic nuclei. One recent approach developed by Iglesias and colleagues (2018) generates segmentations by applying a probabilistic atlas to subject-space anatomical images using the FreeSurfer software. Here, we systematically validate the efficacy of this segmentation approach in delineating thalamic nuclei using Human Connectome Project data. We provide several metrics quantifying the quality of segmentations against the Morel stereotaxic atlas, a widely accepted anatomical atlas based on cyto- and myeloarchitecture. The automated segmentation approach generated clear boundaries between groups of nuclei in the anterior, lateral, posterior, and medial portions of the thalamus. Segmentation efficacy, as measured by metrics of dissimilarity (Average Hausdorff Distance) and overlap (DICE coefficient) within groups was mixed, with regions more clearly delineated in anterior, lateral and medial thalamus compared to the posterior thalamus.

Introduction

Understanding how the brain contributes to cognitive processes is a main goal of human neuroimaging research. Much neuroimaging work has been confined to studying regions within the cerebrum, while the thalamus is traditionally understudied by comparison. However, an increased appreciation for the contribution of the thalamus in cognition is emerging in the neuroscientific literature (Figure 6), and is echoed by recent publications challenging the notion that the thalamus acts simply as a sensory-motor relay, by detailing its influence and modulatory effects on cognition (Wolff & Vann, 2019; Yang et al., 2020). Part of the challenge in studying the activity of the thalamus is due to the small size of its nuclei, relative to the spatial resolution of high-field (3 Tesla) magnetic resonance imaging (MRI). A related issue is delineating the functional and anatomical subdivisions of the thalamus, as the structure appears as largely homogenous when imaged using standard T1-weighted and T2 weighted images, meaning any attempts at manual segmentation would require a high level of anatomical knowledge. To more accurately define the different nuclei by enhancing the visibility of anatomical their boundaries image contrast in the thalamus can be increased by using specially developed sequences, such as cortex attenuated inversion recovery and white-matter-nulled magnetization prepared rapid gradient echo (WMn MP-RAGE), or by combining 3D GRE phase data with optimised MPRAGE images (Bender et al., 2017; Magnotta et al., 2000; Tourdias et al., 2014). However, unless automated supplementary segmentation algorithms are additionally developed (as for WMn MPRAGE, see Su et al, (2019)), specialist expertise in neuroanatomy and neuroradiology is still required to accurately identify thalamic nuclei. Furthermore, the efficacy of these pulse sequences for increasing image contrast are attenuated at typical MRI field strengths (3 Tesla) relative to ultra-high field (7+ Tesla) MRI (Saranathan et al., 2015).

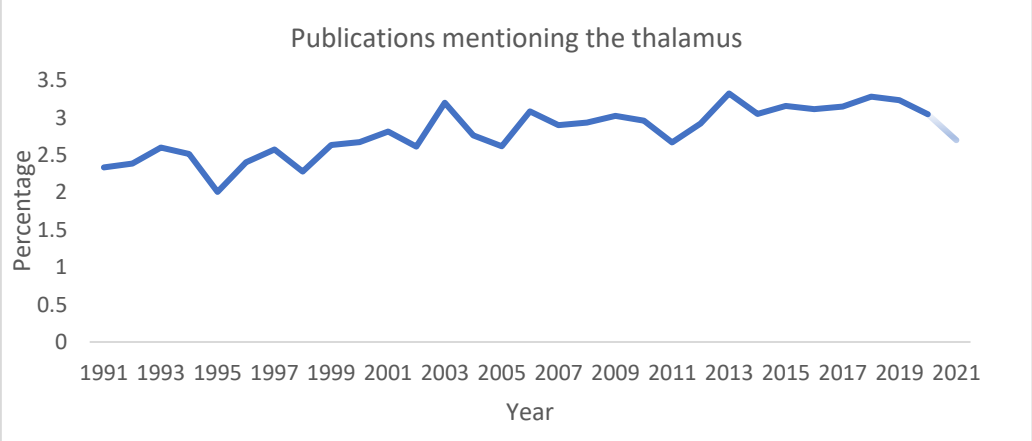

Figure 6 Percentage of neuroimaging papers mentioning the thalamus in their title or abstract as indexed using PubMed (search: 15/03/2021). Search terms: Neuroimaging papers "("MRI"[Title/Abstract] OR "fMRI"[Title/Abstract])", neuroimaging papers mentioning the thalamus "("thalam*"[Title/Abstract]) AND ("MRI"[Title/Abstract] OR "fMRI"[Title/Abstract])".

Recent studies have used MNI space parcellations (Krauth et al., 2010) to study the functional roles for different thalamic nuclei. For instance, Geier et al, (2020) describe different roles for mediodorsal and anterior thalamic nuclei in distinct associative memory processes, while Huang et al, (2019) show how differences in cognitive demand produce dissociable modulatory responses in the mediodorsal nucleus and its functional connectivity with the prefrontal cortex, while also demonstrating that this dissociation is aberrant in schizophrenia.

In both studies, the MNI space thalamic parcellations created by Krauth et al, (2010) are derived from the Morel stereotaxic atlas (Morel, 2007; Morel et al., 1997), a widely used atlas of the thalamus defined on the basis of cytoarchitecture, myeloarchitecture, and functional relevance. This atlas was developed using immunohistochemical staining of the calcium binding proteins parvalbumin, calbindin D-28k, and calretinin to identify anatomical boundaries in five postmortem brain specimens (Figure 7). The Morel atlas thus provides a description of the anatomical structure of the thalamus that is not possible to acquire *in vivo* using magnetic resonance. Yet, the existence of this atlas in MNI space does not allow neuroscientists to infer subject-specific architecture, as it is based on the average of multiple individuals.

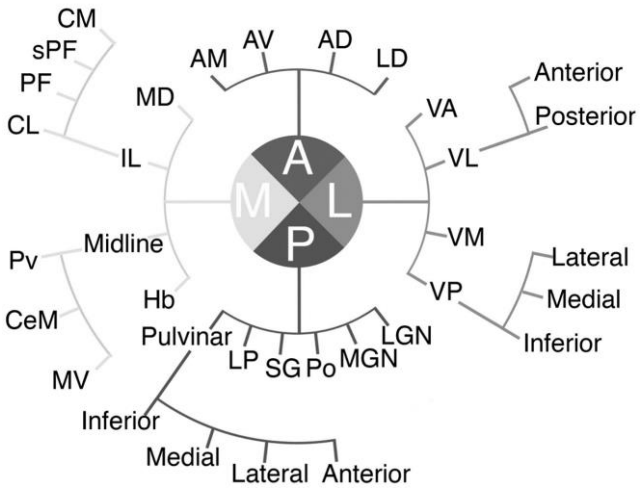

Figure 7 Hierarchical structure of thalamic nuclei as defined by the Morel stereotaxic atlas based on cytoarchitecture, myeloarchitecture, and functional relevance. Figure reproduced from (Lambert et al., 2017).

Numerous methods are described in the neuroimaging literature for defining the anatomical structure of thalamic nuclei using diffusion weighted, resting state, and anatomical data. Automated segmentation techniques first appear just after the turn of the century, initially relying on anatomical (Amini et al., 2004; Deoni et al., 2007) and diffusion data (Behrens et al., 2003; Johansen-Berg et al., 2005; Wiegell et al., 2003), and later on resting state functional data (Kim et al., 2013; Zhang et al., 2008). Parcellation methods have used prior knowledge of distinct cortico-thalamic connectivity to estimate structural boundaries within the thalamus using tractography (Behrens et al., 2003; Johansen-Berg et al., 2005), functional connectivity (Zhang et al., 2008) and machine learning approaches, such as clustering algorithms (Amini et al., 2004; Deoni et al., 2007; Wiegell et al., 2003) or independent component analysis (Kim et al., 2013).

A recent approach was developed by Iglesias et al. (2018), and uses FreeSurfer to provide automated segmentations for thalamic nuclei using anatomical images. This approach involves the application of a probabilistic atlas to anatomical images in subject space using Bayesian inference. This probabilistic atlas is in the form of a tetrahedral mesh that can adapt to changes in subject-specific differences in anatomy. The mesh was formed from a combination of ex-vivo MR images, histological staining, blockface photography, and in-vivo MRI. This approach is favourable relative to techniques using resting state and diffusion data because it is able to delineate more nuclei within the thalamus, and is easier to apply. Additionally, this approach does not require the acquisition of data using specialist sequences, such as WMn MP-RAGE, meaning it is applicable to a wide range of existing and future datasets.

Having good subject-specific parcellation techniques for thalamic nuclei is important for both clinical practice, and empirical research. For instance, these techniques can be used to guide surgeons when implanting deep brain stimulation electrodes to treat Parkinson's disease (Whiting et al., 2018). These techniques can also be used by researchers who may be interested in the role of different thalamic nuclei in functional processes, or the role of anatomical differences in health, development and disease. Nevertheless, the effectiveness of segmentation approaches must first be validated before inferences can be made based on their output. The original publication Iglesias et al. (2018) provides volumetric comparisons between six segmented nuclei and their corresponding regions in the Morel atlas, yet these volumes are not statistically compared to each other, nor is the spatial specificity of segmentations quantified.

Here, we aim to systematically compare the segmentation approach described by Iglesias et al. (2018) to regions in the Morel atlas. We provide volumetric, overlap, and isometric comparisons between all segmented regions and portions of the Morel atlas. These insights will allow clinicians

and researchers to make informed decisions about the applicability of this segmentation approach for identifying specific thalamic nuclei in individuals.

Methods

Data acquisition

Anatomical data were sourced from the publicly available dataset of the Human Connectome Project (HCP) 1200 Subjects Data Release (https://www.humanconnectome.org/study/hcp-young-adult/document/1200-subjects-data-release). The following description of data acquisition and preprocessing steps from the HCP project follow reporting guidelines from Horien et al. (2021) on the use of secondary neuroimaging datasets.

HCP data were acquired using a custom Siemens 3T Connectome Skyra scanner with a 32 channel receiver head coil and custom body transmission coil. Data were acquired over four separate scanning sessions; each session was approximately one hour in length. The structural data were acquired during one of those sessions. Two T1 weighted anatomical images were acquired using a 3D magnetization-prepared rapid gradient-echo (MP-RAGE) sequence with GeneRalized Autocalibrating Partially Parallel Acquisitions (GRAPPA) (R = 2) [TR = 2400ms; TE = 2.14ms; TI = 1000ms; slices = 256; voxel volume = 0.7mm^3; slice thickness = 0.7mm; distance factor = 50%; slice oversampling = 0.0%; FOV = 224 x 224mm; matrix = 320 x 320; flip angle = 8°; phase encoding direction = A → P; interleaved acquisition; echo spacing = 7.6ms].

Preprocessing

Data were preprocessed using the HCP minimal preprocessing pipelines (Glasser et al., 2013; Smith et al., 2013; Sotiropoulos et al., 2013). Firstly, T1 images were corrected for gradient distortions using a customised version of gradient_nonlin_unwarp in FreeSurfer, then each subject's two T1 scans were aligned using FSL FLIRT and averaged. The averaged T1 image was then registered to MNI space using a 12 DOF affine registration with FLIRT, and a subset of 6 DOF transforms were used to align the anterior commissure, the anterior commissure – posterior commissure line, and the inter-hemispheric plane, while preserving the size and shape of the brain in native space. The skull was removed by inverting linear (FLIRT) and non-linear (FNIRT) warps from anatomical to MNI space, applying the warp to the MNI space brain mask, and then applying the mask to the averaged T1 image. Finally, the image was corrected for readout distortion and biases in B_1 and B_1+ fields.

Participants

One hundred participants were pseudorandomly selected for inclusion in analysis. First, participants were filtered on the HCP database to include only subjects with complete anatomical, diffusion, and resting state acquisitions. Then subject IDs were sorted in ascending order and shuffled in MATLAB (2017b) using the seed 03112020 (the date of shuffling). The first one hundred subject IDs were chosen from this list for inclusion in analysis.

Analysis

Data were processed following the method previously described by Iglesias et al., 2018. Data processing was run using a Nipype pipeline integrating FSL (version 6.0.4) and FreeSurfer (version 7.1.1) on Ubuntu 18.04.2. Output files from Nipype nodes were used as analytic checkpoints to confirm each step in the analysis ran as expected. Anatomical T1 images were first processed and parcellated using recon-all in FreeSurfer; the output of recon-all was used to initialise the parcellation of thalamic nuclei for anatomical data using the algorithm described by Iglesias et al. (2018).

Comparison to Morel thalamic atlas

The parcellation of structural data were completed in subject space before being transformed into MNI space. Linear rigid and affine transformations and non-linear warps were generated using the Advanced Normalization Tools (ANTs) package (Version 2.3.5, Ecphorella) script antsRegistrationSyN.sh (Avants et al., 2008). The ANTs package was selected due to its superior performance in registering skull-stripped images compared to other algorithms (Ou et al., 2014). Linear transformations and non-linear warps were then used to convert subject-level parcellations into MNI space. Group-level probabilistic atlases were created by calculating a mean probability map for each parcellation in MNI space (described previously by Najdenovska et al. (2018)). These segmentations were then compared to the Morel probabilistic atlas, which was used as ground truth (Krauth et al., 2010). Each parcellation was compared separately to individual nuclei in the Morel atlas using the EvaluateSegmentation toolbox (Taha & Hanbury, 2015), a threshold of > 0.25 was set for specificity metrics that do not accept non-binary input. The following metrics from the EvaluateSegmentation toolbox were used to assess each parcellation approach.

The DICE coefficient was used as a measure of overlap between segmentations and ground truth; it is a widely used measure in imaging processing for assessing the overlap between segmentation approaches. The DICE coefficient is defined as:

$$DICE(S_x, S_y) = \frac{2|S_x \cap S_y|}{|S_x| + |S_y|}$$

Where $|S_x \cap S_y|$is the cardinality of the intersection between the segmentation and ground truth (this is equal to the number of true positives, or overlapping voxels), divided by the sum of the cardinality of the ground truth $|S_x|$ and the segmentation $|S_y|$ (equal to the sum of true positives, false positives, and false negatives). Because the DICE coefficient is a measure of overlap, it is expressed in terms of the relationship between true positives, false positives, and false negatives, but not the number of true negatives. This is an important consideration when comparing segmentation approaches, since it is necessary that a good segmentation overlap with ground truth, yet overlap is not sufficient for determining the best approach as it cannot account for isometry.

The Average Hausdorff Distance is used as a measure of dissimilarity. Distance based metrics are advantageous, relative to overlap metrics in situations where segmentations are small, because overlap-based metrics disproportionately penalise errors in smaller than larger segmentations (Taha & Hanbury, 2015) as is the case with thalamic nuclei. Importantly, the Average Hausdorff Distance is sensitive to the position of false positives in a segmentation relative to ground truth, and therefore is a useful metric when considering the boundary of a segmentation, and can account for isometry. In relation to image segmentation, the Hausdorff Distance can be defined as the minimum number of voxels (or distance in millimetres) between a point in segmentation X and a point in segmentation Y. Therefore, the Average Hausdorff Distance is the average minimum distance between all points in segmentation A and segmentation B. The Average Hausdorff Distance is defined as:

$$\text{Average Hausdorff Distance}(A, B) = \max(d(A, B), d(B, A))$$

$$d(A, B) = \frac{1}{N} \sum_{a \in A} \min_{b \in B} \|a - b\|$$

Where $d(A, B)$ is the average minimum distance ($min\|a - b\|$) from voxels in the ground truth (A) to the segmentation (B), $d(B, A)$ is the average minimum distance ($min\|a - b\|$) from voxels in the segmentation (B) to the ground truth (A). The Average Hausdorff Distance is then the maximum of either of these two average distance measures.

As part of the volumetric comparison in Table 1, and Figure 10 the following nuclei from the Morel atlas were combined to make them comparable with the segmentations: LGN = (LGNmc + LGNpc), VA = (VAmc + VApc), VLp = (VLpd + VLpv), VPL = (VPLa + VPLp).

Results

Segmentation overlap

DICE coefficients between the Morel atlas and the segmentations of the left and right thalamus are summarised in Figure 8 and Figure 9, respectively. On the x-axis are the thalamic nuclei from the Morel atlas; the segmented regions are displayed along the y-axis. A list of abbreviations used is presented in Table 2; the dendrograms presented above and adjacent to each heatmap show the hierarchical structure of the thalamus as defined by (Morel et al., 1997) and the relative position of each nucleus within that hierarchy. Cells where groups of nuclei are equivalent between the Morel atlas and the segmentation are highlighted. Here, when interpreting DICE coefficients, we use the following terminology, DICE = 0 no agreement, $0 < DICE < 0.2$ slight agreement, $0.2 \leq DICE < 0.4$ fair agreement, $0.4 \leq DICE < 0.6$ moderate agreement, $0.6 \leq DICE < 0.8$ substantial agreement, $0.8 \leq DICE \leq 1$ almost perfect agreement; these values have been used previously by (Pajula et al., 2012) for comparing Nifti images, and are a widely used convention for interpretating DICE coefficients.

DICE coefficients were similar between the left and right thalamus (Wilcoxon Signed-Ranks Test, $Z = 9536$, $p = 0.531$). Figure 8 and Figure 9 show that for the anterior nuclei, the AV had higher overlap than the LD. Overlap for anterior, lateral, medial, and posterolateral divisions of the lateral thalamus generally showed moderate to substantial overlap with nuclei from the same subregion, and mostly only slight overlap between subregions. Posterior thalamic nuclei had overlap values that were generally higher between subregions of the posterior thalamus than for other nuclear groups, and were the only set of nuclei to show greater than slight agreement with nuclei from other nuclear groups. Of the midline nuclei in the medial thalamus, only the CeM was segmented, showing fair and moderate overlap in left and right hemispheres, respectively. For the intralaminar nuclei (CL, CM, Pf) the CM and Pf had higher overlap than the CL, which showed overlap with anterior and posterior at the upper end of slight agreement. Subregions of the mediodorsal thalamus (MDm and MDl) showed slight to moderate overlap with corresponding regions in the Morel atlas, and fair overlap with the CL in the left hemisphere.

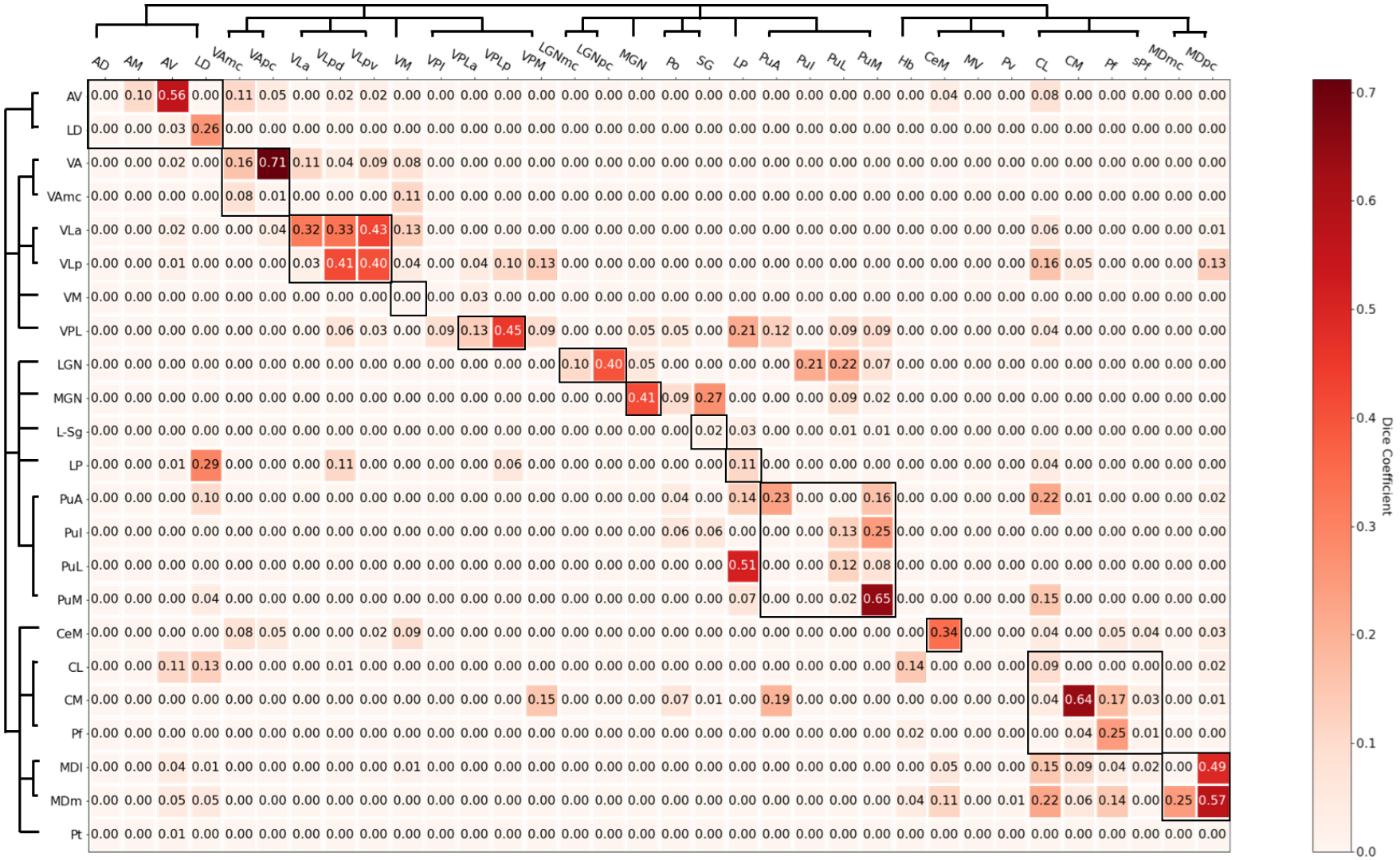
AD AM AV LD VAmc VApc VLa VLpd VLpv VM VPI VPLa VPLp VPM LGNmc LGNpc MGN Po SG LP PuA PuI PuL PuM Hb CeM MV Pv CL CM Pf sPf MDmc MDpc
AV 0.00 0.10 0.56 0.00 0.11 0.05 0.00 0.02 0.02 0.00 0.00 0.00 0.00 0.00 0.00 0.00 0.00 0.00 0.00 0.00 0.00 0.00 0.00 0.00 0.00 0.04 0.00 0.00 0.08 0.00 0.00 0.00 0.00 0.00
LD 0.00 0.00 0.03 0.26 0.00 0.00 0.00 0.00 0.00 0.00 0.00 0.00 0.00 0.00 0.00 0.00 0.00 0.00 0.00 0.00 0.00 0.00 0.00 0.00 0.00 0.00 0.00 0.00 0.00 0.00 0.00 0.00 0.00 0.00
VA 0.00 0.00 0.02 0.00 0.16 0.71 0.11 0.04 0.09 0.08 0.00 0.00 0.00 0.00 0.00 0.00 0.00 0.00 0.00 0.00 0.00 0.00 0.00 0.00 0.00 0.00 0.00 0.00 0.00 0.00 0.00 0.00 0.00 0.00
VAmc 0.00 0.00 0.00 0.00 0.08 0.01 0.00 0.00 0.00 0.11 0.00 0.00 0.00 0.00 0.00 0.00 0.00 0.00 0.00 0.00 0.00 0.00 0.00 0.00 0.00 0.00 0.00 0.00 0.00 0.00 0.00 0.00 0.00 0.00
VLa 0.00 0.00 0.02 0.00 0.00 0.04 0.32 0.33 0.43 0.13 0.00 0.00 0.00 0.00 0.00 0.00 0.00 0.00 0.00 0.00 0.00 0.00 0.00 0.00 0.00 0.00 0.00 0.00 0.06 0.00 0.00 0.00 0.00 0.01
VLp 0.00 0.00 0.01 0.00 0.00 0.00 0.03 0.41 0.40 0.04 0.00 0.04 0.10 0.13 0.00 0.00 0.00 0.00 0.00 0.00 0.00 0.00 0.00 0.00 0.00 0.00 0.00 0.00 0.16 0.05 0.00 0.00 0.00 0.13
VM 0.00 0.00 0.00 0.00 0.00 0.00 0.00 0.00 0.00 0.00 0.00 0.03 0.00 0.00 0.00 0.00 0.00 0.00 0.00 0.00 0.00 0.00 0.00 0.00 0.00 0.00 0.00 0.00 0.00 0.00 0.00 0.00 0.00 0.00
VPL 0.00 0.00 0.00 0.00 0.00 0.00 0.00 0.06 0.03 0.00 0.09 0.13 0.45 0.09 0.00 0.00 0.05 0.05 0.00 0.21 0.12 0.00 0.09 0.09 0.00 0.00 0.00 0.00 0.04 0.00 0.00 0.00 0.00 0.00
LGN 0.00 0.00 0.00 0.00 0.00 0.00 0.00 0.00 0.00 0.00 0.00 0.00 0.00 0.00 0.10 0.40 0.05 0.00 0.00 0.00 0.00 0.21 0.22 0.07 0.00 0.00 0.00 0.00 0.00 0.00 0.00 0.00 0.00 0.00
MGN 0.00 0.00 0.00 0.00 0.00 0.00 0.00 0.00 0.00 0.00 0.00 0.00 0.00 0.00 0.00 0.00 0.41 0.09 0.27 0.00 0.00 0.00 0.09 0.02 0.00 0.00 0.00 0.00 0.00 0.00 0.00 0.00 0.00 0.00
L-Sg 0.00 0.00 0.00 0.00 0.00 0.00 0.00 0.00 0.00 0.00 0.00 0.00 0.00 0.00 0.00 0.00 0.00 0.00 0.02 0.03 0.00 0.00 0.01 0.01 0.00 0.00 0.00 0.00 0.00 0.00 0.00 0.00 0.00 0.00
LP 0.00 0.00 0.01 0.29 0.00 0.00 0.00 0.11 0.00 0.00 0.00 0.00 0.06 0.00 0.00 0.00 0.00 0.00 0.00 0.11 0.00 0.00 0.00 0.00 0.00 0.00 0.00 0.00 0.04 0.00 0.00 0.00 0.00 0.00
PuA 0.00 0.00 0.00 0.10 0.00 0.00 0.00 0.00 0.00 0.00 0.00 0.00 0.00 0.00 0.00 0.00 0.00 0.00 0.04 0.00 0.14 0.23 0.00 0.00 0.16 0.00 0.00 0.00 0.00 0.22 0.01 0.00 0.00 0.02
PuI 0.00 0.00 0.00 0.00 0.00 0.00 0.00 0.00 0.00 0.00 0.00 0.00 0.00 0.00 0.00 0.00 0.00 0.00 0.06 0.06 0.00 0.00 0.00 0.13 0.25 0.00 0.00 0.00 0.00 0.00 0.00 0.00 0.00 0.00
PuL 0.00 0.00 0.00 0.00 0.00 0.00 0.00 0.00 0.00 0.00 0.00 0.00 0.00 0.00 0.00 0.00 0.00 0.00 0.00 0.51 0.00 0.00 0.12 0.08 0.00 0.00 0.00 0.00 0.00 0.00 0.00 0.00 0.00 0.00
PuM 0.00 0.00 0.00 0.04 0.00 0.00 0.00 0.00 0.00 0.00 0.00 0.00 0.00 0.00 0.00 0.00 0.00 0.00 0.00 0.07 0.00 0.00 0.02 0.65 0.00 0.00 0.00 0.00 0.15 0.00 0.00 0.00 0.00 0.00
CeM 0.00 0.00 0.00 0.00 0.08 0.05 0.00 0.00 0.02 0.09 0.00 0.00 0.00 0.00 0.00 0.00 0.00 0.00 0.00 0.00 0.00 0.00 0.00 0.00 0.00 0.34 0.00 0.00 0.04 0.00 0.05 0.04 0.00 0.03
CL 0.00 0.00 0.11 0.13 0.00 0.00 0.00 0.01 0.00 0.00 0.00 0.00 0.00 0.00 0.00 0.00 0.00 0.00 0.00 0.00 0.00 0.00 0.00 0.00 0.00 0.14 0.00 0.00 0.00 0.09 0.00 0.00 0.00 0.02
CM 0.00 0.00 0.00 0.00 0.00 0.00 0.00 0.00 0.00 0.00 0.00 0.00 0.00 0.15 0.00 0.00 0.00 0.07 0.01 0.00 0.19 0.00 0.00 0.00 0.00 0.00 0.00 0.00 0.04 0.64 0.17 0.03 0.00 0.01
Pf 0.00 0.00 0.00 0.00 0.00 0.00 0.00 0.00 0.00 0.00 0.00 0.00 0.00 0.00 0.00 0.00 0.00 0.00 0.00 0.00 0.00 0.00 0.00 0.00 0.00 0.02 0.00 0.00 0.00 0.04 0.25 0.01 0.00 0.00
MDl 0.00 0.00 0.04 0.01 0.00 0.00 0.00 0.00 0.00 0.01 0.00 0.00 0.00 0.00 0.00 0.00 0.00 0.00 0.00 0.00 0.00 0.00 0.00 0.00 0.00 0.05 0.00 0.00 0.15 0.09 0.04 0.02 0.00 0.49
MDm 0.00 0.00 0.05 0.05 0.00 0.00 0.00 0.00 0.00 0.00 0.00 0.00 0.00 0.00 0.00 0.00 0.00 0.00 0.00 0.00 0.00 0.00 0.00 0.00 0.00 0.04 0.11 0.00 0.01 0.22 0.06 0.14 0.00 0.25 0.57
Pt 0.00 0.00 0.01 0.00 0.00 0.00 0.00 0.00 0.00 0.00 0.00 0.00 0.00 0.00 0.00 0.00 0.00 0.00 0.00 0.00 0.00 0.00 0.00 0.00 0.00 0.00 0.00 0.00 0.00 0.00 0.00 0.00 0.00 0.00
Dice Coefficient
0.7
0.6
0.5
0.4
0.3
0.2
0.1
0.0

Figure 8 DICE coefficient between segmented (vertical axis) regions and volumes in the Morel atlas (horizontal axis) in the left thalamus. Higher DICE coefficients show there is greater overlap between segmented regions and volumes in the Morel atlas. Dendrograms show the hierarchical structure of nuclei within the thalamus. DICE coefficients within BOLD boxes along the diagonal are regions that are part of the same nuclear group or sub-group.

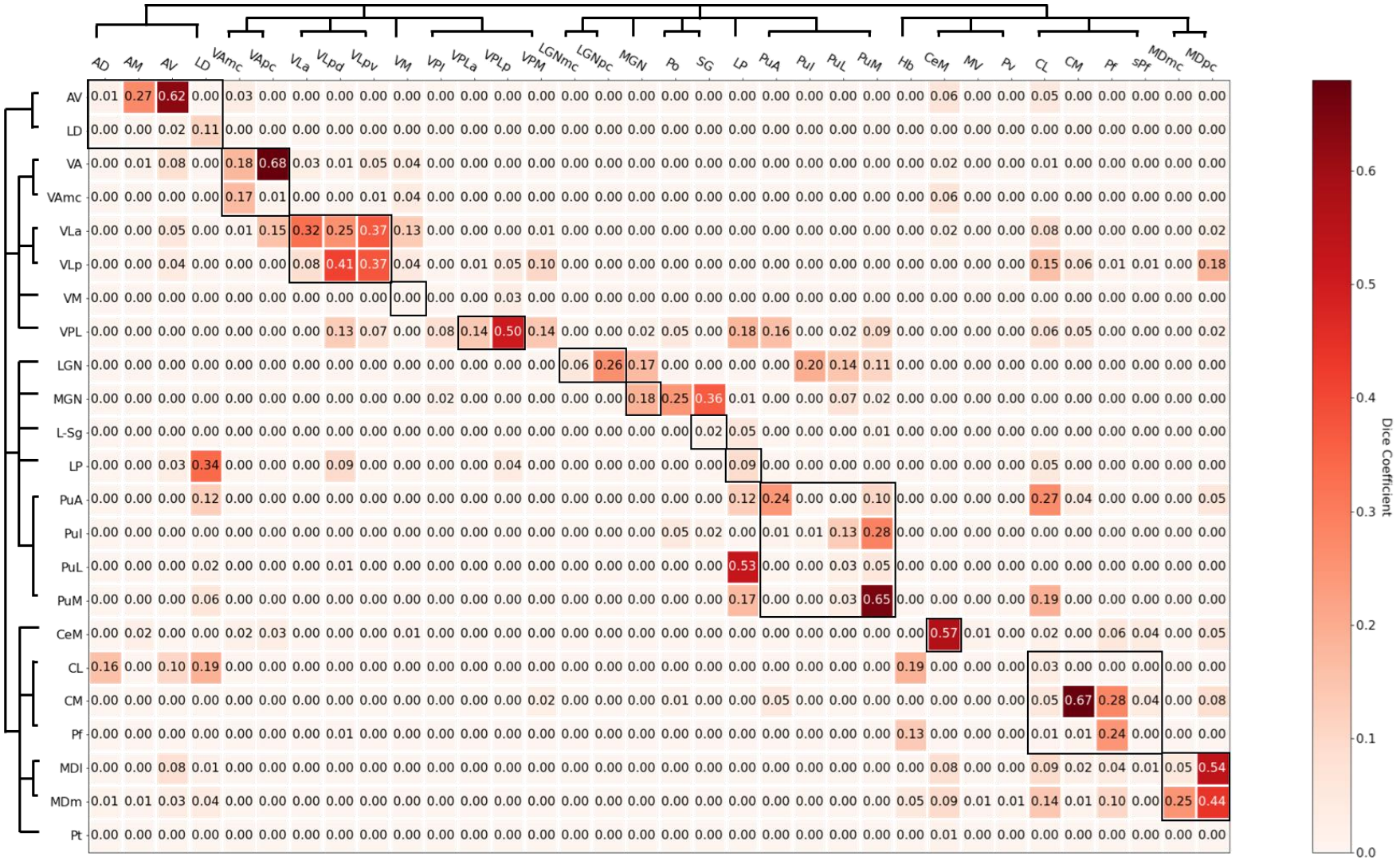
AD AM AV LD VAmc VApc VLa VLpd VLpv VM VPl VPLa VPLp VPM LGNmc LGNpc MGN Po SG LP PuA PuI PuL PuM Hb CeM MV Pv CL CM Pf sPf MDmc MDpc
AV 0.01 0.27 0.62 0.00 0.03 0.00 0.00 0.00 0.00 0.00 0.00 0.00 0.00 0.00 0.00 0.00 0.00 0.00 0.00 0.00 0.00 0.00 0.00 0.00 0.00 0.00 0.06 0.00 0.00 0.05 0.00 0.00 0.00 0.00 0.00
LD 0.00 0.00 0.02 0.11 0.00 0.00 0.00 0.00 0.00 0.00 0.00 0.00 0.00 0.00 0.00 0.00 0.00 0.00 0.00 0.00 0.00 0.00 0.00 0.00 0.00 0.00 0.00 0.00 0.00 0.00 0.00 0.00 0.00 0.00 0.00
VA 0.00 0.01 0.08 0.00 0.18 0.68 0.03 0.01 0.05 0.04 0.00 0.00 0.00 0.00 0.00 0.00 0.00 0.00 0.00 0.00 0.00 0.00 0.00 0.00 0.00 0.00 0.02 0.00 0.00 0.01 0.00 0.00 0.00 0.00 0.00
VAmc 0.00 0.00 0.00 0.00 0.17 0.01 0.00 0.00 0.01 0.04 0.00 0.00 0.00 0.00 0.00 0.00 0.00 0.00 0.00 0.00 0.00 0.00 0.00 0.00 0.00 0.00 0.06 0.00 0.00 0.00 0.00 0.00 0.00 0.00 0.00
VLa 0.00 0.00 0.05 0.00 0.01 0.15 0.32 0.25 0.37 0.13 0.00 0.00 0.00 0.01 0.00 0.00 0.00 0.00 0.00 0.00 0.00 0.00 0.00 0.00 0.00 0.00 0.02 0.00 0.00 0.08 0.00 0.00 0.00 0.00 0.02
VLp 0.00 0.00 0.04 0.00 0.00 0.00 0.08 0.41 0.37 0.04 0.00 0.01 0.05 0.10 0.00 0.00 0.00 0.00 0.00 0.00 0.00 0.00 0.00 0.00 0.00 0.00 0.00 0.00 0.00 0.15 0.06 0.01 0.01 0.00 0.18
VM 0.00 0.00 0.00 0.00 0.00 0.00 0.00 0.00 0.00 0.00 0.00 0.00 0.03 0.00 0.00 0.00 0.00 0.00 0.00 0.00 0.00 0.00 0.00 0.00 0.00 0.00 0.00 0.00 0.00 0.00 0.00 0.00 0.00 0.00 0.00
VPL 0.00 0.00 0.00 0.00 0.00 0.00 0.00 0.13 0.07 0.00 0.08 0.14 0.50 0.14 0.00 0.00 0.02 0.05 0.00 0.18 0.16 0.00 0.02 0.09 0.00 0.00 0.00 0.00 0.06 0.05 0.00 0.00 0.00 0.02
LGN 0.00 0.00 0.00 0.00 0.00 0.00 0.00 0.00 0.00 0.00 0.00 0.00 0.00 0.00 0.06 0.26 0.17 0.00 0.00 0.00 0.00 0.20 0.14 0.11 0.00 0.00 0.00 0.00 0.00 0.00 0.00 0.00 0.00 0.00
MGN 0.00 0.00 0.00 0.00 0.00 0.00 0.00 0.00 0.00 0.00 0.02 0.00 0.00 0.00 0.00 0.00 0.18 0.25 0.36 0.01 0.00 0.00 0.07 0.02 0.00 0.00 0.00 0.00 0.00 0.00 0.00 0.00 0.00 0.00
L-Sg 0.00 0.00 0.00 0.00 0.00 0.00 0.00 0.00 0.00 0.00 0.00 0.00 0.00 0.00 0.00 0.00 0.00 0.00 0.02 0.05 0.00 0.00 0.00 0.01 0.00 0.00 0.00 0.00 0.00 0.00 0.00 0.00 0.00 0.00
LP 0.00 0.00 0.03 0.34 0.00 0.00 0.00 0.09 0.00 0.00 0.00 0.00 0.04 0.00 0.00 0.00 0.00 0.00 0.00 0.09 0.00 0.00 0.00 0.00 0.00 0.00 0.00 0.00 0.05 0.00 0.00 0.00 0.00 0.00
PuA 0.00 0.00 0.00 0.12 0.00 0.00 0.00 0.00 0.00 0.00 0.00 0.00 0.00 0.00 0.00 0.00 0.00 0.00 0.00 0.12 0.24 0.00 0.00 0.10 0.00 0.00 0.00 0.00 0.27 0.04 0.00 0.00 0.00 0.05
PuI 0.00 0.00 0.00 0.00 0.00 0.00 0.00 0.00 0.00 0.00 0.00 0.00 0.00 0.00 0.00 0.00 0.00 0.05 0.02 0.00 0.01 0.01 0.13 0.28 0.00 0.00 0.00 0.00 0.00 0.00 0.00 0.00 0.00 0.00
PuL 0.00 0.00 0.00 0.02 0.00 0.00 0.00 0.01 0.00 0.00 0.00 0.00 0.00 0.00 0.00 0.00 0.00 0.00 0.00 0.53 0.00 0.00 0.03 0.05 0.00 0.00 0.00 0.00 0.00 0.00 0.00 0.00 0.00 0.00
PuM 0.00 0.00 0.00 0.06 0.00 0.00 0.00 0.00 0.00 0.00 0.00 0.00 0.00 0.00 0.00 0.00 0.00 0.00 0.00 0.17 0.00 0.00 0.03 0.65 0.00 0.00 0.00 0.00 0.19 0.00 0.00 0.00 0.00 0.00
CeM 0.00 0.02 0.00 0.00 0.02 0.03 0.00 0.00 0.00 0.01 0.00 0.00 0.00 0.00 0.00 0.00 0.00 0.00 0.00 0.00 0.00 0.00 0.00 0.00 0.00 0.57 0.01 0.00 0.02 0.00 0.06 0.04 0.00 0.05
CL 0.16 0.00 0.10 0.19 0.00 0.00 0.00 0.00 0.00 0.00 0.00 0.00 0.00 0.00 0.00 0.00 0.00 0.00 0.00 0.00 0.00 0.00 0.00 0.00 0.00 0.19 0.00 0.00 0.00 0.03 0.00 0.00 0.00 0.00 0.00
CM 0.00 0.00 0.00 0.00 0.00 0.00 0.00 0.00 0.00 0.00 0.00 0.00 0.00 0.02 0.00 0.00 0.00 0.01 0.00 0.00 0.05 0.00 0.00 0.00 0.00 0.00 0.00 0.00 0.05 0.67 0.28 0.04 0.00 0.08
Pf 0.00 0.00 0.00 0.00 0.00 0.00 0.00 0.01 0.00 0.00 0.00 0.00 0.00 0.00 0.00 0.00 0.00 0.00 0.00 0.00 0.00 0.00 0.00 0.00 0.00 0.13 0.00 0.00 0.00 0.01 0.01 0.24 0.00 0.00 0.00
MDl 0.00 0.00 0.08 0.01 0.00 0.00 0.00 0.00 0.00 0.00 0.00 0.00 0.00 0.00 0.00 0.00 0.00 0.00 0.00 0.00 0.00 0.00 0.00 0.00 0.00 0.00 0.08 0.00 0.00 0.09 0.02 0.04 0.01 0.05 0.54
MDm 0.01 0.01 0.03 0.04 0.00 0.00 0.00 0.00 0.00 0.00 0.00 0.00 0.00 0.00 0.00 0.00 0.00 0.00 0.00 0.00 0.00 0.00 0.00 0.00 0.00 0.05 0.09 0.01 0.01 0.14 0.01 0.10 0.00 0.25 0.44
Pt 0.00 0.00 0.00 0.00 0.00 0.00 0.00 0.00 0.00 0.00 0.00 0.00 0.00 0.00 0.00 0.00 0.00 0.00 0.00 0.00 0.00 0.00 0.00 0.00 0.00 0.00 0.01 0.00 0.00 0.00 0.00 0.00 0.00 0.00 0.00
Dice Coefficient
0.0
0.1
0.2
0.3
0.4
0.5
0.6

Figure 9 DICE coefficient between segmented (vertical axis) regions and volumes in the Morel atlas (horizontal axis) in the right thalamus. Higher DICE coefficients show there is greater overlap between segmented regions and volumes in the Morel atlas. Dendrograms show the hierarchical structure of nuclei within the thalamus. DICE coefficients within BOLD boxes along the diagonal are regions that are part of the same nuclear group or sub-group.

Segmentation volume

Although nuclei volumes in the segmentation and the atlas were correlated ($t(42) = 5.869$, $r = 0.671$, $p < 0.001$; Figure 10), one sample t-tests showed that the volumes were significantly different for all nuclei (Table 1). Most volumes were smaller in the segmentation, except LGN, MDm, PuA, PuI, VLa, and VPL which bilaterally were larger in the segmentation than the equivalent volumes in the Morel atlas.

Bilaterally, the Average Hausdorff Distance (measured in voxels) between segmentations and the Morel atlas was lower along the diagonal (part of the same nuclear subgroup), and larger for nuclei off the diagonal, particularly for nuclei that were part of different nuclear groups (Table 2, Figure 11, Figure 12). Nuclei from the Morel atlas with the lowest Average Hausdorff Distance for each segmentation are summarised in Table 3, and segmented nuclei with the lowest Average Hausdorff Distance for each nuclei in the Morel atlas are summarised in Table 4.

Nucleus	Mean volume (mm^3)	Standard deviation	Minimum (mm^3)	Maximum (mm^3)	*t*-statistic	p-value	N	Morel volume (mm^3)
Left-AV	124.0254	18.205	84.035	174.93	-91.8059	1.3E-97	100	292
Left-CeM	72.74344	12.21982	49.735	109.417	-66.1624	9.34E-84	100	154
Left-CL	13.86406	9.645825	3.43	85.06399	-897.564	2.1E-195	100	884
Left-CM	255.2572	40.31033	173.558	417.431	-13.0186	3.57E-23	100	308
Left-LD	20.6143	8.264449	4.459	45.276	-172.627	1.4E-124	100	164
Left-LGN	285.1942	35.49029	199.969	382.445	6.502605	3.23E-09	100	262
Left-LP	123.0787	19.20904	89.18	180.075	-168.302	1.7E-123	100	448
Left-L-Sg	13.16777	9.164186	2.401	51.793	-49.7616	7.24E-72	100	59
Left-MDl	259.3183	26.47553	213.346	348.831	-291.512	4.6E-147	100	1035
Left-MDm	809.2776	79.1976	643.811	1083.88	75.66626	2.05E-89	100	207
Left-MGN	61.21521	17.20899	22.295	114.562	-87.7587	1.07E-95	100	213
Left-Pf	51.42599	12.4969	28.469	99.46999	-107.942	1.7E-104	100	187
Left-PuA	214.5877	24.80664	169.785	299.096	19.08727	5.98E-35	100	167
Left-PuI	246.9909	41.16957	170.814	355.691	45.43368	4.07E-68	100	59
Left-PuL	180.394	32.57992	125.881	320.019	-63.4027	5.76E-82	100	388
Left-PuM	1158.129	124.1217	906.892	1485.876	-54.019	2.85E-75	100	1832
Left-VA	394.7553	44.87643	293.951	497.693	-54.1532	2.25E-75	100	639
Left-VAmc	7.56658	2.362381	2.401	14.063	-279.804	2.6E-145	100	74
Left-VLa	561.9369	66.39361	411.943	770.0349	36.40699	3.95E-59	100	319
Left-VLp	891.0797	106.9382	662.3329	1262.24	-56.935	1.84E-77	100	1503
Left-VM	1.615819	1.311282	0.343	7.546	-1066.14	1.3E-171	83	156
Left-VPL	926.8751	123.0254	703.4929	1350.734	20.77518	7.15E-38	100	670

Nucleus	Mean volume (mm^3)	Standard deviation	Minimum (mm^3)	Maximum (mm^3)	*t*-statistic	p-value	N	Morel volume (mm^3)
Right-AV	134.823	21.67799	82.32	182.476	-69.847	4.88E-86	100	287
Right-CeM	70.77805	11.77168	43.561	102.214	-86.4019	4.91E-95	100	173
Right-CL	11.92611	6.871285	3.087	61.74	-1222.25	1.1E-208	100	856
Right-CM	256.931	41.84041	184.534	423.262	-11.1933	2.79E-19	100	304
Right-LD	20.16154	7.981011	5.488	44.59	-179.322	3.2E-126	100	164
Right-LGN	275.8269	32.54821	202.37	360.493	5.449611	3.7E-07	100	258
Right-LP	117.0282	18.69873	74.088	163.611	-294.777	1.5E-147	100	671
Right-L-Sg	9.85782	6.783707	0.686	45.276	-70.6116	1.7E-86	100	58
Right-MDl	258.207	26.152	196.882	336.483	-295.541	1.2E-147	100	1035
Right-MDm	821.7388	79.12425	615.685	1072.561	77.0519	3.49E-90	100	209
Right-MGN	73.36427	19.29477	25.725	138.229	-71.4913	5.1E-87	100	212
Right-Pf	58.81078	13.84271	37.387	111.475	-96.4526	1E-99	100	193
Right-PuA	206.3351	23.58036	152.978	277.144	15.75376	1E-28	100	169
Right-PuI	219.0329	38.44851	140.973	320.705	40.63767	1.46E-63	100	62
Right-PuL	166.8009	31.07548	108.388	275.429	-73.7061	2.63E-88	100	397
Right-PuM	1145.116	119.2232	811.1949	1488.277	-57.408	8.29E-78	100	1833
Right-VA	403.9922	49.41994	299.096	566.9789	-48.5229	7.97E-71	100	645
Right-VAmc	9.02776	2.463819	4.459	15.778	-270.46	7.6E-144	100	76
Right-VLa	602.6201	77.34003	443.156	891.114	35.33016	6.25E-58	100	328
Right-VLp	887.7903	111.1463	639.6949	1288.651	-55.8796	1.11E-76	100	1512
Right-VM	1.437333	1.090426	0.343	5.145	-925.229	3.45E-90	42	159
Right-VPL	891.2992	118.3106	647.241	1254.008	19.78856	3.5E-36	100	656

Table 1 Descriptive statistics for segmented thalamic volumes and regions within the Morel atlas. Mean, standard deviation and range are provided for each segmentation bilaterally. Additionally, the number of participants where this nuclei was delineated is specified. The following regions within the Morel atlas are combined for the purpose of statistical analysis (LGN = (LGNmc + LGNpc), VA = (VAmc + VApc), VLp = (VLpd + VLpv), VPL = (VPLa + VPLp).

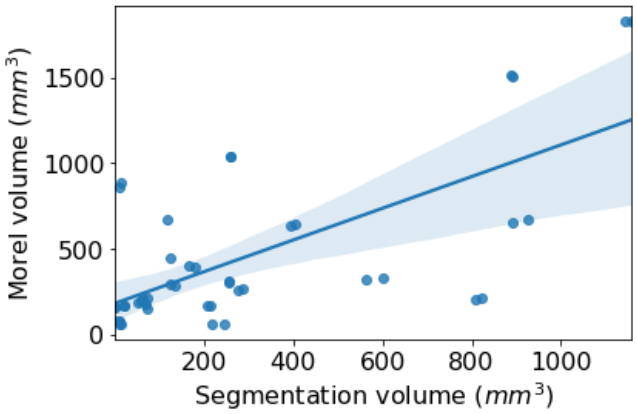

Figure 10 Spearman's correlation between segmentation volumes and volumes from the Morel atlas. A significant moderate correlation was found between segmented volumes and volumes in the Morel atlas (r = 0.671, p < 0.001). The following regions within the Morel atlas are combined for the purpose of statistical analysis (LGN = (LGNmc + LGNpc), VA = (VAmc + VApc), VLp = (VLpd + VLpv), VPL = (VPLa + VPLp).

Nucleus	**Group**		**Morel**	**Segmentation**	
Anterodorsal	Anterior		AD		
Anteromedial			AM		
Anteroventral			AV	AV	
Lateral dorsal			LD	LD	
Ventral anterior, magnocellular division	Lateral	*Ventral anterior*	VAmc	VA	VAmc
Ventral anterior, parvocellular division			VApc		
Ventral lateral anterior		*Ventral lateral*	VLa	VLa	
Ventral lateral posterior, dorsal division			VLpd	VLp	
Ventral lateral posterior, ventral division			VLpv		
Ventral medial			VM	VM	
Ventral posterior inferior		*Ventroposterior complex*	VPI		
Ventral posterior lateral, anterior division			VPLa	VPL	
Ventral posterior lateral, posterior division			VPLp		
Ventral posterior medial			VPM		
Lateral geniculate, magnocellular division	Posterior	*Geniculate*	LGNmc	LGN	
Lateral geniculate, parvocellular division			LGNpc		
Medial geniculate			MGN	MGN	
Posterior		*Posterior complex*	Po		
Suprageniculate			SG	L-Sg	

Lateral posterior			LP	LP
Anterior pulvinar		*Pulvinar*	PuA	PuA
Inferior pulvinar			PuI	PuI
Lateral pulvinar			PuL	PuL
Medial pulvinar			PuM	PuM
Habenula	Medial		Hb	
Central medial		*Midline*	CeM	CeM
Medioventral			MV	
Paraventricular			Pv	
Central lateral		*Intralaminar*	CL	CL
Centromedian			CM	CM
Parafascicular			Pf	Pf
Subparafascicular			sPf	
Mediodorsal, magnocellular division		*Mediodorsal*	MDmc	MDm
Mediodorsal, parvocellular division			MDpc	MDl
Paratenial				Pt

Table 2 Definitions of thalamic nuclei as in the Morel atlas. Nuclei are ordered into their relevant anatomical groups and sub-groups. Abbreviations used in text and in figures to segmented regions and volumes in Morel atlas are also given.

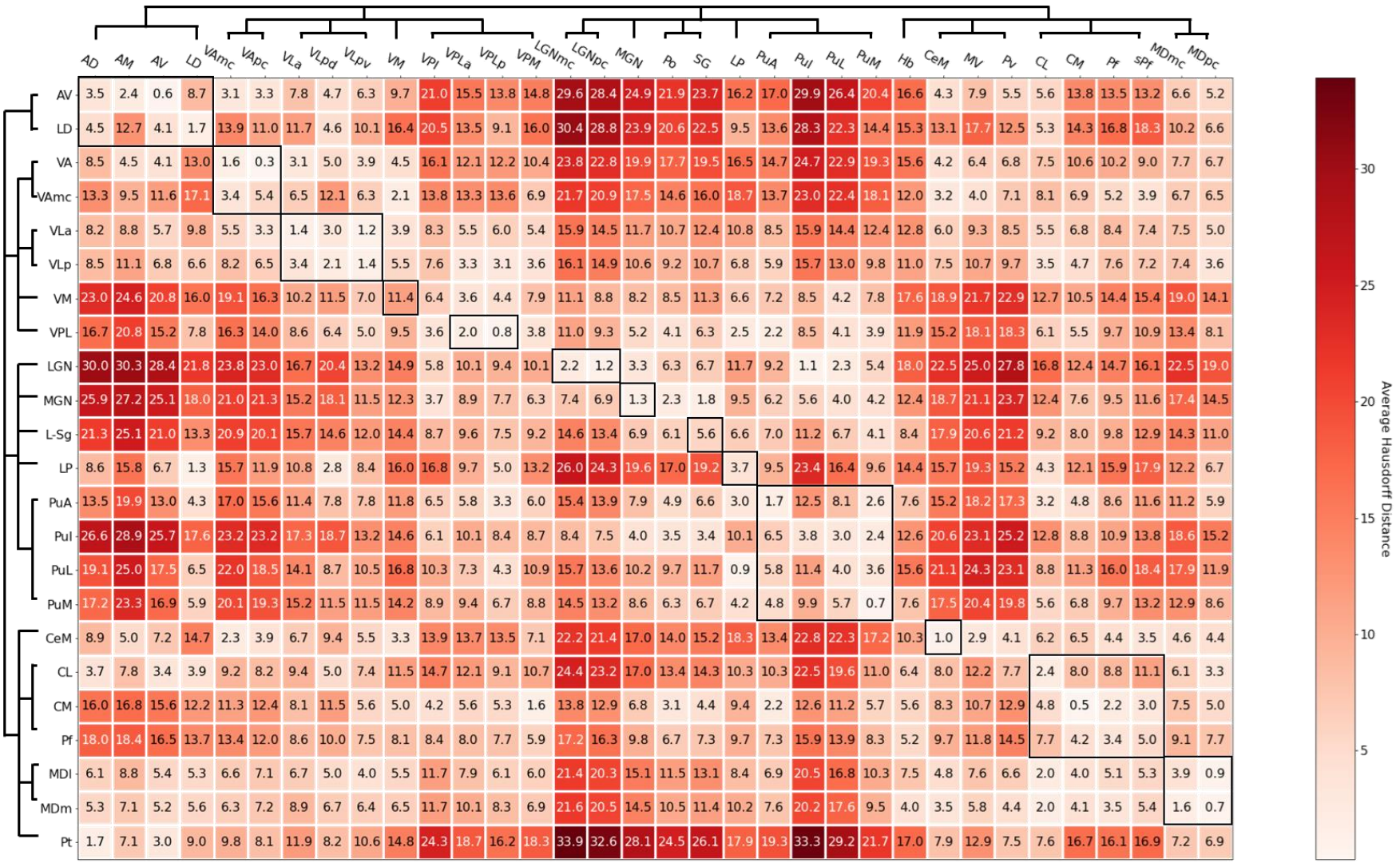
AD AM AV LD VAmc VApc VLa VLpd VLpv VM VPl VPLa VPLp VPM LGNmc LGNpc MGN Po SG LP PuA PuI PuL PuM Hb CeM MV Pv CL CM Pf sPf MDmc MDpc
AV 3.5 2.4 0.6 8.7 3.1 3.3 7.8 4.7 6.3 9.7 21.0 15.5 13.8 14.8 29.6 28.4 24.9 21.9 23.7 16.2 17.0 29.9 26.4 20.4 16.6 4.3 7.9 5.5 5.6 13.8 13.5 13.2 6.6 5.2
LD 4.5 12.7 4.1 1.7 13.9 11.0 11.7 4.6 10.1 16.4 20.5 13.5 9.1 16.0 30.4 28.8 23.9 20.6 22.5 9.5 13.6 28.3 22.3 14.4 15.3 13.1 17.7 12.5 5.3 14.3 16.8 18.3 10.2 6.6
VA 8.5 4.5 4.1 13.0 1.6 0.3 3.1 5.0 3.9 4.5 16.1 12.1 12.2 10.4 23.8 22.8 19.9 17.7 19.5 16.5 14.7 24.7 22.9 19.3 15.6 4.2 6.4 6.8 7.5 10.6 10.2 9.0 7.7 6.7
VAmc 13.3 9.5 11.6 17.1 3.4 5.4 6.5 12.1 6.3 2.1 13.8 13.3 13.6 6.9 21.7 20.9 17.5 14.6 16.0 18.7 13.7 23.0 22.4 18.1 12.0 3.2 4.0 7.1 8.1 6.9 5.2 3.9 6.7 6.5
VLa 8.2 8.8 5.7 9.8 5.5 3.3 1.4 3.0 1.2 3.9 8.3 5.5 6.0 5.4 15.9 14.5 11.7 10.7 12.4 10.8 8.5 15.9 14.4 12.4 12.8 6.0 9.3 8.5 5.5 6.8 8.4 7.4 7.5 5.0
VLp 8.5 11.1 6.8 6.6 8.2 6.5 3.4 2.1 1.4 5.5 7.6 3.3 3.1 3.6 16.1 14.9 10.6 9.2 10.7 6.8 5.9 15.7 13.0 9.8 11.0 7.5 10.7 9.7 3.5 4.7 7.6 7.2 7.4 3.6
VM 23.0 24.6 20.8 16.0 19.1 16.3 10.2 11.5 7.0 11.4 6.4 3.6 4.4 7.9 11.1 8.8 8.2 8.5 11.3 6.6 7.2 8.5 4.2 7.8 17.6 18.9 21.7 22.9 12.7 10.5 14.4 15.4 19.0 14.1
VPL 16.7 20.8 15.2 7.8 16.3 14.0 8.6 6.4 5.0 9.5 3.6 2.0 0.8 3.8 11.0 9.3 5.2 4.1 6.3 2.5 2.2 8.5 4.1 3.9 11.9 15.2 18.1 18.3 6.1 5.5 9.7 10.9 13.4 8.1
LGN 30.0 30.3 28.4 21.8 23.8 23.0 16.7 20.4 13.2 14.9 5.8 10.1 9.4 10.1 2.2 1.2 3.3 6.3 6.7 11.7 9.2 1.1 2.3 5.4 18.0 22.5 25.0 27.8 16.8 12.4 14.7 16.1 22.5 19.0
MGN 25.9 27.2 25.1 18.0 21.0 21.3 15.2 18.1 11.5 12.3 3.7 8.9 7.7 6.3 7.4 6.9 1.3 2.3 1.8 9.5 6.2 5.6 4.0 4.2 12.4 18.7 21.1 23.7 12.4 7.6 9.5 11.6 17.4 14.5
L-Sg 21.3 25.1 21.0 13.3 20.9 20.1 15.7 14.6 12.0 14.4 8.7 9.6 7.5 9.2 14.6 13.4 6.9 6.1 5.6 6.6 7.0 11.2 6.7 4.1 8.4 17.9 20.6 21.2 9.2 8.0 9.8 12.9 14.3 11.0
LP 8.6 15.8 6.7 1.3 15.7 11.9 10.8 2.8 8.4 16.0 16.8 9.7 5.0 13.2 26.0 24.3 19.6 17.0 19.2 3.7 9.5 23.4 16.4 9.6 14.4 15.7 19.3 15.2 4.3 12.1 15.9 17.9 12.2 6.7
PuA 13.5 19.9 13.0 4.3 17.0 15.6 11.4 7.8 7.8 11.8 6.5 5.8 3.3 6.0 15.4 13.9 7.9 4.9 6.6 3.0 1.7 12.5 8.1 2.6 7.6 15.2 18.2 17.3 3.2 4.8 8.6 11.6 11.2 5.9
PuI 26.6 28.9 25.7 17.6 23.2 23.2 17.3 18.7 13.2 14.6 6.1 10.1 8.4 8.7 8.4 7.5 4.0 3.5 3.4 10.1 6.5 3.8 3.0 2.4 12.6 20.6 23.1 25.2 12.8 8.8 10.9 13.8 18.6 15.2
PuL 19.1 25.0 17.5 6.5 22.0 18.5 14.1 8.7 10.5 16.8 10.3 7.3 4.3 10.9 15.7 13.6 10.2 9.7 11.7 0.9 5.8 11.4 4.0 3.6 15.6 21.1 24.3 23.1 8.8 11.3 16.0 18.4 17.9 11.9
PuM 17.2 23.3 16.9 5.9 20.1 19.3 15.2 11.5 11.5 14.2 8.9 9.4 6.7 8.8 14.5 13.2 8.6 6.3 6.7 4.2 4.8 9.9 5.7 0.7 7.6 17.5 20.4 19.8 5.6 6.8 9.7 13.2 12.9 8.6
CeM 8.9 5.0 7.2 14.7 2.3 3.9 6.7 9.4 5.5 3.3 13.9 13.7 13.5 7.1 22.2 21.4 17.0 14.0 15.2 18.3 13.4 22.8 22.3 17.2 10.3 1.0 2.9 4.1 6.2 6.5 4.4 3.5 4.6 4.4
CL 3.7 7.8 3.4 3.9 9.2 8.2 9.4 5.0 7.4 11.5 14.7 12.1 9.1 10.7 24.4 23.2 17.0 13.4 14.3 10.3 10.3 22.5 19.6 11.0 6.4 8.0 12.2 7.7 2.4 8.0 8.8 11.1 6.1 3.3
CM 16.0 16.8 15.6 12.2 11.3 12.4 8.1 11.5 5.6 5.0 4.2 5.6 5.3 1.6 13.8 12.9 6.8 3.1 4.4 9.4 2.2 12.6 11.2 5.7 5.6 8.3 10.7 12.9 4.8 0.5 2.2 3.0 7.5 5.0
Pf 18.0 18.4 16.5 13.7 13.4 12.0 8.6 10.0 7.5 8.1 8.4 8.0 7.7 5.9 17.2 16.3 9.8 6.7 7.3 9.7 7.3 15.9 13.9 8.3 5.2 9.7 11.8 14.5 7.7 4.2 3.4 5.0 9.1 7.7
MDl 6.1 8.8 5.4 5.3 6.6 7.1 6.7 5.0 4.0 5.5 11.7 7.9 6.1 6.0 21.4 20.3 15.1 11.5 13.1 8.4 6.9 20.5 16.8 10.3 7.5 4.8 7.6 6.6 2.0 4.0 5.1 5.3 3.9 0.9
MDm 5.3 7.1 5.2 5.6 6.3 7.2 8.9 6.7 6.4 6.5 11.7 10.1 8.3 6.9 21.6 20.5 14.5 10.5 11.4 10.2 7.6 20.2 17.6 9.5 4.0 3.5 5.8 4.4 2.0 4.1 3.5 5.4 1.6 0.7
Pt 1.7 7.1 3.0 9.0 9.8 8.1 11.9 8.2 10.6 14.8 24.3 18.7 16.2 18.3 33.9 32.6 28.1 24.5 26.1 17.9 19.3 33.3 29.2 21.7 17.0 7.9 12.9 7.5 7.6 16.7 16.1 16.9 7.2 6.9
Average Hausdorff Distance
30
25
20
15
10
5

Figure 11 Average Hausdorff Distance between segmented (vertical axis) regions and volumes in the Morel atlas (horizontal axis) in the left thalamus. Higher Average Hausdorff Distances shows there is greater dissimilarity and that segmented regions and volumes in the Morel atlas are less isometric. Dendrograms show the hierarchical structure of nuclei within the thalamus. Average Hausdorff Distances within BOLD boxes along the diagonal are show regions that are part of the same nuclear group or sub-group.

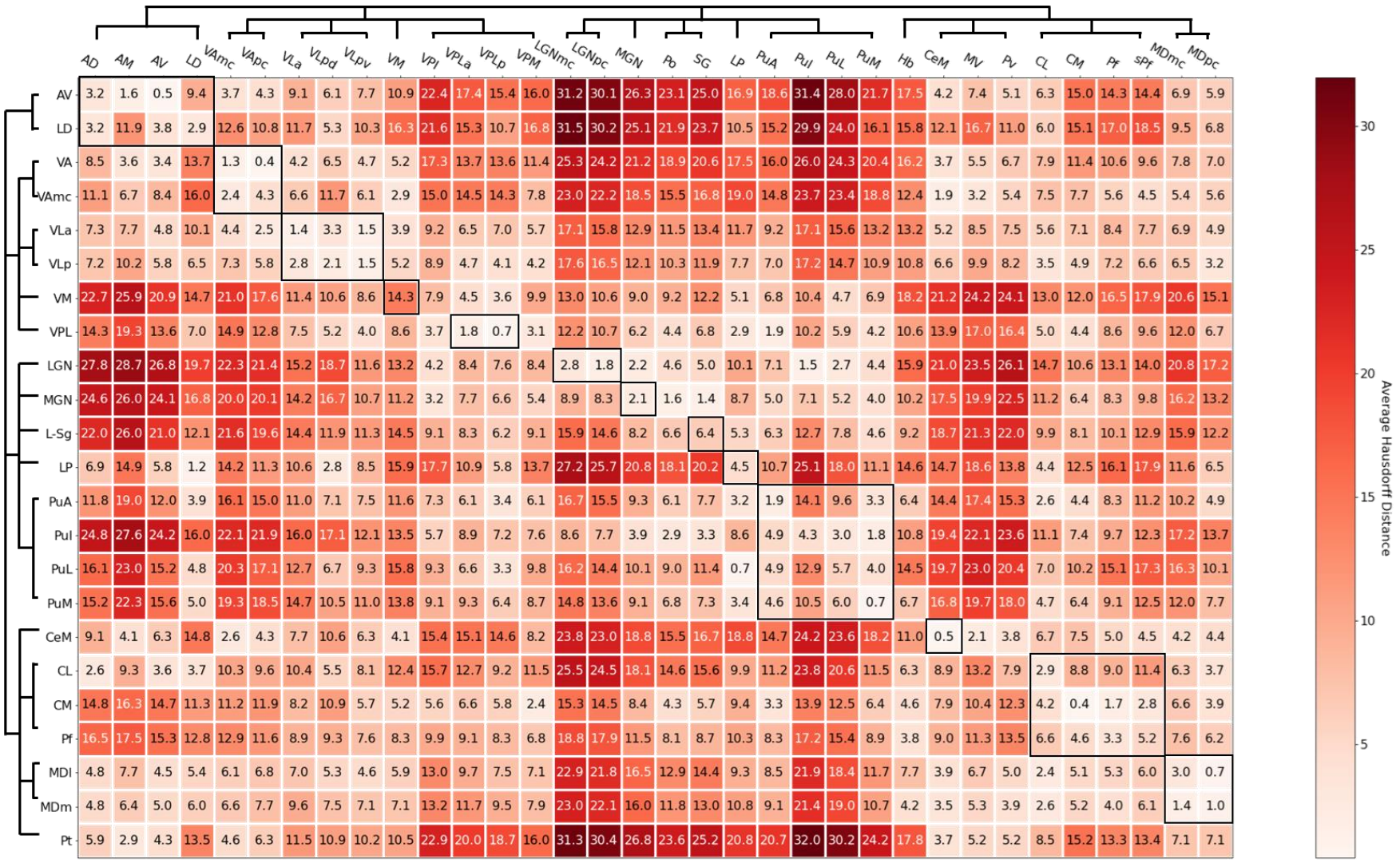
AD AM AV LD VAmc VApc VLa VLpd VLpv VM VPl VPLa VPLp VPM LGNmc LGNpc MGN Po SG LP PuA PuI PuL PuM Hb CeM MV Pv CL CM Pf sPf MDmc MDpc
AV 3.2 1.6 0.5 9.4 3.7 4.3 9.1 6.1 7.7 10.9 22.4 17.4 15.4 16.0 31.2 30.1 26.3 23.1 25.0 16.9 18.6 31.4 28.0 21.7 17.5 4.2 7.4 5.1 6.3 15.0 14.3 14.4 6.9 5.9
LD 3.2 11.9 3.8 2.9 12.6 10.8 11.7 5.3 10.3 16.3 21.6 15.3 10.7 16.8 31.5 30.2 25.1 21.9 23.7 10.5 15.2 29.9 24.0 16.1 15.8 12.1 16.7 11.0 6.0 15.1 17.0 18.5 9.5 6.8
VA 8.5 3.6 3.4 13.7 1.3 0.4 4.2 6.5 4.7 5.2 17.3 13.7 13.6 11.4 25.3 24.2 21.2 18.9 20.6 17.5 16.0 26.0 24.3 20.4 16.2 3.7 5.5 6.7 7.9 11.4 10.6 9.6 7.8 7.0
VAmc 11.1 6.7 8.4 16.0 2.4 4.3 6.6 11.7 6.1 2.9 15.0 14.5 14.3 7.8 23.0 22.2 18.5 15.5 16.8 19.0 14.8 23.7 23.4 18.8 12.4 1.9 3.2 5.4 7.5 7.7 5.6 4.5 5.4 5.6
VLa 7.3 7.7 4.8 10.1 4.4 2.5 1.4 3.3 1.5 3.9 9.2 6.5 7.0 5.7 17.1 15.8 12.9 11.5 13.4 11.7 9.2 17.1 15.6 13.2 13.2 5.2 8.5 7.5 5.6 7.1 8.4 7.7 6.9 4.9
VLp 7.2 10.2 5.8 6.5 7.3 5.8 2.8 2.1 1.5 5.2 8.9 4.7 4.1 4.2 17.6 16.5 12.1 10.3 11.9 7.7 7.0 17.2 14.7 10.9 10.8 6.6 9.9 8.2 3.5 4.9 7.2 6.6 6.5 3.2
VM 22.7 25.9 20.9 14.7 21.0 17.6 11.4 10.6 8.6 14.3 7.9 4.5 3.6 9.9 13.0 10.6 9.0 9.2 12.2 5.1 6.8 10.4 4.7 6.9 18.2 21.2 24.2 24.1 13.0 12.0 16.5 17.9 20.6 15.1
VPL 14.3 19.3 13.6 7.0 14.9 12.8 7.5 5.2 4.0 8.6 3.7 1.8 0.7 3.1 12.2 10.7 6.2 4.4 6.8 2.9 1.9 10.2 5.9 4.2 10.6 13.9 17.0 16.4 5.0 4.4 8.6 9.6 12.0 6.7
LGN 27.8 28.7 26.8 19.7 22.3 21.4 15.2 18.7 11.6 13.2 4.2 8.4 7.6 8.4 2.8 1.8 2.2 4.6 5.0 10.1 7.1 1.5 2.7 4.4 15.9 21.0 23.5 26.1 14.7 10.6 13.1 14.0 20.8 17.2
MGN 24.6 26.0 24.1 16.8 20.0 20.1 14.2 16.7 10.7 11.2 3.2 7.7 6.6 5.4 8.9 8.3 2.1 1.6 1.4 8.7 5.0 7.1 5.2 4.0 10.2 17.5 19.9 22.5 11.2 6.4 8.3 9.8 16.2 13.2
L-Sg 22.0 26.0 21.0 12.1 21.6 19.6 14.4 11.9 11.3 14.5 9.1 8.3 6.2 9.1 15.9 14.6 8.2 6.6 6.4 5.3 6.3 12.7 7.8 4.6 9.2 18.7 21.3 22.0 9.9 8.1 10.1 12.9 15.9 12.2
LP 6.9 14.9 5.8 1.2 14.2 11.3 10.6 2.8 8.5 15.9 17.7 10.9 5.8 13.7 27.2 25.7 20.8 18.1 20.2 4.5 10.7 25.1 18.0 11.1 14.6 14.7 18.6 13.8 4.4 12.5 16.1 17.9 11.6 6.5
PuA 11.8 19.0 12.0 3.9 16.1 15.0 11.0 7.1 7.5 11.6 7.3 6.1 3.4 6.1 16.7 15.5 9.3 6.1 7.7 3.2 1.9 14.1 9.6 3.3 6.4 14.4 17.4 15.3 2.6 4.4 8.3 11.2 10.2 4.9
PuI 24.8 27.6 24.2 16.0 22.1 21.9 16.0 17.1 12.1 13.5 5.7 8.9 7.2 7.6 8.6 7.7 3.9 2.9 3.3 8.6 4.9 4.3 3.0 1.8 10.8 19.4 22.1 23.6 11.1 7.4 9.7 12.3 17.2 13.7
PuL 16.1 23.0 15.2 4.8 20.3 17.1 12.7 6.7 9.3 15.8 9.3 6.6 3.3 9.8 16.2 14.4 10.1 9.0 11.4 0.7 4.9 12.9 5.7 4.0 14.5 19.7 23.0 20.4 7.0 10.2 15.1 17.3 16.3 10.1
PuM 15.2 22.3 15.6 5.0 19.3 18.5 14.7 10.5 11.0 13.8 9.1 9.3 6.4 8.7 14.8 13.6 9.1 6.8 7.3 3.4 4.6 10.5 6.0 0.7 6.7 16.8 19.7 18.0 4.7 6.4 9.1 12.5 12.0 7.7
CeM 9.1 4.1 6.3 14.8 2.6 4.3 7.7 10.6 6.3 4.1 15.4 15.1 14.6 8.2 23.8 23.0 18.8 15.5 16.7 18.8 14.7 24.2 23.6 18.2 11.0 0.5 2.1 3.8 6.7 7.5 5.0 4.5 4.2 4.4
CL 2.6 9.3 3.6 3.7 10.3 9.6 10.4 5.5 8.1 12.4 15.7 12.7 9.2 11.5 25.5 24.5 18.1 14.6 15.6 9.9 11.2 23.8 20.6 11.5 6.3 8.9 13.2 7.9 2.9 8.8 9.0 11.4 6.3 3.7
CM 14.8 16.3 14.7 11.3 11.2 11.9 8.2 10.9 5.7 5.2 5.6 6.6 5.8 2.4 15.3 14.5 8.4 4.3 5.7 9.4 3.3 13.9 12.5 6.4 4.6 7.9 10.4 12.3 4.2 0.4 1.7 2.8 6.6 3.9
Pf 16.5 17.5 15.3 12.8 12.9 11.6 8.9 9.3 7.6 8.3 9.9 9.1 8.3 6.8 18.8 17.9 11.5 8.1 8.7 10.3 8.3 17.2 15.4 8.9 3.8 9.0 11.3 13.5 6.6 4.6 3.3 5.2 7.6 6.2
MDl 4.8 7.7 4.5 5.4 6.1 6.8 7.0 5.3 4.6 5.9 13.0 9.7 7.5 7.1 22.9 21.8 16.5 12.9 14.4 9.3 8.5 21.9 18.4 11.7 7.7 3.9 6.7 5.0 2.4 5.1 5.3 6.0 3.0 0.7
MDm 4.8 6.4 5.0 6.0 6.6 7.7 9.6 7.5 7.1 7.1 13.2 11.7 9.5 7.9 23.0 22.1 16.0 11.8 13.0 10.8 9.1 21.4 19.0 10.7 4.2 3.5 5.3 3.9 2.6 5.2 4.0 6.1 1.4 1.0
Pt 5.9 2.9 4.3 13.5 4.6 6.3 11.5 10.9 10.2 10.5 22.9 20.0 18.7 16.0 31.3 30.4 26.8 23.6 25.2 20.8 20.7 32.0 30.2 24.2 17.8 3.7 5.2 5.2 8.5 15.2 13.3 13.4 7.1 7.1
Average Hausdorff Distance
30
25
20
15
10
5

Figure 12 Average Hausdorff Distance between segmented (vertical axis) regions and volumes in the Morel atlas (horizontal axis) in the right thalamus. Higher Average Hausdorff Distances shows there is greater dissimilarity and that segmented regions and volumes in the Morel atlas are less isometric. Dendrograms show the hierarchical structure of nuclei within the thalamus. Average Hausdorff Distances within BOLD boxes along the diagonal are show regions that are part of the same nuclear group or sub-group.

Segmentation	Morel	Distance (voxels)	Segmentation	Morel	Distance (voxels)
Left			**Right**		
VA	VApc	0.332751	VA	VApc	0.431525
CM	CM	0.460216	CM	CM	0.437139
AV	AV	0.63198	AV	AV	0.515158
PuM	PuM	0.659518	CeM	CeM	0.542475
MDm	MDpc	0.735318	PuL	LP	0.66192
VPL	VPLp	0.782243	VPL	VPLp	0.663946
MDl	MDpc	0.873007	MDl	MDpc	0.709001
PuL	LP	0.878453	PuM	PuM	0.74441
CeM	CeM	1.00372	MDm	MDpc	1.047935
LGN	PuI	1.130774	LP	LD	1.163396
VLa	VLpv	1.19992	MGN	SG	1.354912
LP	LD	1.255153	VLa	VLa	1.363725
MGN	MGN	1.334352	VLp	VLpv	1.453629
VLp	VLpv	1.364389	LGN	PuI	1.493237
PuA	PuA	1.666463	PuI	PuM	1.843849
Pt	AD	1.684479	VAmc	CeM	1.864043
LD	LD	1.743449	PuA	PuA	1.943745
VAmc	VM	2.13865	CL	AD	2.583181
PuI	PuM	2.371877	LD	LD	2.850019
CL	CL	2.379825	Pt	AM	2.938476
Pf	Pf	3.431893	Pf	Pf	3.263468
VM	VPLa	3.63583	VM	VPLp	3.556207
L-Sg	PuM	4.061324	L-Sg	PuM	4.555451

Table 3 Lowest Average Hausdorff Distance between each segmentation and its corresponding volume within the Morel atlas. Higher Average Hausdorff Distances shows there is greater dissimilarity and that segmented regions and volumes in the Morel atlas are less isometric.

Segmentation	Morel	Distance (voxels)	Segmentation	Morel	Distance (voxels)
Left			**Right**		
VA	VApc	0.332751	VA	VApc	0.431525
CM	CM	0.460216	CM	CM	0.437139
AV	AV	0.63198	AV	AV	0.515158
PuM	PuM	0.659518	CeM	CeM	0.542475
MDm	MDpc	0.735318	PuL	LP	0.66192
VPL	VPLp	0.782243	VPL	VPLp	0.663946
PuL	LP	0.878453	MDl	MDpc	0.709001
CeM	CeM	1.00372	PuM	PuM	0.74441
LGN	PuI	1.130774	LP	LD	1.163396
LGN	LGNpc	1.19418	VA	VAmc	1.270166
VLa	VLpv	1.19992	MGN	SG	1.354912
LP	LD	1.255153	VLa	VLa	1.363725
MGN	MGN	1.334352	MDm	MDmc	1.407938
VLa	VLa	1.379999	VLp	VLpv	1.453629
VA	VAmc	1.618183	LGN	PuI	1.493237
CM	VPM	1.636273	AV	AM	1.636578
MDm	MDmc	1.646026	MGN	Po	1.641001
PuA	PuA	1.666463	CM	Pf	1.693499
Pt	AD	1.684479	LGN	LGNpc	1.762076
MGN	SG	1.757686	VPL	VPLa	1.82221
MDm	CL	1.963445	VPL	PuA	1.909816
VPL	VPLa	1.971193	VLp	VLpd	2.062684
VLp	VLpd	2.128442	MGN	MGN	2.08619
VAmc	VM	2.13865	CeM	MV	2.137629
LGN	LGNmc	2.169776	CM	VPM	2.396707
CM	Pf	2.18454	MDl	CL	2.447928
MGN	Po	2.294516	CL	AD	2.583181
LGN	PuL	2.330049	LGN	PuL	2.668344
AV	AM	2.39251	CM	sPf	2.785892
CeM	MV	2.945644	LGN	LGNmc	2.818837
CM	sPf	3.005708	VAmc	VM	2.924402
VPL	VPI	3.562672	MGN	VPI	3.220601
MDm	Hb	4.016412	CeM	Pv	3.809648
CeM	Pv	4.120213	Pf	Hb	3.843084

Table 4 Lowest Average Hausdorff Distance between volumes within the Morel atlas and its corresponding segmentation. Higher Average Hausdorff Distances shows there is greater dissimilarity and that segmented regions and volumes in the Morel atlas are less isometric.

Lastly, we calculated the Spearman's correlation coefficient between the volume of segmentations and their Average Hausdorff Distance to determine whether segmentation size affected dissimilarity and found they were significantly anticorrelated $t(42) = -3.4575$, $r = -0.471$, $p = 0.001$ (Figure 13). Visually, this trend looked like it was driven by segmentations with volumes at the tail end of the plot. Therefore, we performed an exploratory analysis to test what effect removing these values had on the relationship. To do this we removed the five smallest nuclei bilaterally (CL, LD, L-Sg, VAmc, VM) which all had volumes lower than $21mm^3$, and used this as a threshold to re-run the correlation. Removing these values reduced the strength of the relationship, and meant the correlation was non-significant $t(32) = -1.602$, $r = -0.273$, $p = 0.119$.

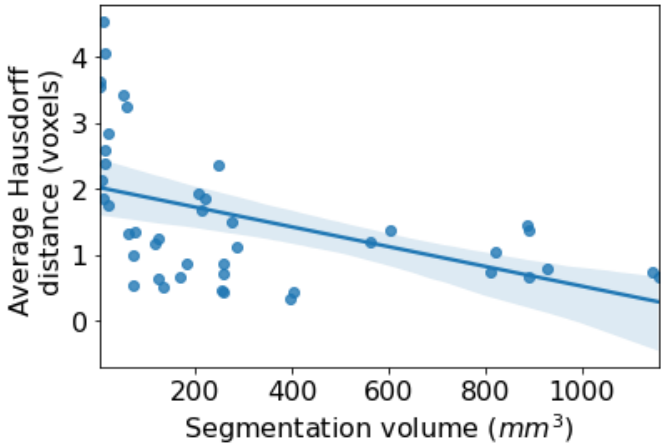

Figure 13 Spearman's correlation between segmentation volumes and Average Hausdorff Distances. A significant weak correlation was found between segmented volumes and Average Hausdorff Distances (r = -0.471, p = 0.001). This correlation was no longer significant after segmented volumes < $21mm^3$ were removed from analysis, suggesting this negative relationship was driven by regions that were not properly segmented and as such had very small volumes. The following regions within the Morel atlas are combined for the purpose of statistical analysis (LGN = (LGNmc + LGNpc), VA = (VAmc + VApc), VLp = (VLpd + VLpv), VPL = (VPLa + VPLp).

Discussion

The thalamus is known to be important for a wide range of cognitive processes, yet delineating and studying the roles of specific nuclei in aspects of cognition is a non-trivial problem in human neuroimaging. Here, we systematically compare the segmentation approach developed by Iglesias et al. (2018) to the Morel atlas of the thalamus (Krauth et al., 2010; Morel et al., 1997) using data from the Human Connectome project. We use DICE coefficients to measure volume overlap, and the Average Hausdorff Distance to compare the closeness and how isometric the segmentations are relative to the nuclei in the Morel atlas. Firstly, we found mixed levels of overlap across anterior, lateral, posterior and medial portions of the thalamus, and at the group level we found the volumes for all nuclei were significantly different to the defined regions within the Morel atlas. Nuclei had lower Average Hausdorff Distances within groups than across groups, showing segmentations clearly discriminated between anterior, lateral, medial and posterior portions of the thalamus.

We assessed whether there was a systematic effect of geometry on the isometry of segmented nuclei relative to the atlas. We found a significant negative correlation between the size of the segmented volume and the Average Hausdorff Distance; this significance did not remain after the five smallest nuclei (all with a volume < 21mm^3) were removed from the analysis, suggesting this relationship was driven by an inability to segment these nuclei with smaller values, rather than changes in isometry across nuclei size.

The segmentation approach developed by Iglesias et al. (2018) showed substantial overlap as indexed using the DICE coefficient for one nucleus within each of the anterior, lateral, posterior and midline thalamus (AV, VA, PuM, and CM respectively). Conversely, slight overlap between segmentations and their corresponding region in the Morel atlas was seen for a single segmentation in the anterior thalamus (VAmc), and four regions in the posterior thalamus (LGN, MGN, L-Sg, and LP). The geniculate nuclei may be particularly difficult for the algorithm to segment due to their location on the exterior of the thalamus, adjacent to the pulvinar. Indeed, we see comparable DICE coefficients, particularly for the LGN, between the segmented LGN region and the inferior and lateral pulvinar regions as defined by the Morel atlas. The posterior region was also the only portion of the thalamus to show greater than slight overlap with nuclei in other regions of the thalamus; both the LP and PuA showed fair bilateral overlap with the LD in the anterior thalamus, and the CL in the medial thalamus. Therefore, this segmentation approach formed clear anatomical boundaries between the anterior, lateral and medial thalamus, but not the posterior thalamus. Additionally, the delineation of nuclei within each sub-region of the anterior, lateral, and medial thalamus appeared to be more distinct than in the posterior thalamus, as indicated by an increased

number of nuclei with only slight overlap and being the only group of nuclei showing greater than slight overlap with nuclei from other groups.

There were significant volumetric differences for all nuclei between the volume as segmented by the automated algorithm and the Morel atlas. One potential explanation for this is that the Morel atlas, which was converted into MNI space (Krauth et al., 2010) was not corrected for the effects of fixation during the preparation of the tissue. Fixation with solutions such as formalin or paraformaldehyde is an important step when working with biological specimens as it limits the decomposition of biological tissue; yet fixation also causes tissue to shrink. The atlas derived by Morel from cyto- and myeloarchitecture was not corrected for shrinkage due to fixation (Bender et al., 2011), therefore, the atlas produced by Krauth et al, (2010) may include slight distortions of the morphometry of thalamic nuclei in-vivo. Another possible reason for our observed volumetric differences between the segmentation and the atlas is that the initial template used to begin segmentation is the whole thalamus volume estimated by *recon-all* in FreeSurfer. *Recon-all* has previously been shown to over-estimate the volume of the thalamus relative to manually derived segmentations of the whole thalamus, and in particular for participants with volumes at the lower end of the distribution (Makowski et al., 2018). Nevertheless, these explanations cannot fully describe why we observed volumetric differences for most nuclei as segmentations were generally smaller than those produced by the Morel atlas, with the exceptions being the LGN, MDm, PuA, PuI, and VLa. One reason may be that certain nuclei are overestimated, and others are underestimated, while the general trend for nuclei volume remains consistent between segmentations and the Morel atlas. Our correlational results between segmented and atlas volumes suggest this may be the case, as we see a moderate positive correlation between the two sets of volumes. Reductions of these volumetric differences may be improved by combining diffusion and anatomical data as proposed by (Iglesias et al., 2019), yet there is currently no publicly available implementation for the approach they describe.

In their original paper describing their segmentation algorithm, Iglesias and colleagues do provide volumetric comparisons for six regions within the thalamus, namely the AV, LP, CM, MD (composite of MDl and MDm), VL (composite of VLa and VLp), and the pulvinar (PuA, PuM, PuL, and PuI combined) in 66 subjects. However, their approach involves the transformation of the equivalent Morel nuclei into subject space before plotting the distributions for each nucleus. Though this provides a visual overview of the relationship between segmented volumes and the Morel atlas, no inferential statistics are used to characterise this relationship. Additionally, though the authors state these regions were chosen based on their functional and structural connectivity, it is unclear why other nuclei were not also selected. Based on our metrics we see these regions appear

well segmented at the group level, except for the LP. Here, we systematically show that, although there is a positive relationship between segmented volumes and volumes in the Morel atlas, these volumes are significantly different across all regions. Furthermore, we also extend upon the work of Iglesias et al. (2018) by describing differences in the overlap and isometry between segmented nuclei and regions within the Morel atlas, and show that not all regions can be delineated as clearly as those selected in the original paper for comparison. These insights are important if this segmentation approach is used to make inferences about the role these nuclei play in cognitive processes, or how aberrant changes in the thalamus occur in disease (Elvsåshagen et al., 2021; Park et al., 2020).

While it is important to have segmentations that are faithful to their underlying neuroanatomy, it is also worth being pragmatic about the limitations of automated segmentations and how we use them. At the implementation level it is likely that heterogeneity in segmentation results will be observed across and within participants. For example, these differences could be driven by changes in signal, intensity, and noise across multiple acquisitions within the same individual (Kiar et al., 2020). Other implementation-based sources of variance include differences across operating system and software versions. For example, estimates of anatomical volumes is known to be inconsistent across versions of FreeSurfer (Gronenschild et al., 2012), while differences if floating point arithmetic across operating systems and versions have also been shown to influence analyses (Glatard et al., 2015). Practical solutions, such as the use of Docker and Singularity containers, enable the homogenisation of computational resource, yet they cannot address inherent differences in image acquisition.

More broadly, the biological plausibility of measures should also be considered when applying automated segmentation processes to study structure and function. Differences, such as those that are clinically relevant or that change across developmental trajectories, should be observed at a level that is greater than noise that could be due to within-individual variance or computational set-up. These differences, even if small should be shown to be at least qualitatively reproducible.

Additional considerations regarding biological plausibility include the application of automatic segmentation tools. As an example, the original pipeline in this study involved the use of FLIRT and FNIRT in FSL to convert images from subject space to MNI space. Yet, we found that these algorithms were unsuitable in terms of their accuracy for providing transformations within the thalamus. We therefore amended our pipeline to use ANTs, rather than FSL for normalisation. Additionally, it is worth considering the utility of applying these methods to studying functional activation. For instance, the use of these segmentation techniques in studies with typical 3 tesla

acquisition and analysis parameters (e.g. $3mm^3$ voxels, 8mm smoothing kernel) would mean that it is likely that functionally relevant signal is not localised to specific thalamic nuclei. Therefore, we suggest that those wishing to study the relevance of thalamic nuclei to functional processes carefully consider acquisition and processing pipelines with respect to the metrics provided here to restrict the integration of signal across regions of the thalamus. For instance, investigators may find it beneficial to combine segmentations from regions with high overlap and functional homogeneity, such as the subnuclei of the mediodorsal thalamus, to improve the anatomical definition of their region of interest. Furthermore, consideration of the size of segmented nuclei in relation to acquisition and processing parameters are important to determine whether it could be considered feasible to acquire clean signal from a given region.

In conclusion, this paper aimed to systematically validate the thalamic nuclei segmentation approach developed by Iglesias et al. (2018) using Human Connectome Project data and the Morel thalamic atlas derived from histological staining post-mortem (Krauth et al., 2010). We show using volumetric, overlap, and isometry measures that the automated segmentation approach clearly delineates between groups of nuclei across anterior, lateral, posterior and medial portions of the thalamus, and that there is mixed segmentation efficacy within groups. Furthermore, although we find a positive relationship between segmented nuclei and their equivalent volumes in the Morel atlas, we do find that segmentation volumes are significantly different from those defined in the atlas. We also suggest important considerations related to the functional relevance of these segmentations and describe potential pitfalls researchers may face when using these segmentations within their own research.

Acknowledgements:

The authors would like to thank ETH Zurich and the University of Zurich for the provision of the Morel atlas in MNI space as described in (Krauth et al., 2010).

Appendix:

Appendix 1: HCP subject IDs used for analysis

192237	907656	131419	118831	281135
871762	105923	186545	325129	932554
180937	814548	660951	486759	371843
919966	782561	233326	188751	169444
217126	128127	129634	108828	210415
180129	809252	108121	305830	441939
207123	197348	760551	154532	186444
111413	547046	198451	251833	580650
189349	657659	103818	581450	156536
153025	581349	517239	436239	894774
971160	145834	300719	148335	111211
209329	102614	250932	146432	217429
379657	172130	155938	194443	194746
886674	679568	955465	173940	395251
633847	192540	179245	448347	570243
202719	135225	562345	307127	529549
654552	615744	133928	150928	172332
318637	611938	127933	180230	167440
286650	594156	654754	209228	154229

161832	576255	133625	917558	220721

References:

Amini, L., Soltanian-Zadeh, H., Lucas, C., & Gity, M. (2004). Automatic segmentation of thalamus from brain MRI integrating fuzzy clustering and dynamic contours. *IEEE Transactions on Biomedical Engineering*, *51*(5), 800–811. https://doi.org/10.1109/TBME.2004.826654

Avants, B. B., Epstein, C. L., Grossman, M., & Gee, J. C. (2008). Symmetric diffeomorphic image registration with cross-correlation: Evaluating automated labeling of elderly and neurodegenerative brain. *Medical Image Analysis*, *12*(1), 26–41. https://doi.org/10.1016/j.media.2007.06.004

Battistella, G., Najdenovska, E., Maeder, P., Ghazaleh, N., Daducci, A., Thiran, J.-P., Jacquemont, S., Tuleasca, C., Levivier, M., Bach Cuadra, M., & Fornari, E. (2017). Robust thalamic nuclei segmentation method based on local diffusion magnetic resonance properties. *Brain Structure & Function*, *222*(5), 2203–2216. https://doi.org/10.1007/s00429-016-1336-4

Behrens, T. E. J., Johansen-Berg, H., Woolrich, M. W., Smith, S. M., Wheeler-Kingshott, C. A. M., Boulby, P. A., Barker, G. J., Sillery, E. L., Sheehan, K., Ciccarelli, O., Thompson, A. J., Brady, J. M., & Matthews, P. M. (2003). Non-invasive mapping of connection between human thalamus and cortex using diffusion imaging. *Nature Neuroscience*, *6*(7), 750–757. https://doi.org/10.1038/nn1075

Bender, B., Mänz, C., Korn, A., Nägele, T., & Klose, U. (2011). Optimized 3D Magnetization-Prepared Rapid Acquisition of Gradient Echo: Identification of Thalamus Substructures at 3T. *American Journal of Neuroradiology*, *32*(11), 2110–2115. https://doi.org/10.3174/ajnr.A2705

Bender, B., Wagner, S., & Klose, U. (2017). Optimized depiction of thalamic substructures with a combination of T1-MPRAGE and phase: MPRAGE*. *Clinical Neuroradiology*, *27*(4), 511–518. https://doi.org/10.1007/s00062-016-0513-4

Deoni, S. C. L., Rutt, B. K., Parrent, A. G., & Peters, T. M. (2007). Segmentation of thalamic nuclei using a modified k-means clustering algorithm and high-resolution quantitative magnetic resonance imaging at 1.5 T. *NeuroImage*, *34*(1), 117–126. https://doi.org/10.1016/j.neuroimage.2006.09.016

Elvsåshagen, T., Shadrin, A., Frei, O., van der Meer, D., Bahrami, S., Kumar, V. J., Smeland, O., Westlye, L. T., Andreassen, O. A., & Kaufmann, T. (2021). The genetic architecture of the human thalamus and its overlap with ten common brain disorders. *Nature Communications*, *12*(1), 2909. https://doi.org/10.1038/s41467-021-23175-z

Geier, K. T., Buchsbaum, B. R., Parimoo, S., & Olsen, R. K. (2020). The role of anterior and medial dorsal thalamus in associative memory encoding and retrieval. *Neuropsychologia*, *148*, 107623. https://doi.org/10.1016/j.neuropsychologia.2020.107623

Glasser, M. F., Sotiropoulos, S. N., Wilson, J. A., Coalson, T. S., Fischl, B., Andersson, J. L., Xu, J., Jbabdi, S., Webster, M., Polimeni, J. R., Van Essen, D. C., & Jenkinson, M. (2013). The minimal preprocessing pipelines for the Human Connectome Project. *NeuroImage*, *80*, 105–124. https://doi.org/10.1016/j.neuroimage.2013.04.127

Glatard, T., Lewis, L. B., Ferreira da Silva, R., Adalat, R., Beck, N., Lepage, C., Rioux, P., Rousseau, M.-E., Sherif, T., Deelman, E., Khalili-Mahani, N., & Evans, A. C. (2015).

Reproducibility of neuroimaging analyses across operating systems. *Frontiers in Neuroinformatics*, *9*. https://doi.org/10.3389/fninf.2015.00012

Gronenschild, E. H. B. M., Habets, P., Jacobs, H. I. L., Mengelers, R., Rozendaal, N., Os, J. van, & Marcelis, M. (2012). The Effects of FreeSurfer Version, Workstation Type, and Macintosh Operating System Version on Anatomical Volume and Cortical Thickness Measurements. *PLOS ONE*, *7*(6), e38234. https://doi.org/10.1371/journal.pone.0038234

Horien, C., Noble, S., Greene, A. S., Lee, K., Barron, D. S., Gao, S., O'Connor, D., Salehi, M., Dadashkarimi, J., Shen, X., Lake, E. M. R., Constable, R. T., & Scheinost, D. (2021). A hitchhiker's guide to working with large, open-source neuroimaging datasets. *Nature Human Behaviour*, *5*(2), 185–193. https://doi.org/10.1038/s41562-020-01005-4

Huang, A. S., Rogers, B. P., & Woodward, N. D. (2019). Disrupted modulation of thalamus activation and thalamocortical connectivity during dual task performance in schizophrenia. *Schizophrenia Research*, *210*, 270–277. https://doi.org/10.1016/j.schres.2018.12.022

Iglesias, J. E., Insausti, R., Lerma-Usabiaga, G., Bocchetta, M., Van Leemput, K., Greve, D. N., van der Kouwe, A., Fischl, B., Caballero-Gaudes, C., & Paz-Alonso, P. M. (2018). A probabilistic atlas of the human thalamic nuclei combining ex vivo MRI and histology. *NeuroImage*, *183*, 314–326. https://doi.org/10.1016/j.neuroimage.2018.08.012

Iglesias, J. E., Van Leemput, K., Golland, P., & Yendiki, A. (2019). Joint inference on structural and diffusion MRI for sequence-adaptive Bayesian segmentation of thalamic nuclei with probabilistic atlases. *Information Processing in Medical Imaging : Proceedings of the ... Conference*, *11492*, 767–779. https://doi.org/10.1007/978-3-030-20351-1_60

Johansen-Berg, H., Behrens, T. E. J., Sillery, E., Ciccarelli, O., Thompson, A. J., Smith, S. M., & Matthews, P. M. (2005). Functional–Anatomical Validation and Individual Variation of Diffusion Tractography-based Segmentation of the Human Thalamus. *Cerebral Cortex*, *15*(1), 31–39. https://doi.org/10.1093/cercor/bhh105

Kiar, G., Castro, P. de O., Rioux, P., Petit, E., Brown, S. T., Evans, A. C., & Glatard, T. (2020). Comparing perturbation models for evaluating stability of neuroimaging pipelines: *The International Journal of High Performance Computing Applications*. https://doi.org/10.1177/1094342020926237

Kim, D.-J., Park, B., & Park, H.-J. (2013). Functional connectivity-based identification of subdivisions of the basal ganglia and thalamus using multilevel independent component analysis of resting state fMRI. *Human Brain Mapping*, *34*(6), 1371–1385. https://doi.org/10.1002/hbm.21517

Krauth, A., Blanc, R., Poveda, A., Jeanmonod, D., Morel, A., & Székely, G. (2010). A mean three-dimensional atlas of the human thalamus: Generation from multiple histological data. *NeuroImage*, *49*(3), 2053–2062. https://doi.org/10.1016/j.neuroimage.2009.10.042

Lambert, C., Simon, H., Colman, J., & Barrick, T. R. (2017). Defining thalamic nuclei and topographic connectivity gradients in vivo. *NeuroImage*, *158*, 466–479. https://doi.org/10.1016/j.neuroimage.2016.08.028

Magnotta, V. A., Gold, S., Andreasen, N. C., Ehrhardt, J. C., & Yuh, W. T. C. (2000). Visualization of Subthalamic Nuclei with Cortex Attenuated Inversion Recovery MR Imaging. *NeuroImage*, *11*(4), 341–346. https://doi.org/10.1006/nimg.2000.0552

Makowski, C., Béland, S., Kostopoulos, P., Bhagwat, N., Devenyi, G. A., Malla, A. K., Joober, R., Lepage, M., & Chakravarty, M. M. (2018). Evaluating accuracy of striatal, pallidal, and thalamic segmentation methods: Comparing automated approaches to manual delineation. *NeuroImage*, *170*, 182–198. https://doi.org/10.1016/j.neuroimage.2017.02.069

Morel, A. (2007). *Stereotactic Atlas of the Human Thalamus and Basal Ganglia*. CRC Press.

Morel, A., Magnin, M., & Jeanmonod, D. (1997). Multiarchitectonic and stereotactic atlas of the human thalamus. *Journal of Comparative Neurology*, *387*(4), 588–630. https://doi.org/10.1002/(SICI)1096-9861(19971103)387:4<588::AID-CNE8>3.0.CO;2-Z

Najdenovska, E., Alemán-Gómez, Y., Battistella, G., Descoteaux, M., Hagmann, P., Jacquemont, S., Maeder, P., Thiran, J.-P., Fornari, E., & Bach Cuadra, M. (2018). In-vivo probabilistic atlas of human thalamic nuclei based on diffusion- weighted magnetic resonance imaging. *Scientific Data*, *5*. https://doi.org/10.1038/sdata.2018.270

Ou, Y., Akbari, H., Bilello, M., Da, X., & Davatzikos, C. (2014). Comparative Evaluation of Registration Algorithms in Different Brain Databases With Varying Difficulty: Results and Insights. *IEEE Transactions on Medical Imaging*, *33*(10), 2039–2065. https://doi.org/10.1109/TMI.2014.2330355

Pajula, J., Kauppi, J.-P., & Tohka, J. (2012). Inter-Subject Correlation in fMRI: Method Validation against Stimulus-Model Based Analysis. *PLOS ONE*, *7*(8), e41196. https://doi.org/10.1371/journal.pone.0041196

Park, J., Park, K. M., Jo, G., Lee, H., Choi, B. S., Shin, K. J., Ha, S., Park, S., Lee, H., & Kim, H. Y. (2020). An investigation of thalamic nuclei volumes and the intrinsic thalamic structural network based on motor subtype in drug naïve patients with Parkinson's disease. *Parkinsonism & Related Disorders*, *81*, 165–172. https://doi.org/10.1016/j.parkreldis.2020.10.044

Saranathan, M., Tourdias, T., Bayram, E., Ghanouni, P., & Rutt, B. K. (2015). Optimization of white-matter-nulled magnetization prepared rapid gradient echo (MP-RAGE) imaging. *Magnetic Resonance in Medicine*, *73*(5), 1786–1794. https://doi.org/10.1002/mrm.25298

Smith, S. M., Beckmann, C. F., Andersson, J., Auerbach, E. J., Bijsterbosch, J., Douaud, G., Duff, E., Feinberg, D. A., Griffanti, L., Harms, M. P., Kelly, M., Laumann, T., Miller, K. L., Moeller, S., Petersen, S., Power, J., Salimi-Khorshidi, G., Snyder, A. Z., Vu, A. T., … Glasser, M. F. (2013). Resting-state fMRI in the Human Connectome Project. *NeuroImage*, *80*, 144–168. https://doi.org/10.1016/j.neuroimage.2013.05.039

Sotiropoulos, S. N., Jbabdi, S., Xu, J., Andersson, J. L., Moeller, S., Auerbach, E. J., Glasser, M. F., Hernandez, M., Sapiro, G., Jenkinson, M., Feinberg, D. A., Yacoub, E., Lenglet, C., Van Essen, D. C., Ugurbil, K., & Behrens, T. E. J. (2013). Advances in diffusion MRI acquisition and processing in the Human Connectome Project. *NeuroImage*, *80*, 125–143. https://doi.org/10.1016/j.neuroimage.2013.05.057

Su, J. H., Thomas, F. T., Kasoff, W. S., Tourdias, T., Choi, E. Y., Rutt, B. K., & Saranathan, M. (2019). Thalamus Optimized Multi Atlas Segmentation (THOMAS): Fast, fully automated segmentation of thalamic nuclei from structural MRI. *NeuroImage*, *194*, 272–282. https://doi.org/10.1016/j.neuroimage.2019.03.021

Taha, A. A., & Hanbury, A. (2015). Metrics for evaluating 3D medical image segmentation: Analysis, selection, and tool. *BMC Medical Imaging*, *15*(1), 29. https://doi.org/10.1186/s12880-015-0068-x

Tourdias, T., Saranathan, M., Levesque, I. R., Su, J., & Rutt, B. K. (2014). Visualization of intra-thalamic nuclei with optimized white-matter-nulled MPRAGE at 7T. *NeuroImage*, *84*, 534–545. https://doi.org/10.1016/j.neuroimage.2013.08.069

van Oort, E. S. B., Mennes, M., Navarro Schröder, T., Kumar, V. J., Zaragoza Jimenez, N. I., Grodd, W., Doeller, C. F., & Beckmann, C. F. (2018). Functional parcellation using time courses of instantaneous connectivity. *NeuroImage*, *170*, 31–40. https://doi.org/10.1016/j.neuroimage.2017.07.027

Whiting, B. B., Whiting, A. C., & Whiting, D. M. (2018). Thalamic Deep Brain Stimulation. *Current Concepts in Movement Disorder Management*, *33*, 198–206. https://doi.org/10.1159/000481104

Wiegell, M. R., Tuch, D. S., Larsson, H. B. W., & Wedeen, V. J. (2003). Automatic segmentation of thalamic nuclei from diffusion tensor magnetic resonance imaging. *NeuroImage*, *19*(2), 391–401. https://doi.org/10.1016/S1053-8119(03)00044-2

Wolff, M., & Vann, S. D. (2019). The Cognitive Thalamus as a Gateway to Mental Representations. *Journal of Neuroscience*, *39*(1), 3–14. https://doi.org/10.1523/JNEUROSCI.0479-18.2018

Yang, S., Meng, Y., Li, J., Li, B., Fan, Y.-S., Chen, H., & Liao, W. (2020). The thalamic functional gradient and its relationship to structural basis and cognitive relevance. *NeuroImage*, *218*, 116960. https://doi.org/10.1016/j.neuroimage.2020.116960

Zhang, D., Snyder, A. Z., Fox, M. D., Sansbury, M. W., Shimony, J. S., & Raichle, M. E. (2008). Intrinsic Functional Relations Between Human Cerebral Cortex and Thalamus. *Journal of Neurophysiology*, *100*(4), 1740–1748. https://doi.org/10.1152/jn.90463.2008

Reliability of magnetic resonance spectroscopy of regional cholinergic metabolites in the cortex and striatum of humans

Brendan Williams[1,2], Shan Shen[1], Tiffany Bell[3], Anastasia Christakou[1,2]

1. Centre for Integrative Neuroscience and Neurodynamics, University of Reading, UK
2. School of Psychology and Clinical Language Sciences, University of Reading, UK
3. Cumming School of Medicine, University of Calgary, Canada

Abstract

Typical approaches for studying choline-containing compounds (CCCs) using proton magnetic resonance spectroscopy (^{1}H-MRS) treat these metabolites as a single component due to their proximity on the metabolite spectra. Nevertheless, previous work has demonstrated that choline can be separated from glycerophosphocholine and phosphocholine, and that functionally relevant changes in choline are aligned with expected changes in acetylcholine. As no method for non-invasively studying acetylcholine in humans *in vivo* currently exists, measuring choline may act as an appropriate proxy. The aim for this study was to quantify the reliability of ^{1}H-MRS measures of choline-containing compounds in two distinct cholinergic systems, in the striatum and parieto-occipital cortex, both within and between sessions. Estimates of metabolite concentrations using single and separate peaks for CCCs showed good consistency. Greater variability in choline and the sum of CCCs were seen within and across sessions than for glycerophosphocholine and phosphocholine. However, all metabolite concentrations appear to be relatively stable at the group level over time. We predict that some variability in choline is related to its functional relationship with acetylcholine.

Introduction

Proton magnetic resonance spectroscopy (^{1}H-MRS) is a technique that is used to non-invasively study the chemical composition of biological tissue *in vivo*. Its application in neuroimaging enables the study of more than thirty brain metabolites and macromolecules related to various biological processes. These include neuronal activity (such as glutamate, and Gamma Aminobutyric Acid (GABA)), brain health (such as N-acetylaspartate (NAA), glutathione, myo-inositol), and energy metabolism (such as creatine) (Barker & Lin, 2006; Bittšanský et al., 2012; Zhu & Barker, 2011). Included in these metabolites, the choline-containing compounds (CCCs) choline (Cho, 3.19 ppm), glycerophosphocholine (GPC, 3.23 ppm) and phosphocholine (PC, 3.22ppm) are also identifiable on the MRS spectra (Figure 14). The CCCs form part of a biochemical cycle that is involved in the synthesis and hydrolysis of the neurotransmitter acetylcholine (Figure 14). Although acetylcholine is also detectable at 3.21ppm using ^{1}H-MRS, its concentrations are much lower than Cho, GPC, PC, meaning its peak cannot be distinguished from the other CCCs on the metabolite spectrum *in vivo*. Additionally, spectroscopy studies commonly quantify the CCCs as a single peak on the metabolite spectra (tCho), due their closeness on the metabolite spectra (Figure 14).

Nevertheless, previous work from our lab, using functional magnetic resonance spectroscopy (fMRS), has demonstrated that Cho can be separated from the other CCCs (GPC+PC) on the metabolite spectra, and that relative differences in the concentrations of these compounds are behaviourally relevant. fMRS is an application of standard ^{1}H-MRS and is used to study the temporal dynamics of metabolite concentrations, and how these changes are related to concurrent behaviour. For instance, fMRS was used by Lindner et al. (2017) to investigate the role of the ascending cholinergic system in visuospatial attention in the parieto-occipital cortex (POC). Significant changes in Cho were observed following attention shifting in the hemifield contralateral to the spectroscopy acquisition, while ipsilateral attention shifting or a control task did not significantly change Cho concentrations. These differences were in line with *a priori* hypotheses regarding the laterality of visuospatial attention and provided the first *in vivo* non-pharmacological evidence for the involvement of the human cholinergic system in visuospatial attention shifting. Lindner et al. (2017) also showed that modelling Cho as a separate peak from GPC and PC could reliably recover metabolite concentrations from simulated data at various spectral noise levels, and that the recovered concentrations of Cho and the other CCCs were independent of each other.

fMRS has also be used to study the involvement of the striatal cholinergic system in cognitive flexibility. To do this Bell et al. (2018) had participants complete a multi-alternative probabilistic reversal learning task while ^{1}H-MRS spectra were acquired in the dorsal striatum. During this task

participants learned associations between multiple stimuli and how frequently they produced favourable or unfavourable outcomes. Midway through the task, unbeknownst to the participants, these associations reversed so that stimuli that had produced favourable outcomes more frequently now produced unfavourable outcomes, and *vice versa*. Bell et al. (2018) found that there was a significant change in the concentration of Cho following the reversal of stimulus-outcome associations, even though there was no overall change in the total concentration of CCCs. These findings were in line with evidence from animal literature that suggests that the striatal cholinergic system is important for reversal learning (Bradfield et al., 2013; Brown et al., 2010; Ragozzino et al., 2009). Furthermore, resting levels of Cho were also reported to be associated with performance during probabilistic reversal learning (Bell et al., 2019).

Based on these findings we posit that function-related changes in Cho concentrations may be reflective of the multi-scale dynamics of acetylcholine release (Lindner et al., 2017). Following its exocytosis from the presynaptic terminal, acetylcholine is hydrolysed into Cho and acetate by acetylcholinesterase in the synaptic cleft. There is then rapid reuptake of Cho back into the presynaptic neuron, where choline is converted into PC by choline kinase. PC can then either be converted into phosphatidylcholine and stored in the cell membrane or converted back into Cho. Cho is then combined with acetyl coenzyme A (acetyl-CoA) to produce acetylcholine via the enzyme choline acetyltransferase. As part of this cycle, Cho is the rate limiting factor in the synthesis of acetylcholine by choline acetyltransferase (Cuello, 1993; White & Wu, 1973). Therefore, increased exocytosis of acetylcholine from the presynaptic terminal into the synaptic cleft would increase demand for acetylcholine biosynthesis, and this would decrease the concentration of freely available Cho that is detectable using ^{1}H-MRS (Löffelholz, 1998). Indeed, the functional changes we observe are also in-line with phasic changes in Cho seen following the stimulation of cholinergic neurons (Löffelholz, 1998).

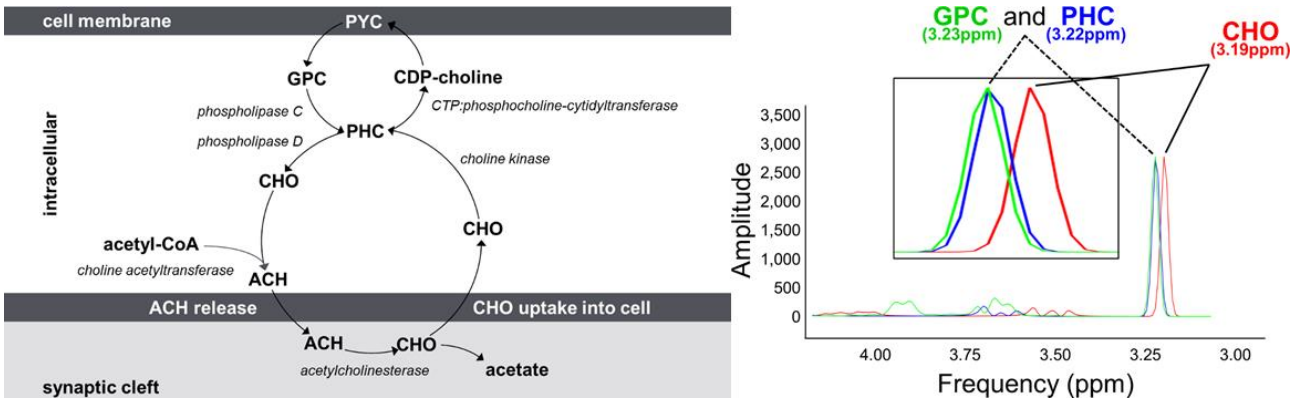

Figure 14 Overview of the acetylcholing cycle (left), and the locations of the choline containing metabolites on an MRS spectra. Figures reproduced from Lindner et al. (2017).

A number of previous studies have quantified the reliability of point resolved spectroscopy (PRESS) sequences for ^{1}H-MRS. These include studies investigating the relationship between metabolite concentration variability and signal-to-noise ratio (Okada et al., 2007), metabolite quantitation approaches (Fayed et al., 2009), and inter-scanner differences (Chard et al., 2002). ^{1}H-MRS imaging was used by (Chard et al., 2002) to study intra-individual and inter-scanner variability in metabolite concentrations. By calculating coefficients of variation, a measure of an assay's precision and repeatability, they found that intra-individual differences in tCho were 12.3%, while inter scanner (same model, different site) variability was 10.1%, suggesting that intra-individual differences in tCho concentrations over time are greater than differences due to distinct, but equivalent hardware. Differences in striatal metabolite concentrations were investigated by Soreni et al. (2006), who quantified time of day and laterality effects on NAA and creatine in the striatum; Soreni et al. (2006) found a significant effet of time of day on NAA and NAA/creatine ratios, but not on creatine levels. Additionally, no laterality effects were found for either metabolites, or the ratio between them. Regional differences in tCho measures in the cerebellum were previously reported by Currie et al. (2013), however no previous studies, to the best of our knowledge, have investigated regional differences in Cho and GPC+PC separately, nor how consistent measures of Cho and GPC+PC are in the dorsal striatum and POC over time.

Here, we assess within session how consistent estimates of choline metabolites are for spectra that are averaged from 128 and 256 transients, and we also quantify whether these metabolite concentrations are stable over time by acquiring spectra at two time points, one week apart. We aim to describe differences in metabolite concentrations over time, individual differences in metabolite estimates for acquisitions over different numbers of transients, and the consistency in metabolite estimates when quantifying CCCs as single and separate peaks. These outcomes will

help us better understand how to use ^{1}H-MRS to study Cho and its predicted relationship with acetylcholine. Furthermore, our findings will inform future work on the functional relevance of Cho, including the use of fMRS to study behaviourally relevant changes in neurochemistry.

Methods

Participants

Twenty-three healthy adult participants (mean age = 24.552 years; SD = 7.442; 16 female) were recruited. Exclusion criteria were self-reported regular use of cigarettes, recreational drugs, or psychoactive medication, or clinical diagnosis of a neurological or psychiatric condition. Twenty participants (mean age = 25.191 years; SD = 7.792, 15 female) returned for the second scanning session. The repeat scans of each participant were performed one week apart (mean = 7.1 days; SD = 0.447 days), at approximately the same time of day (mean difference = 10.5 minutes; SD = 26.253 min) to control for diurnal effects on metabolite concentrations (Soreni et al., 2006). All participants gave written informed consent before taking part in the study. Participants took part in the study on a voluntary basis, or for credit via the Research Panel of the School of Psychology and Clinical Language Sciences, University of Reading. The study was approved by the University of Reading Research Ethics Committee (ref.: UREC 19/14).

MRS Data Acquisition

^{1}H-MRS spectra and MR images were acquired at the Centre for Integrative Neuroscience and Neurodynamics, University of Reading, on a 3 Tesla Siemens Magnetom Prisma-fit scanner using a single channel transmit-receive head coil. A high-resolution whole-brain T1 structural image was acquired using an MPRAGE sequence (TR = 2020 ms; TE = 2.99 ms; FOV = 250 x 250mm; flip angle = 9^{o}; voxel = 1 mm isotropic; 192 slices). T2 HASTE images (TR = 1500 ms; TE = 82 ms; FOV = 220 x 220mm; flip angle = 150^{o}; voxel = 0.7 x 0.7 x 3 mm; 15 slices) were acquired immediately prior to the acquisition of MRS spectra in the striatum and POC, positioning the axial plane of the voxel in the isocenter of the magnetic field, optimizing the homogenization of the magnetic field using manual shimming. The native scanner PRESS sequence (striatal voxel = 15 x 10 x 15 mm; POC voxel = 15 x 15 x 15 mm; TR = 2000 ms; TE = 30ms) was used to acquire three spectra in the left striatum and left POC of all participants, as in our previous studies (Bell et al., 2018, 2019; Lindner et al., 2017). The first was a spectrum averaged from 256 transients. The second was a water-unsuppressed spectrum, averaged from 15 transients. The third was a spectrum averaged from 128 transients. Order of spectral acquisition in the striatum and POC was counterbalanced between subjects. MR acquisition sessions were always the first of the day to minimize the effects of artifacts due to previous use of the scanner (such as frequency drift) on MRS signal acquisition (El-Sharkawy et al., 2006; Harris et al., 2014; Lange et al., 2011).

Data Analysis

Pre-processing and Metabolite Quantitation

Data preprocessing and metabolite quantitation were performed using java-based Magnetic Resonance User Interface software (jMRUI, version 6.0; http://www.jmrui.eu/; (Garcia et al., 2010; Naressi et al., 2001; Stefan et al., 2009)). Spectra were phase corrected using the corresponding regional water peak and the residual water peak was removed using the Hankel-Lanczos Singular Value Decomposition filter tool. Apodization of the spectra was not carried out following recent recommendations (Wilson et al., 2019). Metabolite basis sets were generated using the MATLAB FID-A toolbox (Simpson et al., 2015). Two basis set models were generated. The first contained a single peak for quantifying CCCs. This single peak ($tCho_1$) was the average of the simulated phosphocholine (PC) and glycerophosphocholine (GPC) metabolites. The first basis set contained fifteen metabolites in total (acetate, aspartate, creatine, gamma‐aminobutyric acid (GABA), glucose, glutamate, glutamine, $tCho_1$ (GPC+PC), lactate, myo-inositol, N‐acetyl aspartate (NAA), phosphocreatine, scyllo‐inositol, succinate, and taurine). The second basis set contained the same metabolites as the first, but also included a separate peak for choline. For the second basis set, $tCho_2$ is the sum of Cho and GPC+PC. Metabolites were simulated at a field strength of 3T using a PRESS pulse sequence (TE1 = 16.6 ms, TE2 = 13.4 ms, 2048 points, spectral width = 2399.8Hz, linewidth = 12.684Hz).

Automatic quantification of metabolites from the spectra were calculated using the jMRUI tool Accurate Quantification of Short Echo time domain Signals (AQSES). The NAA peak in the spectra was shifted to 2.02 ppm to correct for chemical shift displacement, the metabolite model was realigned with the NAA peak in the spectra, and the exact position of the model was refined to align with the separate choline peaks. The following settings were used for quantification: equal phase for all metabolites; begin fixed timing; delta damping -10 to 40 Hz; delta frequency -10 to 10 Hz, no background handling; 0 truncated points; 2048 points in AQSES; normalization on. Metabolite concentrations were corrected by calculating their amplitude relative to the corresponding regional water peak (acquisition correction=1, tissue correction=0.5555).

MRS voxels were co-registered with high resolution T1 anatomical images using CoRegStandAlong in Gannet 3.1 and SPM-12 (Ashburner & Friston, 2005; Edden et al., 2014). During registration, the fraction of grey matter, white matter, and cerebrospinal fluid was calculated

for each spectral acquisition. These fractional tissue compositions were used to correct concentrations for partial volume and relaxation effects using the MATLAB toolbox MRSParVolCo (https://github.com/DrMichaelLindner/MRSParVolCo), based on the formulae described by Gasparovic et al. (2006).

Statistical analysis

Statistical analyses and data visualisations were performed using the R programming language (Bengtsson, 2020; Gamer et al., 2019; Harrell Jr & Dupont, 2020; Lehnert, 2015; Mangiafico, 2021; Papadakis et al., 2021; Phillips, 2017; R Core Team, 2020; Revelle, 2020; Wickham, 2016; Wickham & Bryan, 2019; Wilke, 2020). The Shapiro-Wilk test of normality was used to determine whether metabolite concentrations were normally distributed. Equivalent non-parametric tests were used for metabolite concentrations found to be non-normally distributed. Pearson's r correlation coefficients were used to measure the strength of association between $tCho_1$ and $tCho_2$, and for intra- and inter-session measurements of metabolite concentrations using spectra averaged from 128 and 256 transients for $tCho_1$, Cho, and GPC+PC in the striatum and POC separately. Paired sample t-tests were used to determine whether the difference between concentrations measured using spectra averaged from 128 and 256 transients were statistically different at the group level. Intraclass-correlation coefficients were used to determine intra and inter-session consistency in metabolite concentrations for spectra averaged from 128 and 256 transients. Intraclass-correlation coefficients were interpreted as: Poor: ICC < 0.4; moderate: ≤ 0.4 ICC < 0.6; good: 0.6 ≤ ICC < 0.75; excellent: 0.75 ≥ ICC, following the approach used by Baeshen et al. (2020). Intra-class correlation coefficients were calculated separately in the striatum and POC, and for $tCho_1$, Cho and GPC+PC. The coefficient of variation (CV) was used as a measure of the intra- and inter-session precision and reliability of metabolite concentrations and is the ratio of a measure's standard deviation and mean ($CV = \frac{\sigma}{\mu}$). Bland-Altman plots were used to visualize agreement for within and between session measurements.

Results

MRS Voxel Placement

To localize voxel positioning MRS voxels were co-registered with high resolution T1 anatomical images using CoRegStandAlone in Gannet 3.1 (Ashburner & Friston, 2005; Edden et al., 2014). Subject space masks of voxel positioning were normalized into standard space and binarized using SPM-12. The sum of all standard space binary masks is visualized in Figure 15.

To calculate the consistency of MRS voxel positioning between sessions within subjects we calculated the Hadamard product of the binary masks for sessions one and two in MNI space for the POC and Striatum. This gave the conjunction of the voxels included in the MRS volume for both sessions. The number of overlapping voxels was then divided by the mean number of voxels in the masks for sessions one and two and converted to percentage. Voxel placement consistencies were calculated for 19 of the participants who completed two scanning sessions (one participant did not have a T1 for co-registration in session one). The average consistency of voxel positioning in the striatum was 68.3% (SD = 15.6; range = 32.4 → 90.9), in the POC consistency was 53.8% (SD = 23.468; range = 8.0 → 87.2).

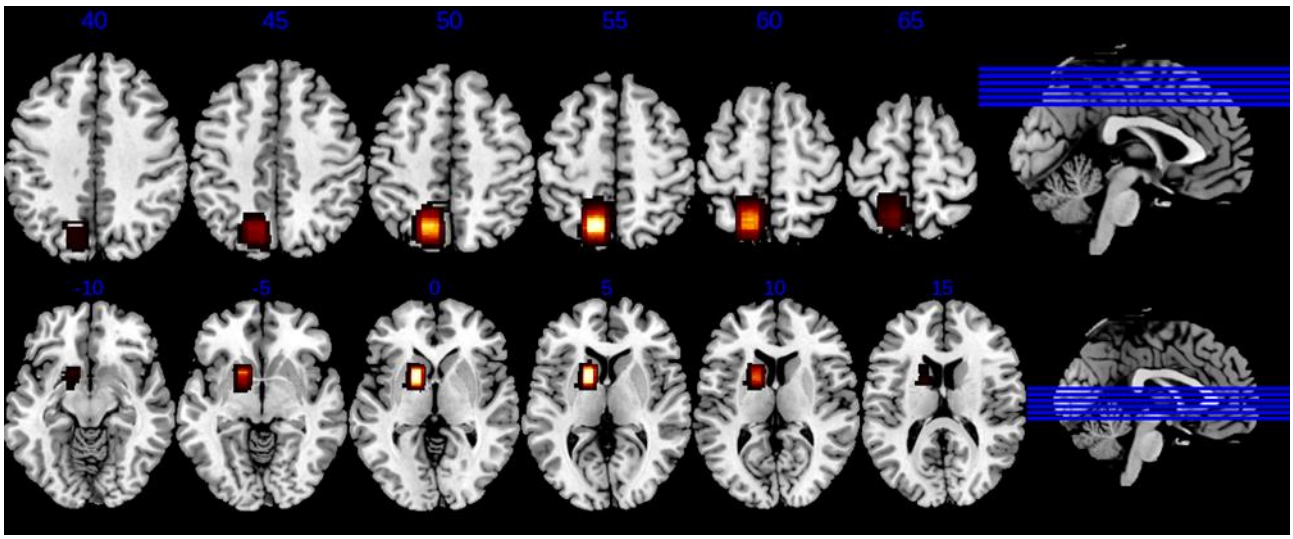

Figure 15 Heatmap of voxel positioning in the parieto-occipital cortex (top) and striatum (bottom) for all participants in standard space.

Choline measures using single and separate peaks

Firstly, we correlated concentrations of $tCho_1$ and $tCho_2$ to quantify the strength of the association between CCCs quantified using single and separate choline peaks. We observed strong positive correlations between $tCho_1$ and $tCho_2$ concentrations in the striatum for spectra averaged from 128 and 256 transients in both sessions ($p < 0.05$ for all correlations; Figure 16). Significant positive correlations for $tCho_1$ and $tCho_2$ in the POC were found in session one for spectra averaged from 256 transients ($t(14) = 3.268$, $p = 0.006$, 95% CI [0.241, 0.870], $r = 0.657$), and in session two for spectra averaged from 128 transients ($r_S(38) = 0.895$, $p < 0.001$) (Figure 17). A summary of the number of participants for whom separate peaks for Cho and GPC were quantifiable across sessions, regions, and averages is summarised in Table 5.

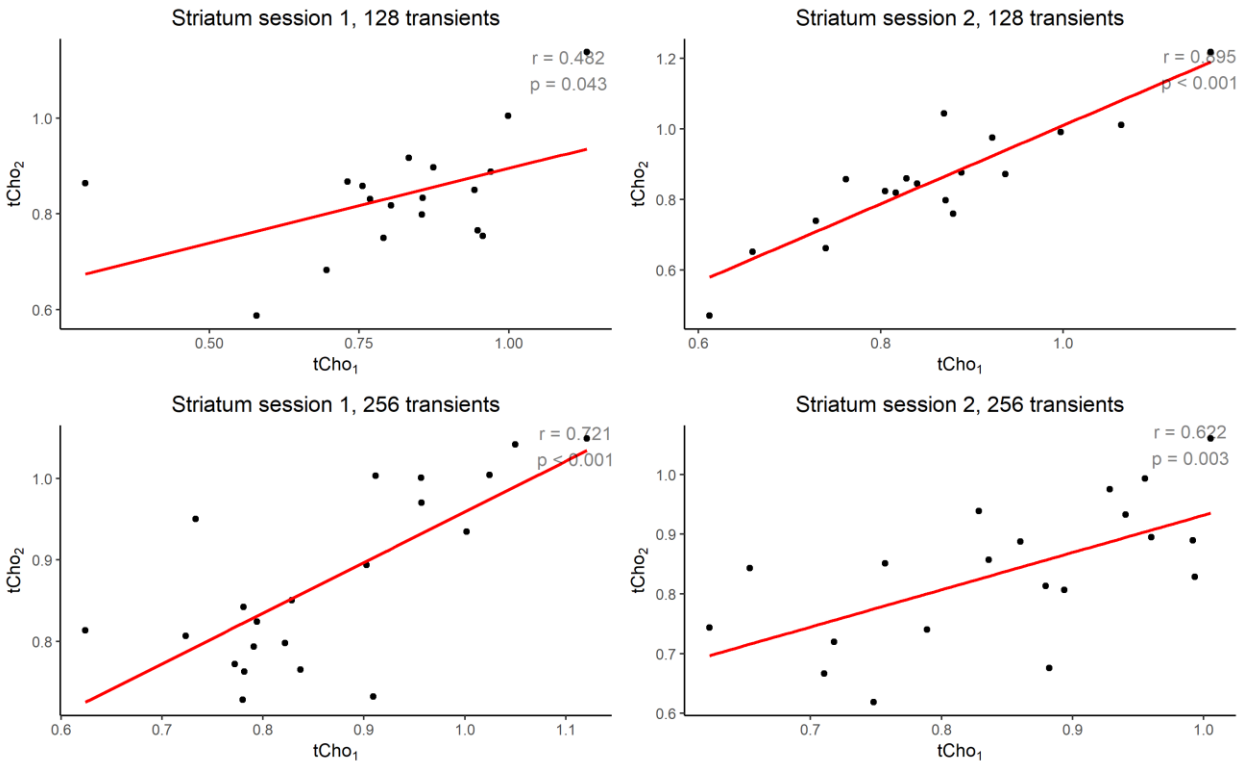

Figure 16 correlation between $tCho_1$ and $tCho_2$ measures in the striatum

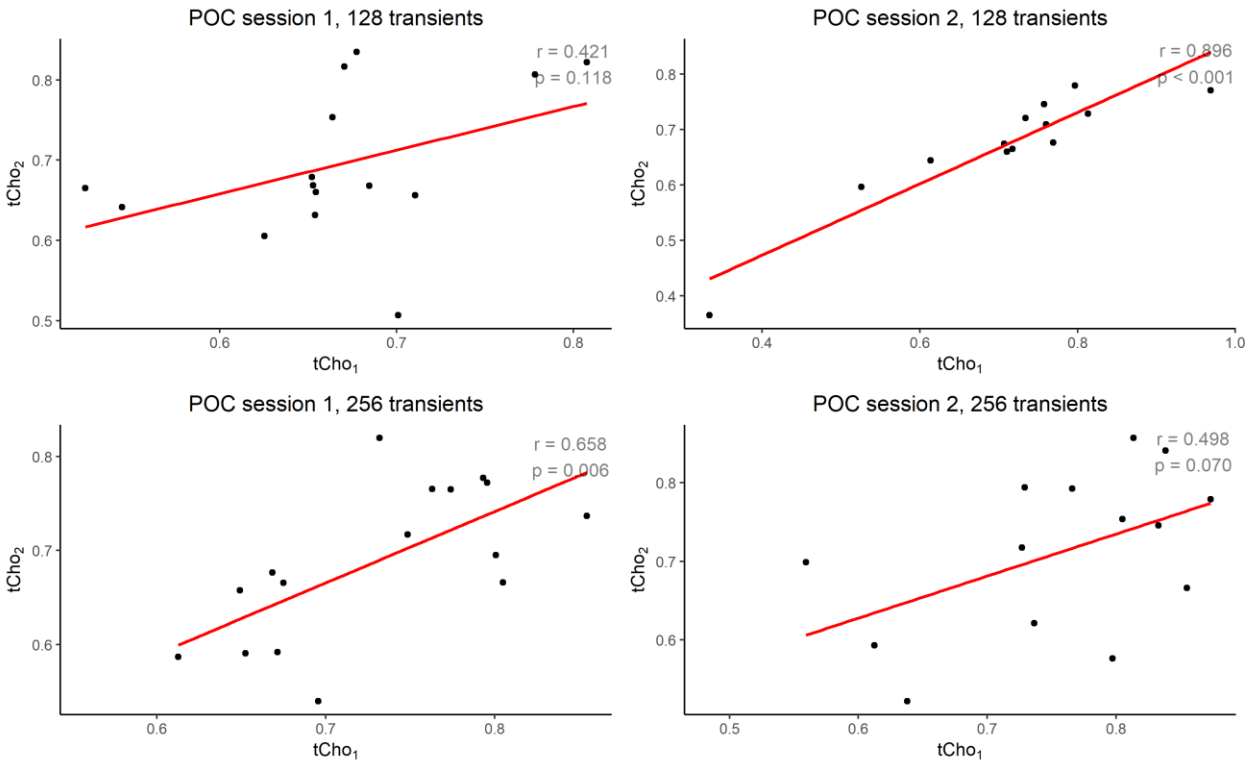

Figure 17 correlation between $tCho_1$ and $tCho_2$ measures in the POC

Session	Region	Transients	N Spectra Acquired	N Spectra Quantified
1	POC	128	23	16
		256	23	16
	STR	128	22	19
		256	22	22
2	POC	128	20	13
		256	20	15
	STR	128	20	18
		256	20	20

Table 5 number of spectra acquired for each scan and the number of spectra where separate peaks for Cho and GPC+PC were quantified.

Within Session analysis

Single choline peak

Paired sample t-tests were used to determine whether there were significant differences in $tCho_1$ concentrations in the striatum and POC for spectra averaged from 128 and 256 transients at the group level. No significant differences in metabolite concentrations were found in the striatum in the first ($t(20) = -1.262$, $p = 0.221$, 95% CI [-0.142, 0.035], mean difference = -0.054) or second

($t(19) = -0.014$, $p = 0.989$, 95% CI [-0.071, 0.070], mean difference = -0.0005) session; nor were differences found in the POC in either session (first session: $t(21) = -1.774$, $p = 0.091$, 95% CI [-0.089, 0.007], mean difference = -0.041; second session: ($t(19) = -0.878$, $p = 0.391$, 95% CI [-0.090, 0.037], mean difference = -0.027). Within session consistency of $tCho_1$ in the striatum for spectra averaged from 128 and 256 transients, assessed using intra-class correlation coefficient, showed poor consistency ($F(20,21) = 1.37$, $p = 0.241$, ICC = 0.156, ICC 95% CI [-0.278, 0.54]) in the first session, and poor consistency ($F(19,20) = 1.75$, $p = 0.111$, ICC = 0.273, ICC 95% CI [-0.172, 0.629]) in the second session. POC $tCho_1$ concentrations showed poor consistency ($F(21,22) = 0.988$, $p = 0.51$, ICC = 0.006, ICC 95% CI [-0.412, 0.406]) in the first session, and poor consistency ($F(19,20) = 2.23$, $p = 0.041$, ICC = 0.381, ICC 95% CI [-0.053, 0.697]) in the second session for spectra averaged from 128 and 256 transients. No significant association between spectra averaged from 128 and 256 transients were observed in the striatum or the POC in either session ($p > 0.05$, Figure 18). The coefficient of variance for spectra averaged from 128 and 256 transients for each participant is summarised in Figure 20. In session one, the mean coefficient of variance was 8.529 in the striatum and 6.598 in the POC; in session two the mean coefficient of variance in the striatum and POC was 7.459 and 8.316, respectively. One participant had a coefficient of variance higher than 20% in the striatum for sessions one and two, and two participants had coefficients of variance greater than 20% in the POC in session two; this level has previously been used as a threshold below which a measurement is considered to be reliable (Baeshen et al., 2020).

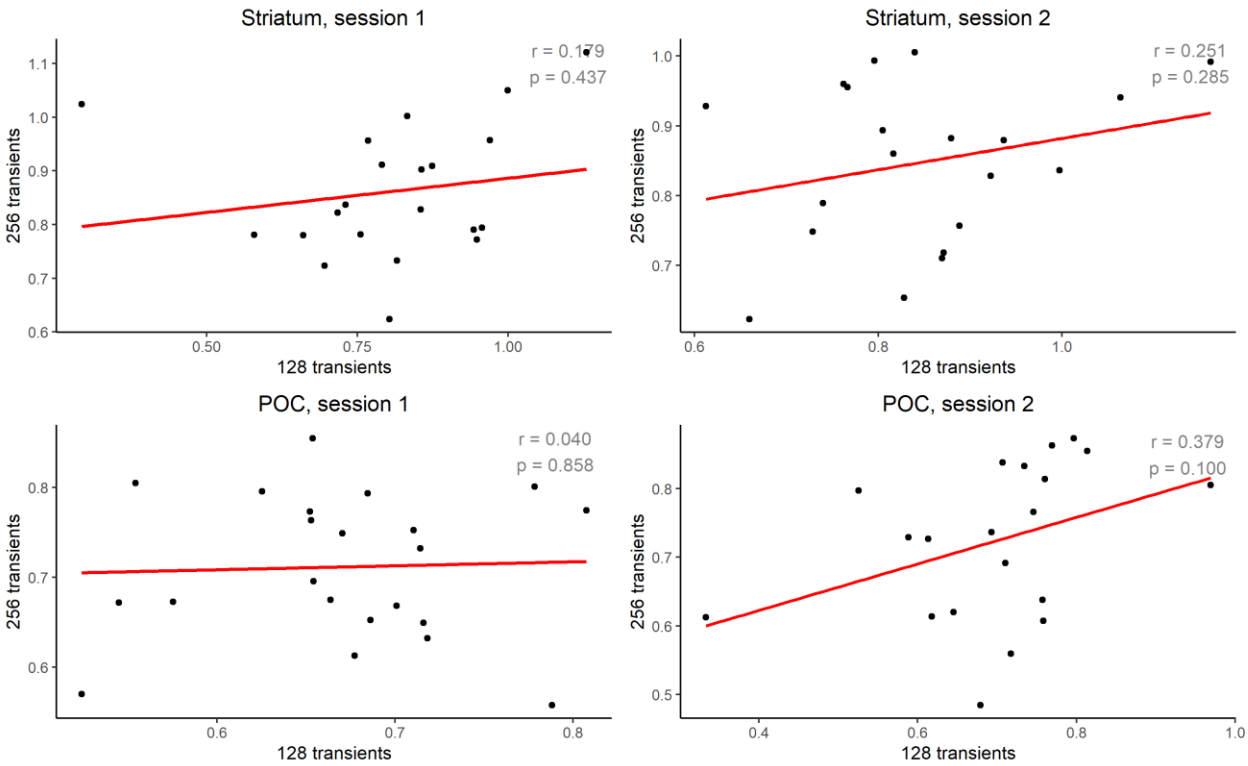

Figure 18 Correlation between spectra averaged from 128 and 256 transients for $tCho_1$

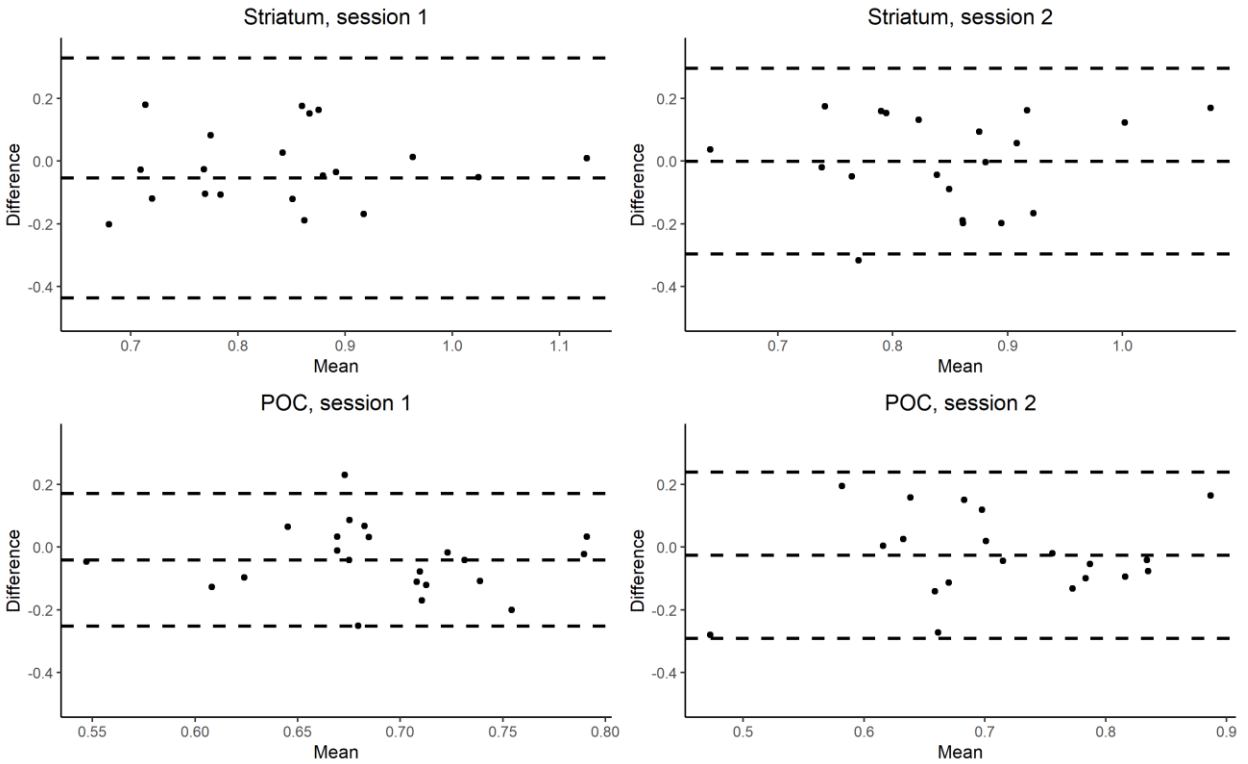

Figure 19 Bland-Altman plot of the difference between spectra averaged from 128 and 256 transients for $tCho_1$

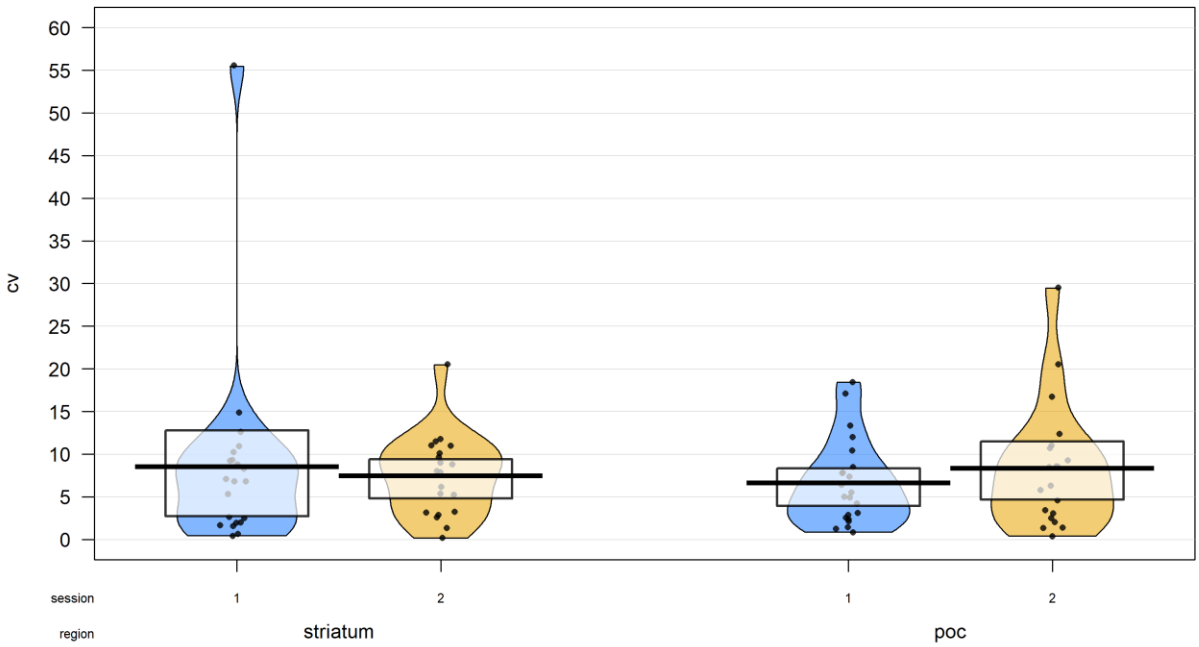

Figure 20 Coefficient of variance for spectra averaged from 128 and 256 transients (denoted session 1 and 2 respectively) for $tCho_1$

Separate choline peaks

No significant correlations in Cho concentrations were found for spectra averaged from 128 and 256 transients in the striatum and POC in sessions one and two ($p > 0.05$, Figure 21). A significant positive correlation for GPC+PC concentrations were observed in the striatum in session one ($t(16) = 2.521$, $p = 0.023$, 95% CI [0.088, 0.701], $r = 0.533$), but not in session two nor in the POC in either sessions one or two ($p > 0.05$, Figure 24). Cho concentrations were not significantly different for spectra averaged from 128 and 256 transients at the group level in the striatum (first session: Z = -0.131, $p = 0.899$, 95% CI [-0.111, 0.075], median difference = -0.016, second session: Z = -1.22, $p = 0.229$, 95% CI [-0.204, 0.063], median difference = -0.088), or in the POC (first session: Z = -0.745, $p = 0.470$, 95% CI [-0.085, 0.040], median difference = -0.024, second session: Z = -0.489, $p = 0.638$, 95% CI [-0.052, 0.015], median difference = -0.004). GPC+PC concentrations were also not significantly different for spectra averaged from 128 and 256 transients at the group level in the striatum (first session: $t(17) = -0.524$, $p = 0.607$, 95% CI [-0.093, 0.056], mean difference = -0.019, second session: $t(17) = 1.56$, $p = 0.137$, 95% CI [-0.031, 0.205], mean difference = 0.087), nor the POC (first session: $t(11) = 0.716$, $p = 0.489$, 95% CI [-0.047, 0.092], mean difference = 0.023, second session: $t(10) = -0.487$, $p = 0.637$, 95% CI [-0.106, 0.068], mean

difference = -0.019). Cho concentrations in the striatum had poor consistency between spectra averaged from 128 and 256 transients in sessions one and two, as measured using intra-class correlation (first session: $F(17,18) = 1.53$, $p = 0.188$, ICC = 0.211, ICC 95% CI [-0.261, 0.606], second session: $F(17,18) = 0.61$, $p = 0.843$, ICC = -0.242, ICC 95% CI [-0.622, 0.236]); POC measures had poor consistency in the first session, and good consistency in the second session (first session: $F(11,12) = 0.589$, $p = 0.805$, ICC = -0.259, ICC 95% CI [-0.699, 0.338], second session: $F(10,11) = 5.89$, $p = 0.004$, ICC = 0.71, ICC 95% CI [0.251, 0.911]). GPC+PC concentrations had moderate consistency in the striatum in session one and the POC in session two (striatum: $F(17,18) = 3.22$, $p = 0.009$, ICC = 0.526, ICC 95% CI [0.103, 0.79], POC: $F(10,11) = 3.01$, $p = 0.042$, ICC = 0.502, ICC 95% CI [-0.078, 0.834]); consistency was poor in the POC in session one, and in the striatum in session two (POC: $F(11,12) = 1.72$, $p = 0.183$, ICC = 0.264, ICC 95% CI [-0.318, 0.71], striatum: $F(17,18) = 1.18$, $p = 0.362$, ICC = 0.084, ICC 95% CI [-0.377, 0.517]). The mean coefficient of variance for Cho in the striatum was 42.564 in session one, and 48.972 in session two, four participants in session one and five participants in session two had coefficients lower than 20%; in the POC the mean coefficient of variance was 52.831 in session one and 26.227 in session two, three participants in session one and five in session two had values below 20% (Figure 23). GPC+PC measures in the striatum had a mean coefficient of variance of 10.019 in session one and 17.724 in session two, sixteen participants in session one, and twelve in session two had values less than 20%. The mean coefficient of variance for GPC+PC in the POC was 7.387 in session one, and 8.441 in session two, all participants had values below 20% in session one and only one participant in session two had a value that was now lower than 20%.

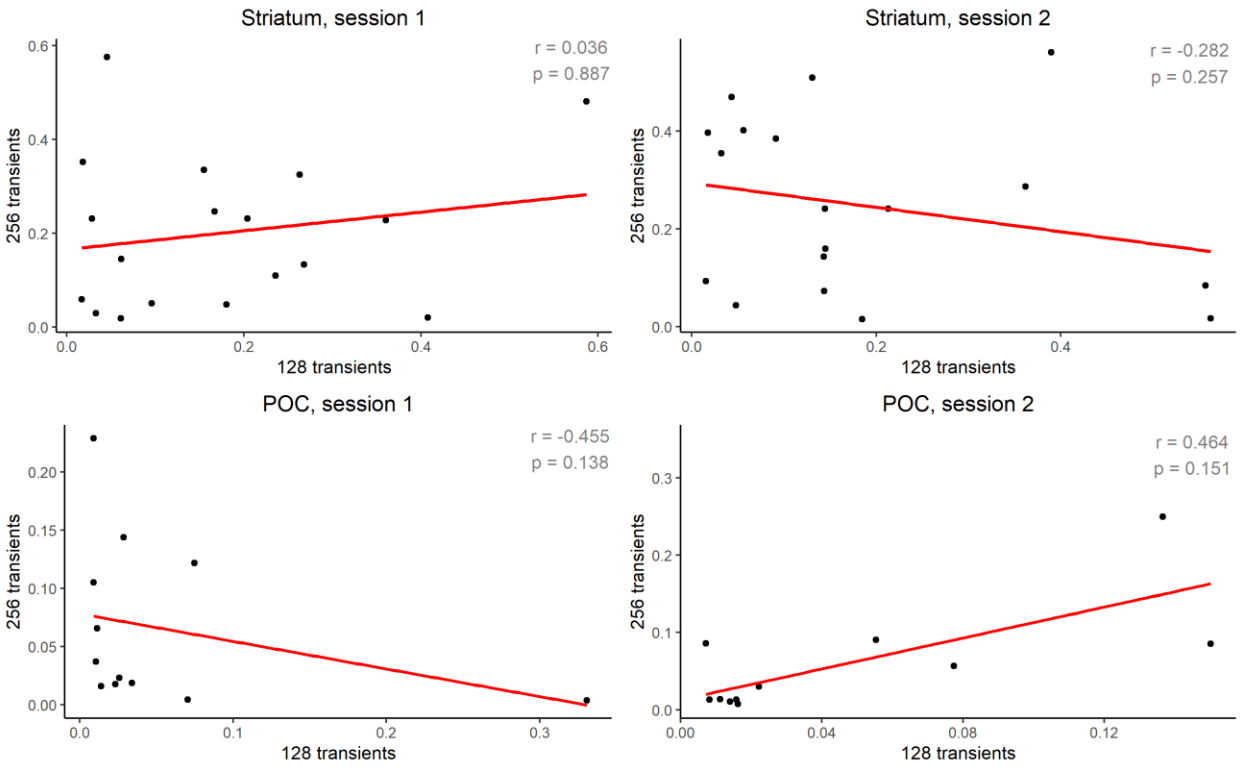

Figure 21 Correlation between spectra averaged from 128 and 256 transients for Cho

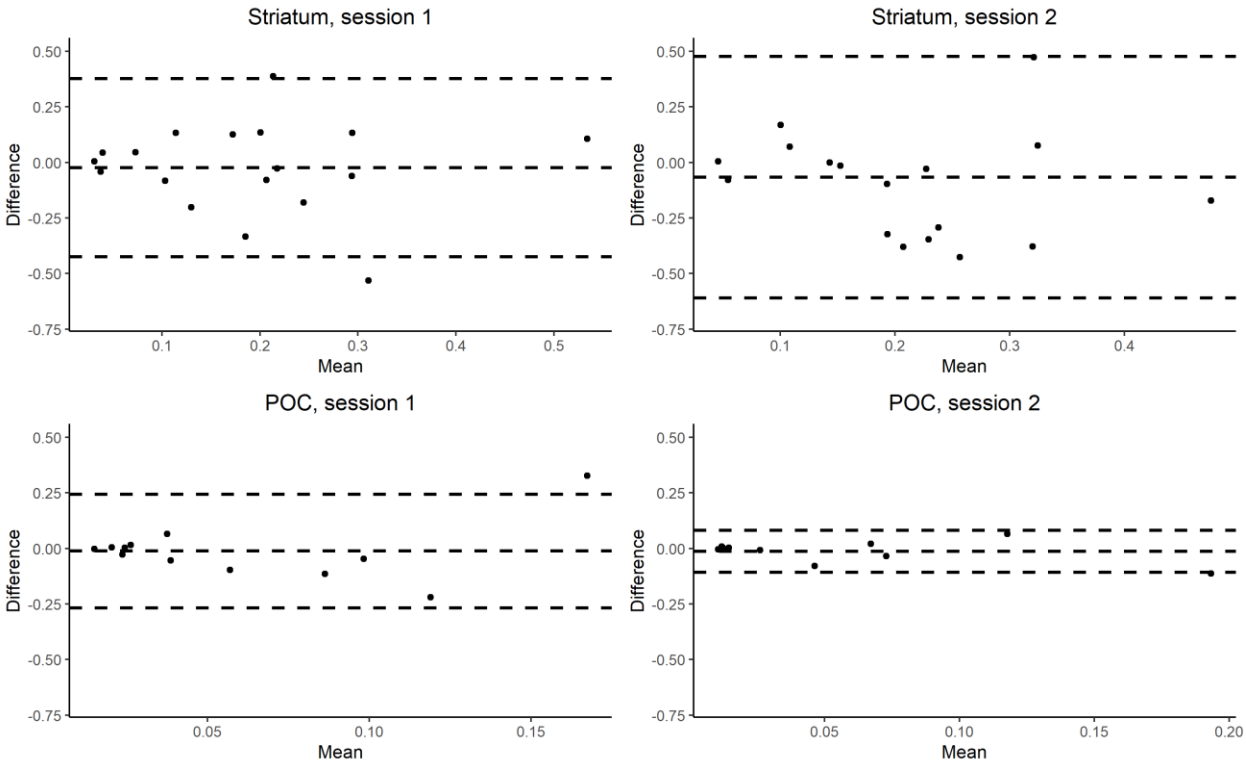

Figure 22 Bland-Altman plot of the difference between spectra averaged from 128 and 256 transients for Cho

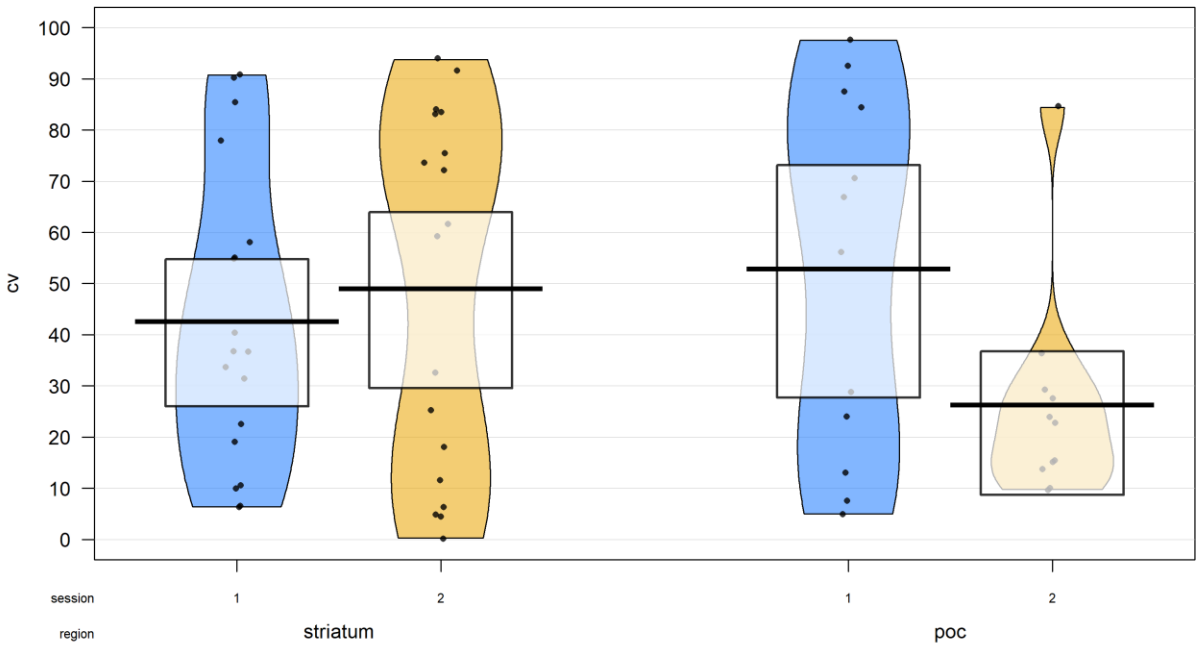

Figure 23 Coefficient of variance for spectra averaged from 128 and 256 transients for Cho

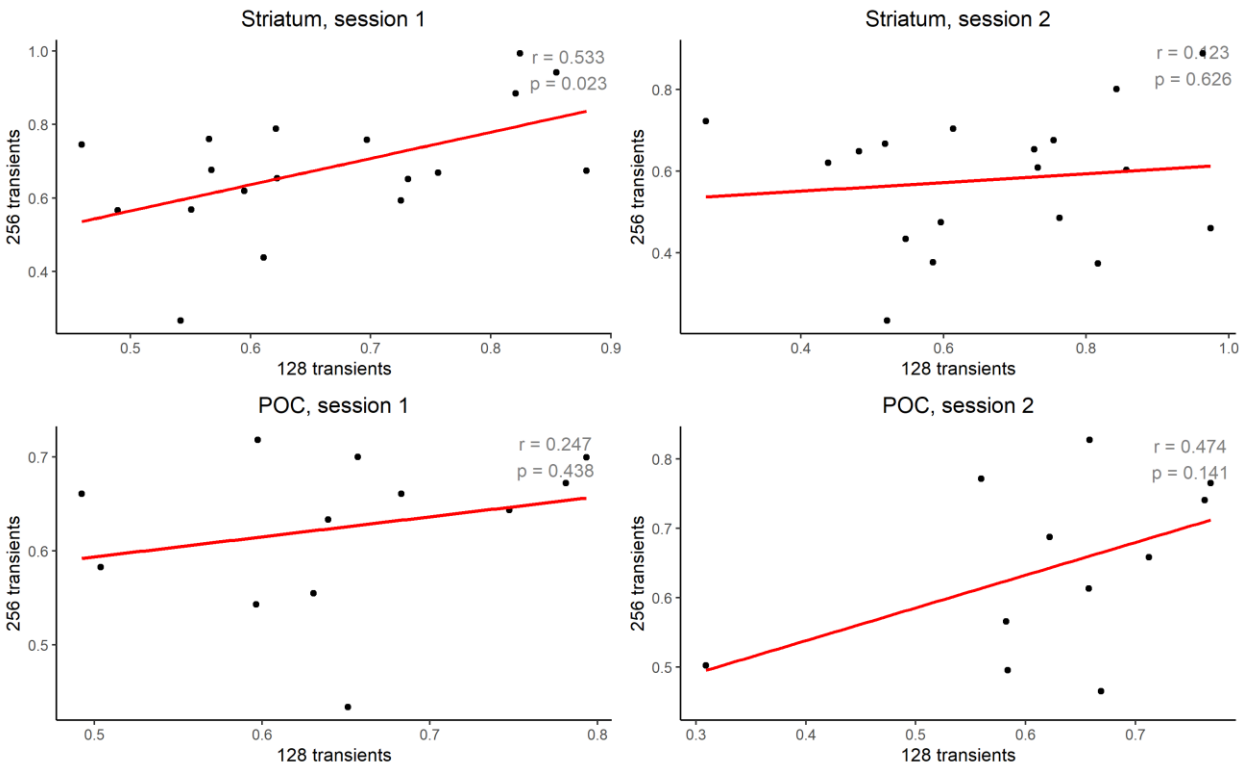

Figure 24 Correlation between spectra averaged from 128 and 256 transients for GPC+PC

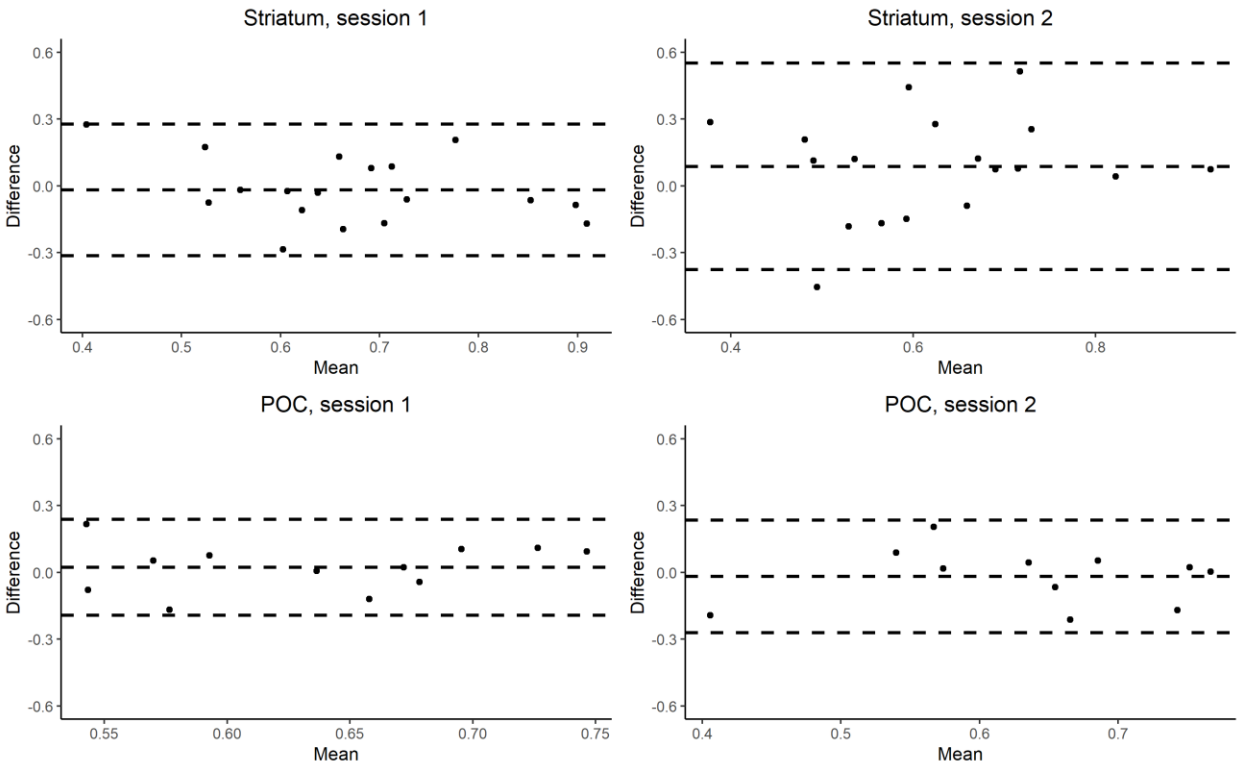

Figure 25 Bland-Altman plot of the difference between spectra averaged from 128 and 256 transients for GPC+PC

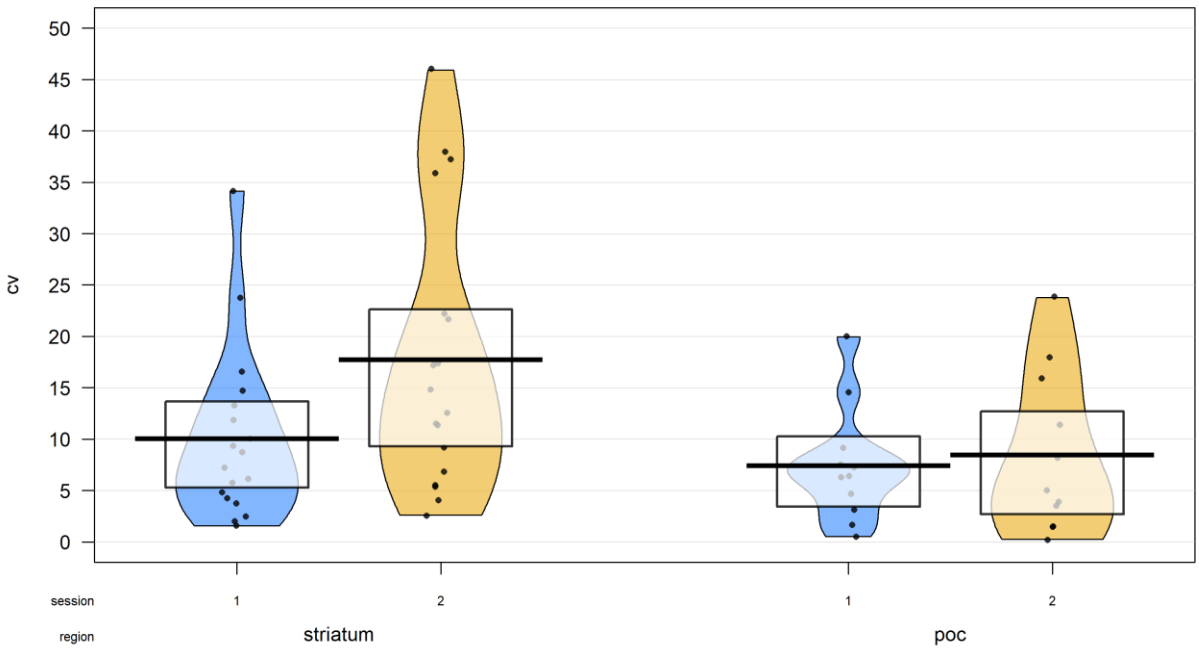

Figure 26 coefficient of variance for spectra averaged from 128 and 256 transients for GPC+PC

Across Sessions analysis

Single choline peak

Paired sample t-tests were run to test whether $tCho_1$ concentrations were significantly different between session one and session two. No significant difference in metabolite concentrations between sessions were found in the striatum for spectra averaged from 128 transients ($t(17) = -0.857$, $p = 0.403$, 95% CI [-0.145, 0.061], mean difference = -0.042) or 256 transients ($t(17) = 0.642$, $p = 0.530$, 95% CI [-0.048, 0.090], mean difference = 0.021), nor in the POC for spectra averaged from 128 transients ($t(18) = -1.134$, $p = 0.272$, 95% CI [-0.103, 0.031], mean difference = -0.036) or 256 transients ($t(18) = -0.609$, $p = 0.550$, 95% CI [-0.072, 0.039], mean difference = -0.016). Between session consistency in $tCho_1$ concentrations within the striatum, assessed using intra-class correlation coefficient, showed poor consistency ($F(17,18) = 1.49$, $p = 0.204$, ICC = 0.197, ICC 95% CI [-0.274, 0.596]) for spectra averaged from 128 transients, and for spectra averaged from 256 transients ($F(17,18) = 2.3$, $p = 0.044$, ICC = 0.394, ICC 95% CI [-0.064, 0.719]). POC $tCho_1$ concentrations showed poor consistency for spectra averaged from 128 transients ($F(18,19) = 1.28$, $p = 0.3$, ICC = 0.122, ICC 95% CI [-0.332, 0.534]), and poor consistency for spectra averaged from 256 transients ($F(18,19) = 1.92$, $p = 0.084$, ICC = 0.315, ICC 95% CI [-0.14, 0.664]). No significant correlations in $tCho_1$ concentrations between sessions one and two were observed for spectra acquired from 128 and 256 transients in the striatum and POC (Figure 27). Coefficients of variance between sessions are summarised in Figure 29. In the striatum, the mean coefficient of variance for $tCho_1$ concentrations for spectra averaged from 128 transients was 9.202, for spectra from 256 transients the mean coefficient of variance was 7.324. In the POC these coefficients of variance were 8.363 and 6.338 for averages of 128 and 256 transients, respectively. One participant had a coefficient of variance that exceeded 20% in the striatum and POC for spectra averaged from 128 transients.

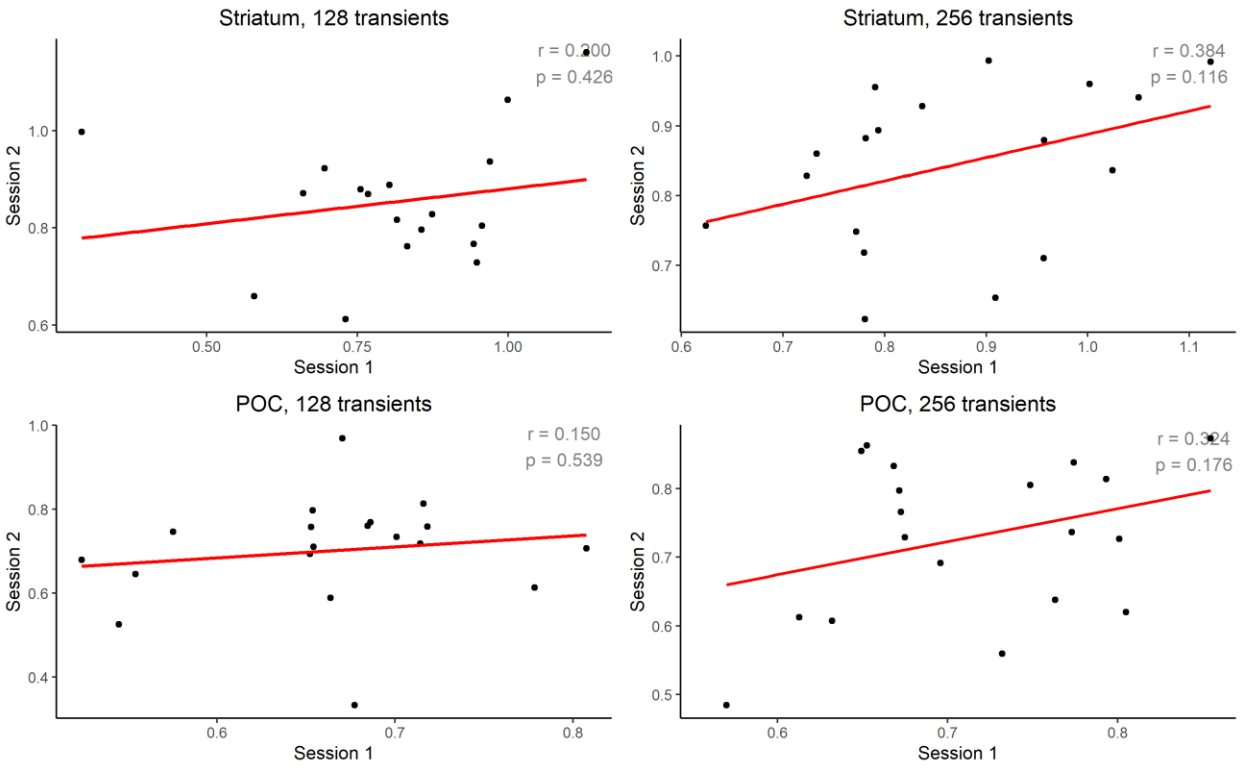

Figure 27 Correlation of across session difference for spectra averaged from 128 and 256 transients for $tCho_1$

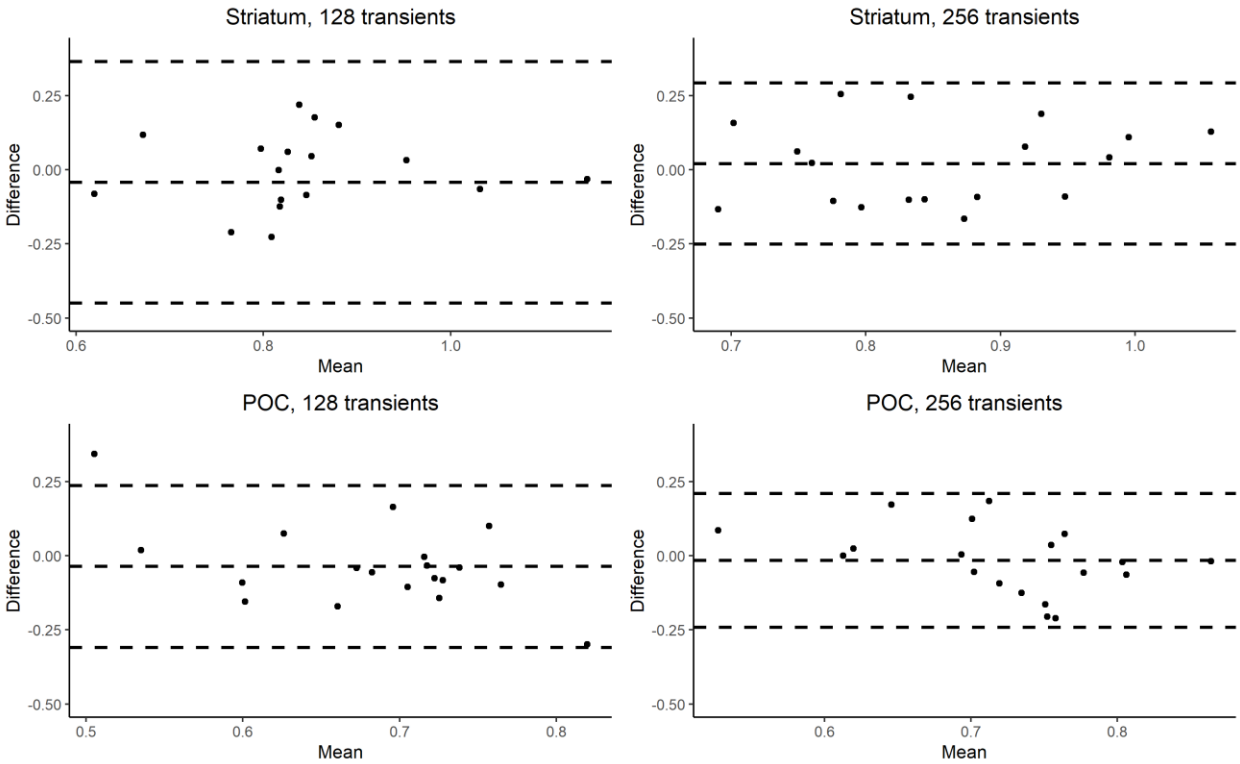

Figure 28 Bland-Altman plot of across session difference for spectra averaged from 128 and 256 transients for $tCho_1$

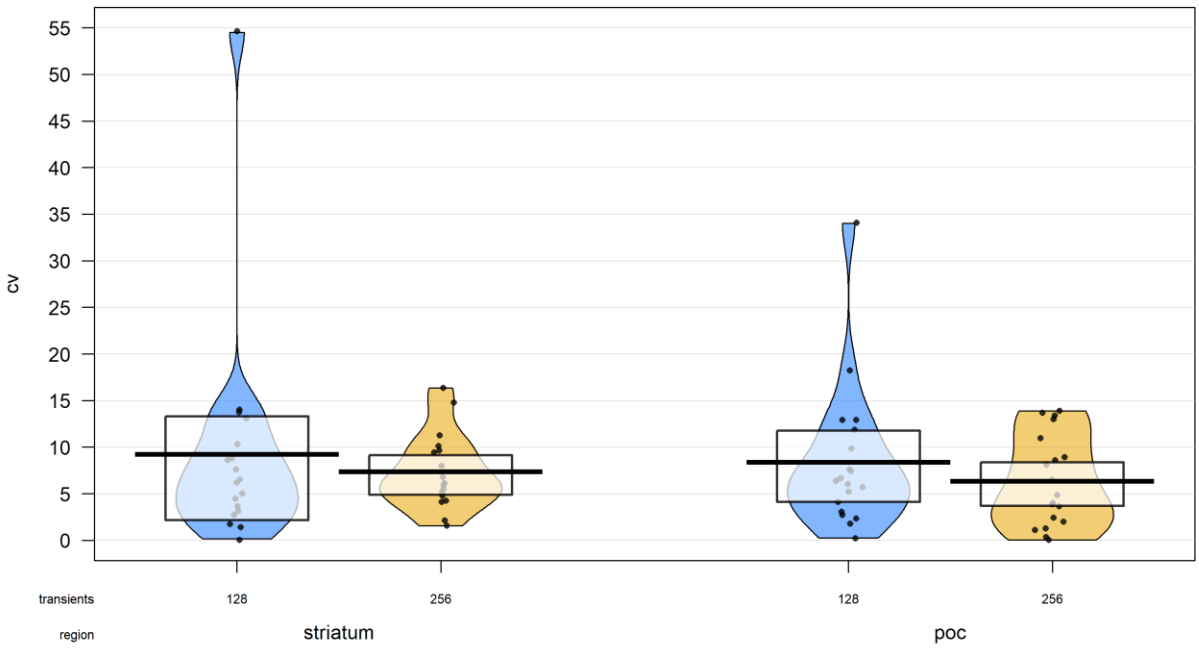

Figure 29 coefficient of variance of across session difference for spectra averaged from 128 and 256 transients for $tCho_1$

Separate choline peaks

Cho concentrations were not significantly different across sessions for spectra averaged from 128 and 256 transients at the group level in the striatum (128 transients: Z = -0.314, p = 0.761, 95% CI [-0.177, 0.107], median difference = -0.026, 256 transients: Z = -0.958, p = 0.347, 95% CI [-0.180, 0.051], median difference = -0.054), or in the POC (128 transients: Z = 0, p = 1, 95% CI [-0.066, 0.136], median difference = -0.000016, 256 transients: Z = -0.275, p = 0.791, 95% CI [-0.120, 0.043], median difference = 0.005). A significant difference in GPC+PC concentration between sessions was found in the striatum for spectra averaged from 256 transients (t(17) = 2.793, p = 0.012, 95% CI [0.026, 0.186], mean difference = 0.106), but not for spectra averaged from 128 transients (t(13) = 0.266, p = 0.795, 95% CI [-0.093, 0.118], mean difference = 0.013). No significant differences in GPC+PC concentrations were found in the POC for spectra averaged from 128 transients (t(9) = 0.949, p = 0.367, 95% CI [-0.045, 0.111], mean difference = 0.033) nor 256 transients (t(11) = 0.645, p = 0.532, 95% CI [-0.059, 0.108], mean difference = 0.024).Consistency of Cho concentrations in the striatum and POC across sessions, as measured using intra-class correlation, showed poor consistency for spectra averaged from 128 transients (striatum: F(13,14) = 1.35, p = 0.292, ICC = 0.149, ICC 95% CI [-0.381, 0.612], POC: F(9,10) =

1.1, p = 0.437, ICC = 0.049, ICC 95% CI [-0.548, 0.628]), and 256 transients (striatum: F(17,18) = 1.5, p = 0.202, ICC = 0.199, ICC 95% CI [-0.272, 0.597], POC: F(11,12) = 0.728, p = 0.697, ICC = -0.157, ICC 95% CI [-0.64, 0.428]). Intra-class correlation coefficients for GPC+PC showed spectra averaged from 128 and 256 transients both had moderate consistency in the striatum (128 transients: F(13,14) = 2.88, p = 0.030, ICC = 0.485, ICC 95% CI [-0.022, 0.798], 256 transients: F(17,18) = 2.77, p = 0.019, ICC = 0.47, ICC 95% CI [0.029, 0.761]); moderate consistency for spectra averaged from 128 transients and poor consistency for spectra averaged from 256 transients were observed in the POC (128 transients: F(9,10) = 3.62, p = 0.029, ICC = 0.567, ICC 95% CI [-0.022, 0.87], 256 transients: F(11,12) = 1.38, p = 0.293, ICC = .16, ICC 95% CI [-0.412, 0.652]). No significant correlations for Cho concentrations across sessions for spectra averaged from 128 and 256 transients were observed in the striatum or the POC (p > 0.05, Figure 30). GPC+PC concentrations had a significant positive correlation in the striatum across sessions for spectra averaged from 256 transients (t(16) = 2.926, p = 0.010, 95% CI [0.170, 0.829], r = 0.590), however no other GPC+PC concentrations were significantly correlated across sessions (p > 0.05, Figure 33). In the striatum the mean coefficient of variance for Cho measures across sessions was 51.787 for spectra averaged from 128 transients, and 45.187 for 256 transients. For Cho in the striatum two participants had coefficients that were below 20% for spectra averaged from 128 transients, and three participants had coefficients lower than 20% for spectra averaged from 256 transients. In the POC the average coefficient of variance for Cho was 48.050 and 46.534 for spectra averaged from 128 and 256 transients, respectively. Three participants had coefficients of variance that were lower than 20% in the POC for spectra averaged from 128 transients, and four had coefficients lower than 20% for spectra averaged from 256 transients for Cho (Figure 32). Mean coefficients of variance for GPC+PC measures across sessions were 9.290 and 12.145 across sessions for spectra averaged from 128 and 256 transients, respectively. Mean GPC+PC coefficients of variance in the POC were 7.616 and 8.120 for spectra averaged from 128 and 256 transients, respectively. In the striatum two spectra averaged from 128 transients, and five from 256 transients had coefficients of variance that were greater than 20 % for GPC+PC, and in the POC one participant had a coefficient greater than 20% for both spectra averaged from 128 and 256 transients (Figure 35).

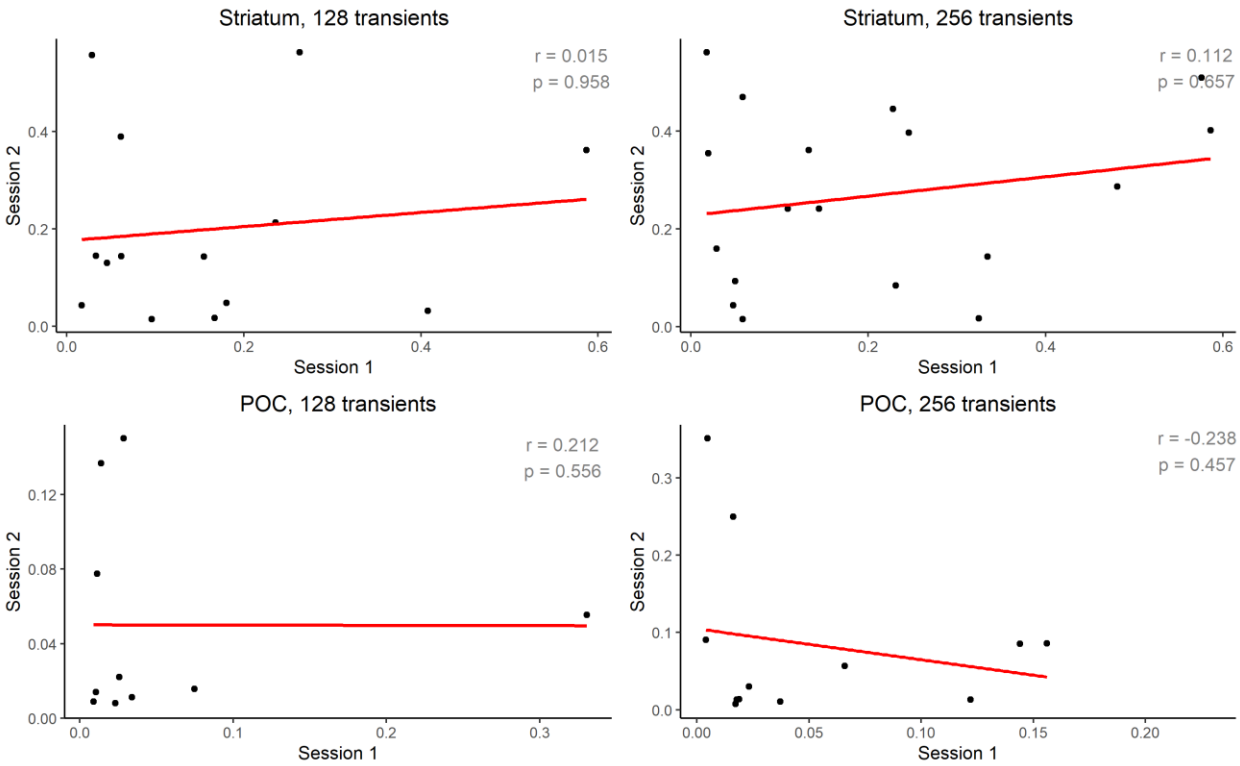

Figure 30 Correlation of across session difference for spectra averaged from 128 and 256 transients for Cho

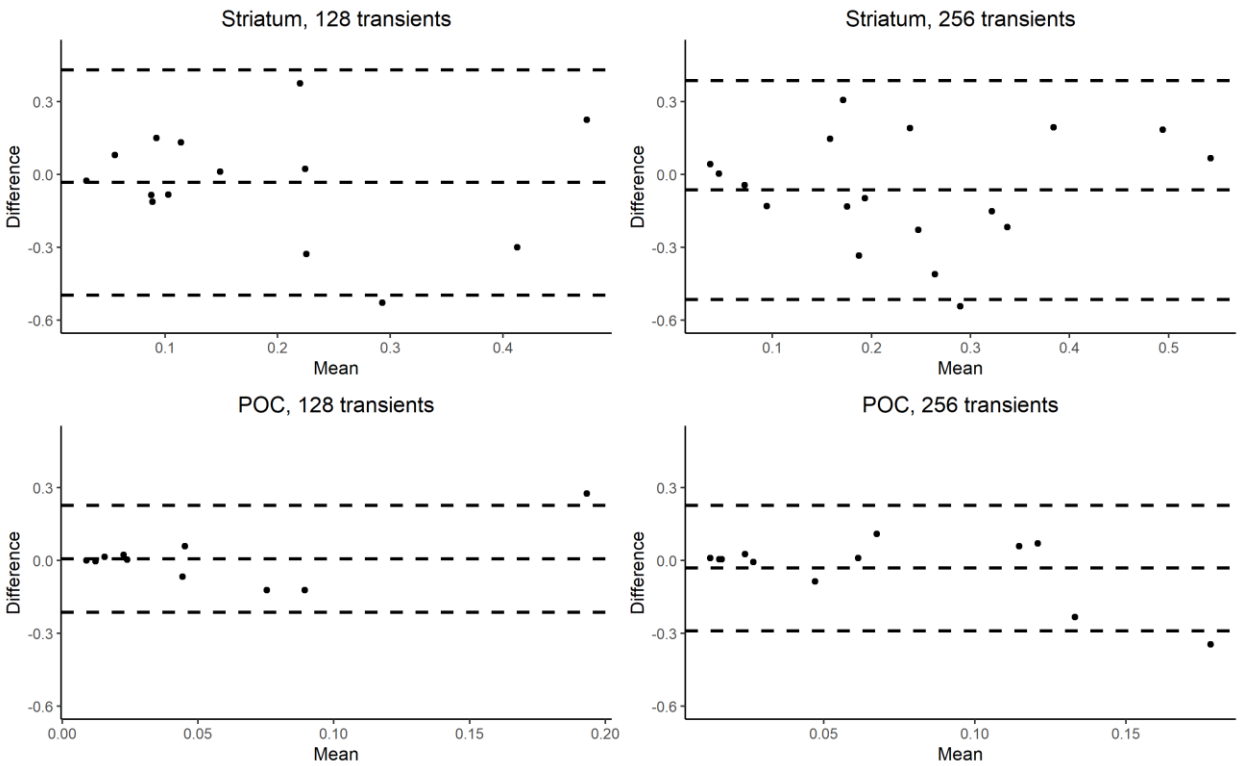

Figure 31 Bland-Altman plot of across session difference for spectra averaged from 128 and 256 transients for Cho

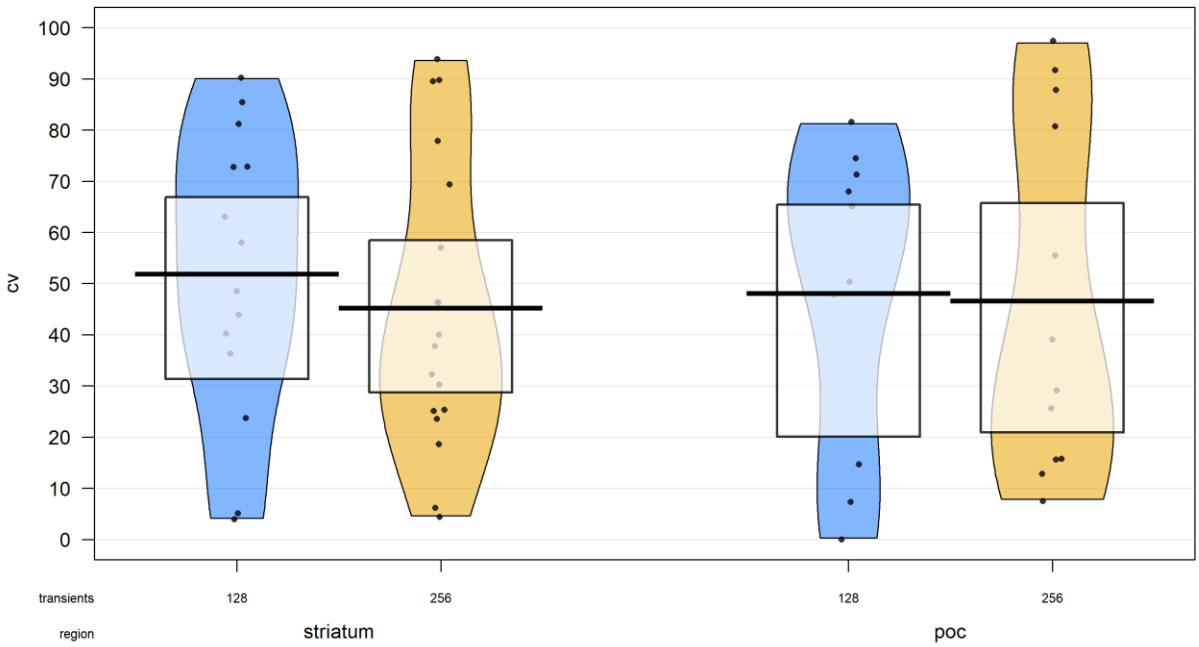

Figure 32 Coefficient of variance of across session difference for spectra averaged from 128 and 256 transients for Cho

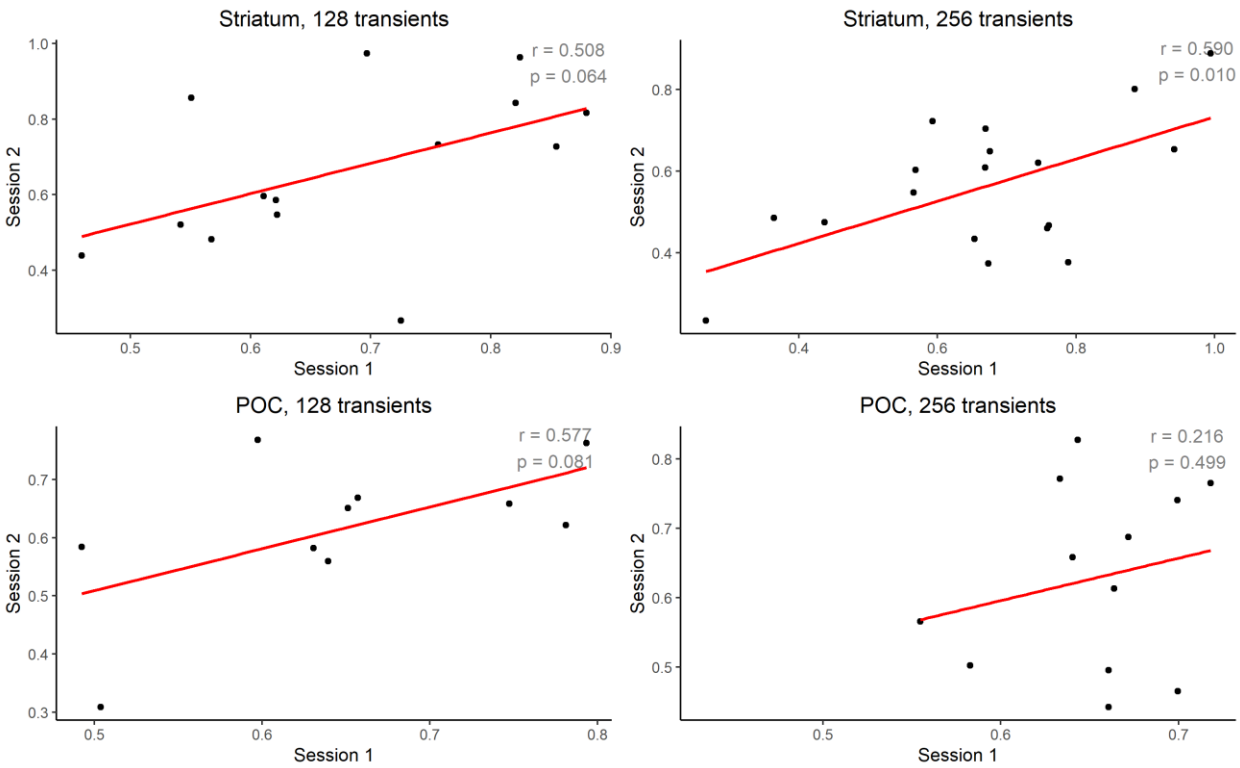

Figure 33 Correlation of across session difference for spectra averaged from 128 and 256 transients for GPC+PC

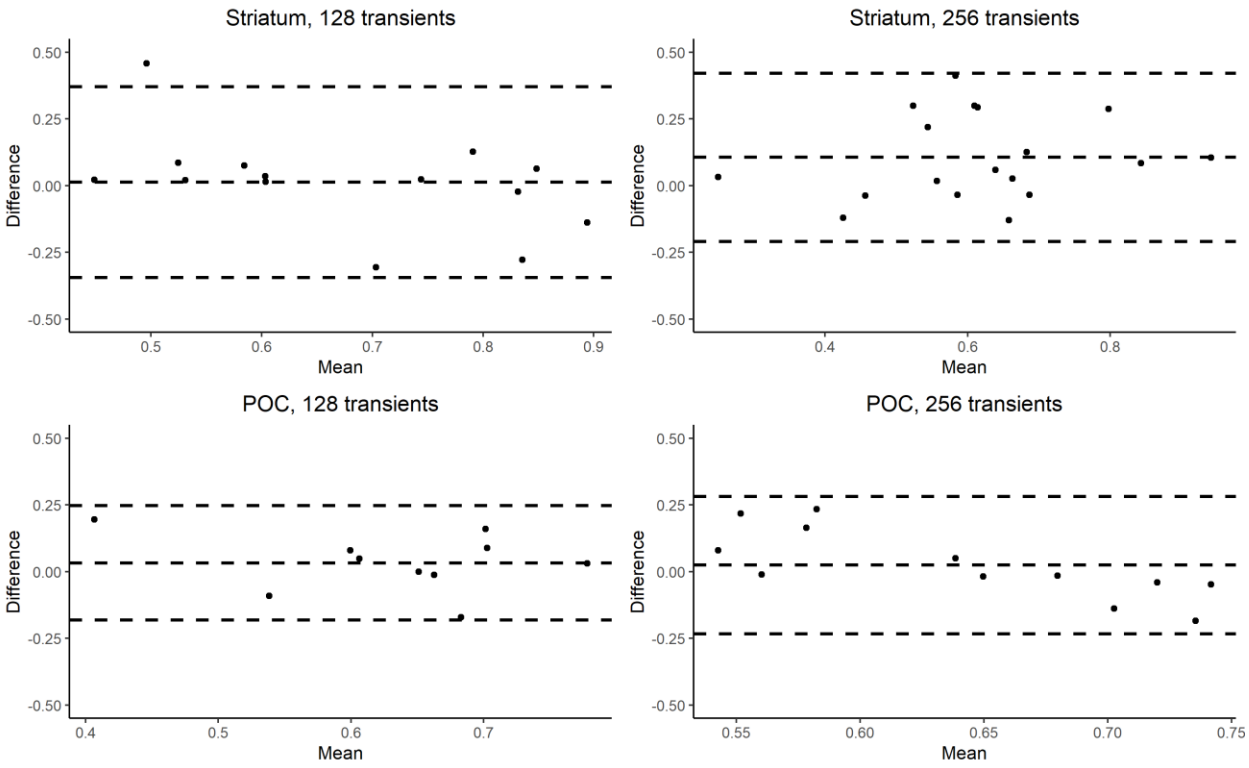

Figure 34 Bland-Altman plot of across session difference for spectra averaged from 128 and 256 transients for GPC+PC

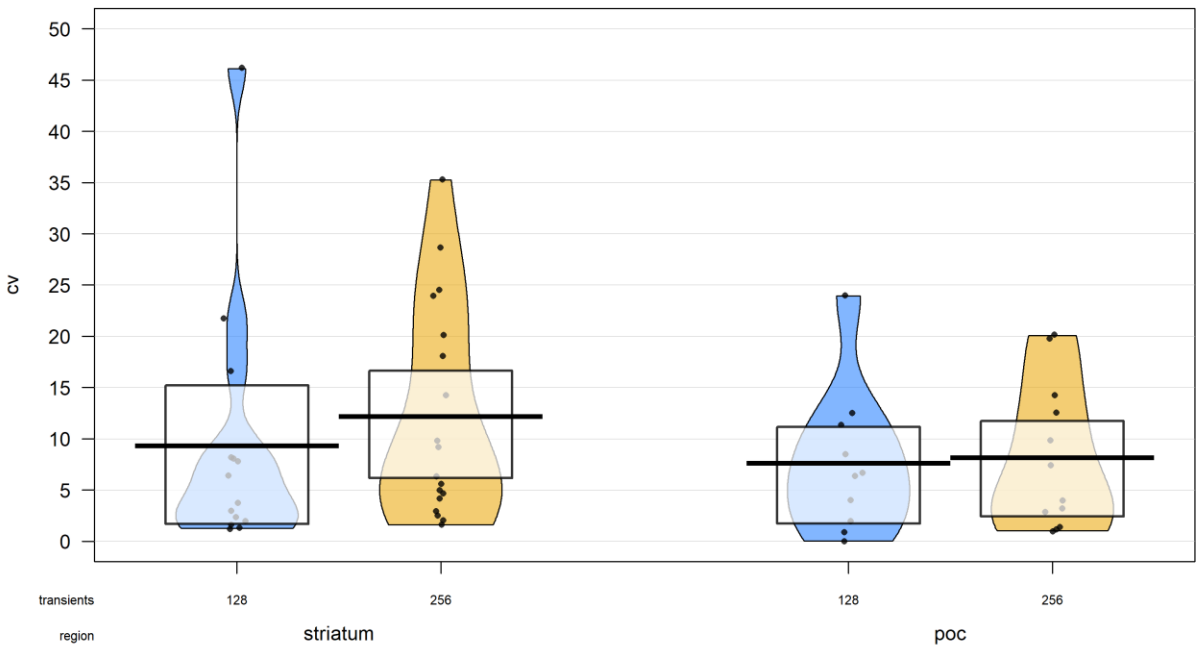

Figure 35 Coefficient of variance of across session difference for spectra averaged from 128 and 256 transients for GPC+PC

Discussion

We used ^{1}H-MRS to assess the reliability of cholinergic metabolites in the striatum and cortex. We analysed averages of 128 and 256 transients in the dorsal striatum and POC in spectra acquired one week apart. Cholinergic metabolites were quantified using two different basis sets: one quantified cholinergic metabolites as a single peak ($tCho_1$), while the other separated choline (Cho) from glycerophosphocholine and phosphocholine (GPC+PC). We found quantifying CCCs using separate peaks for choline and GPC+PC resulted in concentrations that were consistent with estimates when using a single peak in the striatum, but not in the POC. Additionally, we find $tCho_1$ and choline concentrations were inconsistent at the individual level within and between sessions, but there were no differences at the group level. Conversely, within session GPC+PC concentrations were consistent in the striatum at the individual level in one session. Between session GPC+PC were consistent between sessions for spectra averaged from 256 transients at the individual level, but were significantly different at the group level. GPC+PC concentrations were inconsistent within and between sessions in the POC, but showed no significant difference at the group level.

$tCho_1$ levels in the striatum were highly correlated with the sum of Cho and GPC+PC ($tCho_2$) for both averages in both sessions. $tCho_1$ and $tCho_2$ were significantly correlated for 256 transients in session one, and 128 transients in session two for the POC, and for both acquisitions in both sessions in the striatum. Separate peaks for Cho and GPC+PC were also quantified more frequently in the striatum than in the POC. Within session $tCho_1$ concentrations were inconsistent at the subject level in the striatum and POC between spectra averaged from 128 and 256 transients, but no significant differences in metabolite concentrations were observed at the group level. The same results as $tCho_1$ were found at the individual and group level for Cho. GPC+PC concentrations for spectra averaged from 128 and 256 transients were consistent at the subject level for the first but not the second session in the striatum, and for neither session in the POC; no group level differences were observed for GPC+PC. Across session $tCho_1$ concentrations were inconsistent at the subject level in the striatum and POC for spectra averaged from 128 and 256 transients, but no significant differences in metabolite concentrations were observed at the group level. Cho concentrations showed the same trend as $tCho_1$ across sessions. GPC+PC concentrations were consistent at the subject level across sessions for the striatum but not the POC. Significant group level differences were found for GPC+PC across sessions for spectra averaged from 256 transients, but no other group level differences were significant. These differences in metabolite concentrations are not due

to diurnal effects as participants were scanned at the same time of day, nor were they due to the heating of gradient coils causing scanner drift as all sessions were the first scan of each day.

Conventional approaches for quantifying the choline containing metabolites from ^{1}H-MRS spectra treat these metabolites as a single peak, however we have previously demonstrated that Cho can be separated from GPC+PC, and that this can be used to measure functionally relevant changes in metabolites (Bell et al., 2018, 2019; Lindner et al., 2017). Here, we again show that separate peaks for the CCCs can be quantified, and that the sum of these separate metabolites are positively associated with metabolite estimates with a single peak. This suggests that quantifying metabolites with a single peak for the CCCs quantifies equivalent parts of the metabolite spectra as when using separate peaks but oversimplifies the underlying biochemistry as it masks the functionally relevant Cho signal that is present within the metabolite signal. The between session coefficients of variance observed for GPC+PC in the striatum and POC are in line with previously reported values by Chard et al. (2002), however the coefficients we observed for Cho between sessions was around five times greater than we observed for GPC+PC. The difference in consistency between GPC+PC and Cho suggests that GPC+PC is a more stable measure over time, and that differences in $tCho_1$ over time may be driven more by differences in Cho than in GPC+PC concentrations. This interpretation is in line with the fundings of Bell et al. (2018), who show that while there are functionally relevant changes in Cho following behavioural change, there was no significant changes in total choline, or other CCCs. We therefore interpret this difference in consistency over time as being relevant for the functional role that Cho plays in acetylcholine neurotransmission, and that variation in resting Cho levels over time may also explain some variance in intra-individual performance on tasks requiring the recruitment of the cholinergic system (Bell et al., 2019).

Within sessions, quantified concentrations of $tCho_1$, Cho, and GPC+PC from spectra averaged from 128 and 256 transients in the striatum and POC were not significantly correlated, except for GPC+PC in the striatum in session one. These differences may be due to increased precision in metabolite concentration estimation during spectral acquisition and quantitation following an increase in the number of averaged transients. Conversely, these differences may reflect fluctuations in resting metabolite concentrations during acquisition, or noise due to participant movement. In either case, we found no significant differences in metabolite concentrations at the group level, suggesting that this variance may average out when inferences do not need to be drawn at the individual level. We are unable to explore these alternative explanations further with this dataset using approaches like bootstrapping because our archived spectral data were averages for each acquisition; therefore, we do not have individual spectra for each transient. Nevertheless, the difference in metabolite concentrations from spectra of different lengths raises important

considerations for work employing functional ^{1}H-MRS to studying changes in metabolite concentrations in relation to behaviour. Experimental design should balance the trade-off between the temporal resolution required to study the behaviour of interest, and the signal to noise ratio in the metabolite spectra.

One limitation of this study is that some unaccounted variance in between session metabolite estimates is likely to be due to inconsistency in voxel positioning. Though voxel positioning was guided by an individual's anatomy, and the average consistency of voxel positioning was good, we also had a wide range in voxel positioning consistency in both the striatum and POC. Striatal voxel positioning consistency was in line with previous reports, but POC positioning was lower than previously reported voxel positioning consistency (~70%) (Dou et al., 2015). Furthermore, unlike Lindner et al. (2017), our POC voxel position was driven by anatomical boundaries, rather than a functional localiser. These issues could be addressed in future by using an automated voxel positioning, such as the Automated Voxel Placement procedure described by Woodcock et al. (2018). Furthermore, participant head motion during spectral acquisition could be controlled for by using prospective motion correction to ensure the anatomical location of the voxel is consistent across time and within each spectral acquisition (Zaitsev et al., 2010).

In summary, we assess the use of ^{1}H-MRS to investigate the reliability of measures of cholinergic metabolites in the striatum and POC. Quantifying CCCs with single and separate peaks showed these metabolite concentrations were related, and that using separate peaks for Cho and GPC+PC may more clearly explain functionally relevant cholinergic signals. Separate peaks were more frequently delineated in the striatum than in the POC and suggests there are regional differences in how these metabolites can be quantified. We observed greater intra-individual variability in $tCho_1$ and Cho than in GPC+PC. Disproportionate variability in Cho may reflect its functional relationship with acetylcholine dynamics, and therefore quantifying the CCCs using a single peak may mask functionally relevant information in the metabolite spectra. Further work is required to clarify the use of ^{1}H-MRS to study the human cholinergic system *in vivo* including the use of standardised routines for positioning the spectroscopy voxel, and methods for online correction of motion artefacts during spectral acquisition.

Acknowledgments

We would like to thank Dan James for assistance with recruitment & Michael Lindner for initial methods development work.

References

Ashburner, J., & Friston, K. J. (2005). Unified segmentation. *NeuroImage*, *26*(3), 839–851. https://doi.org/10.1016/j.neuroimage.2005.02.018

Baeshen, A., Wyss, P. O., Henning, A., O'Gorman, R. L., Piccirelli, M., Kollias, S., & Michels, L. (2020). Test–Retest Reliability of the Brain Metabolites GABA and Glx With JPRESS, PRESS, and MEGA‐PRESS MRS Sequences in vivo at 3T. *Journal of Magnetic Resonance Imaging*, *51*(4), 1181–1191. https://doi.org/10.1002/jmri.26921

Barker, P. B., & Lin, D. D. M. (2006). In vivo proton MR spectroscopy of the human brain. *Progress in Nuclear Magnetic Resonance Spectroscopy*, *49*(2), 99–128. https://doi.org/10.1016/j.pnmrs.2006.06.002

Bell, T., Lindner, M., Langdon, A., Mullins, P. G., & Christakou, A. (2019). Regional Striatal Cholinergic Involvement in Human Behavioral Flexibility. *The Journal of Neuroscience*, *39*(29), 5740–5749. https://doi.org/10.1523/JNEUROSCI.2110-18.2019

Bell, T., Lindner, M., Mullins, P. G., & Christakou, A. (2018). Functional neurochemical imaging of the human striatal cholinergic system during reversal learning. *European Journal of Neuroscience*, *47*(10), 1184–1193. https://doi.org/10.1111/ejn.13803

Bengtsson, H. (2020). *matrixStats: Functions that Apply to Rows and Columns of Matrices (and to Vectors)*. https://CRAN.R-project.org/package=matrixStats

Bittšanský, M., Výbohová, D., & Dobrota, D. (2012). Proton magnetic resonance spectroscopy and its diagnostically important metabolites in the brain. *General Physiology and Biophysics*, *31*(1), 101–112. https://doi.org/10.4149/gpb_2012_007

Bradfield, L. A., Bertran-Gonzalez, J., Chieng, B., & Balleine, B. W. (2013). The thalamostriatal pathway and cholinergic control of goal-directed action: Interlacing new with existing learning in the striatum. *Neuron*, *79*(1), 153–166. https://doi.org/10.1016/j.neuron.2013.04.039

Brown, H. D., Baker, P. M., & Ragozzino, M. E. (2010). The Parafascicular Thalamic Nucleus Concomitantly Influences Behavioral Flexibility and Dorsomedial Striatal Acetylcholine Output in Rats. *Journal of Neuroscience*, *30*(43), 14390–14398. https://doi.org/10.1523/JNEUROSCI.2167-10.2010

Chard, D. T., McLean, M. A., Parker, G. J. M., MacManus, D. G., & Miller, D. H. (2002). Reproducibility of in vivo metabolite quantification with proton magnetic resonance spectroscopic imaging. *Journal of Magnetic Resonance Imaging*, *15*(2), 219–225. https://doi.org/10.1002/jmri.10043

Cuello, A. C. (Ed.). (1993). *Cholinergic Function and Dysfunction* (1st ed., Vol. 98). Elsevier.

Currie, S., Hadjivassiliou, M., Wilkinson, I. D., Griffiths, P. D., & Hoggard, N. (2013). Magnetic Resonance Spectroscopy of the Normal Cerebellum: What Degree of Variability Can Be Expected? *The Cerebellum*, *12*(2), 205–211. https://doi.org/10.1007/s12311-012-0415-1

Dou, W., Speck, O., Benner, T., Kaufmann, J., Li, M., Zhong, K., & Walter, M. (2015). Automatic voxel positioning for MRS at 7 T. *Magnetic Resonance Materials in Physics, Biology and Medicine*, *28*(3), 259–270. https://doi.org/10.1007/s10334-014-0469-9

Edden, R. A. E., Puts, N. A. J., Harris, A. D., Barker, P. B., & Evans, C. J. (2014). Gannet: A batch-processing tool for the quantitative analysis of gamma-aminobutyric acid–edited MR spectroscopy spectra. *Journal of Magnetic Resonance Imaging*, *40*(6), 1445–1452. https://doi.org/10.1002/jmri.24478

El-Sharkawy, A. M., Schär, M., Bottomley, P. A., & Atalar, E. (2006). Monitoring and correcting spatio-temporal variations of the MR scanner's static magnetic field. *Magnetic Resonance Materials in Physics, Biology and Medicine*, *19*(5), 223–236. https://doi.org/10.1007/s10334-006-0050-2

Fayed, N., Modrego, P. J., & Medrano, J. (2009). Comparative test–retest reliability of metabolite values assessed with magnetic resonance spectroscopy of the brain. The LCModel versus the manufacturer software. *Neurological Research*, *31*(5), 472–477. https://doi.org/10.1179/174313209X395481

Gamer, M., Lemon, J., & Singh, I. F. P. (2019). *irr: Various Coefficients of Interrater Reliability and Agreement*. https://CRAN.R-project.org/package=irr

Garcia, M. I. O., Sima, D., Nielsen, F., Himmelreich, U., & Van Huffel, S. (2010). Quantification of in vivo Magnetic Resonance Spectroscopy signals with baseline and lineshape corrections. *2010 IEEE International Conference on Imaging Systems and Techniques*, 349–352. https://doi.org/10.1109/IST.2010.5548503

Gasparovic, C., Song, T., Devier, D., Bockholt, H. J., Caprihan, A., Mullins, P. G., Posse, S., Jung, R. E., & Morrison, L. A. (2006). Use of tissue water as a concentration reference for proton spectroscopic imaging. *Magnetic Resonance in Medicine*, *55*(6), 1219–1226. https://doi.org/10.1002/mrm.20901

Harrell Jr, F. E., & Dupont, C. (2020). *Hmisc: Harrell Miscellaneous*. https://CRAN.R-project.org/package=Hmisc

Harris, A. D., Glaubitz, B., Near, J., Evans, C. J., Puts, N. A. J., Schmidt-Wilcke, T., Tegenthoff, M., Barker, P. B., & Edden, R. A. E. (2014). Impact of frequency drift on gamma-aminobutyric acid-edited MR spectroscopy. *Magnetic Resonance in Medicine*, *72*(4), 941–948. https://doi.org/10.1002/mrm.25009

Lange, T., Zaitsev, M., & Buechert, M. (2011). Correction of frequency drifts induced by gradient heating in 1H spectra using interleaved reference spectroscopy. *Journal of Magnetic Resonance Imaging: JMRI*, *33*(3), 748–754. https://doi.org/10.1002/jmri.22471

Lehnert, B. (2015). *BlandAltmanLeh: Plots (Slightly Extended) Bland-Altman Plots*. https://CRAN.R-project.org/package=BlandAltmanLeh

Lindner, M., Bell, T., Iqbal, S., Mullins, P. G., & Christakou, A. (2017). In vivo functional neurochemistry of human Cortical cholinergic function during visuospatial attention. *PLoS ONE*, *12*(2), e0171338. https://doi.org/10.1371/journal.pone.0171338

Löffelholz, K. (1998). Brain choline has a typical precursor profile. *Journal of Physiology Paris*, *92*(3–4), 235–239. https://doi.org/10.1016/S0928-4257(98)80025-9

Mangiafico, S. (2021). *rcompanion: Functions to Support Extension Education Program Evaluation*. https://CRAN.R-project.org/package=rcompanion

Naressi, A., Couturier, C., Devos, J. M., Janssen, M., Mangeat, C., de Beer, R., & Graveron-Demilly, D. (2001). Java-based graphical user interface for the MRUI quantitation package. *Magnetic Resonance Materials in Physics, Biology and Medicine*, *12*(2–3), 141–152.

Okada, T., Sakamoto, S., Nakamoto, Y., Kohara, N., & Senda, M. (2007). Reproducibility of magnetic resonance spectroscopy in correlation with signal-to-noise ratio. *Psychiatry Research: Neuroimaging*, *156*(2), 169–174. https://doi.org/10.1016/j.pscychresns.2007.03.007

Papadakis, M., Tsagris, M., Dimitriadis, M., Fafalios, S., Tsamardinos, I., Fasiolo, M., Borboudakis, G., Burkardt, J., Zou, C., Lakiotaki, K., & Chatzipantsiou, C. (2021). *Rfast: A Collection of Efficient and Extremely Fast R Functions*. https://CRAN.R-project.org/package=Rfast

Phillips, N. (2017). *Yarrr: A Companion to the e-Book 'YaRrr!: The Pirate's Guide to R'*. https://CRAN.R-project.org/package=yarrr

R Core Team. (2020). *R: A Language and Environment for Statistical Computing*. R Foundation for Statistical Computing. https://www.R-project.org/

Ragozzino, M. E., Mohler, E. G., Prior, M., Palencia, C. A., & Rozman, S. (2009). Acetylcholine activity in selective striatal regions supports behavioral flexibility. *Neurobiology of Learning and Memory*, *91*(1), 13–22. https://doi.org/10.1016/j.nlm.2008.09.008

Revelle, W. (2020). *psych: Procedures for Psychological, Psychometric, and Personality Research*. Northwestern University. https://CRAN.R-project.org/package=psych

Simpson, R., Devenyi, G. A., Jezzard, P., Hennessy, T. J., & Near, J. (2015). Advanced processing and simulation of MRS data using the FID appliance (FID-A)—An open source, MATLAB-based toolkit. *Magnetic Resonance in Medicine*, *77*(1), 23–33. https://doi.org/10.1002/mrm.26091

Soreni, N., Noseworthy, M. D., Cormier, T., Oakden, W. K., Bells, S., & Schachar, R. (2006). Intraindividual variability of striatal (1)H-MRS brain metabolite measurements at 3 T. *Magnetic Resonance Imaging*, *24*(2), 187–194. https://doi.org/10.1016/j.mri.2005.10.027

Stefan, D., Cesare, F. D., Andrasescu, A., Popa, E., Lazariev, A., Vescovo, E., Strbak, O., Williams, S., Starcuk, Z., Cabanas, M., Ormondt, D. van, & Graveron-Demilly, D. (2009). Quantitation of magnetic resonance spectroscopy signals: The jMRUI software package. *Measurement Science and Technology*, *20*(10), 104035. https://doi.org/10.1088/0957-0233/20/10/104035

White, H. L., & Wu, J. C. (1973). Kinetics of Choline Acetyltransferases (ec 2.3.1.6) from Human and Other Mammalian Central and Peripheral Nervous Tissues. *Journal of Neurochemistry*, *20*(2), 297–307. https://doi.org/10.1111/j.1471-4159.1973.tb12129.x

Wickham, H. (2016). *ggplot2: Elegant Graphics for Data Analysis*. Springer-Verlag. https://ggplot2.tidyverse.org

Wickham, H., & Bryan, J. (2019). *readxl: Read Excel Files*. https://CRAN.R-project.org/package=readxl

Wilke, C. O. (2020). *cowplot: Streamlined Plot Theme and Plot Annotations for 'ggplot2'*. https://CRAN.R-project.org/package=cowplot

Wilson, M., Andronesi, O., Barker, P. B., Bartha, R., Bizzi, A., Bolan, P. J., Brindle, K. M., Choi, I., Cudalbu, C., Dydak, U., Emir, U. E., Gonzalez, R. G., Gruber, S., Gruetter, R., Gupta, R. K., Heerschap, A., Henning, A., Hetherington, H. P., Huppi, P. S., … Howe, F. A. (2019). Methodological consensus on clinical proton MRS of the brain: Review and recommendations. *Magnetic Resonance in Medicine*, *82*(2), 527–550. https://doi.org/10.1002/mrm.27742

Woodcock, E. A., Arshad, M., Khatib, D., & Stanley, J. A. (2018). Automated Voxel Placement: A Linux-based Suite of Tools for Accurate and Reliable Single Voxel Coregistration. *Journal of Neuroimaging in Psychiatry & Neurology*, *3*(1), 1–8. https://doi.org/10.17756/jnpn.2018-020

Zaitsev, M., Speck, O., Hennig, J., & Büchert, M. (2010). Single-voxel MRS with prospective motion correction and retrospective frequency correction. *NMR in Biomedicine*, *23*(3), 325–332. https://doi.org/10.1002/nbm.1469

Zhu, H., & Barker, P. B. (2011). MR Spectroscopy and Spectroscopic Imaging of the Brain. In M. Modo & J. W. M. Bulte (Eds.), *Magnetic Resonance Neuroimaging: Methods and Protocols* (pp. 203–226). Humana Press. https://doi.org/10.1007/978-1-61737-992-5_9

Cortical and thalamic influences on striatal involvement in instructed, serial reversal learning; implications for the organisation of flexible behaviour

Brendan Williams[1,2], Anastasia Christakou[1,2]

1. Centre for Integrative Neuroscience and Neurodynamics, University of Reading, UK
2. School of Psychology and Clinical Language Sciences, University of Reading, UK

Abstract

Cognitive flexibility is essential for enabling an individual to respond adaptively to changes in their environment. Evidence from human and animal research suggests that the control of cognitive flexibility is dependent on an array of neural architecture. Cortico-basal ganglia circuits have long been implicated in cognitive flexibility. In particular, the role of the striatum is pivotal, acting as an integrative hub for inputs from the prefrontal cortex and thalamus, and modulation by dopamine and acetylcholine. Striatal cholinergic modulation has been implicated in the flexible control of behaviour, driven by input from the centromedian-parafascicular nuclei of the thalamus. However, the role of this system in humans is not clearly defined as much of the current literature is based on animal work. Here, we aim to investigate the roles corticostriatal and thalamostriatal connectivity in serial reversal learning. Functional connectivity between the left centromedian-parafascicular nuclei and the associative dorsal striatum was significantly increased for negative feedback compared to positive feedback. Similar differences in functional connectivity were observed for the right lateral orbitofrontal cortex, but these were localised to when participants switched to using an alternate response strategy following reversal. These findings suggest that connectivity between the centromedian-parafascicular nuclei and the striatum may be used to generally identify potential changes in context based on negative outcomes, and the effect of this signal on striatal output may be influenced by connectivity between the lateral orbitofrontal cortex and the striatum.

Introduction

Flexible control over behaviour enables goal directed action by allowing an individual to respond to changes in its environment. Being adaptive to change means an individual can adjust their behaviour while maintaining their current goal, which is particularly important in ambiguous or volatile environments where there is uncertainty around optimal behaviours. One common behavioural assay is the reversal learning task (Izquierdo et al., 2017; Yaple & Yu, 2019). During reversal learning participants learn associations between actions and outcomes, with the aim of maximising reward. Some actions are more rewarding, while others are less so. These associations between actions and outcomes change during the task and therefore participants need to alter how they respond to continue maximising reward. Perseverative responding, the inability to effectively switch to an alternate response strategy following reversal, is indicative of inflexibility, and elevated in conditions characterised by repetitive behaviour including addiction (De Ruiter et al., 2009; Ersche et al., 2011; Verdejo-Garcia et al., 2015), autism (Crawley et al., 2020; though also see D'Cruz et al., 2016) and obsessive compulsive disorder (Remijnse et al., 2006).

Cognitive flexibility requires the orchestration of signals from across the cortical surface and subcortical brain regions. Previous work has shown that the striatum, with its afferent projections from the cerebral cortex, thalamus, amygdala, and hippocampus (among other regions) is well positioned to act as an integrative information hub (Haber, 2016) and supports reversal learning (Bradfield, Hart, et al., 2013; Cools et al., 2002; Ruge & Wolfensteller, 2016). One striatal afferent consistently implicated in studies of reversal learning is the orbitofrontal cortex (Dalton et al., 2016; Rudebeck & Murray, 2008; Rygula et al., 2010; Tsuchida et al., 2010). Reduced orbitofrontal activation during reversal learning is associated with increased inflexibility in obsessive compulsive disorder, (Remijnse et al., 2006), and with a reduced capacity to use negative outcomes to guide behaviour (Groman et al., 2019). Within the context of reversal learning, the orbitofrontal cortex is broadly thought to be involved in the shifting of behaviour following the reversal of outcome contingencies (Izquierdo et al., 2017; Uddin, 2021). More specifically, the medial and lateral portions of the orbitofrontal cortex are thought to have dissociable roles, with the former involved in outcome evaluation, and the latter representing the current state of the task and its associated contingencies (Hampshire et al., 2012; Hervig et al., 2020; Noonan et al., 2017). Therefore, though the medial division of the orbitofrontal cortex is generally important for goal directed learning, the lateral portion is specifically involved in reversal learning and changing behaviour following the reversal of reward contingencies (Dalton et al., 2016; Hampshire et al., 2012; Morris et al., 2016). Previous work from Bell, Langdon, et al. (2019) used a multi-alternative

reversal learning task with a single uninstructed reversal to investigate the neural mechanisms underlying reversal learning. This task closely mimics the setup of animal studies of reversal learning. It has a protracted period of initial and reversal learning where participants learn correct and incorrect choices from experiencing trial-and-error. These protracted learning periods are like learning in animal reversal learning task (e.g. in T-mazes Izquierdo et al, (2017)), where many trials are required for learning stimulus-outcome contingencies. This is because participants are not instructed about the reversal of reward contingencies. Instead, they rely on ongoing outcome processing to signal a potential change in environmental contingencies. Increased functional connectivity between the medial orbitofrontal cortex and ventral striatum was found after initial learning, and before reversal; at this time participants should have a stable initial representation of the task to guide goal-directed behaviour. This finding supports the proposed role of the medial orbitofrontal cortex in outcome evaluation and goal directed behaviour. Conversely, increased functional connectivity between the lateral orbitofrontal cortex and the dorsal striatum was found during reversal learning. The strength of functional connectivity was inversely correlated with trials to criterion during reversal learning and was found to be mediated by the learning rate for positive prediction errors. This suggests lateral orbitofrontal connectivity with the dorsal striatum promotes changes in behaviour following reversal via learning from positive outcomes, reducing response perseveration.

Another region important for cognitive flexibility is the thalamus. While traditionally viewed as a relay for sensory and motor signals, there is an increasing appreciation for the role of the thalamus in cognitive processes (Wolff & Vann, 2019). This includes cognitive flexibility and reversal learning, where several thalamic nuclei are known to have an important role. For instance, animal literature has shown that lesions to the mediodorsal nucleus of the thalamus does not impair initial discrimination learning but does impair reversal learning (Chudasama et al., 2001). More specifically, lesions to the mediodorsal thalamus are thought to impair reversal learning by preventing the use of recent history to guide future choice, and thus choice behaviour is increasingly stochastic following the reversal of reward contingencies (Chakraborty et al., 2016). In addition to the mediodorsal thalamus, the centromedian-parafascicular nuclei are also important for flexibility. However, while the mediodorsal projects primarily to the cortex with axon collaterals to the striatum, the centromedian-parafascicular nuclei project primarily to the striatum, with afferents that are preferentially connected with the striatal cholinergic system (Smith et al., 2009). Thalamic connectivity between the parafascicular nucleus of the thalamus (the rodent homologue of the primate centromedian-parafascicular (Smith et al., 2011)) and the striatal cholinergic system is important for reversal learning (Bradfield, Hart, et al., 2013); disconnection of these circuits

impairs reversal learning by reducing striatal acetylcholine efflux, which in turn increases interference between new and existing contingency encoding following reversal (Bradfield, Bertran-Gonzalez, et al., 2013; Brown et al., 2010). Therefore, though both the mediodorsal and centromedian-parafascicular nuclei support cognitive flexibility, they show distinct roles and connectivity patterns.

Thalamostriatal connections between the centromedian-parafascicular nuclei and the striatal cholinergic system are also thought to be important for flexibility in humans. For instance, magnetic resonance spectroscopy has previously been used during uninstructed reversal learning, to demonstrate functionally relevant changes in dorsal striatal choline that are specific to the reversal of reward contingencies and are not present during initial learning (Bell et al., 2018). Moreover, baseline striatal choline levels are also associated with reversal learning performance, and suggests that the state of the striatal cholinergic system explains some variability in cognitive flexibility (Bell, Lindner, et al., 2019). Additionally, changes in functional connectivity between the centromedian-parafascicular nucleus in the thalamus and the dorsal striatum have been seen during reversal, but not initial learning in the same task (Bell, Langdon, et al., 2019). Based on evidence from animal and human literature we think the thalamostriatal connectivity between the centromedian-parafascicular nuclei and the dorsal striatal system is important for producing internal representations that are context dependent and support cognitive flexibility. More specifically, thalamostriatal connections are believed to recruit cholinergic interneurons to support new learning without "overwriting" prior knowledge (Bradfield, Bertran-Gonzalez, et al., 2013). Cholinergic involvement, alongside dopaminergic prediction errors, enables behaviour that can adaptively and efficiently respond to change by making the system sensitive to the broader behavioural context, beyond simply outcome contingencies. Furthermore, the striatal cholinergic system may enable the representation of context by modulating the output of striatal projection neurons (Stayte et al., 2021). Therefore, the concurrent representation of context-dependent contingencies in the striatum facilitates flexible behaviour that is responsive to change. Indeed, this preposition is supported by computational work from Franklin & Frank (2015), who show the inclusion of cholinergic interneurons in a model of the basal ganglia enables learning rates to respond to environmental noise and uncertainty. Cholinergic interneurons are tonically active and show a transient pause and rebound response to phasic activity. Changes in length of this transient pause in Franklin & Frank's (2015) model were associated with balancing flexibility and stability, with pause length inversely associated with learning rate during reversal. Shorter pauses facilitated faster updating of expected values but meant the system was more perturbed by noise, while the inverse was true for longer pauses. Importantly, a pause length that was reciprocally modulated by

medium spiny neuron activity (compared to models with fixed pause lengths), enabled the system to respond adaptively to change, minimising errors during probabilistic reversal. These dynamics may ultimately regulate the effects of dopamine on the plasticity of corticostriatal synapses, enabling the striatum to generate internal representations that are responsive to change and uncertainty in the environment. Furthermore, these dynamics are in line with our understanding of how variability in cholinergic transmission influences sensitivity to volatility and noise during reversal learning.

Previous evidence in animals has shown that thalamostriatal connectivity between the centromedian-parafascicular nuclei and the striatal cholinergic system is important for preventing interference when integrating new and existing learning (Bradfield, Bertran-Gonzalez, et al., 2013). This is supported by our previous work in humans where we show that the striatal cholinergic system, recruited by corticostriatal and thalamostriatal connectivity, is involved in reversal learning (Bell et al., 2018; Bell, Langdon, et al., 2019; Bell, Lindner, et al., 2019). These works from Bell and colleagues bridge the gap between animal and human neuroscience, using a homologous task setup to consolidate how we think cortical, striatal, and thalamic systems interact during initial and reversal learning. However, most reversal learning tasks used in human neuroimaging work are more like serial reversal learning than the multi-alternative task of the Bell et al. studies. Internal representations of task context are readily acquired in serial reversal learning, and once an "if not A, then B" heuristic for correct and incorrect choices exists, no additional information is relevant for representing task structure. Therefore, task representation in serial reversal learning may be considered as "saturated". However, task representations for the multi-alternative task can be considered as "unsaturated", since participants are not instructed on the structure of the task and only compile mature task representations following both the protracted initial and reversal learning periods. Therefore, these differences in task representation may explain evidence suggesting dissociable roles for choline in serial and multi-alternative reversal learning in chapter 5 and Bell, Lindner, et al. (2019). We propose having a higher cholinergic "tone" at rest is beneficial under a saturated task representation, by limiting learning disproportionately from probabilistic and regressive errors, thereby promoting stability. By contrast, a lower tone is beneficial for unsaturated task representations, by maximising contrast between periods of stability and change, thereby promoting flexibility.

However, it is unclear how cortical and thalamic regions interact with the striatum and produce flexible behaviour in a context with a saturated task representation. In such a context, there is no new contextual information following initial discrimination and reversal learning, because the reversal has been instructed. Therefore, connectivity specifically from the centromedian-

parafascicular nuclei to the striatum may not contribute to serial reversal learning in the same way as in the uninstructed multi-alternative task, where the reversal needs to be discovered. Instead, behaviour may be mediated via cortically driven mechanisms, using prior knowledge to guide action in line with the known task representation. This is supported by evidence demonstrating that inputs from the orbitofrontal cortex to striatal cholinergic interneurons are necessary for generating internal representations in the striatum (Stalnaker et al., 2016). Alternatively, these thalamic connections may continue to be important after initial and reversal learning. For instance, they signal behaviourally relevant sensory events (Matsumoto et al., 2001; Schepers et al., 2017), and respond to changes in context (Yamanaka et al., 2018). Therefore, thalamostriatal connectivity may be relevant for identifying contextual change to promote flexibility in serial reversal as in the multi-alternative task.

To arbitrate between these possibilities, we use recent advances in parcellation approaches and functional magnetic resonance acquisition optimised for spatial specificity to examine the roles of orbitofrontal, striatal, and thalamic regions in producing cognitive flexibility in serial probabilistic reversal learning (Iglesias et al., 2018; Volz et al., 2019). In our task we define two distinct phases that appear consistently over successive reversal episodes. The "*re-learning phase*" is the period between the reversal of outcome contingencies and participants reaching the learning criterion. Once they reach criterion participants are in the "*stability phase*" until outcome contingencies reverse again. We used psychophysiological interaction analysis to study the functional connectivity between regions of interest in subdivisions of the cortex, striatum, and thalamus during re-learning and stability. Additionally, we conducted exploratory analyses investigating how reward and error signals may be used to guide behaviour during re-learning and stability phases.

Methods

Participants

36 healthy adult participants (mean age = 24.38 years; SD = 6.51; range = 18-49; 23 female) were recruited via opportunity sampling from the University of Reading community. Participants were eligible for participation if they were right-handed, and did not self-report the use of cigarettes, recreational drugs, or psychoactive medication or have a formal diagnosis of psychiatric or mental health condition. Participants were reimbursed £15 for their time. Seven participants were excluded from the final dataset. One participant had artifacts in MR data due to braces; one participant had technical errors during scanning; one participant had registration issues; four participants responded on less than 95% of trials during the task.

Materials

Magnetic resonance images were collected on a Siemens MAGNETOM Prisma 3T MRI Scanner with a 32-channel receiver head coil at the Centre for Integrative Neuroscience and Neurodynamics at the University of Reading. The probabilistic reversal learning task was programmed using MATLAB (2017b, The Mathworks, Inc, Natick, MA, United States) and Psychtoolbox-3 (Brainard, 1997) on a Macintosh running macOS Sierra. The task was presented on a BOLDscreen LCD (Cambridge Research Systems Ltd, Rochester, Kent, United Kingdom) during scanning and displayed to the participant via a mirror placed above their eyes. Task presentation, synchronised with functional volume acquisition, was controlled by a computer running Windows 7, MATLAB 2015b and Psychtoolbox-3.

Learning task

Two abstract images of fractal patterns were shown on the left and right hemifield of the visual display. Participants had to choose one of the two images within 2000ms by pressing the corresponding button on a button box, else a "too late" message was displayed. After selection, the chosen stimulus was immediately highlighted (duration: min = 1500ms, max = 2500ms, $\overline{x}$ = 2000ms, plus a jitter sampled from an exponential distribution (min = 500ms, max = 6000ms, $\overline{x}$ = 1000ms)). The outcome of the participant's choice was then presented for 1000ms. A jittered fixation cross sampled from an exponential distribution (min = 500ms, max = 3000ms, $\overline{x}$ = 1000ms) followed and was presented in the centre of the display. The participant's cumulative points total was then presented for 500ms and the trial ended with a second jittered fixation cross in the centre

of the screen, sampled from a different exponential distribution to the first fixation cross (min = 500ms, max = 6000ms, $\bar{x}$ = 1000ms). Delays and jitters were optimised to separate events of interest without compromising the psychological features of the trial, desynchronise trial timings from the fMRI acquisition repetition time, and to fully sample across the hemodynamic response function. Figure 36 shows a schematic of the task trial structure and timings.

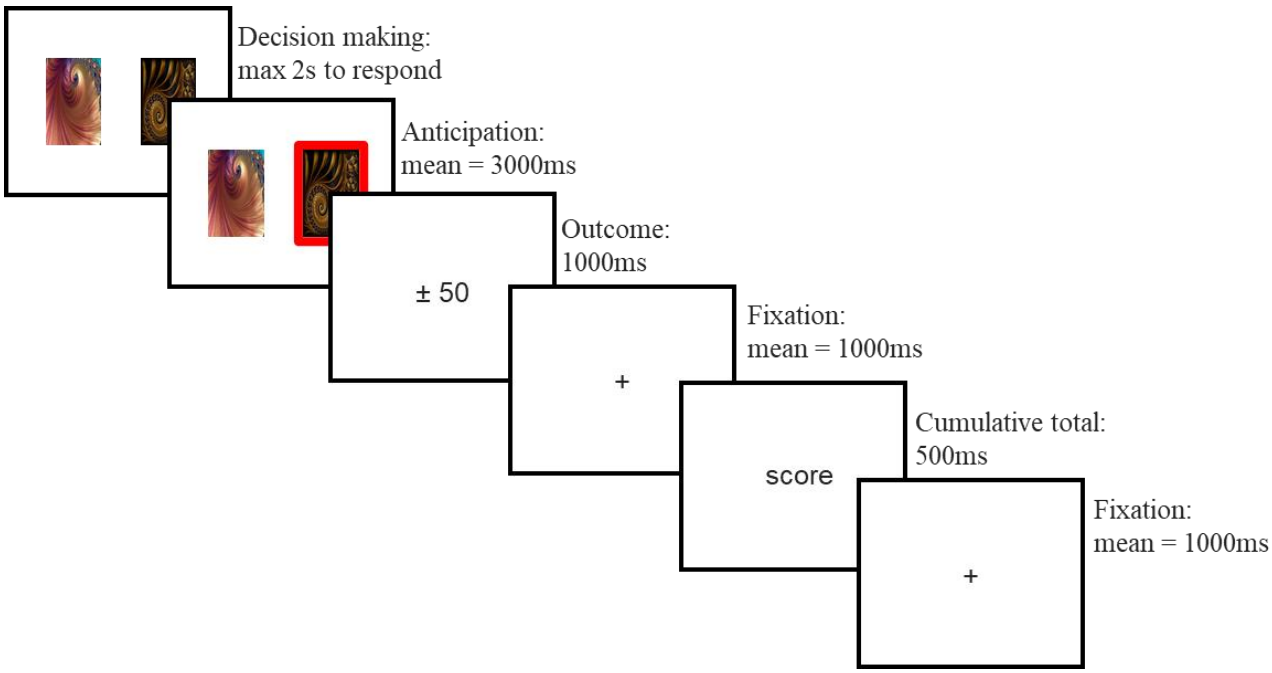

Figure 36: Overview of a single trial. Participants are initially shown two abstract fractal images and given two seconds to choose one image. Their choice is then highlighted. The participant is then shown the outcome of their choice; this will either be an increase or decrease of 50 points if they selected an image, or 0 points if they made no choice. The outcome is followed by a fixation cross, their cumulative total so far, and finally another fixation cross.

At the beginning of the task, one of the two images were randomly assigned as the correct image, and the other as the incorrect image. The probability of winning points on the correct image was 0.8, and the probability of losing points was 0.2. The inverse was true for the incorrect image. Outcomes were pseudo-randomised such that the assigned probabilities were true for blocks of 20 consecutive selections of the correct or incorrect choice. Additionally, no more than six of the same outcomes (win or loss) would be consecutively presented for the correct or incorrect choice. If participants won, their cumulative total increased by 50. If they lost, their cumulative total decreased by 50. If they did not choose an image, their cumulative total did not change. For outcome probabilities to reverse participants had to reach and maintain a predefined learning criterion: the selection of the correct image on five of the previous six trials. After reaching criterion

participants entered a *stability phase* where the probability of reversal was equal to the number of trials where criterion had been maintained, divided by 10 (adapted from (Hampton et al., 2006)). If criterion was not maintained, then the probability of reversal was reset to 0 and restarted once criterion was reached. This variable length was included to minimise identification of the learning criterion and anticipation of the reversal event. The reversal event involved the switching of outcome probabilities, with the correct image becoming incorrect and *vice versa*. On reversal, participants had to re-reach and maintain the learning criterion for the reassigned outcome probabilities (*re-learning phase*) before outcome probabilities would reverse again. Participants completed 360 trials of the reversal learning task. There was no limit on the number of reversal events a participant could experience. Left-right stimulus presentation was randomised across trials. Before starting, participants were instructed that: their aim was to collect as many points as possible; the outcome was dependent on the image they chose; one choice may be better than the other; and the better choice could change during the task. Participants completed 20 practice trials prior to entering the MRI scanner. Practice trials followed the same structure as trials in the scanner, but participants did not receive any feedback for their choices. Instead, hashtags were presented in place of outcome and cumulative total feedback.

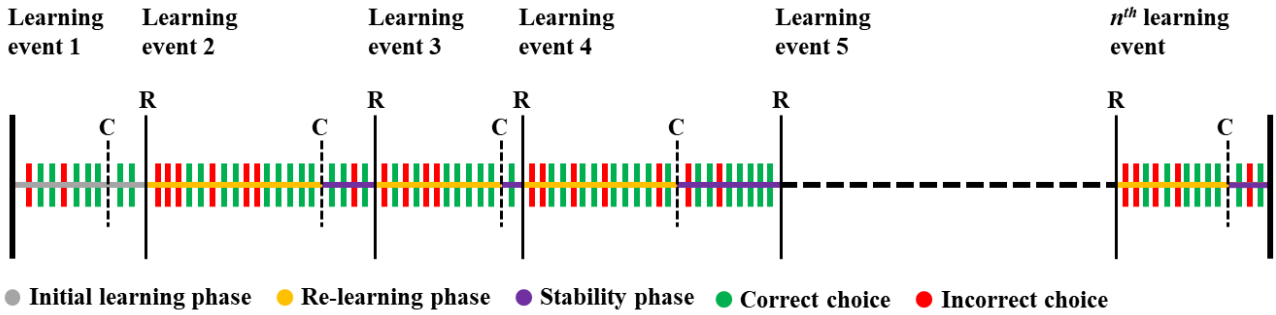

Figure 37 Trial and task phase overview of the serial reversal learning task. Dashed vertical lines show when criterion was reached (C); thin vertical lines show where outcome contingencies reversed (R) and a new learning event starts. Initial learning is the first learning event. After each reversal (R) participants are in the re-learning phase until they reach criterion (C). Participants are then in the stability phase until outcome contingencies reverse (R). The learning criterion must be maintained during the stability phase before reward contingencies reverse. Incorrect choices during the re-learning phase are defined as reversal errors, and the last reversal error of each re-learning phase is defined as the final reversal error. Each participant completes a total of 360 trials.

fMRI acquisition

T2-weighted whole-brain blood oxygen level-dependent (BOLD) functional images were acquired using a multi-band 2D-echo-planar imaging sequence with GeneRalized Autocalibrating Partially Parallel Acquisitions (GRAPPA) (acceleration factor = 2) [TR = 2160ms; TE = 30ms; slices = 93; voxel volume ≈ 1.6mm^3; slice thickness = 1.6mm; distance factor = 0%; FOV = 205 x 205 mm; matrix = 128 x 128; flip angle = 90°; multiband acceleration factor = 3; phase encoding direction = A → P (negative polarity); interleaved acquisition; echo spacing = 0.75ms; fat suppression]. BOLD acquisition parameters were optimised for spatial resolution due to the scale of thalamic nuclei relative to standard parameters used at 3T (2.5-3mm isotropic), and because smaller voxels decreases signal loss in the orbitofrontal cortex as field inhomogeneities cause partial volume distortions for fewer voxels (Volz et al., 2019; Weiskopf et al., 2007). Fieldmap images were acquired to correct for distortions in the acquired data due to inhomogeneities in the magnetic field [TR = 2900ms; TE = 53.8ms; slices = 93; voxel volume ≈ 1.6mm^3; slice thickness = 1.6mm; distance factor = 0%; FOV = 205 x 205 mm; matrix = 128 x 128; flip angle = 90°; multiband acceleration factor = 3; phase encoding direction = A → P and P → A; interleaved acquisition; echo spacing = 0.75ms; fat suppression; GRAPPA acceleration factor = 2]. High resolution T1-weighted anatomical images were acquired with a magnetization-prepared rapid gradient-echo (MP-RAGE) sequence with GRAPPA (acceleration factor = 2) [TR = 2300ms; TE = 2.29ms; TI = 900ms slices = 192; voxel volume ≈ 0.9mm^3; slice thickness = 0.94mm; distance factor = 50%; slice oversampling = 16.7%; FOV = 240 x 240mm; matrix = 256 x 256; flip angle = 8 °; phase encoding direction = A → P; echo spacing = 7ms].

Analysis of fMRI data

fMRI image analysis was performed principally using the FSL (6.0.4) toolbox from the Oxford Centre for Functional MRI of the Brain (FMRIB's Software Library, www.fmrib.ox.ac.uk/fsl), and the FreeSurfer image analysis suite (version 6.0.0).

Preprocessing

fMRI data pre-processing was carried out using FEAT (FMRI Expert Analysis Tool) Version 6.00. Registration of high resolution structural, functional and standard space images was carried out using FLIRT (Normal search, 12 DOF) (Jenkinson et al., 2002; Jenkinson & Smith, 2001); structural registration to standard space was further refined using FNIRT nonlinear registration (Normal search, 12 DOF, warp resolution = 10mm) (Andersson et al., 2007a, 2007b). MCFLIRT

was used to identify motion artefacts in functional data. Motion and distortion correction were simultaneously applied to functional data using MCFLIRT parameters and B0 unwarping parameters from fieldmap images respectively. Functional data were spatially smoothed using a smoothing kernel (3.2 FWHM).

Anatomical segmentation

Cortical reconstruction and volumetric segmentation were performed with FreeSurfer. Firstly, anatomical images were processed using the FreeSurfer recon-all pipeline, which included the generation of subject specific parcellations of the medial and lateral orbitofrontal cortex. We then used the ThalamicNuclei tool in FreeSurfer to perform thalamus segmentation. This tool performs segmentation of the thalamus using Bayesian Inference, and is based on a probabilistic atlas constructed from histological and *ex vivo* MRI data (Iglesias et al., 2018). Subject space masks for the centromedian, parafascicular, mediodorsal (medial), and mediodorsal (lateral) nuclei of the thalamus and the medial and lateral portions of the orbitofrontal cortex were generated from the automated FreeSurfer parcellations. Masks were transposed from anatomical space to functional space using FLIRT affine transformation parameters and re-binarised. Centromedian and parafascicular nuclei masks were combined to create a single mask for the Centromedian-parafascicular complex; mediodorsal (medial), and mediodorsal (lateral) masks were combined to create a mask for the mediodorsal nucleus.

Statistical analysis

First level and higher-level statistical analyses for the fMRI data were performed using FEAT. At the first level, two general linear models were run.

Model 1 – trial-wide modelling for activation comparison across task phases

The first modelled different trial types as separate regressors. These regressors were modelled as boxcar functions, the onset coincided with the onset of choice stimuli (the start of the trial as depicted in Figure 36) and the offset with the removal of the cumulative total (the start of the intertrial fixation cross; Figure 36). Twelve regressors were used to model different trial types at the subject level; Trial regressors are defined in Table 6, and are based on the phase of the task (initial learning, re-learning, or stability), the choice made (correct or incorrect), and the outcome of the choice (positive or negative feedback). A regressor to separate final reversal errors (Figure 37) from other reversal errors was also included. Each regressor and its temporal derivative were

convolved with the canonical (double gamma) haemodynamic response function. Activation maps for each regressor were generated at the subject level by creating contrast estimates relative to an implicit baseline derived from fixation periods (Figure 36). Contrast estimates for this model were generated at the whole-brain level.

<table>
<tr><td></td><td colspan="2">Initial learning</td><td colspan="3">Re-learning</td><td colspan="2">Stability</td></tr>
<tr><td></td><td>Correct</td><td>Incorrect</td><td>Correct</td><td colspan="2">Incorrect</td><td>Correct</td><td>Incorrect</td></tr>
<tr><td>Win</td><td>CI</td><td></td><td>CRe</td><td colspan="2"></td><td>CSt</td><td></td></tr>
<tr><td>Loss</td><td></td><td>II</td><td></td><td>Re
Re_par</td><td>FRe</td><td>PESt</td><td>ISt</td></tr>
</table>

Abbreviation	Description
CI	Correct response and positive feedback during initial learning
CRe	Correct response and positive feedback during re-learning
CSt	Correct response and positive feedback during stability
CR = (CI + CRe + CSt)	All correct response and positive feedback trials
II	Incorrect response and negative feedback during initial learning
Re	Reversal error – Incorrect response and negative feedback during re-learning (excluding the last Re trial for each learning event)
Re_par	Reversal error – As above, but with EV the parametrically modulated such that activation decreases from 1 to (excluding) 0 in each learning event.
FRe	Final reversal error – The last incorrect response and negative feedback during re-learning (for each learning event)
PESt	Probabilistic error - Correct response but negative feedback during stability
ISt	Incorrect response and negative feedback during stability

Table 6 Definitions of trial types within the task used for the analysis of functional magnetic resonance imaging data based on the task phase, the participant's choice, and the outcome of their choices. Task phases are described as based on definitions in Figure 37; correct choices are choices of the option with the higher probability of positive feedback, regardless of whether positive feedback was received; incorrect choices are choices with the higher probability of negative feedback. Positive feedback is the gain of 50 points irrespective of the participant's choice, negative feedback is the loss of 50 points irrespective of the participant's choice.

Model 2 – epoch-wide modelling across task phases for PPI analysis

The second general linear model modelled each epoch of the trial as a separate regressor and was used as the basis for our psychophysiological interaction analyses (PPI). These epochs were the decision-making phase, the anticipation phase, the outcome phase, and the cumulative total phase for each trial (see Figure 36 for a schematic of the trial epochs). The decision-making phase was

subdivided into decision making during initial learning, re-learning and the stability phase. The outcome phase was subdivided into positive, negative, and neutral (i.e. no choice on that given trial) feedback during each of the initial learning, re-learning, and stability phases separately.

The purpose of the PPI analysis was to interrogate the functional connectivity of regions of interest in the orbitofrontal cortex and the thalamus with specific subregions of the striatum (Friston et al., 1997; O'Reilly et al., 2012).

Unilateral seed timeseries for the medial and lateral portions of the orbitofrontal cortex, and the mediodorsal and centromedian-parafascicular nuclei of the thalamus were extracted using subject-space masks generated using FreeSurfer, and subjects pre-processed BOLD data. Medial orbitofrontal cortex was included as a control region for the lateral orbitofrontal cortex due to their dissociable roles in reversal learning. The mediodorsal thalamus was included as a control region as although it has some projections to the striatum (which do not project to cholinergic interneurons), the cortex is its main target. Conversely, the centromedian-parafascicular nuclei project preferentially to the striatal cholinergic interneurons, and these projections have been implicated specifically in reversal learning (Bell, Langdon, et al., 2019). The centromedian-parafascicular nuclei and the mediodorsal nucleus also appear to have distinct functional roles during reversal learning. Previous evidence suggests the mediodorsal nucleus is important for using recent reward history to guide behaviour and minimising perseveration (Chakraborty et al., 2016), while the centromedian-parafascicular nuclei are important for generating multiple concurrent representations of contingencies that are relevant in different contexts, signalling behaviourally relevant sensory stimuli that signal a change in context, and minimising regressive error (Bradfield & Balleine, 2017; Brown et al., 2010; Matsumoto et al., 2001; Schepers et al., 2017; Yamanaka et al., 2018).

For each general linear model, the timeseries of a seed region was included as a regressor, and the interaction between the psychological regressors and the seed timeseries was calculated. Therefore, each general linear model contained sixteen regressors. Each permutation of psychological regressor and seed timeseries was run as a separate model; these are summarised in Table 7. This resulted in forty-eight PPI models for each subject. Contrast estimates were generated using the interaction term from each PPI to identify differences in functional connectivity for positive and negative feedback during the outcome epoch and differences in functional connectivity between the re-learning and stability phases for the decision making and feedback epoch. Region of interest analysis was used to restrict our PPI results to three functional subdivisions of the striatum (associative, limbic and motor) that were defined *a priori* as target areas (Bell, Langdon, et al.,

2019; Choi et al., 2012). Regions of interest were ipsilateral to the seed region used for PPI analysis, based on the predominant anatomical connectivity of corticostriatal and thalamostriatal circuits (Bradfield, Bertran-Gonzalez, et al., 2013; Gourley et al., 2013).

Physiological regressors	Psychological regressors
Left-CM-Pf, Left-MD, Left-lOFC, Left-mOFC, Right-CM-Pf, Right -MD, Right -lOFC, Right -mOFC	Decision making (Re-learning), Decision making (Stability), Positive feedback (Re-learning), Positive feedback (Stability), Negative feedback (Re-learning), Negative feedback (Stability)

Table 7 Overview of physiological and psychological regressors used in the general linear model for psychophysiological interaction analysis.

Group-level Estimates

Higher analysis was used to calculate group level activation for our contrast estimates. Age was included as a covariate of no interest in our higher level analysis to control for maturational effects on our results, given the age range of our participants (Boehme et al., 2017); the number of reversals was also included to control for the number of learning events each participant completed. Group estimates were calculated using FLAME 1 (FMRIB's Local Analysis of Mixed Effects) in FSL using familywise error corrected (FWE) cluster thresholding ($Z = 2.3$, $p < 0.05$). For whole-brain contrasts, global and local maxima within each cluster were identified using a custom python script (https://github.com/bwilliams96/pyCL/blob/master/Label_copes.ipynb) that used atlasquery in FSL to produce an html report of the most probable region using the Harvard-Oxford cortical subcortical structural atlases. For each region, the coordinates, size, and p(FWE) corresponding to the highest z-value are reported. Our results follow published reporting guidelines for functional neuroimaging studies (Poldrack et al., 2008).

Results

Behavioural summary

All subjects included in the analysis experienced an average of 24.62 (SD = 5.67; Range = 10 - 37) reversals during the task and selected an image on >95% of trials. Correct responses, regardless of outcome, were made at significantly greater than chance level (mean correct choices = 254.38, 95% CI [248.66, ∞], $t(28) = 22.13$, $p < .001$, SD = 18.10, Range = 193 - 290), and participants experienced an average of 24.62 (SD = 5.77; Range = 10 - 37) reversals (Figure 38). The average number of trials taken to reach criterion was 8.76 (SD = 4.33; Range = 5 - 40); an average of 3.07 (SD = 2.30; Range = 0 - 18) perseverative errors were made following the reversal of contingencies before reaching criterion in each learning event. Participants did not respond on an average 2.79 trials (SD = 3.59; Range = 0 - 15) during the task. An average of 4,718.97 (SD = 1,065.31, Range = 1200 - 6800) points were collected by the end of the task. The average reaction time of participants to choose following the onset of the stimuli was 621.57 milliseconds (SD = 123.86, Range = 367.07 - 917.30).

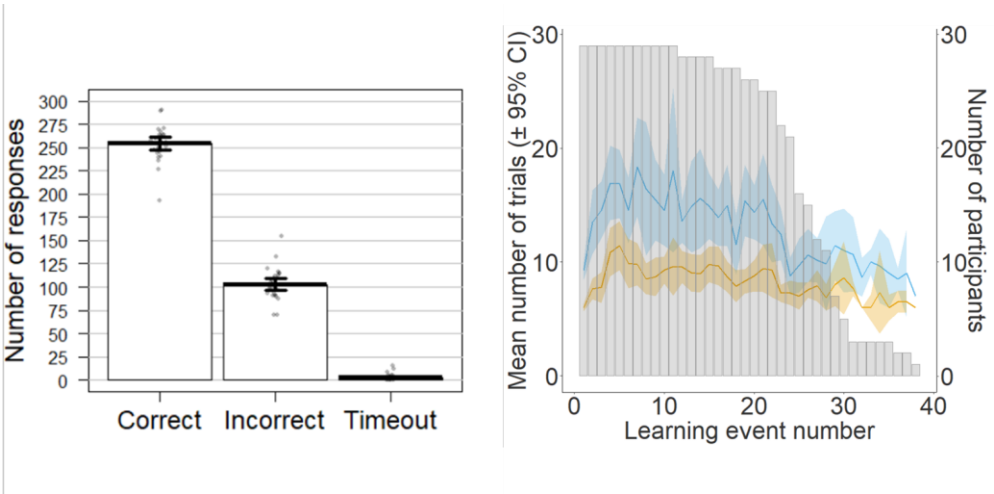

Figure 38 Mean (±95% confidence intervals) number of correct, incorrect, and missed responses for each participant across the task. Mean (±95% confidence intervals) number of trials (blue) and trials to criterion (orange) in each learning event; grey bars are the number of participants who reached each learning event.

fMRI results

Task-related activations are in line with previous studies of probabilistic reversal learning.

First, we wanted to understand whether our data was in line with previous reports of probabilistic reversal learning. If results from these analyses are aligned with previous reports, then this suggests our task is broadly comparable with other designs. Significant bilateral insula activation was found when contrasting final reversal errors and correct responses (FRe > CR), in line with previous findings (Table 8, Figure 39) (Cools et al., 2002; Dodds et al., 2008; Freyer et al., 2009; Waegeman et al., 2014; Yaple & Yu, 2019; Zeuner et al., 2016). Reversal errors that did not lead to a change in behaviour (Re > CR) showed activation consistent with past findings in the anterior cingulate/paracingulate cortex (Kringelbach & Rolls, 2003), bilateral insular cortex and right frontal operculum cortex/inferior frontal gyrus (Table 8) (Mitchell et al., 2008).

		Final reversal error > Correct					
Region	**L/R**	x	y	z	**Size**	$z(max)$	$p(FWE)$
Frontal operculum/orbitofrontal cortex	R	46	20	-4	297	4.24	< 0.001
Insula	L	-32	24	-2	158	3.75	< 0.001
Insula	R	32	26	2	297	3.62	< 0.001
		Reversal error > Correct					
Region	**L/R**	x	y	z	**Size**	$z(max)$	$p(FWE)$
Anterior cingulate/paracingulate cortex	R	8	22	40	275	3.84	< 0.001
Cerebellum	L	-40	-50	-30	110	3.71	< 0.001
Frontal operculum cortex/inferior frontal gyrus	R	46	18	2	1811	3.77	< 0.001
Frontal pole	R	36	46	6	162	3.51	< 0.001
Insula	L	-42	18	-4	202	3.68	< 0.001
Insula	R	32	26	2	1811	3.75	< 0.001
Superior frontal gyrus	R	14	10	62	233	3.71	< 0.001

Table 8 Significant clusters from whole brain analysis of contrasts used in previous studies of probabilistic reversal learning (see text for details and citations).

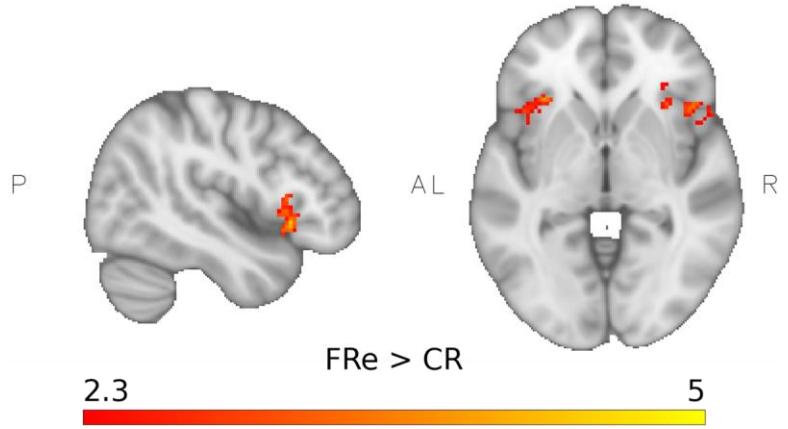

Figure 39 Whole brain analysis shows similar activations for final reversal errors versus correct response as in previous studies of reversal learning (see text for details). Significant clusters were identified in bilateral insula (peak coordinates were $x = -32,\ y = 24,\ z = -2,\ z(max) = 3.75$ for the left insula; $x = 32,\ y = 26,\ z = 2,\ z(max) = 3.75$ for the right insula) and in the right orbitofrontal cortex (peak coordinates $x = 46,\ y = 20,\ z = -4,\ z(max) = 4.24$). A significance threshold of $p(FWE) < 0.05$ and a cluster threshold of z > 2.3 was used.

Centromedian-parafascicular nuclei and lateral orbitofrontal cortex show increased functional connectivity with striatal regions during the processing of negative feedback.

We were next interested in assessing functional connectivity between the orbitofrontal cortex and striatum, and between the thalamus and the striatum. To do this we use psychophysiological interaction analysis. We used unilateral seed regions in the medial and lateral orbitofrontal cortex, and in the centromedian-parafascicular and mediodorsal nuclei of the thalamus. We measured ipsilateral functional connectivity with the striatum and restricted our analysis to regions of the associative dorsal striatum, motor dorsal striatum, and limbic ventral striatum (Bell, Langdon, et al., 2019; Choi et al., 2012). For the outcome epoch we assessed differences in functional connectivity between the re-learning and stability phases, and between positive and negative feedback. For the decision-making epoch we assessed differences in functional connectivity between the re-learning and stability phases (Table 7).

Outcome valence

Functional connectivity between the left centromedian-parafascicular nucleus of the thalamus and the associative dorsal striatum during the outcome epoch was significantly greater for negative feedback than positive feedback ($z(max) = 3.57$, MNI coordinates = [-26, 4, -2], 38 voxels, $p = 0.012$, Figure 40B & C). We also found significantly greater functional connectivity for negative feedback than positive feedback between the right lateral orbitofrontal cortex, and the associative dorsal striatum ($z(max) = 4.14$, MNI coordinates = [18, 16, -4], 39 voxels, $p = 0.008$, Figure 40E). Increased functional connectivity for negative feedback, relative to positive feedback suggests that thalamostriatal and corticostriatal circuits may use negative outcomes to guide adaptive behaviour during serial reversal learning.

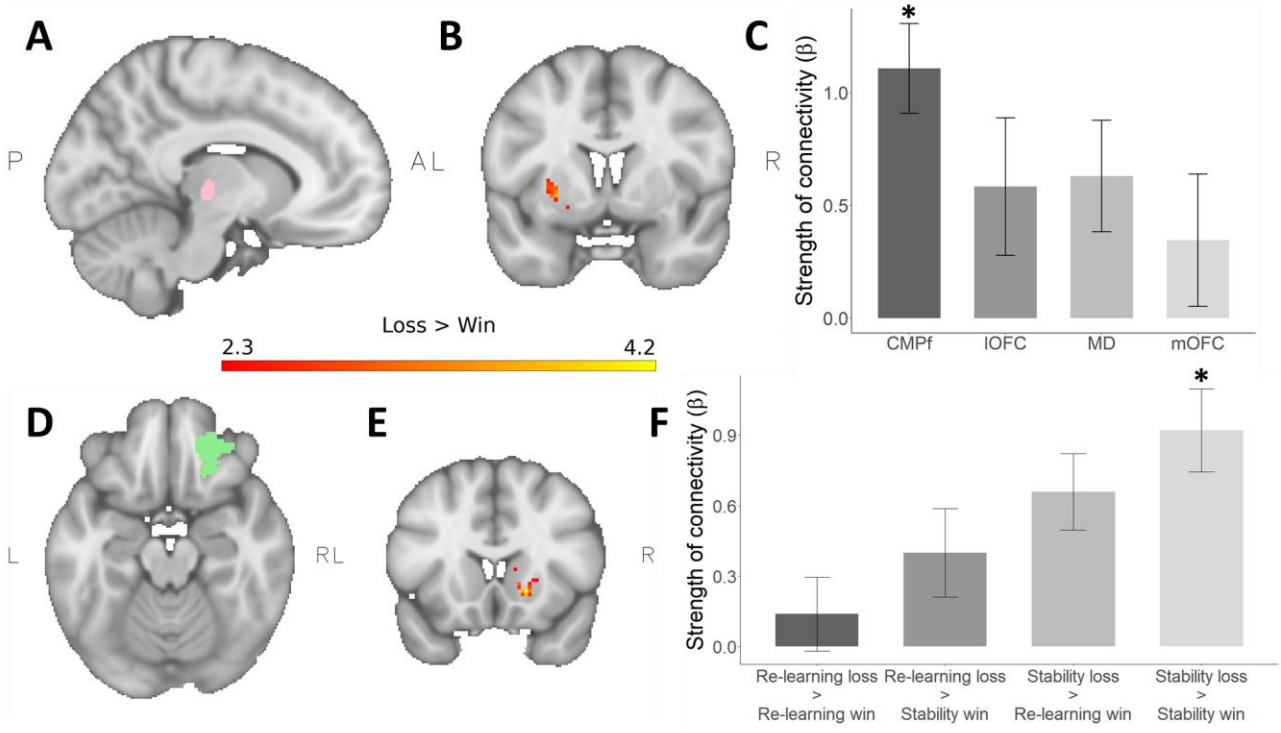

Figure 40 A: Left centromedian-parafascicular (CMPf) seed region. B: Functional connectivity between the left centromedian-parafascicular and the left associative striatum was significantly greater during the processing of negative feedback versus positive feedback (peak coordinates $x = -26,\ y = 4,\ z = -2,\ z(max) = 3.57$). No significant differences in this contrast were seen when comparing between phases of the task. C: Strength of functional connectivity between left cortical (lOFC: lateral orbitofrontal cortex, mOFC: medial orbitofrontal cortex) and thalamic (CMPf, MD: mediodorsal nucleus) seeds with the associative dorsal striatum for negative feedback versus positive feedback. Significant functional connectivity was observed between the left centromedian-parafascicular nuclei and the striatum, but other regions did not show significant functional connectivity. D: Right lOFC seed region. E: Functional connectivity between the right lOFC and the right associative striatum was significantly greater during the processing of negative feedback versus positive feedback (peak coordinates $x = -18,\ y = 16,\ z = -4,\ z(max) = 4.14$). F: Significant differences in functional connectivity were observed for negative versus positive feedback during the stability phase, but not between other phases of the task. A significance threshold of $p(FWE) < 0.05$ and a cluster threshold of z >2.3 was used.

To determine whether differences in functional connectivity between the centromedian-parafascicular nucleus or the lateral orbitofrontal cortex and the associative striatum were localised

to a specific phase of the task we calculated differences in functional connectivity for negative and positive feedback across the re-learning and stability phases of the task. Functional connectivity between the lateral orbitofrontal cortex and the associative striatum was significantly greater for negative feedback than positive feedback during the stability phase (z(max) = 3.21, MNI coordinates = [14, 16, 0], 40 voxels, p = 0.006, Figure 40F). No differences were found between the centromedian-parafascicular and the associative striatum for negative and positive feedback across re-learning and stability. These findings are suggestive of a general error signal between the centromedian-parafascicular and the associative striatum used to guide behaviour by signalling potential changes in context based on negative feedback. Conversely, error signals between the lateral orbitofrontal cortex and associative striatum may be specifically used to implement a change in response strategy, in line with previous literature (Hampshire et al., 2012; Rygula et al., 2010). Importantly, no differences in functional connectivity between the medial orbitofrontal cortex and mediodorsal thalamus with our striatal regions of interest was observed during the outcome epoch of the task. These regions were included as control regions, and support the specificity of the thalamus with the dorsal striatal cholinergic system, and the lateral orbitofrontal cortex during serial reversal learning. The dorsal striatal cholinergic system is preferentially innervated by the centromedian and parafascicular nuclei, while the mediodorsal nucleus has few projections to the striatal cholinergic system (Smith et al., 2009). The striatal cholinergic system has an important role during reversal learning, and is associated with the generation and flexible use of multiple internal representations (Bell et al., 2018; Bradfield, Bertran-Gonzalez, et al., 2013; Bradfield & Balleine, 2017; Brown et al., 2010; Ragozzino et al., 2009; Stalnaker et al., 2016). Therefore, although we have not measured striatal cholinergic activity directly, the specificity of these results suggests that functional connectivity between the centromedian-parafascicular nucleus and the dorsal striatum might be associated with striatal cholinergic interneuron activity. Additionally, while the medial orbitofrontal cortex is involved in outcome evaluation and goal-directed behaviour, its inactivation is associated with general impairments in probabilistic learning (Dalton et al., 2016). Conversely, lateral orbitofrontal inactivation preferentially impairs reversal learning (Dalton et al., 2016), in line with other work suggesting the lateral orbitofrontal cortex is important for initiating change and minimising perseveration after the reversal of outcome contingencies (Bell, Langdon, et al., 2019; Hampshire et al., 2012; Hervig et al., 2020). Therefore, the specificity of lateral orbitofrontal result suggests its functional connectivity with the dorsal striatum changed as a function of reversal learning, while no differences in functional connectivity for the medial orbitofrontal cortex suggests the strength of its connectivity was consistent across the task.

Decision-making

Next, we assessed functional connectivity between our seed regions in the orbitofrontal cortex and thalamus with the striatum during decision making. Functional connectivity between the right mediodorsal thalamus and the ventral striatum was significantly greater during the decision-making epoch of the re-learning phase than the stability phase (z(max) = 3.03, MNI coordinates = [16, 6, -12], 8 voxels, p = 0.046).

Although the mediodorsal thalamus was included as control regions based on the specificity of centromedian-parafascicular connectivity with the dorsal-striatal cholinergic system, there is prior evidence from animal and human literature for a role for the mediodorsal thalamus and ventral striatum in reversal learning. For instance the ventral striatopallidal circuit, which includes the ventral striatum and mediodorsal thalamus, helps the inhibition of responding to previously rewarded stimuli after contingency reversal, as lesions to the circuit impair reversal learning, but not stimulus discrimination or simple stimulus-outcome association learning (Ferry et al., 2000; Price, 2005).

In the present study, increased coherence between the mediosorsal thalamus and ventral striatum during decision making may help prevent perseverative errors during re-learning, i.e. after the reversal has been instigated. We ran supplementary analyses to test this hypothesis but found no correlation between participant's average number of perseverative errors and the difference in functional connectivity between the re-learning and stability phases (r = -0.029, p = 0.881).

No differences in functional connectivity during decision making between the orbitofrontal cortex or centromedian-parafascicular nucleus and the striatum were observed during re-learning and stability phases.

Cortical error signals are parametrically modulated by response perseveration.

Following our findings describing the role of thalamostriatal and corticostriatal connectivity in reversal learning, we next ran a series of whole brain exploratory analyses. These analyses aimed to investigate further how negative and positive feedback may guide adaptive behaviour during serial reversal learning; we modelled different trial types as individual explanatory variables (Table 6).

We first tested for error signals that could relate to a change in behavioural strategy. To do this we compared final reversal errors, as defined by Cools et al. (2002), with errors unrelated to reversal

learning. Specifically, we compared final reversal errors with incorrect choices during initial learning (FRe > II) and found significant increases in activation in the orbitofrontal and insular cortices and middle frontal, paracingulate, and superior frontal gyri (Table 9). However, these differences do not provide causal evidence of activation resulting in behavioural change, since the difference could merely be due to differences in responding to negative outcomes during initial and reversal learning. Therefore, we compared error signals leading to a change in strategy with those that did not (FRe > II) > (Re > II) to test whether these effects were specifically associated with strategy change. None of our initial clusters survived thresholding. One potential explanation for this lack of overall statistical effect is that evidence leading to a change in strategy is accumulated gradually. Therefore, this gradient could be averaged out when grouping trial types.

To test this hypothesis, we parametrically modulated reversal errors not leading to a change in strategy (Re_par), scaled descending from one to (excluding) zero. Re_par was then de-meaned, allowing us to combine learning events of differing lengths. We used a descending parametric modulator because we expect early reversal errors to produce greater responsivity than late reversal errors, akin to a prediction error signal. Reversal errors showed significant parametric modulation in regions involved in error processing, including the posterior insula, Heschl's gyrus, and the posterior cingulate cortex (Table 9). These findings suggest activation may be related to the accumulation of evidence to determine when to reverse.

		Final reversal error > Incorrect $_{\text{Initial learning}}$					
Region	**L/R**	x	y	z	**Size**	$z(max)$	$p(FWE)$
Angular gyrus	R	52	-46	58	477	3.79	< 0.001
Frontal operculum cortex	L	-40	18	0	163	3.68	0.001
Frontal operculum/orbitofrontal cortex	R	44	20	-4	497	4.71	< 0.001
Inferior frontal gyrus	R	52	20	-4	497	3.78	< 0.001
Insula	L	-34	20	-2	163	3.36	0.001
Insula	R	32	26	4	497	3.85	< 0.001
Lateral occipital cortex	R	42	-58	56	477	3.74	< 0.001
Middle frontal gyrus	R	46	24	44	122	3.23	0.013
Orbitofrontal cortex	L	-32	24	-4	163	3.86	0.001
Paracingulate gyrus	R	2	14	52	464	4.32	< 0.001
Superior frontal gyrus	R	2	28	52	464	3.91	< 0.001
Supramarginal gyrus	R	56	-44	50	477	4.12	< 0.001

		Reversal error $_{\text{Parametric modulation}}$ **> Incorrect** $_{\text{Initial learning}}$					
Region	**L/R**	x	y	z	**Size**	$z(max)$	$p(FWE)$
Central opercular cortex	L	-58	-6	8	162	3.43	< 0.001
Central opercular cortex	R	56	2	4	375	3.70	< 0.001
Heschl's gyrus	L	-46	-24	12	120	3.47	0.003
Heschl's gyrus	R	44	-26	12	416	3.63	< 0.001

Insula	R	40	-16	6	375	3.50	< 0.001
Lateral occipital cortex	L	-52	-70	36	92	2.77	0.024
Lingual gyrus	L	-30	-56	4	192	4.56	< 0.001
Paracingulate gyrus	L	0	44	-8	327	4.38	< 0.001
Parietal operculum cortex	L	-52	-26	12	120	2.77	0.003
Parietal operculum cortex	R	56	-24	18	416	3.86	< 0.001
Planum temporale	L	-64	-24	14	184	2.96	< 0.001
Postcentral gyrus	R	66	-12	14	416	3.58	< 0.001
Posterior cingulate cortex	L	-4	-52	14	191	3.71	< 0.001
Precentral gyrus	L	-58	6	2	162	3.43	< 0.001
Precentral gyrus	R	62	4	6	375	3.49	< 0.001
Precuneous	L	-8	-56	26	191	3.81	< 0.001
Subcallosal cortex	L	0	22	-14	327	3.47	< 0.001
Supramarginal gyrus	L	-66	-24	26	184	3.34	< 0.001
Supramarginal gyrus	R	62	-28	24	416	4.02	< 0.001

Table 9 Significant clusters from whole brain analysis of contrasts that describe how perseverative error processing may be used to guide adaptive behaviour following the reversal of outcome contingencies.

Prefrontal regions supporting the implementation of cognitive flexibility.

Considering our findings describing how errors may be used to guide behaviour, we next wanted to explore differences in activation for choices made during the re-learning and stability phases. We contrasted trials where participants made correct responses during the stability versus the re-learning phase (CSt > CRe) and found a single significant cluster in the left frontal pole (Table 10, Figure 41). During the stability phase, participants demonstrate behaviourally that they understand which is the choice that is most likely to lead to a positive outcome. However, the relationship between actions and outcomes may be more uncertainty during the re-learning phase, given the recent reversal of reward contingencies. It has been suggested that the frontal polar cortex tracks the relative advantage of alternative response strategies, and recruits prefrontal regions to shift behaviour when the alternative strategy becomes advantageous (Mansouri et al., 2017). Therefore, while participants use a single response strategy during stability to gain positive outcomes, they may use the frontal polar cortex to track the relative advantage of the unchosen option.

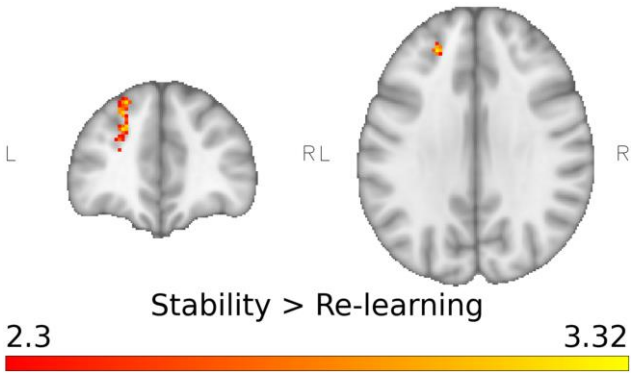

Figure 41 The frontal pole showed significantly increased activation when participants made correct choices during the stability phase versus re-learning (peak coordinates $x = -22,\ y = 40,\ z = 30,\ z(max) = 3.28$). This signal may reflect tracking the reliability of the alternative task strategy during reversal learning. Participants have demonstrated behaviourally that they understand the currently correct action policy once they have reached the stability phase, whereas the correct policy would be more ambiguous during re-learning, and therefore there is not a clear correct and alternative action policy. A significance threshold of $p(FWE) < 0.05$ and a cluster threshold of z >2.3 was used.

Outcomes that deviate from expectations are also likely to guide behaviour given that correct and incorrect choice are mutually exclusive in our task. Therefore, we next compared activation when feedback was congruent or incongruent with a participant's expectations by contrasting correct choices during the stability phase that led to negative versus positive feedback (PESt > CSt). This type of negative feedback, i.e. following a choice they considered correct, could indicate to the participant that reward contingencies changed as they are incongruent with expectations. The contrast showed increased activation across the cortex, including regions involved in feedback monitoring such as the angular gyrus, anterior cingulate, inferior frontal gyrus, insula, and orbitofrontal cortex (Table 10, Figure 42A). To confirm the specificity of this result we looked for the effect over and above activation differences due to positive and negative feedback (PESt > CSt) > (ISt > CSt). Activation in several regions discriminated between incongruent negative feedback and congruent positive feedback for correct responses during the stability phase, over and above responsivity to punishment (Table 10, Figure 42B). Most notably, significant activation was consistently found in the anterior cingulate and paracingulate cortex for activation over and above differences due to positive and negative feedback; significant activation in the lingual and precentral gyri was also observed in both analyses ((PESt > CSt) > (ISt > CSt) and PESt > CSt). Anterior cingulate has been found to support adaptive behaviour in macaques by using errors to

guide choice, while lesions to the anterior cingulate led to impairments in reversal learning (Chudasama et al., 2013).

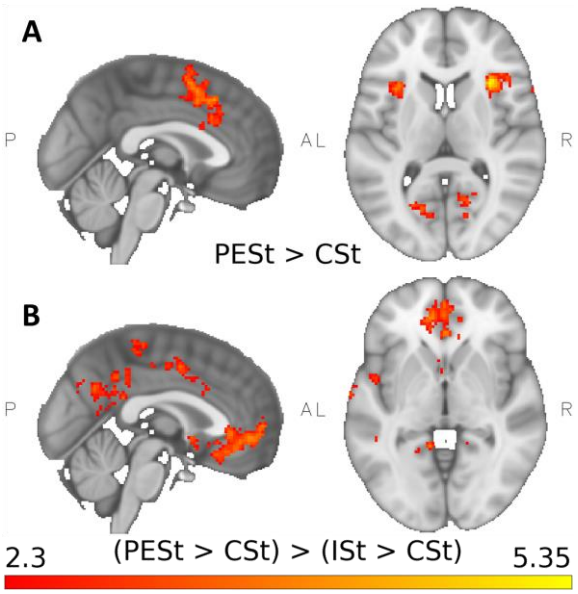

Figure 42 A: Significantly greater activation for probabilistic loss errors than correct choices during the stability phase was seen in the anterior cingulate, orbitofrontal cortex, insula, and inferior frontal gyrus (full details on regions and cluster statistics in Table 10). This contrast shows differences in activation when actual outcomes are incongruent with expected outcomes and may indicate regions that are involved in signalling unexpected outcomes that could lead to a change in behaviour. B: Significant differences in activation for probabilistic loss errors than correct choices, above activation for negative versus positive feedback (Probabilistic loss error > correct) > (Incorrect > correct) (all stability). Several regions, including the anterior cingulate cortex (see Table 10 for full details) show increased activation to probabilistic loss errors specifically. These regions may use probabilistic loss errors to signal a potential change in context that could lead to the reversal of behaviour. A significance threshold of $p(FWE) < 0.05$ and a cluster threshold of z >2.3 was used.

		Stability $_{\text{Correct}}$ > Re-learning $_{\text{Correct}}$					
Region	**L/R**	x	y	z	**Size**	$z(max)$	$p(FWE)$
Frontal pole	L	-22	40	30	145	3.28	0.002

		Stability $_{\text{Probabilistic loss error}}$ > Stability $_{\text{Correct}}$					
Region	**L/R**	x	y	z	**Size**	$z(max)$	$p(FWE)$
Angular gyrus	R	40	-48	44	198	3.21	< 0.001
Anterior cingulate cortex	L	-8	24	28	1356	4.21	< 0.001
Anterior cingulate cortex	R	6	12	42	1356	3.96	< 0.001
Frontal operculum cortex	L	-42	14	-2	261	3.80	< 0.001

Frontal operculum cortex	R	40	26	6	380	3.70	< 0.001
Inferior frontal gyrus	L	-48	18	2	261	3.28	< 0.001
Inferior frontal gyrus	R	44	22	8	380	3.43	< 0.001
Insula	L	-30	18	10	261	4.25	< 0.001
Insula	R	32	20	8	380	5.30	< 0.001
Intracalcarine cortex	L	-16	-68	6	134	3.94	0.002
Intracalcarine cortex	R	14	-60	6	118	3.95	0.005
Lingual gyrus	L	-18	-56	2	134	3.15	0.002
Middle frontal gyrus	L	-28	-2	58	307	3.65	< 0.001
Middle frontal gyrus	R	42	18	28	94	2.70	0.027
Orbitofrontal cortex	R	34	28	2	380	3.14	< 0.001
Paracingulate gyrus	L	0	22	44	1356	4.17	< 0.001
Paracingulate gyrus	R	4	14	50	1356	4.21	< 0.001
Precentral gyrus	L	-30	-6	64	307	3.50	< 0.001
Precentral gyrus	R	54	10	18	94	3.79	0.027
Precuneous	R	22	-58	6	118	3.16	0.005
Superior frontal gyrus	L	-26	4	54	307	3.54	< 0.001
Superior frontal gyrus	R	16	12	64	1356	4.18	< 0.001
Superior parietal lobule	L	-36	-54	48	183	3.62	< 0.001
Superior parietal lobule	R	32	-44	40	198	3.59	< 0.001
Supramarginal gyrus	L	-32	-46	38	183	3.51	< 0.001
Supramarginal gyrus	R	42	-42	42	198	3.46	< 0.001

		Stability (Probabilistic loss error > Correct) > Stability (Incorrect > Correct)					
Region	**L/R**	x	y	z	**Size**	$z(max)$	$p(FWE)$
Anterior cingulate cortex	L	0	34	-2	827	3.75	< 0.001
Central Opercular cortex	L	-54	-16	10	943	3.64	< 0.001
Central Opercular cortex	R	64	-12	10	105	3.26	0.033
Frontal pole	L	0	56	4	827	3.76	< 0.001
Lateral occipital cortex	L	-46	-76	28	189	3.53	< 0.001
Lingual gyrus	L	-10	-46	-2	1125	3.70	< 0.001
Middle temporal gyrus	L	-48	-48	8	943	3.87	< 0.001
Paracingulate gyrus	L	0	48	-4	827	3.99	< 0.001
Planum temporale	L	-62	-14	8	943	3.55	< 0.001
Postcentral gyrus	L	-6	-36	66	134	2.71	0.006
Postcentral gyrus	R	58	-10	20	105	2.54	0.033
Precentral gyrus	L	-2	-32	56	134	3.39	0.006
Precuneus	L	-6	-54	14	1125	3.83	< 0.001
Precuneus	R	12	-54	14	1125	3.80	< 0.001
Posterior cingulate cortex	L	-10	-42	32	1125	4.06	< 0.001
Superior temporal gyrus	L	-62	0	-10	943	3.99	< 0.001
Supplementary motor cortex	R	10	-2	48	193	3.59	< 0.001

Table 10 Significant clusters from whole brain analysis of contrasts showing differences between making correct choices at during different phases of the task, and how unexpected feedback may be used to prepare switching behaviour in response to negative feedback.

Discussion

The present study aimed to investigate the influences of cortical and thalamic brain regions on striatal activity during probabilistic reversal learning. We found that functional connectivity between the centromedian-parafascicular nuclei of the thalamus and a portion of the associative striatum was significantly greater during the processing of negative compared to positive feedback. A similar pattern of functional connectivity was observed between the lateral orbitofrontal cortex and the associative striatum. These results suggest the centromedian-parafascicular nuclei, and the dorsal striatum use negative feedback as a general error signal to promote flexibility. Lateral orbitofrontal cortex and dorsal striatum connectivity was specific to when participants were using the alternative response strategy, suggesting connectivity may be involved in the implementation of change to an alternate strategy. Additionally, we explored how cortical activity may influence cognitive flexibility. Following the reversal of contingencies, parametric modulation of regions involved in error processing, including the posterior cingulate and insula cortices, and Heschl's gyrus, was observed. This modulation may be related to the gradual accumulation of evidence that contingencies have reversed from negative feedback in preparation for change. Orbitofrontal and insular cortices and middle frontal, paracingulate, and superior frontal gyri showed significant activation for probabilistic loss errors during the stability phase. These regions have previously been reported to be important for error processing and change detection, and therefore activation may be related to anticipating future reversals. Lastly, we provide evidence suggesting that the frontal polar cortex is involved in monitoring the relative advantage of alternate response strategy, and a set of regions including the inferior frontal gyrus, anterior cingulate and orbitofrontal cortices that may signal when a reversal has occurred.

Connectivity between the centromedian-parafascicular nuclei and striatum has previously reported to be involved in the expression of adaptive behaviour in rodents and humans (Bell, Langdon, et al., 2019; Bradfield, Bertran-Gonzalez, et al., 2013; Bradfield, Hart, et al., 2013; Brown et al., 2010; Yamanaka et al., 2018). Here we provide further evidence for the premise that thalamostriatal circuits are important for adaptive behaviour by showing that functional connectivity is significantly greater during the processing of negative versus positive feedback in a task where behavioural adaptation relies on the reliable tracking of negative outcomes. This difference in functional connectivity is in line with the purported role of the centromedian-parafascicular in signalling contextual change (Bradfield, Bertran-Gonzalez, et al., 2013; Yamanaka et al., 2018). In a simple, two-choice task, actual outcomes are likely to match expected outcomes; therefore, incongruent feedback might suggest that outcome contingencies had reversed. Thus, in this task,

the centromedian-parafascicular may be involved in detecting changes in behavioural context by tracking negative feedback. This information could then be used to infer that the current behavioural policy needs to be changed.

Indeed, this suggestion is in line with previous research showing greater activation in the centromedian-parafascicular nuclei when overcoming bias and responding to unexpected outcomes (Matsumoto et al., 2001; Minamimoto et al., 2005, 2014). Centromedian-parafascicular activity may indicate a general error signal that is used to guide behaviour by signalling a potential change in context following negative outcomes. This may also explain why significant differences in connectivity were not found during feedback in different phases of the task, i.e. thalamostriatal connectivity did not discriminate between losses and wins during stability or re-learning. This is in line with previous work showing that centromedian-parafascicular neurons habituate to non-reward but not reward-related stimulation (Alloway et al., 2014; Matsumoto et al., 2001). If we did see differences between phases of the task, then this would suggest the centromedian-parafascicular nuclei, and the dorsal striatum have reduced connectivity during some phases compared to others.

Conversely, the lateral orbitofrontal cortex and the striatum show increased connectivity during negative feedback, but only during the stability phase, suggesting this connectivity may support changes in behaviour following reversal. This finding is in line with previous evidence that suggests the lateral orbitofrontal cortex is involved in the implementation of changes in behaviour during reversal learning (Hampshire et al., 2012; Rygula et al., 2010).

Thalamic and cortical connections may be integrated within the striatum to coordinate cognitive flexibility. For instance, thalamostriatal connections have the potential to signal changes in context to the cholinergic interneurons at any time, simply by virtue of a non-specific error signal. Meanwhile, corticostriatal connections may either attenuate or enhance the influence of this thalamostriatal input to the striatum. For instance, other external inputs to the orbitofrontal cortex may signal that a change in behaviour is required, at which point connections from the orbitofrontal cortex to the striatum will modulate the influence of cholinergic interneurons on the output of the striatum.

Previous studies using reversal learning have indicated that quantitative activation differences exist between final reversal errors and errors not leading to a change in strategy (Cools et al., 2002; Culbreth et al., 2016; Remijnse et al., 2006), although, we did not find such differences in our data. One potential explanation is the differences in the design of our probabilistic learning task. For instance, Cools et al. (2002) had participants complete thirty minutes of probabilistic discrimination learning training, Culbreth et al. (2016) also had participants complete practice trials (though they

do not describe the extent of practice), and instructed them to stick with a response. Therefore, participants in these studies received more training than our participants did. In terms of prior experience, the participants of Remijnse et al. (2006) are closest to our own, as they completed thirty trials of probabilistic discrimination learning without reversal. Yet, although Remijnse et al. (2006) used probabilistic feedback for correct choices, incorrect choices were always deterministic, and participants were told what stimulus would initially be correct. Therefore, discrimination of correct and incorrect choices should require less effort from the participant. By contrast, participants in our task were relatively naïve to probabilistic discrimination learning, and though they received instruction about probabilistic feedback and the existence of reversals they were not explicated instructed how to make choices in the task. We therefore cannot assume that reversal errors and final reversal errors in our task are necessarily equivalent with those of Cools et al. (2002), Culbreth et al. (2016) and Remijnse et al. (2006). Importantly, we also observe parametric modulation of reversal error signals in regions involved in change detection such as the insula and Heschl's gyrus, and the posterior cingulate cortex. Furthermore, these differences in activation exist over and above negative feedback during initial learning. This may explain why Cools et al. (2002) did not see any modulatory effect of the number of preceding reversal errors on the final reversal error; here, we find that the insula appears to be modulated by preceding perseverative errors. Alternatively, the relatively small sample size of thirteen subjects used by Cools et al. (2002) could mean parametric modulation could not be detected in their dataset due to insufficient statistical power.

Model-based approaches to learning assume mental representations of an environment are used to guide goal-directed behaviour. This representation could include multiple plausible environmental contexts, with representation of the current context being driven by recent experience. The orbitofrontal cortex is associated with the representation of the current context (Schuck et al., 2016; Wilson et al., 2014); in particular medial orbitofrontal and ventromedial prefrontal activity is thought to be related to the reliability of the inferred context (Domenech & Koechlin, 2015). However, an environment with multiple contexts requires arbitration between them for an individual to respond adaptively to change. The frontal polar cortex, found exclusively in primates, is well placed to support such adaptive responding (Bunge, 2004; Bunge et al., 2005; Koechlin, 2014; Sakai & Passingham, 2006), and is associated with monitoring alternative strategies (Boorman et al., 2009). Here, we find increased activation in the frontal polar cortex during correct choices in stability compared to re-learning, and postulate that this is related to monitoring the reliability of the alternative task context. Though this study was not specifically designed to test this hypothesis, our reversal learning task is structured in such a way that once participants reach

the stability phase, they have demonstrated behaviourally that they understand the current context of the task due to our stringent learning criterion. During the re-learning phase, the reversal of contingencies increases the relative uncertainty around the currently correct choice, making the likelihood for each choice more similar. Participants need to determine whether contingencies have reversed or not. Because either choice could currently be correct, there is no alternative context during re-learning. However, after reaching the stability phase participants have demonstrated behaviourally that they understand the current task context. Therefore, the frontopolar cortex can track the relative reliability of the alternative context, while the medial orbitofrontal cortex implements the behavioural policy associated with the current context during the stability phase. This proposition is supported by the error signals we found when participants received probabilistically incorrect feedback to correct choices during stability as compared to rewarded correct choices. Here we see increased activation in regions often associated with error feedback, such as the insula and inferior frontal gyrus, but we also see increased activation in the orbitofrontal and anterior cingulate cortices. Error-dependent changes in activity within the orbitofrontal cortex may indicate a decrease in the reliability of the current context, due to choice outcomes being incongruent with the estimate of the current context (Ghahremani et al., 2010). Alternatively, orbitofrontal cortex activity may indicate preparation to switch responding as is suggested by our functional connectivity results. Anterior cingulate activation may signal outcomes that are unexpected based on the current context and this salient event may increase attentional resources for monitoring outcomes with a view to potentially change strategy (Behrens et al., 2007; Chudasama et al., 2013; Liu et al., 2015).

There are several limitations with the current study which also provide possible avenues for future research. The first is the spatial specificity of our functional signal within subregions of the thalamus. In this study we aimed to minimise cross-contamination of our functional signal between nuclei within the thalamus by reducing our voxel size and smoothing kernel during preprocessing. Nevertheless, it is likely that signal blurring would still occur at the anatomical boundaries of nuclei within the thalamus, meaning that our timeseries used for psychophysiological interaction analysis may be influenced by more than one anatomical region. Therefore, it would be useful to validate these findings using ultra-high field magnetic resonance imaging as this would allow for greater spatial specificity and would provide further evidence that this signal is localised within the centromedian-parafascicular nuclei. Secondly, despite efforts taken to optimise echo-planar image acquisition to reduce dropout in the orbitofrontal cortex (Volz et al., 2019; Weiskopf et al., 2007), we found that for some participants there was still partial signal loss in the most rostral portions of the orbitofrontal cortex. Therefore, though we detected significant functional connectivity between

the lateral orbitofrontal cortex and the striatum, it would be worth undertaking further work optimising signal within the orbitofrontal cortex to further investigate how it interacts with thalamostriatal connections during reversal learning.

In summary, we show that functional connectivity between the centromedian-parafascicular nuclei of the thalamus and the associative dorsal striatum contributes to adaptive behaviour. Functional connectivity is increased when processing negative versus positive outcomes and points to a simple system that utilises negative outcomes to detect potential changes in behavioural context and guide adaptive behaviour. This information may be used by the striatum to signal potential changes in context. Functional connectivity between the lateral orbitofrontal cortex and the associative dorsal striatum was also increased, but only during the stability phase. We believe this specificity is related to the role of the orbitofrontal cortex in flexibly implementing a change in behaviour when required. We also describe how task context might be represented and tracked within the prefrontal cortex. We suggest that activity within the frontal polar cortex is related to tracking the reliability of an alternative context to determine when a change in behaviour is required. Furthermore, we suggest that activity in the orbitofrontal cortex, anterior cingulate, insula, and inferior frontal gyrus may prepare neural architecture for change after receiving evidence that is incongruent with current expectations.

References

Alloway, K. D., Smith, J. B., & Watson, G. D. R. (2014). Thalamostriatal projections from the medial posterior and parafascicular nuclei have distinct topographic and physiologic properties. *Journal of Neurophysiology*, *111*(1), 36–50. https://doi.org/10.1152/jn.00399.2013

Andersson, J. L. R., Jenkinson, M., & Smith, S. (2007a). *Non-linear optimisation; FMRIB Technial Report TR07JA1*.

Andersson, J. L. R., Jenkinson, M., & Smith, S. (2007b). *Non-linear registration aka spatial normalisation; FMRIB Technical Report TR07JA2*.

Behrens, T. E. J., Woolrich, M. W., Walton, M. E., & Rushworth, M. F. S. (2007). Learning the value of information in an uncertain world. *Nature Neuroscience*, *10*(9), 1214–1221. https://doi.org/10.1038/nn1954

Bell, T., Langdon, A., Lindner, M., Lloyd, W., & Christakou, A. (2019). *Orbitofrontal and Thalamic Influences on Striatal Involvement in Human Reversal Learning* (p. 246371). https://doi.org/10.1101/246371

Bell, T., Lindner, M., Langdon, A., Mullins, P. G., & Christakou, A. (2019). Regional Striatal Cholinergic Involvement in Human Behavioral Flexibility. *The Journal of Neuroscience*, *39*(29), 5740–5749. https://doi.org/10.1523/JNEUROSCI.2110-18.2019

Bell, T., Lindner, M., Mullins, P. G., & Christakou, A. (2018). Functional neurochemical imaging of the human striatal cholinergic system during reversal learning. *European Journal of Neuroscience*, *47*(10), 1184–1193. https://doi.org/10.1111/ejn.13803

Boehme, R., Lorenz, R. C., Gleich, T., Romund, L., Pelz, P., Golde, S., Flemming, E., Wold, A., Deserno, L., Behr, J., Raufelder, D., Heinz, A., & Beck, A. (2017). Reversal learning strategy in adolescence is associated with prefrontal cortex activation. *European Journal of Neuroscience*, *45*(1), 129–137. https://doi.org/10.1111/ejn.13401

Boorman, E. D., Behrens, T. E. J., Woolrich, M. W., & Rushworth, M. F. S. (2009). How Green Is the Grass on the Other Side? Frontopolar Cortex and the Evidence in Favor of Alternative Courses of Action. *Neuron*, *62*(5), 733–743. https://doi.org/10.1016/j.neuron.2009.05.014

Bradfield, L. A., & Balleine, B. W. (2017). Thalamic Control of Dorsomedial Striatum Regulates Internal State to Guide Goal-Directed Action Selection. *The Journal of Neuroscience*, *37*(13), 3721–3733. https://doi.org/10.1523/JNEUROSCI.3860-16.2017

Bradfield, L. A., Bertran-Gonzalez, J., Chieng, B., & Balleine, B. W. (2013). The thalamostriatal pathway and cholinergic control of goal-directed action: Interlacing new with existing learning in the striatum. *Neuron*, *79*(1), 153–166. https://doi.org/10.1016/j.neuron.2013.04.039

Bradfield, L. A., Hart, G., & Balleine, B. W. (2013). The role of the anterior, mediodorsal, and parafascicular thalamus in instrumental conditioning. *Frontiers in Systems Neuroscience*, *7*, 51. https://doi.org/10.3389/fnsys.2013.00051

Brainard, D. H. D. H. (1997). The Psychophysics Toolbox. *Spatial Vision*, *10*(4), 433–436. https://doi.org/10.1163/156856897X00357

Brown, H. D., Baker, P. M., & Ragozzino, M. E. (2010). The Parafascicular Thalamic Nucleus Concomitantly Influences Behavioral Flexibility and Dorsomedial Striatal Acetylcholine Output in Rats. *Journal of Neuroscience*, *30*(43), 14390–14398. https://doi.org/10.1523/JNEUROSCI.2167-10.2010

Bunge, S. A. (2004). How we use rules to select actions: A review of evidence from cognitive neuroscience. *Cognitive, Affective, & Behavioral Neuroscience*, *4*(4), 564–579. https://doi.org/10.3758/CABN.4.4.564

Bunge, S. A., Wallis, J. D., Parker, A., Brass, M., Crone, E. A., Hoshi, E., & Sakai, K. (2005). Neural Circuitry Underlying Rule Use in Humans and Nonhuman Primates. *Journal of Neuroscience*, *25*(45), 10347–10350. https://doi.org/10.1523/JNEUROSCI.2937-05.2005

Chakraborty, S., Kolling, N., Walton, M. E., & Mitchell, A. S. (2016). Critical role for the mediodorsal thalamus in permitting rapid reward-guided updating in stochastic reward environments. *ELife*, *5*, e13588. https://doi.org/10.7554/eLife.13588

Choi, E. Y., Yeo, B. T. T., & Buckner, R. L. (2012). The organization of the human striatum estimated by intrinsic functional connectivity. *Journal of Neurophysiology*, *108*(8), 2242–2263. https://doi.org/10.1152/jn.00270.2012

Chudasama, Y., Bussey, T. J., & Muir, J. L. (2001). Effects of selective thalamic and prelimbic cortex lesions on two types of visual discrimination and reversal learning. *European Journal of Neuroscience*, *14*(6), 1009–1020. https://doi.org/10.1046/j.0953-816x.2001.01607.x

Chudasama, Y., Daniels, T. E., Gorrin, D. P., Rhodes, S. E. V., Rudebeck, P. H., & Murray, E. A. (2013). The Role of the Anterior Cingulate Cortex in Choices based on Reward Value and Reward Contingency. *Cerebral Cortex (New York, NY)*, *23*(12), 2884–2898. https://doi.org/10.1093/cercor/bhs266

Cools, R., Clark, L., Owen, A. M., & Robbins, T. W. (2002). Defining the neural mechanisms of probabilistic reversal learning using event-related functional magnetic resonance imaging. *The Journal of Neuroscience : The Official Journal of the Society for Neuroscience*, *22*(11), 4563–4567. https://doi.org/20026435

Crawley, D., Zhang, L., Jones, E. J. H., Ahmad, J., Oakley, B., Cáceres, A. S. J., Charman, T., Buitelaar, J. K., Murphy, D. G. M., Chatham, C., Ouden, H. den, Loth, E., & Group, the E.-A. L. (2020). Modeling flexible behavior in childhood to adulthood shows age-dependent learning mechanisms and less optimal learning in autism in each age group. *PLOS Biology*, *18*(10), e3000908. https://doi.org/10.1371/journal.pbio.3000908

Culbreth, A. J., Gold, J. M., Cools, R., & Barch, D. M. (2016). Impaired activation in cognitive control regions predicts reversal learning in schizophrenia. *Schizophrenia Bulletin*, *42*(2), 484–493. https://doi.org/10.1093/schbul/sbv075

Dalton, G. L., Wang, X. N. Y., Phillips, X. A. G., Floresco, X. S. B., Wang, N. Y., Phillips, A. G., & Floresco, S. B. (2016). Multifaceted Contributions by Different Regions of the Orbitofrontal and Medial Prefrontal Cortex to Probabilistic Reversal Learning. *The Journal of Neuroscience*, *36*(6), 1996–2006. https://doi.org/10.1523/JNEUROSCI.3366-15.2016

D'Cruz, A. M., Mosconi, M. W., Ragozzino, M. E., Cook, E. H., & Sweeney, J. A. (2016). Alterations in the functional neural circuitry supporting flexible choice behavior in autism spectrum disorders. *Translational Psychiatry*, *6*(10), e916. https://doi.org/10.1038/tp.2016.161

De Ruiter, M. B., Veltman, D. J., Goudriaan, A. E., Oosterlaan, J., Sjoerds, Z., & Van Den Brink, W. (2009). Response perseveration and ventral prefrontal sensitivity to reward and punishment in male problem gamblers and smokers. *Neuropsychopharmacology*, *34*(4), 1027–1038. https://doi.org/10.1038/npp.2008.175

Dodds, C. M., Müller, U., Clark, L., van Loon, A., Cools, R., & Robbins, T. W. (2008). Methylphenidate has differential effects on blood oxygenation level-dependent signal related to cognitive subprocesses of reversal learning. *The Journal of Neuroscience: The Official Journal of the Society for Neuroscience*, *28*(23), 5976–5982. https://doi.org/10.1523/JNEUROSCI.1153-08.2008

Domenech, P., & Koechlin, E. (2015). Executive control and decision-making in the prefrontal cortex. *Current Opinion in Behavioral Sciences*, *1*, 101–106. https://doi.org/10.1016/j.cobeha.2014.10.007

Ersche, K. D., Roiser, J. P., Abbott, S., Craig, K. J., Müller, U., Suckling, J., Ooi, C., Shabbir, S. S., Clark, L., Sahakian, B. J., Fineberg, N. A., Merlo-Pich, E. V., Robbins, T. W., & Bullmore, E. T. (2011). Response perseveration in stimulant dependence is associated with striatal dysfunction and can be ameliorated by a D(2/3) receptor agonist. *Biological Psychiatry*, *70*(8), 754–762. https://doi.org/10.1016/j.biopsych.2011.06.033

Ferry, A. T., Lu, X.-C. M., & Price, J. L. (2000). Effects of excitotoxic lesions in the ventral striatopallidal–thalamocortical pathway on odor reversal learning: Inability to extinguish an incorrect response. *Experimental Brain Research*, *131*(3), 320–335. https://doi.org/10.1007/s002219900240

Franklin, N. T., & Frank, M. J. (2015). A cholinergic feedback circuit to regulate striatal population uncertainty and optimize reinforcement learning. *ELife*, *4*, e12029. https://doi.org/10.7554/eLife.12029

Freyer, T., Valerius, G., Kuelz, A.-K., Speck, O., Glauche, V., Hull, M., & Voderholzer, U. (2009). Test-retest reliability of event-related functional MRI in a probabilistic reversal learning task. *Psychiatry Research*, *174*(1), 40–46. https://doi.org/10.1016/j.pscychresns.2009.03.003

Friston, K. J., Buechel, C., Fink, G. R., Morris, J., Rolls, E., & Dolan, R. J. (1997). Psychophysiological and Modulatory Interactions in Neuroimaging. *NeuroImage*, *6*(3), 218–229. https://doi.org/10.1006/nimg.1997.0291

Ghahremani, D. G., Monterosso, J., Jentsch, J. D., Bilder, R. M., & Poldrack, R. A. (2010). Neural Components Underlying Behavioral Flexibility in Human Reversal Learning. *Cerebral Cortex*, *20*(8), 1843–1852. https://doi.org/10.1093/cercor/bhp247

Gourley, S. L., Olevska, A., Zimmermann, K. S., Ressler, K. J., DiLeone, R. J., & Taylor, J. R. (2013). The orbitofrontal cortex regulates outcome-based decision-making via the lateral striatum. *The European Journal of Neuroscience*, *38*(3). https://doi.org/10.1111/ejn.12239

Groman, S. M., Keistler, C., Keip, A. J., Hammarlund, E., DiLeone, R. J., Pittenger, C., Lee, D., & Taylor, J. R. (2019). Orbitofrontal Circuits Control Multiple Reinforcement-Learning Processes. *Neuron*, *103*(4), 734-746.e3. https://doi.org/10.1016/j.neuron.2019.05.042

Haber, S. N. (2016). Corticostriatal circuitry. *Dialogues in Clinical Neuroscience*, *18*(1), 7–21.

Hampshire, A., Chaudhry, A. M., Owen, A. M., & Roberts, A. C. (2012). Dissociable roles for lateral orbitofrontal cortex and lateral prefrontal cortex during preference driven reversal learning. *NeuroImage*, *59*(4), 4102–4112. https://doi.org/10.1016/j.neuroimage.2011.10.072

Hampton, A. N., Bossaerts, P., & O'Doherty, J. P. (2006). The Role of the Ventromedial Prefrontal Cortex in Abstract State-Based Inference during Decision Making in Humans. *Journal of Neuroscience*. https://doi.org/10.1523/JNEUROSCI.1010-06.2006

Hervig, M. E., Fiddian, L., Piilgaard, L., Božič, T., Blanco-Pozo, M., Knudsen, C., Olesen, S. F., Alsiö, J., & Robbins, T. W. (2020). Dissociable and Paradoxical Roles of Rat Medial and Lateral Orbitofrontal Cortex in Visual Serial Reversal Learning. *Cerebral Cortex*, *30*(3), 1016–1029. https://doi.org/10.1093/cercor/bhz144

Iglesias, J. E., Insausti, R., Lerma-Usabiaga, G., Bocchetta, M., Van Leemput, K., Greve, D. N., van der Kouwe, A., Fischl, B., Caballero-Gaudes, C., & Paz-Alonso, P. M. (2018). A probabilistic atlas of the human thalamic nuclei combining ex vivo MRI and histology. *NeuroImage*, *183*, 314–326. https://doi.org/10.1016/j.neuroimage.2018.08.012

Izquierdo, A., Brigman, J. L., Radke, A. K., Rudebeck, P. H., & Holmes, A. (2017). The neural basis of reversal learning: An updated perspective. *Neuroscience*, *345*, 12–26. https://doi.org/10.1016/j.neuroscience.2016.03.021

Jenkinson, M., Bannister, P., Brady, M., & Smith, S. (2002). Improved optimization for the robust and accurate linear registration and motion correction of brain images. *NeuroImage*, *17*(2), 825–841. https://doi.org/10.1016/S1053-8119(02)91132-8

Jenkinson, M., & Smith, S. (2001). A global optimisation method for robust affine registration of brain images. *Medical Image Analysis*, *5*(2), 143–156. https://doi.org/10.1016/S1361-8415(01)00036-6

Koechlin, E. (2014). An evolutionary computational theory of prefrontal executive function in decision-making. *Philosophical Transactions of the Royal Society B: Biological Sciences*, *369*(1655), 20130474. https://doi.org/10.1098/rstb.2013.0474

Kringelbach, M. L., & Rolls, E. T. (2003). Neural correlates of rapid reversal learning in a simple model of human social interaction. *NeuroImage*, *20*(2), 1371–1383. https://doi.org/10.1016/S1053-8119(03)00393-8

Liu, Z., Braunlich, K., Wehe, H. S., & Seger, C. A. (2015). Neural networks supporting switching, hypothesis testing, and rule application. *Neuropsychologia*, *77*, 19–34. https://doi.org/10.1016/j.neuropsychologia.2015.07.019

Mansouri, F. A., Koechlin, E., Rosa, M. G. P., & Buckley, M. J. (2017). Managing competing goals—A key role for the frontopolar cortex. *Nature Reviews Neuroscience*, *18*(11), 645–657. https://doi.org/10.1038/nrn.2017.111

Matsumoto, N., Minamimoto, T., Graybiel, A. M., & Kimura, M. (2001). Neurons in the Thalamic CM-Pf Complex Supply Striatal Neurons With Information About Behaviorally Significant Sensory Events. *Journal of Neurophysiology*, *85*(2), 960–976. https://doi.org/10.1152/jn.2001.85.2.960

Minamimoto, T., Hori, Y., & Kimura, M. (2005). Complementary Process to Response Bias in the Centromedian Nucleus of the Thalamus. *Science*, *308*(5729), 1798–1801. https://doi.org/10.1126/science.1109154

Minamimoto, T., Hori, Y., Yamanaka, K., & Kimura, M. (2014). Neural signal for counteracting pre-action bias in the centromedian thalamic nucleus. *Frontiers in Systems Neuroscience*, *8*. https://doi.org/10.3389/fnsys.2014.00003

Mitchell, D. G. V., Rhodes, R. A., Pine, D. S., & Blair, R. J. R. (2008). The contribution of ventrolateral and dorsolateral prefrontal cortex to response reversal. *Behavioural Brain Research*, *187*(1), 80–87. https://doi.org/10.1016/j.bbr.2007.08.034

Morris, L. S., Kundu, P., Dowell, N., Mechelmans, D. J., Favre, P., Irvine, M. A., Robbins, T. W., Daw, N., Bullmore, E. T., Harrison, N. A., & Voon, V. (2016). Fronto-striatal organization: Defining functional and microstructural substrates of behavioural flexibility. *Cortex*, *74*, 118–133. https://doi.org/10.1016/j.cortex.2015.11.004

Noonan, M. P., Chau, B. K. H., Rushworth, M. F. S., & Fellows, L. K. (2017). Contrasting effects of medial and lateral orbitofrontal cortex lesions on credit assignment and decision-making in humans. *Journal of Neuroscience*, *37*(29), 7023–7035. https://doi.org/10.1523/JNEUROSCI.0692-17.2017

O'Reilly, J. X., Woolrich, M. W., Behrens, T. E. J., Smith, S. M., & Johansen-Berg, H. (2012). Tools of the trade: Psychophysiological interactions and functional connectivity. *Social Cognitive and Affective Neuroscience*, *7*(5), 604–609. https://doi.org/10.1093/scan/nss055

Poldrack, R. A., Fletcher, P. C., Henson, R. N., Worsley, K. J., Brett, M., & Nichols, T. E. (2008). Guidelines for reporting an fMRI study. *NeuroImage*, *40*(2), 409–414. https://doi.org/10.1016/j.neuroimage.2007.11.048

Price, J. L. (2005). Free will versus survival: Brain systems that underlie intrinsic constraints on behavior. *Journal of Comparative Neurology*, *493*(1), 132–139. https://doi.org/10.1002/cne.20750

Ragozzino, M. E., Mohler, E. G., Prior, M., Palencia, C. A., & Rozman, S. (2009). Acetylcholine activity in selective striatal regions supports behavioral flexibility. *Neurobiology of Learning and Memory*, *91*(1), 13–22. https://doi.org/10.1016/j.nlm.2008.09.008

Remijnse, P. L., Nielen, M. M. A., van Balkom, A. J. L. M., Cath, D. C., van Oppen, P., Uylings, H. B. M., & Veltman, D. J. (2006). Reduced orbitofrontal-striatal activity on a reversal learning task in obsessive-compulsive disorder. *Archives of General Psychiatry*, *63*(11), 1225–1236. https://doi.org/10.1001/archpsyc.63.11.1225

Rudebeck, P. H., & Murray, E. A. (2008). Amygdala and Orbitofrontal Cortex Lesions Differentially Influence Choices during Object Reversal Learning. *The Journal of Neuroscience*, *28*(33), 8338–8343. https://doi.org/10.1523/JNEUROSCI.2272-08.2008

Ruge, H., & Wolfensteller, U. (2016). Distinct contributions of lateral orbito-frontal cortex, striatum, and fronto-parietal network regions for rule encoding and control of memory-based implementation during instructed reversal learning. *NeuroImage*, *125*, 1–12. https://doi.org/10.1016/j.neuroimage.2015.10.005

Rygula, R., Walker, S. C., Clarke, H. F., Robbins, T. W., & Roberts, A. C. (2010). Differential Contributions of the Primate Ventrolateral Prefrontal and Orbitofrontal Cortex to Serial Reversal Learning. *Journal of Neuroscience*, *30*(43), 14552–14559. https://doi.org/10.1523/JNEUROSCI.2631-10.2010

Sakai, K., & Passingham, R. E. (2006). Prefrontal Set Activity Predicts Rule-Specific Neural Processing during Subsequent Cognitive Performance. *Journal of Neuroscience*, *26*(4), 1211–1218. https://doi.org/10.1523/JNEUROSCI.3887-05.2006

Schepers, I. M., Beck, A. K., Bräuer, S., Schwabe, K., Abdallat, M., Sandmann, P., Dengler, R., Rieger, J. W., & Krauss, J. K. (2017). Human centromedian-parafascicular complex signals sensory cues for goal-oriented behavior selection. *NeuroImage*, *152*, 390–399. https://doi.org/10.1016/j.neuroimage.2017.03.019

Schuck, N. W., Cai, M. B., Wilson, R. C., & Niv, Y. (2016). Human Orbitofrontal Cortex Represents a Cognitive Map of State Space. *Neuron*, *91*(6), 1402–1412. https://doi.org/10.1016/j.neuron.2016.08.019

Smith, Y., Raju, D., Nanda, B., Pare, J.-F., Galvan, A., & Wichmann, T. (2009). The thalamostriatal systems: Anatomical and functional organization in normal and parkinsonian states. *Brain Research Bulletin*, *78*(2), 60–68. https://doi.org/10.1016/j.brainresbull.2008.08.015

Smith, Y., Surmeier, D. J., Redgrave, P., & Kimura, M. (2011). Thalamic Contributions to Basal Ganglia-Related Behavioral Switching and Reinforcement. *Journal of Neuroscience*, *31*(45), 16102–16106. https://doi.org/10.1523/JNEUROSCI.4634-11.2011

Stalnaker, T. A., Berg, B., Aujla, N., & Schoenbaum, G. (2016). Cholinergic Interneurons Use Orbitofrontal Input to Track Beliefs about Current State. *The Journal of Neuroscience : The Official Journal of the Society for Neuroscience*, *36*(23), 6242–6257. https://doi.org/10.1523/JNEUROSCI.0157-16.2016

Stayte, S., Dhungana, A., Vissel, B., & Bradfield, L. A. (2021). Parafascicular Thalamic and Orbitofrontal Cortical Inputs to Striatum Represent States for Goal-Directed Action Selection. *Frontiers in Behavioral Neuroscience*, *15*. https://doi.org/10.3389/fnbeh.2021.655029

Tsuchida, A., Doll, B. B., & Fellows, L. K. (2010). Beyond reversal: A critical role for human orbitofrontal cortex in flexible learning from probabilistic feedback. *The Journal of Neuroscience: The Official Journal of the Society for Neuroscience*, *30*(50), 16868–16875. https://doi.org/10.1523/JNEUROSCI.1958-10.2010

Uddin, L. Q. (2021). Cognitive and behavioural flexibility: Neural mechanisms and clinical considerations. *Nature Reviews Neuroscience*, *22*(3), 167–179. https://doi.org/10.1038/s41583-021-00428-w

Verdejo-Garcia, A., Clark, L., Verdejo-Román, J., Albein-Urios, N., Martinez-Gonzalez, J. M., Gutierrez, B., & Soriano-Mas, C. (2015). Neural substrates of cognitive flexibility in

cocaine and gambling addictions. *The British Journal of Psychiatry: The Journal of Mental Science*, *207*(2), 158–164. https://doi.org/10.1192/bjp.bp.114.152223

Volz, S., Callaghan, M. F., Josephs, O., & Weiskopf, N. (2019). Maximising BOLD sensitivity through automated EPI protocol optimisation. *NeuroImage*, *189*, 159–170. https://doi.org/10.1016/j.neuroimage.2018.12.052

Waegeman, A., Declerck, C. H., Boone, C., Seurinck, R., & Parizel, P. M. (2014). Individual differences in behavioral flexibility in a probabilistic reversal learning task: An fMRI study. *Journal of Neuroscience, Psychology, and Economics*, *7*(4), 203–218. https://doi.org/10.1037/npe0000026

Weiskopf, N., Hutton, C., Josephs, O., Turner, R., & Deichmann, R. (2007). Optimized EPI for fMRI studies of the orbitofrontal cortex: Compensation of susceptibility-induced gradients in the readout direction. *Magnetic Resonance Materials in Physics, Biology and Medicine*, *20*(1), 39. https://doi.org/10.1007/s10334-006-0067-6

Wilson, R. C., Takahashi, Y. K., Schoenbaum, G., & Niv, Y. (2014). Orbitofrontal cortex as a cognitive map of task space. *Neuron*, *81*(2), 267–279. https://doi.org/10.1016/j.neuron.2013.11.005

Wolff, M., & Vann, S. D. (2019). The Cognitive Thalamus as a Gateway to Mental Representations. *Journal of Neuroscience*, *39*(1), 3–14. https://doi.org/10.1523/JNEUROSCI.0479-18.2018

Yamanaka, K., Hori, Y., Minamimoto, T., Yamada, H., Matsumoto, N., Enomoto, K., Aosaki, T., Graybiel, A. M., & Kimura, M. (2018). Roles of centromedian parafascicular nuclei of thalamus and cholinergic interneurons in the dorsal striatum in associative learning of environmental events. *Journal of Neural Transmission*, *125*(3), 501–513. https://doi.org/10.1007/s00702-017-1713-z

Yaple, Z. A., & Yu, R. (2019). Fractionating adaptive learning: A meta-analysis of the reversal learning paradigm. *Neuroscience & Biobehavioral Reviews*, *102*, 85–94. https://doi.org/10.1016/j.neubiorev.2019.04.006

Zeuner, K. E., Knutzen, A., Granert, O., Sablowsky, S., Götz, J., Wolff, S., Jansen, O., Dressler, D., Schneider, S. A., Klein, C., Deuschl, G., van Eimeren, T., & Witt, K. (2016). Altered brain activation in a reversal learning task unmasks adaptive changes in cognitive control in writer's cramp. *NeuroImage. Clinical*, *10*, 63–70. https://doi.org/10.1016/j.nicl.2015.11.006

Dissociable roles for the striatal cholinergic system in different flexibility contexts

Brendan Williams[1,2], Anastasia Christakou[1,2]

1. Centre for Integrative Neuroscience and Neurodynamics, University of Reading, UK
2. School of Psychology and Clinical Language Sciences, University of Reading, UK

Abstract

The production of cognitive flexibility requires the coordination and integration of information from across the brain, by the dorsal striatum. In particular, the striatal cholinergic system is thought to be important for the modulation of striatal activity. Research from animal literature has shown that chemical inactivation of the dorsal striatum leads to impairments in reversal learning. Furthermore, proton magnetic resonance spectroscopy work has shown that the striatal cholinergic system is also important for reversal learning in humans. Here, we aim to assess whether the state of the dorsal striatal cholinergic system at rest is related to flexible behaviour in reversal learning. We provide preliminary results showing that variability in choline in the dorsal striatum is significantly related to both the number perseverative and regressive errors that participants make, and their rate of learning from positive and negative prediction errors. These findings, in line with previous work, suggest the resting state of dorsal striatal cholinergic system has important implications for producing flexible behaviour. However, these results also suggest the system may have heterogeneous functionality across different types of tasks measuring cognitive flexibility. These findings provide a starting point for further interrogation into understanding the functional role of the striatal cholinergic system in flexibility.

Introduction

Cognitive flexibility enables an individual to generate complex behavioural output that allows them to adaptively respond changes in their world. The neurotransmitter acetylcholine is thought to play a critical role in this ability (Yamanaka et al., 2018). Evidence of the importance of the striatal cholinergic system has mostly come from the animal literature, where cholinergic interneurons in the dorsomedial striatum have been shown to be important for flexibility (Bradfield & Balleine, 2017)[8]. The reversal learning task is a commonly used paradigm for studying cognitive flexibility, with reversal learning associated with increases in acetylcholine release in the dorsomedial striatum (Ragozzino et al., 2009). Cholinergic neurotransmission modulates medium spiny neuron activity directly via the expression of muscarinic receptors on medium spiny neurons (Assous, 2021), and indirectly via the expression of acetylcholine receptors on glutamatergic and dopaminergic projection neurons, GABAergic interneurons, and as autoreceptors on cholinergic interneurons (Ding et al., 2010; English et al., 2012; Kljakic et al., 2017; Kreitzer, 2009). Inactivation of cholinergic interneurons, and antagonism of cholinergic receptors on medium spiny neurons in the dorsomedial striatum impairs reversal learning performance (McCool et al., 2008; Ragozzino et al., 2009; Tzavos et al., 2004). These impairments, as indexed by a reduced ability to update outcome contingencies following reversal and an increase in regressive errors are seen following the loss of cholinergic interneuron activity, or input from parafascicular nucleus of the thalamus to cholinergic interneurons (Brown et al., 2010; Ragozzino et al., 2002).

The response of cholinergic interneurons to changes in outcome contingency is thought to be dependent on input from the parafascicular nucleus of the thalamus in rodents, and its homologue in human and non-human primates, the centromedian-parafascicular nuclei (Smith et al., 2011). Unlike other thalamostriatal pathways, connections between the centromedian-parafascicular nuclei and the striatum show preferential connectivity with cholinergic interneurons in the striatum (Smith et al., 2009). Moreover, these thalamostriatal connections are crucial for the role of cholinergic interneurons for flexible behaviour. For instance, inactivation of parafascicular nucleus in rodents impaired reversal learning performance, with similar behavioural impairments seen in studies where cholinergic interneurons were chemically inactivated (Brown et al., 2010). The importance of input from the parafascicular nucleus to the striatal cholinergic system is thought to be specific for reversal learning, and direct evidence for the role of these thalamostriatal connections for flexible behaviour is provided by Bradfield et al. (2013). Firstly, they show bilateral lesions of the parafascicular nucleus impair reversal, but not initial learning. Next contralateral

[8] See Chapter 1, "Reversal learning, the striatum, and acetylcholine" for a detailed overview.

lesions of the parafascicular nucleus and dorsomedial striatum, but not ipsilateral lesions of the same regions are also shown to impair reversal learning. This is because unilateral lesions spare thalamostriatal connections in the hemisphere contralateral to the lesions, while contralateral lesions leave no intact connectivity because at least one node of the circuit is ablated in each hemisphere. Finally, unilateral lesions of the parafascicular and the chemical inactivation of cholinergic interneurons in the contralateral hemisphere also leave reversal learning impaired, emphasising that it is the inactivation of these thalamic connections specifically that impair reversal learning, providing compelling evidence for the role thalamostriatal connectivity with the striatal cholinergic system in the production of cognitive flexibility.

Compared with animal research, where invasive experiments can interrogate causal interactions, studying the role of thalamostriatal connectivity and the striatal cholinergic system in cognitive flexibility in humans is not trivial. Nevertheless, proton magnetic resonance spectroscopy (^{1}H-MRS) is a non-invasive application of nuclear magnetic resonance spectroscopy, and is used to measure brain metabolites *in vivo* (Keeler, 2010). Theoretically, ^{1}H-MRS can be used to directly measure acetylcholine, but its concentration is so low *in vivo* that its signal is masked by other choline containing compounds (Bell, Lindner, et al., 2019). These choline containing compounds are choline, glycerophosphocholine (GPC), and phosphocholine (PC). These metabolites could be used to indirectly study acetylcholine function. For instance, choline is the rate-limiting factor in synthesis of acetylcholine (Lockman & Allen, 2002), and synaptic choline levels are related to cholinergic interneuron activity with prolonged activation of cholinergic interneurons decreasing the concentration of choline in the synaptic cleft (Löffelholz, 1998). However, typical ^{1}H-MRS approaches to quantifying choline containing compounds model them as a single peak due to their proximity on the spectrum. Doing so masks any functionally relevant choline effects as choline concentrations are anti-correlated with other choline-containing compounds (Lindner et al., 2017). Therefore, if we were able to separably measure choline from GPC and PC, then we could use this to indirectly and non-invasively study cholinergic system in humans. Previous work from our lab has demonstrated that choline can be separated from GPC and PC using ^{1}H-MRS at three tesla by modelling choline as a separate peak from a combined GPC and PC peak. We observed task related functional changes in choline that were in line with expected changes in acetylcholine release during visuospatial attention (Lindner et al., 2017) which suggests that quantifying choline separately from GPC+PC using ^{1}H-MRS may be an appropriate proxy for measuring acetylcholine activity in vivo.

We have previously used ^{1}H-MRS to study the role of the dorsal striatal cholinergic system in cognitive flexibility using a multi-alternative probabilistic reversal learning task. Functional ^{1}H-

MRS was previously used by Bell et al. (2018) to study changes in choline that functionally relate to flexible behaviour. ^{1}H-MRS data were acquired in the dorsal striatum while participants completed a multi-alternative probabilistic reversal learning task, and levels of choline and GPC+PC were quantified from metabolite spectra. The reversal of reward contingencies coincided with a significant decrease in the concentration of choline, but not GPC+PC or the total sum of choline containing metabolites, in line with previous findings of choline kinetics following the stimulation of cholinergic neurons in animals (Löffelholz, 1998), and from previous work using ^{1}H-MRS to study visuospatial attention (Lindner et al., 2017). These results show the functional relevance of choline for cognitive flexibility and demonstrate the specificity of this metabolite as a proxy for acetylcholine release.

Performance during reversal learning can be summarised in several ways. Direct measures of performance include the number of trials taken to reach a predefined learning criterion, number of correct responses, or the number of perseverative and regressive errors participants make. Following the reversal of reward contingencies in the task, the continued selection of the previously correct response strategy is known as response perseveration and the number trials before switching to using a difference response strategy is a measure of perseverative errors. Following a change in response strategy and in the absence of any reversal of outcome contingencies, trials where participants revert to using the now incorrect response strategy are used to measure regressive errors. Latent variables of performance can be inferred by fitting models to behavioural data. For instance, temporal difference reinforcement learning models can be used to model how participants learn from experience (Sutton & Barto, 2018). These models describe how people learn associations between actions and outcomes. Learning is driven by reward prediction errors, which describe the difference between actual and expected outcomes and are used to generate future estimates of expected value (Schultz et al., 1997). The rate of expected value updating is determined by the learning rate, and can be symmetric (a single learning rate α) or asymmetric for positive (α^{+}) and negative (α^{-}) prediction errors (Niv et al., 2012). Reversal learning performance is associated with dorsal striatal choline levels at rest, with Bell, Lindner et al. (2019) finding choline concentrations were positively correlated with perseverative errors, and negatively correlated with α^{-}. Additionally, α^{-} was negatively correlated with perseverative errors during reversal learning. These results show that lower levels of choline in the dorsal striatum at rest are associated with a quicker change in behaviour following the onset of reversal during multi-alternative probabilistic reversal learning and suggests that participants who reversed more quickly had lower levels of acetylcholine at rest, or more efficient re-uptake of choline following acetylcholine release.

In comparison to multi-alternative probabilistic reversal learning, two-choice serial reversal learning task is computationally simpler to solve. This simplicity means participants can feasibly complete multiple reversals over the course of the task. In chapter 4, we show that functional connectivity between the centromedian-parafascicular nuclei and the associative dorsal striatum is significantly increased during the processing of negative feedback relative to positive feedback. This change in functional connectivity could reflect a general error signal from the thalamus to cholinergic interneurons to promote flexible behaviour. However, these results do not directly implicate the striatal cholinergic system in the generation of flexible behaviour. Therefore, we next want to use ^{1}H-MRS to determine whether, in line with animal literature and our previous human work, serial reversal learning performance is associated with the striatal cholinergic system. More specifically, we are interested in the relationship between reversal learning and choline in the dorsal striatum at rest. Participants completed a probabilistic reversal learning task and we then acquired spectroscopy data from the dorsal striatum while at rest. Based on previous results, we predict reversal learning performance, as indexed by perseverative and regressive errors and parameter estimates from reinforcement learning models, will be associated with levels of choline in the dorsal striatum at rest.

Methods

Participants

Thirty three healthy adult participants were recruited to take part in this study. Thirty one of these participants were a subset of participants who also took part in the study described in chapter 4. Participants were recruited through opportune sampling within the University of Reading community. Eligible participants were right-handed, and self-reported no use of cigarettes, recreational drugs, prescription of psychoactive medication, and that they had no formal diagnosis of a psychiatric or neurological condition. Participants received £15 compensation for their time. Participants were included in the analysis reported here if they responded on at least 95% of the trials in the learning task, if their MRS spectral acquisition appeared correctly aligned within the striatum on their T1 acquisition, and if we were able to quantify separate peaks for choline and glycerophosphocholine plus phosphocholine. Three participants were excluded because they responded on fewer than 95% of trials, one had registration issues, one had no behavioural data, one was manually removed as their behaviour suggested they did not understand the task, one had spectroscopy data lost, four had spectra that were corrupted during acquisition, and nine had choline peaks that could not be separated. Our sample used for statistical analyses consisted of thirteen participants (mean age = 22.69 years; SD = 3.20; range = 18-29; 11 female). The study was approved by the research ethics committee of the University of Reading [UREC 19/42].

Probabilistic reversal learning task

This task has been described previously in chapter 4. Briefly, two abstract images of fractal patterns were shown on the left and right hemifield of the visual display. Participants had to choose one of the two images within 2000ms by pressing the corresponding button on a button box, else a "too late" message was displayed. The outcome of the participant's choice was then presented, followed by their cumulative points total. Figure 43 shows a schematic of the task trial structure and timings.

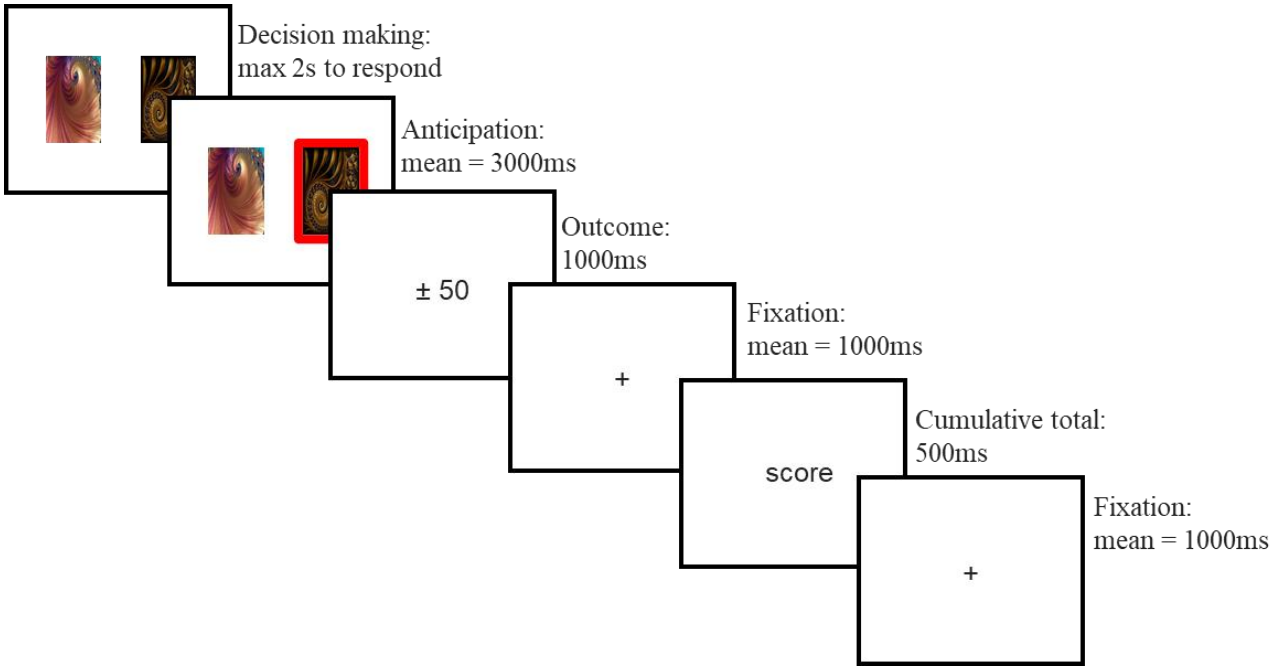

Figure 43 Overview of a single trial. Participants are initially shown two abstract fractal images and given two seconds to choose one image. Their choice is then highlighted. The participant is then shown the outcome of their choice; this will either be an increase or decrease of 50 points if they selected an image, or 0 points if they made no choice. The outcome is followed by a fixation cross, their cumulative total so far, and finally another fixation cross.

At the beginning of the task, one of the two images were randomly assigned as the correct image, and the other as the incorrect image. The probability of winning points on the correct image was 0.8, and the probability of losing points was 0.2. The inverse was true for the incorrect image. Outcomes were pseudo-randomised such that the assigned probabilities were true for blocks of 20 consecutive selections of the correct or incorrect choice. Additionally, no more than six of the same outcomes (win or loss) would be consecutively presented for the correct or incorrect choice. If participants won, their cumulative total increased by 50. If they lost, their cumulative total decreased by 50. If they did not choose an image, their cumulative total did not change. For outcome probabilities to reverse participants had to reach and maintain a predefined learning criterion: the selection of the correct image on five of the previous six trials. After reaching criterion participants entered a stability phase where the probability of reversal was equal to the number of trials where criterion had been maintained, divided by 10 (adapted from (Hampton et al., 2006)). If criterion was not maintained, then the probability of reversal was reset to 0 and restarted once criterion was reached. The reversal event involved the switching of outcome probabilities, with the correct image becoming incorrect and *vice versa*. After reversal, participants had to re-reach and

maintain the learning criterion for the reassigned outcome probabilities before outcome probabilities would reverse again. Participants completed 360 trials of the reversal learning task. Participants completed 20 practice trials. Practice trials followed the same structure as trials in the scanner, but participants did not receive any feedback for their choices. Instead, hashtags were presented in place of outcome and cumulative total feedback.

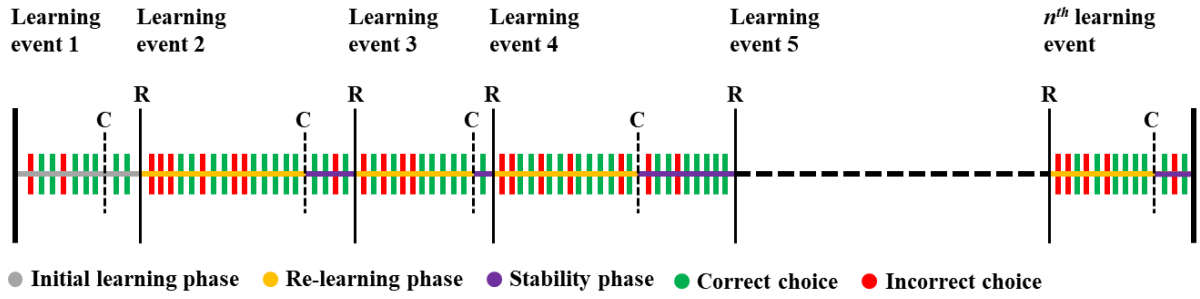

Figure 44 Trial and task phase overview of the serial reversal learning task. Dashed vertical lines show when criterion was reached (C); thin vertical lines show where outcome contingencies reversed (R) and a new learning event starts. Initial learning is the first learning event. After each reversal (R) participants are in the re-learning phase until they reach criterion (C). Participants are then in the stability phase until outcome contingencies reverse (R). The learning criterion must be maintained during the stability phase before reward contingencies reverse. Incorrect choices during the re-learning phase are defined as reversal errors, and the last reversal error of each re-learning phase is defined as the final reversal error. Each participant completes a total of 360 trials.

Computational Modelling

Overview

Two models were fit using mean-field variational Bayes to perform hierarchical Bayesian inference on our behavioural data using the MATLAB computational/behavioural modelling toolbox (Piray, Dezfouli, et al., 2019). Calculating parameter distributions at the population level using hierarchical Bayesian inference is advantageous over hierarchical parameter estimation, since one of the assumptions of hierarchical parameter estimation is that a given model is responsible for generating data from all subjects. During hierarchical parameter estimation, each participant equally influences group level parameters as model identity is included as a fixed effect despite it not

necessarily being true that one given model best explains the behaviour of each subject. By contrast, hierarchical Bayesian inference takes a random effects approach to parameter estimation and model comparison (Piray & Daw, 2020).Therefore, an advantage of hierarchical Bayesian inference over hierarchical parameter estimation is that it includes a step where the responsibility of each model for generating a given dataset is calculated, and this responsibility influences group parameter estimation. The modelling approach described below follows recommendations from Wilson & Collins (2019).

Models

Model one is a model-free reinforcement learning model with a single learning rate parameter (α), and an inverse temperature parameter (β). The learning rate parameter defines the rate that value estimates are updated based on the difference between expected and actual outcomes, also known as a prediction error. The inverse temperature parameter describes the degree to which choices are based on value estimates. The lower an agent's inverse temperature parameter, the more stochastic their choices will be. When β=0, choices would be made completely at random; when $\beta = \infty$ the choice with the largest expected value would be deterministically chosen. In this model the softmax function is used to calculate the probability of making choice k at time t (p_t^k), and is based on expected values Q and the inverse temperature parameter β. These probabilities are used during model fitting to calculate parameters that best describe the data. The softmax choice rule is defined as:

$$p_t^k = \frac{e^{\beta Q_t^k}}{\sum_{i=1}^{K} e^{\beta Q_t^i}} \quad (1)$$

where Q_t^k is defined as:

$$Q_t^k = V_t^k \quad (2)$$

The expected value for choice k is updated such that V_{t+1}^k is equal to V_t^k plus the product of the learning rate (α) and the prediction error (δ) (eq. 3). The prediction error δ is defined as the difference between the actual λ_t and expected value V_t^k for choice k at time t (eq. 4).

$$V_{t+1}^k = V_t^k + \alpha\delta_t \quad (3)$$

$$\delta_t = (\lambda_t - V_t^k) \tag{4}$$

Model two is a model-free reinforcement learning model with separate learning rates for positive (α^+) and negative (α^-) prediction and errors (eq. 5) and an inverse temperature parameter (β). The softmax function (eq. 1) is used to calculate the probability of making choice k at time t (p_t^k). The expected value for choice k is updated such that V_{t+1}^k is equal to V_t^k plus the product of the learning rate ($\alpha^{+/-}$) and the prediction error (δ) (eq. 5). The prediction error δ is defined as the difference between the actual λ_t and expected value V_t^k for choice k at time t (eq. 4). Separate learning rates for positive and negative prediction errors were included in this model because they have been shown to have asymmetric effects on expected value updating (Niv et al., 2012).

$$V_{t+1}^k = \begin{cases} V_t^k + \alpha^+ \delta_t & \text{if } \delta > 0 \\ V_t^k + \alpha^- \delta_t & \text{otherwise} \end{cases} \tag{5}$$

Model fitting

Model fitting and parameter estimation was performed using hierarchical Bayesian inference as implemented in the Computational/Behavioural Modelling toolbox (Piray, Dezfouli, et al., 2019). Model fitting was performed using behavioural data from the twenty-nine participants who successfully completed the reversal learning task; data from these participants were modelled to produce better estimates of group-level parameter distributions. In the first step of model fitting each model was fitted to participant's data using Laplace approximation for non-hierarchical inference to generate a maximum a-posteriori estimates for each parameter for each subject, and log-model evidence for each subject. This non-hierarchical model fit requires that parameters have Gaussian priors; for all parameters these priors were specified as having mean=0, variance =6.25, in line with previous reports (Piray, Dezfouli, et al., 2019; Piray, Ly, et al., 2019). These values were selected because it creates a wide range of values that parameters could take. These values were then used during hierarchical Bayesian inference, implemented using mean-field variational Bayes. Each iteration of model fitting contained the following steps 1. Calculate summary statistics, 2. Update estimates of the posterior distribution for group parameters, 3. Update estimates of the posterior for individual parameters, 4. Update estimates of responsibility for each model in generating given data. Model fitting was iterated until the model reached convergence. The best fitting model was determined by the model with the highest exceedance probability, which is the probability that a given model is more commonly expressed than other candidate models in model

space. Lastly, Model fitting was re-run, but this time under the hypothesis that observed differences in model fit are due to chance. This returns the protected exceedance probability, and a more conservative approach for finding the best fitting model (Piray, Dezfouli, et al., 2019).

Magnetic Resonance Spectroscopy

Data acquisition

^{1}H-MRS spectra and MR images were acquired at the Centre for Integrative Neuroscience and Neurodynamics, University of Reading, using a Siemens Magnetom Prisma-fit scanner 3T scanner and a 32 channel receiver head coil. High resolution T1-weighted anatomical images were acquired with a magnetization-prepared rapid gradient-echo (MP-RAGE) with GeneRalized Autocalibrating Partially Parallel Acquisitions (GRAPPA) (R = 2) sequence [TR = 2300ms; TE = 2.29ms; TI = 900ms slices = 192; voxel volume ≈ 0.9mm3; slice thickness = 0.94mm; distance factor = 50%; slice oversampling = 16.7%; FOV = 240 x 240mm; matrix = 256 x 256; flip angle = 8°; phase encoding direction = A → P; echo spacing = 7ms]. T2 HASE images [TR = 1500 ms; TE = 82 ms; FOV = 220 x 220mm; flip angle = 150º; voxel = 0.7 x 0.7 x 3 mm; 15 slices] were acquired immediately prior to the acquisition of the MRS spectra; this positioned the axial plane of the voxel in the isocenter of the magnetic field, optimizing the homogenization of the magnetic field during shimming. The native scanner PRESS sequence [striatal voxel = 15 x 10 x 15 mm; TR = 2000 ms; TE = 30ms; 256 transients; water suppression bandwidth = 50 Hz; automatic shimming] was used to acquire spectra in the left dorsal striatum of all participants, similar to Bell et al. (2018), and Bell, Lindner, et al. (2019). The same PRESS sequence was used to acquire a water unsuppressed peak for eddy current correction and calculating absolute metabolite concentrations [15 transients]. PRESS data were acquired following the acquisition of echo planar data presented in chapter 4.

Preprocessing

^{1}H-MRS data analysis was performed in line with experts' consensus recommendations published by (Near et al., 2020). MRS data pre-processing was carried out using the MATLAB toolbox FID-A (Simpson et al., 2015). Firstly, radiofrequency coil channels were combined, and bad individual spectra (spectra > 4 standard deviations used as rejection threshold) were removed. Spectra were then aligned to correct for frequency drift and averaged to create a single spectrum. The averaged spectrum was brought in phase (first-order phasing), and zero-order phase correction was applied using the creatine peak. The spectrum was frequency shifted so that creatine appeared at 3.027ppm

for the water suppressed spectrum, and water appeared at 4.65ppm in the water unsuppressed spectrum. eddy current correction was applied to remove distortion in the spectrum due to fluctuations in the B_0 field, then the water peak was subtracted from the water suppressed spectrum using Hankel-Lanczos Singular Value Decomposition (Pijnappel et al., 1992) as implemented in FID-A.

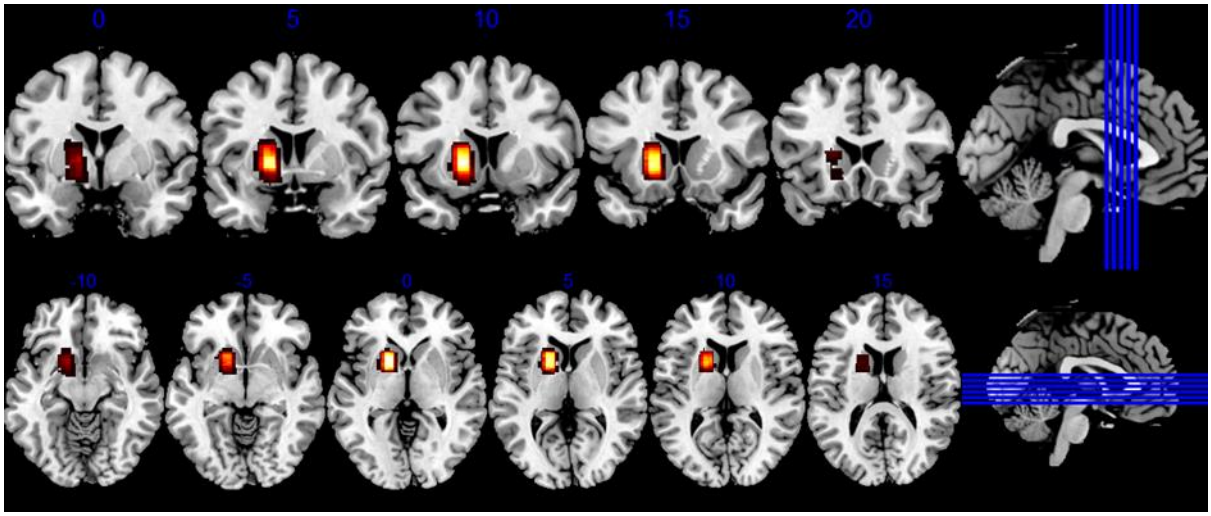

Figure 45 Coronal and axial slices visualising voxel positioning within the striatum for all participants in standard space. Heatmap denotes extent of spatial overlap, from maximum/yellow to minimum/red.

Spectral quantitation

A metabolite basis set was generated using the MATLAB FID-A toolbox (Simpson et al., 2015). Sixteen metabolites (acetate, aspartate, choline, creatine, gamma‐aminobutyric acid (GABA), glucose, glutamate, glutamine, lactate, myo‐inositol, N‐acetyl aspartate (NAA), phosphocreatine, phosphocholine (PC), glycerophosphocholine (GPC), scyllo‐inositol, and taurine) were simulated at a field strength of 3T using a PRESS pulse sequence (TE1 = 16.6 ms, TE2 = 13.4 ms, 4096 points, spectral width = 2399.8Hz, linewidth = 12.684Hz). Choline was modelled separately from PC and GPC, which were added following simulation to form a single peak (GPC+PC).

Automatic quantification of metabolites from the spectra were calculated using the jMRUI tool Accurate Quantification of Short Echo time domain Signals (AQSES) (jMRUI, version 6.0; http://www.jmrui.eu/; Garcia et al., 2010; Naressi et al., 2001; Stefan et al., 2009). The NAA peak

in the spectra was shifted to 2.02 ppm to correct for chemical shift displacement, and the metabolite model was realigned with the NAA peak in the spectra. The following settings were used for quantification: equal phase for all metabolites; begin fixed timing; delta damping -10 to 40 Hz; delta frequency -10 to 10 Hz, no background handling; 0 truncated points; 4096 points in AQSES; normalization on. Metabolite concentrations were corrected by calculating their amplitude relative to the corresponding regional water peak (acquisition correction=1, tissue correction=0.5555).

MRS voxels were co-registered with high resolution T1 anatomical images using CoRegStandAlong in Gannet 3.1 and SPM-12 (Ashburner & Friston, 2005; Edden et al., 2014). During registration, the fraction of grey matter, white matter, and cerebrospinal fluid was calculated for each spectral acquisition. These fractional tissue compositions were used to correct the concentrations of choline and GPC+PC for partial volume and relaxation effects using the MATLAB toolbox MRSParVolCo (https://github.com/DrMichaelLindner/MRSParVolCo), based on the formulae described by (Gasparovic et al., 2006).

Statistical analysis

Statistical analyses were performed using the R programming language (R Core Team, 2020; Wei & Simko, 2021; Wickham, 2016; Wickham et al., 2020) and SPSS (IBM Corp. Released 2017. IBM SPSS Statistics for Windows, Version 25.0. Armonk, NY: IBM Corp.). Correlational analyses were used to assess the relationship between metabolite concentrations, model parameter estimates, and behavioural performance. Hierarchical multiple regression was used to assess whether variance in choline concentrations could be explained by participants' model parameter estimates and behaviour. As part of this analysis we included GPC+PC concentration, since we know it is anti-correlated with choline concentrations (Bell, Lindner, et al., 2019; Lindner et al., 2017), and number of reversals as covariates of no interest. Lastly, to assess the specificity of these results to choline, we re-ran our regression analysis using NAA.

Results

Reversal learning performance

Participants made correct choices at significantly greater than chance level (mean correct choices = 252.71, 95% CI [244, ∞], $t(13) = 14.19$, $p < .001$, SD = 19.18, Range = 193 - 269), and experienced an average of 24.21 (SD = 4.96; Range = 10-29) reversals. The average number of trials taken to reach criterion was 8.756 (SD = 4.371; Range = 5 - 40); an average of 3.044 (SD = 2.161; Range = 0 - 17) perseverative errors were made following the reversal of contingencies before reaching criterion in each learning event. On 3.357 (SD = 3.734; Range = 0 - 12) trials participants did not respond to either of the two images presented to them. An average of 4617.857 (SD = 1099.407, Range = 1200 - 5550) points were collected by the end of the task. The average time taken by participants to make a choice following the onset of the stimuli was 595.746 milliseconds (SD = 110.104, Range = 398.713 - 782.612).

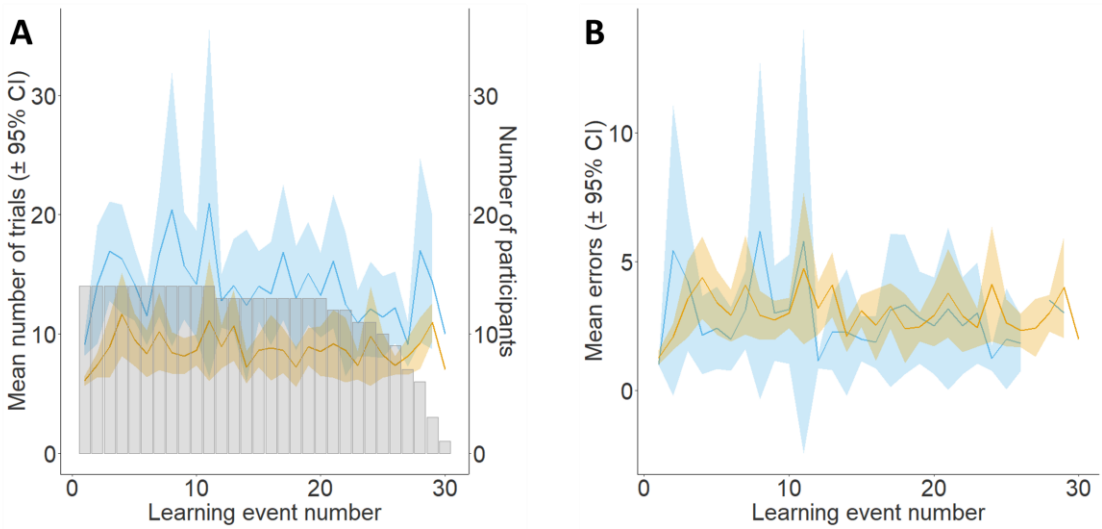

Figure 46 A: Average number of trials to reach criterion (orange) and reversal (blue) for each learning event (± 95% confidence intervals). Number of participants who reached each learning event (grey bars). B: Average number of perseverative (orange) and regressive (blue) errors for each learning event (± 95% confidence intervals).

Model fit

Two reinforcement learning models were fit to participants behavioural data from the reversal learning task. The first was a model-free reinforcement learning model with a single learning rate α, and an inverse temperature parameter β. The second model was a model-free reinforcement

learning model with two learning rates, α^+ and α^- for positive and negative prediction errors, and an inverse temperature parameter β. Model fitting was performed using hierarchical Bayesian inference with the MATLAB Computational/Behavioural Modelling toolbox (Piray, Dezfouli, et al., 2019). Overall, the dual-learning rate model out-performed the single learning rate model with respect to its protected exceedance probability (0.9727 for the dual learning rate model, 0.0273 for the single learning rate model), and the goodness of fit to each participant's data (the dual learning rate model had a higher responsibility for eleven of the fourteen participants included in the analysis of spectroscopy data). The group-mean learning rate for positive prediction errors (α^+) was 0.4605 and 0.9786 for negative prediction errors (α^-); the group-mean inverse temperature parameter (β) was 1.8533.

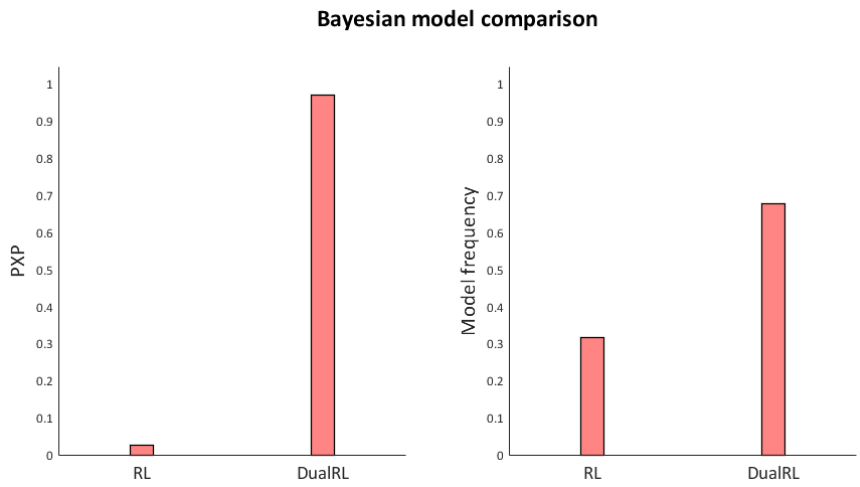

Figure 47 Protected exceedance probability and model frequency for the single and dual learning rate reinforcement learning models. The exceedance probability is the probability that a given model is the most commonly expressed model across particiapants, given the null hypothesis none of the models are sufficiently supported by the data

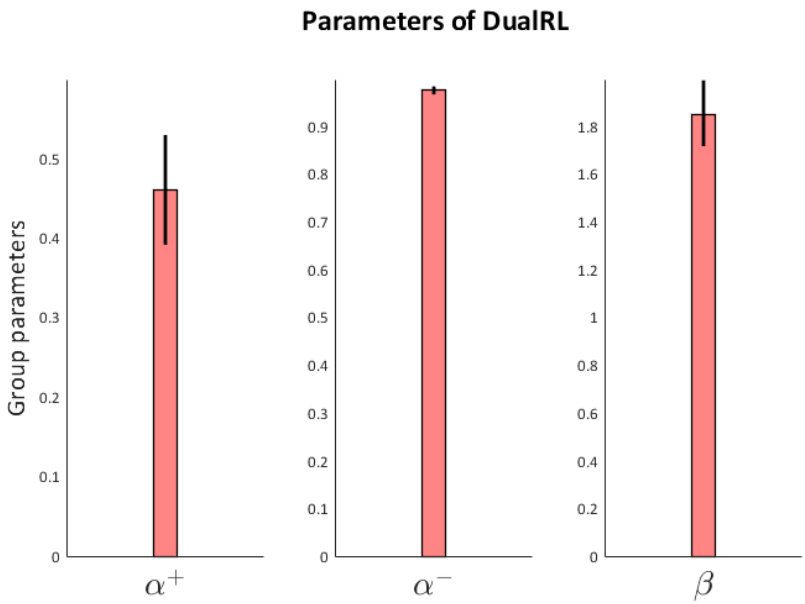

Figure 48 Group level parameter estimates for the learning rate for positive (α^+) and negative (α^-) prediction errors and the inverse temperature parameter (β). The error bars for all plots are the standard error of the mean.

Metabolite quantitation

Metabolite spectra were quantified for twenty-one participants to measure concentrations of choline and glycerophosphocholine plus phosphocholine (GPC+PC) in the dorsal striatum. Separate measures of choline and GPC+PC could be quantified for fourteen participants. The mean concentration of choline in the dorsal striatum was 0.797 millimolar (mM) (SD = 0.253, Range = 0.481 - 1.351); for GPC+PC the mean concentration was 0.854 mM (SD = 0.241, Range = 0.323 - 1.238). As previously reported, we found that concentrations of choline and GPC+PC were anti-correlated (r = -0.912 $t(11)$ = -7.379, 95% CI = [-0.974, -0.726], $p < 0.001$) (Bell et al., 2018; Lindner et al., 2017; Miller et al., 1996).

Relationship between choline measures and behaviour

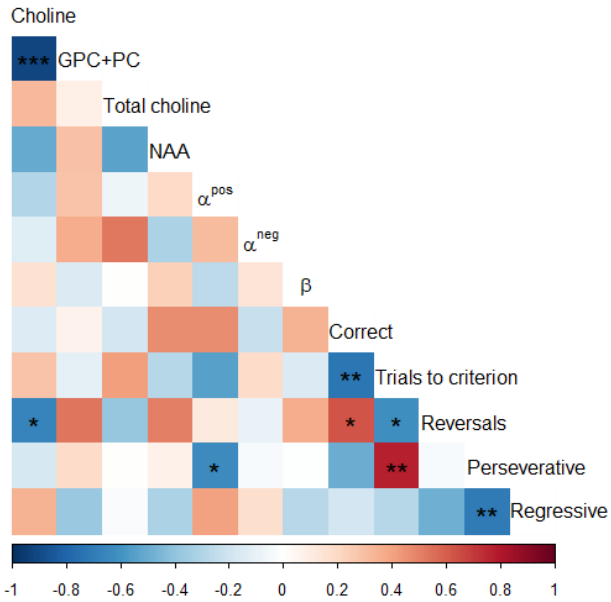

Figure 49 Correlations between metabolite concentrations, reinforcement learning model parameter estimates, and measures of reversal learning behaviour. Significant correlations are denoted with asterisks (*p < 0.05, **p < 0.01, ***p < 0.001)

To investigate the relationship between neurochemistry and behaviour we first ran correlations between our measures of task performance (correct choices, perseverative errors, regressive errors, and number of reversals), modelling parameters (α^+, α^-, β) and metabolite concentrations in the dorsal striatum (Cho, GPC+PC, total choline, and NAA). Increases in dorsal striatal choline were associated with decreases in dorsal striatal GPC+PC (r = -0.912 $t(11)$ = -7.379, 95% CI = [-0.974, -0.726], $p < 0.001$), and decreases in the number of reversals participants experienced (r = -0.667 $t(11)$ = -2.971, 95% CI = [-0.891, -0.184], p = 0.013). Increases in the number of reversals was associated with an increase in the number of correct responses made (r = 0.630 $t(11)$ = 2.688, 95% CI = [0.120, 0.877], p = 0.021). An increase in the number of perseverative errors was associated with a decrease in the learning rate for positive prediction errors (α^+; r = -0.632 $t(11)$ = -2.701, 95% CI = [-0.877, -0.123], p = 0.021), and a decrease in the number of regressive errors made (r = -0.709 $t(11)$ = -3.333, 95% CI = [-0.906, -0.259], p = 0.007). No other significant correlations were identified at a threshold of $p < 0.05$.

Before running our hierarchical multiple regression, the following assumptions were tested. We tested for multicollinearity by calculating variance inflation factors (VIF) for our predictor

variables; no variables had a VIF greater than 10, suggesting they have not violated assumptions of multicollinearity (Field, 2013). To test the assumption that the residuals of predictors are uncorrelated, we used the Durbin-Watson test and found this assumption was met (Durbin-Watson = 2.288); values of two suggest residuals are uncorrelated, while values less than one or greater than three suggest indicate there are problematic positive or negative correlations (Field, 2013). Plots of standardised residuals and standardised predicted values suggested the assumptions of homogeneity of variance were met; P-P plots of standardised residuals suggested that the assumption of normality may have been violated, however regression results are unlikely to be biased by violations of normality when there are ten or more observations for each variable (Schmidt & Finan, 2018). Cook's distance for two participants were greater than one and suggests these participants may have a disproportionate influence on the model, however these participants were not excluded from analysis given the size of the dataset.

A two-stage hierarchical multiple regression model was run to investigate the relationship between levels of choline and task performance. The GPC+PC concentration and number of reversals were included in the first stage as a covariates of no interest. Perseverative and regressive errors, positive (α^+) and negative (α^-) learning rates, and the inverse temperature parameter (β) were included in the second stage of the model. One participant was excluded from our regression model because their behaviour suggested they did not understand the task, but this did not influence model fitting. The first stage of the regression revealed that GPC+PC and the number of reversals were significant predictors of choline concentrations in the dorsal striatum F (2,12) = 35.522, $p < 0.001$, and explained 87.6% of the variance in choline concentration. The inclusion of model parameters and number of errors at the second stage of the regression increased the variance explained by 10.6%, and this was a significant increase in explained variance F (7,12) = 39.802, $p < 0.001$, $f^2 = 0.119$ (Table 11).

Variable	Unstandardised β / Standardised β	*t*	R	R^2	ΔR^2
Stage 1			.936	.876	
GPC+PC	-.820 / -.778	-5.913***			
Reversals	-.023 / -.250	-1.903			
Stage 2			.991	.982	.149*
GPC+PC	-.894 / -.848	-7.083**			
Reversals	-.037 / -.400	-3.407*			
α^+	-.493 / -.303	-2.914*			
α^-	1.891 / .328	3.275*			
β	-.067 / -.125	-1.192			
Perseverative err	-.014 / -.619	-4.397**			
Regressive err	-.015 / -.574	-4.197**			

N = 13; **p* < .05; ***p* <.01; ****p* <.001

Table 11 Hierarchical regression model predicting concentrations of choline. At the first stage GPC+PC concentration and the number of reversals are included as covariates of no interest. In the second stage reinforcement learning model parameter estimates, perseverative and regressive errors are included in the model.

To test whether these results were specific to the concentration of choline, we re-ran the same regression model with the concentration of N - acetyl aspartate (NAA) as our dependent variable. GPC+PC and the number of reversals were not significant predictors of NAA concentration in the first stage of the regression model F (2,12) = 1.704, p = 0.231, and explained 25.4% of the variance in NAA concentration. The addition of our modelling parameters and measures of error increased the explained variance in NAA to 79%, however this was not a significant increase in explained variance and the model did not significantly explain concentrations of NAA F (7,12) = 2.693, p = 0.146.

Variable	Unstandardised β / Standardised β	*t*	R	R^2	ΔR^2
Stage 1			.504	.254	
GPC+PC	.091 / .033	.103			
Reversals	.117 / .485	1.501			
Stage 2			.889	.790	.536
GPC+PC	1.836 / .672	1.628			
Reversals	-.018 / -.073	-.181			
α^+	4.083 / .967	2.701*			
α^-	-16.326 / -1.092	-3.164*			
β	1.367 / .976	2.703*			
Perseverative err	.059 / .995	2.050			
Regressive err	.045 / .668	1.417			

N = 13; **p* < .05; ***p* <.01; ****p* <.001

Table 12 Hierarchical regression model predicting concentrations of NAA. NAA model was used as a control metabolite to demonstrate the specificity of the model for choline. At the first stage GPC+PC concentration and the number of reversals are included as covariates of no interest. In the second stage reinforcement learning model parameter estimates, perseverative and regressive errors are included in the model.

Discussion

We used ^{1}H-MRS to investigate whether variability in resting levels of choline in the dorsal striatum are related to reversal learning performance and reinforcement learning model parameter estimates in a two-alternative serial reversal learning task. Positive and negative learning rates, and the number of perseverative and regressive errors were significant predictors of dorsal striatal choline, and their inclusion in our regression model explained significantly more variance in choline than when we only included GPC+PC and number of reversals as covariates of no interest. Almost all the variability in choline was explained by this regression model (98.2%). Conversely, when we re-ran the same analyses for a metabolite that we consider a functional control we observed no association with performance. Specifically, using NAA as our predicted outcome, we found that neither level of our hierarchical model significantly predicted NAA concentrations.

Further correlational analyses are in line with previous findings. Firstly, we show that levels of choline in the dorsal striatum are inversely correlated with GPC+PC concentrations (Bell, Lindner, et al., 2019; Lindner et al., 2017). We believe this relationship is not due to issues with model fitting, as Lindner et al. (2017) previously demonstrated using synthetic spectra that relative differences in concentrations of choline and GPC+PC are faithfully recovered during model fitting when separate peaks for choline and GPC+PC are used. Secondly, we found that concentrations of choline are rest are negatively correlated with the number of reversals participants made. This mirrors previous findings that participants who were quicker to reverse had lower levels of dorsal striatal choline at rest (Bell, Lindner, et al., 2019), and that participants who learned during reversal had lower levels of choline at rest than those who did not (Bell et al., 2018).

Previous work on deterministic reversal learning by D'Cruz et al. (2011) has demonstrated that unexpected outcomes during two- and four-choice tasks activate similar brain areas, but that activation during four choice learning is significantly greater in several regions, including the thalamus. Although D'Cruz et al. (2011) do not localise this activation to specific nuclei in the thalamus, based on our understanding of the roles of thalamostriatal connections in flexibility, especially in signalling unexpected outcomes (Bell, Langdon, et al., 2019; Bradfield et al., 2013; Matsumoto et al., 2001), we would expect this cluster to include the centromedian-parafascicular nuclei. If the centromedian-parafascicular nuclei show different levels of activation in two and four choice reversal learning, then their efferent projections to the cholinergic interneurons of the dorsal striatum may have different effects on the striatal cholinergic system during reversal learning. If resting levels of choline were consistent for participants completing both reversal learning tasks,

then variability in input to the striatal cholinergic system could have a differential effect on subsequent behaviour in the two tasks.

Here we provide evidence suggesting choline levels at rest may have dissociable effects on behaviour, depending on task context. During multi-alternative reversal learning, there is a protracted period of learning where the participant's experience closely mimics the experience in animal studies, with no prior knowledge of task context or structure. Conversely, in serial reversal learning, such as the task used here, participants are provided with instruction about the general structure of the task which can be used to scaffold task representations. This prior knowledge should enable participants to readily form mature task representations. Once participants develop an "if not A, then B" heuristic for choice, their task representation can be considered as "saturated", as no other contextual information is available that might further support adaptive behaviour. However, task representations in the multi-alternative task can be considered as "unsaturated", because participants only form mature task representations after experiencing both the protracted periods of initial and reversal learning. These differences could explain why resting cholinergic "tone" has dissociable effects during serial and multi-alternative reversal learning. Here, we found that dorsal striatal choline concentration was negatively associated with perseverative errors but positively associated with the learning rate for negative prediction errors. Conversely, Bell, Lindner et al. (2019) found that dorsal striatal choline was positively correlated with perseverative errors, but negatively correlated with the learning rate for negative prediction errors. In an unsaturated context (multi-alternative task), a low cholinergic tone may be beneficial for generating contrast between periods of stability and change. This increased contrast could detect change more clearly, enabling flexibility when required. However, in the saturated context (serial reversal learning task), a high cholinergic tone may be more beneficial: participants with higher choline at rest were influenced more by negative than positive prediction errors and showed fewer perseverative and regressive errors. By contrast, lower cholinergic tone may disproportionately increase learning from positive feedback for perseverative errors and decrease learning from negative feedback from regressive errors. These participants would then be slower to reverse and less likely to maintain behaviour. However, these participants do not appear to be any more stochastic in their behaviour than participants with higher cholinergic tone, as the inverse temperature parameter did not significantly predict choline levels at rest. Task performance in different contexts thus appears to be modulated by the state of the cholinergic system at rest, with the saturation of task representation modulating its relationship with performance.

One potential factor that may also account for differences between the serial and multi-alternative reversal learning tasks is the model fitting procedure. Although both studies use the same

reinforcement learning model, Bell, Lindner et al. (2019) fitted their model to initial and reversal learning separately, while here we fit the model to all trials at once. Therefore, parameter estimates in both studies do not describe exactly equivalent aspects of behaviour. This difference is inevitable due to the structure of our task. Combining trials across different phases would produce invalid results, as the model would be fit to non-contiguous trials that do not reflect the experience of the participant. Additionally, the model fitting approach taken here uses Hierarchical Bayesian Inference, while Bell, Lindner et al. (2019) use Maximum Likelihood Estimation. Hierarchical Bayesian methods have been shown to more accurately provide point estimates of individual parameters (Farrell & Ludwig, 2008; Katahira, 2016), and therefore some difference between our results and those of Bell, Lindner et al. (2019) may also be due to model fitting approaches. Most probable is that differences between our results and those of Bell, Lindner et al. (2019) are due to a combination of psychological and methodological factors, given none of the explanations given are mutually exclusive of one-another.

Given the preliminary nature of this study, it is important that the results presented here are received with caution. Despite strong evidence from the animal literature and from our previous work in humans describing the roles of the striatal cholinergic system in flexibility (e.g. Bell et al., 2018; Bell, Lindner, et al., 2019; Bradfield et al., 2013; Brown et al., 2010; Ragozzino et al., 2002, 2009), these results need to be replicated. Several limitations of this study are related to the sample size. Firstly, although data were acquired for thirty-three participants, only thirteen datasets were used in our final analysis. Of the twenty excluded participants, thirteen had issues related to the acquisition or analysis of their metabolite spectra. One potential explanation for this data loss is the ^{1}H-MRS spectra were acquired following the acquisition of fMRI data using echo-planar imaging sequences, which can cause frequency drift, leading to the distortion of metabolite spectra (El-Sharkawy et al., 2006; Harris et al., 2014; Lange et al., 2011). Future work could aim to minimise the effects of frequency drift by leaving time for the gradient coils to cool prior to the acquisition of spectroscopy data. Further, given the size of the sample size reported here it is worth noting that the implied α for ΔR^2 (based on f^2, sample size, and number of predictors) in the stage 2 choline regression model was 0.183. This inflated α increases the risk of type 1 error, so the results reported here may have an increased likelihood of being due to type 1 error. Furthermore, two participants had Cook's distances that were greater than the recommended threshold and therefore these participants could disproportionately affect regression coefficient estimation (Field, 2013).

As it stands, and in line with previous work, this study provides further evidence for the role of the dorsal striatal cholinergic system in flexibility, and particularly during reversal learning. We find that levels of choline are associated with learning rates for positive and negative prediction errors,

and the number of perseverative and regressive errors. These findings show that the dorsal striatal cholinergic system appears to be involved in producing flexible behaviour during reversal learning, in line with previous work. Importantly, however, we find potential differences in how the system may be involved during instructed serial reversal learning and during uninstructed multi-alternative probabilistic reversal learning. Together, these results suggest an important role for the cholinergic system in flexibility in humans, as is suggested by findings from animal literature, and describe how the system may function in different contexts.

References

Ashburner, J., & Friston, K. J. (2005). Unified segmentation. *NeuroImage*, *26*(3), 839–851. https://doi.org/10.1016/j.neuroimage.2005.02.018

Assous, M. (2021). Striatal cholinergic transmission. Focus on nicotinic receptors' influence in striatal circuits. *European Journal of Neuroscience*, *53*(8), 2421–2442. https://doi.org/10.1111/ejn.15135

Bell, T., Langdon, A., Lindner, M., Lloyd, W., & Christakou, A. (2019). *Orbitofrontal and Thalamic Influences on Striatal Involvement in Human Reversal Learning* (p. 246371). https://doi.org/10.1101/246371

Bell, T., Lindner, M., Langdon, A., Mullins, P. G., & Christakou, A. (2019). Regional Striatal Cholinergic Involvement in Human Behavioral Flexibility. *Journal of Neuroscience*, *39*(29), 5740–5749. https://doi.org/10.1523/JNEUROSCI.2110-18.2019

Bell, T., Lindner, M., Mullins, P. G., & Christakou, A. (2018). Functional neurochemical imaging of the human striatal cholinergic system during reversal learning. *European Journal of Neuroscience*, *47*(10), 1184–1193. https://doi.org/10.1111/ejn.13803

Bradfield, L. A., & Balleine, B. W. (2017). Thalamic Control of Dorsomedial Striatum Regulates Internal State to Guide Goal-Directed Action Selection. *The Journal of Neuroscience*, *37*(13), 3721–3733. https://doi.org/10.1523/JNEUROSCI.3860-16.2017

Bradfield, L. A., Bertran-Gonzalez, J., Chieng, B., & Balleine, B. W. (2013). The thalamostriatal pathway and cholinergic control of goal-directed action: Interlacing new with existing learning in the striatum. *Neuron*, *79*(1), 153–166. https://doi.org/10.1016/j.neuron.2013.04.039

Brown, H. D., Baker, P. M., & Ragozzino, M. E. (2010). The Parafascicular Thalamic Nucleus Concomitantly Influences Behavioral Flexibility and Dorsomedial Striatal Acetylcholine Output in Rats. *Journal of Neuroscience*, *30*(43), 14390–14398. https://doi.org/10.1523/JNEUROSCI.2167-10.2010

D'Cruz, A.-M., Ragozzino, M. E., Mosconi, M. W., Pavuluri, M. N., & Sweeney, J. A. (2011). Human reversal learning under conditions of certain versus uncertain outcomes. *NeuroImage*, *56*(1), 315–322. https://doi.org/10.1016/j.neuroimage.2011.01.068

Ding, J. B., Guzman, J. N., Peterson, J. D., Goldberg, J. A., & Surmeier, D. J. (2010). Thalamic Gating of Corticostriatal Signaling by Cholinergic Interneurons. *Neuron*, *67*(2), 294–307. https://doi.org/10.1016/j.neuron.2010.06.017

Edden, R. A. E., Puts, N. A. J., Harris, A. D., Barker, P. B., & Evans, C. J. (2014). Gannet: A batch-processing tool for the quantitative analysis of gamma-aminobutyric acid–edited MR spectroscopy spectra. *Journal of Magnetic Resonance Imaging*, *40*(6), 1445–1452. https://doi.org/10.1002/jmri.24478

El-Sharkawy, A. M., Schär, M., Bottomley, P. A., & Atalar, E. (2006). Monitoring and correcting spatio-temporal variations of the MR scanner's static magnetic field. *Magnetic Resonance*

Materials in Physics, Biology and Medicine, *19*(5), 223–236. https://doi.org/10.1007/s10334-006-0050-2

English, D. F., Ibanez-Sandoval, O., Stark, E., Tecuapetla, F., Buzsáki, G., Deisseroth, K., Tepper, J. M., & Koos, T. (2012). GABAergic circuits mediate the reinforcement-related signals of striatal cholinergic interneurons. *Nature Neuroscience*, *15*(1), 123–130. https://doi.org/10.1038/nn.2984

Farrell, S., & Ludwig, C. J. H. (2008). Bayesian and maximum likelihood estimation of hierarchical response time models. *Psychonomic Bulletin & Review*, *15*(6), 1209–1217. https://doi.org/10.3758/PBR.15.6.1209

Field, A. P. (2013). *Discovering statistics using IBM SPSS statistics: And sex and drugs and rock 'n' roll* (4th edition). Sage.

Garcia, M. I. O., Sima, D., Nielsen, F., Himmelreich, U., & Van Huffel, S. (2010). Quantification of in vivo Magnetic Resonance Spectroscopy signals with baseline and lineshape corrections. *2010 IEEE International Conference on Imaging Systems and Techniques*, 349–352. https://doi.org/10.1109/IST.2010.5548503

Gasparovic, C., Song, T., Devier, D., Bockholt, H. J., Caprihan, A., Mullins, P. G., Posse, S., Jung, R. E., & Morrison, L. A. (2006). Use of tissue water as a concentration reference for proton spectroscopic imaging. *Magnetic Resonance in Medicine*, *55*(6), 1219–1226. https://doi.org/10.1002/mrm.20901

Hampton, A. N., Bossaerts, P., & O'Doherty, J. P. (2006). The Role of the Ventromedial Prefrontal Cortex in Abstract State-Based Inference during Decision Making in Humans. *Journal of Neuroscience*. https://doi.org/10.1523/JNEUROSCI.1010-06.2006

Harris, A. D., Glaubitz, B., Near, J., Evans, C. J., Puts, N. A. J., Schmidt-Wilcke, T., Tegenthoff, M., Barker, P. B., & Edden, R. A. E. (2014). Impact of frequency drift on gamma-aminobutyric acid-edited MR spectroscopy. *Magnetic Resonance in Medicine*, *72*(4), 941–948. https://doi.org/10.1002/mrm.25009

Katahira, K. (2016). How hierarchical models improve point estimates of model parameters at the individual level. *Journal of Mathematical Psychology*, *73*, 37–58. https://doi.org/10.1016/j.jmp.2016.03.007

Keeler, J. (2010). *Understanding NMR Spectroscopy* (2nd ed.). John Wiley & Sons. https://www.wiley.com/en-gb/Understanding+NMR+Spectroscopy%2C+2nd+Edition-p-9780470746080

Kljakic, O., Janickova, H., Prado, V. F., & Prado, M. A. M. (2017). Cholinergic/glutamatergic co-transmission in striatal cholinergic interneurons: New mechanisms regulating striatal computation. *Journal of Neurochemistry*, *142*(S2), 90–102. https://doi.org/10.1111/jnc.14003

Kreitzer, A. C. (2009). Physiology and Pharmacology of Striatal Neurons. *Annual Review of Neuroscience*, *32*(1), 127–147. https://doi.org/10.1146/annurev.neuro.051508.135422

Lange, T., Zaitsev, M., & Buechert, M. (2011). Correction of frequency drifts induced by gradient heating in 1H spectra using interleaved reference spectroscopy. *Journal of Magnetic Resonance Imaging: JMRI*, *33*(3), 748–754. https://doi.org/10.1002/jmri.22471

Lindner, M., Bell, T., Iqbal, S., Mullins, P. G., & Christakou, A. (2017). In vivo functional neurochemistry of human cortical cholinergic function during visuospatial attention. *PLOS ONE*, *12*(2), e0171338. https://doi.org/10.1371/journal.pone.0171338

Lockman, P. R., & Allen, D. D. (2002). The transport of choline. *Drug Development and Industrial Pharmacy*, *28*(7), 749–771. https://doi.org/10.1081/DDC-120005622

Löffelholz, K. (1998). Brain choline has a typical precursor profile. *Journal of Physiology Paris*, *92*(3–4), 235–239. https://doi.org/10.1016/S0928-4257(98)80025-9

Matsumoto, N., Minamimoto, T., Graybiel, A. M., & Kimura, M. (2001). Neurons in the Thalamic CM-Pf Complex Supply Striatal Neurons With Information About Behaviorally Significant Sensory Events. *Journal of Neurophysiology*, *85*(2), 960–976. https://doi.org/10.1152/jn.2001.85.2.960

McCool, M. F., Patel, S., Talati, R., & Ragozzino, M. E. (2008). Differential involvement of M1-type and M4-type muscarinic cholinergic receptors in the dorsomedial striatum in task switching. *Neurobiology of Learning and Memory*, *89*(2), 114–124. https://doi.org/10.1016/j.nlm.2007.06.005

Miller, B. L., Chang, L., Booth, R., Ernst, T., Cornford, M., Nikas, D., McBride, D., & Jenden, D. J. (1996). In vivo 1H MRS choline:Correlation with in vitro chemistry/histology. *Life Sciences*, *58*(22), 1929–1935. https://doi.org/10.1016/0024-3205(96)00182-8

Naressi, A., Couturier, C., Devos, J. M., Janssen, M., Mangeat, C., de Beer, R., & Graveron-Demilly, D. (2001). Java-based graphical user interface for the MRUI quantitation package. *Magnetic Resonance Materials in Physics, Biology and Medicine*, *12*(2–3), 141–152.

Near, J., Harris, A. D., Juchem, C., Kreis, R., Marjańska, M., Öz, G., Slotboom, J., Wilson, M., & Gasparovic, C. (2020). Preprocessing, analysis and quantification in single‐voxel magnetic resonance spectroscopy: Experts' consensus recommendations. *NMR in Biomedicine*. https://doi.org/10.1002/nbm.4257

Niv, Y., Edlund, J. A., Dayan, P., & O'Doherty, J. P. (2012). Neural Prediction Errors Reveal a Risk-Sensitive Reinforcement-Learning Process in the Human Brain. *Journal of Neuroscience*, *32*(2), 551–562. https://doi.org/10.1523/JNEUROSCI.5498-10.2012

Pijnappel, W. W. F., van den Boogaart, A., de Beer, R., & van Ormondt, D. (1992). SVD-based quantification of magnetic resonance signals. *Journal of Magnetic Resonance (1969)*, *97*(1), 122–134. https://doi.org/10.1016/0022-2364(92)90241-X

Piray, P., & Daw, N. D. (2020). A simple model for learning in volatile environments. *PLOS Computational Biology*, *16*(7), e1007963. https://doi.org/10.1371/journal.pcbi.1007963

Piray, P., Dezfouli, A., Heskes, T., Frank, M. J., & Daw, N. D. (2019). Hierarchical Bayesian inference for concurrent model fitting and comparison for group studies. *PLOS Computational Biology*, *15*(6), e1007043. https://doi.org/10.1371/journal.pcbi.1007043

Piray, P., Ly, V., Roelofs, K., Cools, R., & Toni, I. (2019). Emotionally Aversive Cues Suppress Neural Systems Underlying Optimal Learning in Socially Anxious Individuals. *Journal of Neuroscience*, *39*(8), 1445–1456. https://doi.org/10.1523/JNEUROSCI.1394-18.2018

R Core Team. (2020). *R: A Language and Environment for Statistical Computing*. R Foundation for Statistical Computing. https://www.R-project.org/

Ragozzino, M. E., Jih, J., & Tzavos, A. (2002). Involvement of the dorsomedial striatum in behavioral flexibility: Role of muscarinic cholinergic receptors. *Brain Research*, *953*(1–2), 205–214. https://doi.org/10.1016/S0006-8993(02)03287-0

Ragozzino, M. E., Mohler, E. G., Prior, M., Palencia, C. A., & Rozman, S. (2009). Acetylcholine activity in selective striatal regions supports behavioral flexibility. *Neurobiology of Learning and Memory*, *91*(1), 13–22. https://doi.org/10.1016/j.nlm.2008.09.008

Schmidt, A. F., & Finan, C. (2018). Linear regression and the normality assumption. *Journal of Clinical Epidemiology*, *98*, 146–151. https://doi.org/10.1016/j.jclinepi.2017.12.006

Schultz, W., Dayan, P., & Montague, P. R. (1997). A Neural Substrate of Prediction and Reward. *Science*, *275*(5306), 1593–1599. https://doi.org/10.1126/science.275.5306.1593

Simpson, R., Devenyi, G. A., Jezzard, P., Hennessy, T. J., & Near, J. (2015). Advanced processing and simulation of MRS data using the FID appliance (FID-A)—An open source, MATLAB-based toolkit. *Magnetic Resonance in Medicine*, *77*(1), 23–33. https://doi.org/10.1002/mrm.26091

Smith, Y., Raju, D., Nanda, B., Pare, J.-F., Galvan, A., & Wichmann, T. (2009). The thalamostriatal systems: Anatomical and functional organization in normal and parkinsonian states. *Brain Research Bulletin*, *78*(2), 60–68. https://doi.org/10.1016/j.brainresbull.2008.08.015

Smith, Y., Surmeier, D. J., Redgrave, P., & Kimura, M. (2011). Thalamic Contributions to Basal Ganglia-Related Behavioral Switching and Reinforcement. *Journal of Neuroscience*, *31*(45), 16102–16106. https://doi.org/10.1523/JNEUROSCI.4634-11.2011

Stefan, D., Cesare, F. D., Andrasescu, A., Popa, E., Lazariev, A., Vescovo, E., Strbak, O., Williams, S., Starcuk, Z., Cabanas, M., Ormondt, D. van, & Graveron-Demilly, D. (2009). Quantitation of magnetic resonance spectroscopy signals: The jMRUI software package. *Measurement Science and Technology*, *20*(10), 104035. https://doi.org/10.1088/0957-0233/20/10/104035

Sutton, R. S., & Barto, A. G. (2018). *Reinforcement learning: An introduction* (Second edition). The MIT Press.

Tzavos, A., Jih, J., & Ragozzino, M. E. (2004). Differential effects of M1 muscarinic receptor blockade and nicotinic receptor blockade in the dorsomedial striatum on response reversal learning. *Behavioural Brain Research*, *154*(1), 245–253. https://doi.org/10.1016/j.bbr.2004.02.011

Wei, T., & Simko, V. (2021). *R package 'corrplot': Visualization of a Correlation Matrix*. https://github.com/taiyun/corrplot

Wickham, H. (2016). *ggplot2: Elegant Graphics for Data Analysis*. Springer-Verlag. https://ggplot2.tidyverse.org

Wickham, H., François, R., Henry, L., & Müller, K. (2020). *dplyr: A Grammar of Data Manipulation*. https://CRAN.R-project.org/package=dplyr

Wilson, R. C., & Collins, A. G. (2019). Ten simple rules for the computational modeling of behavioral data. *ELife*, *8*, e49547. https://doi.org/10.7554/eLife.49547

Yamanaka, K., Hori, Y., Minamimoto, T., Yamada, H., Matsumoto, N., Enomoto, K., Aosaki, T., Graybiel, A. M., & Kimura, M. (2018). Roles of centromedian parafascicular nuclei of thalamus and cholinergic interneurons in the dorsal striatum in associative learning of environmental events. *Journal of Neural Transmission*, *125*(3), 501–513. https://doi.org/10.1007/s00702-017-1713-z

General discussion

Overview

The main aim of this thesis was to investigate cortical, striatal, and thalamic involvement in cognitive flexibility, and to assess the practicability of using functional magnetic resonance imaging and magnetic resonance spectroscopy to study the functional connectivity and neurochemistry of this system. Studies from both the animal and human literature point to the importance of the striatal cholinergic system (Bell et al., 2018; Bell, Lindner, et al., 2019; McCool et al., 2008; Ragozzino et al., 2002, 2009; Ragozzino & Choi, 2004), the connections between the centromedian-parafascicular nuclei of the thalamus and the dorsal striatum (Bell, Langdon, et al., 2019; Bradfield et al., 2013; Bradfield & Balleine, 2017; Brown et al., 2010) and the connections between the orbitofrontal cortex and dorsal striatum (Bell, Langdon, et al., 2019; Stalnaker et al., 2016) for flexibility. Previous human work (Bell et al., 2018; Bell, Langdon, et al., 2019; Bell, Lindner, et al., 2019) has used a multi-alternative reversal learning task with four options and a single uninstructed reversal. This task has a behavioural context characterised by unexpected volatility, and where different contingencies need to be learned during initial and reversal learning phases.

It is unclear whether these systems are similarly involved in the more commonly used serial reversal learning task with two choices, where prior knowledge of the reversal rule saturates the task representation needed for effective behaviour. In tackling this question in the work presented, we aimed to address methodological hurdles related to the application of non-conventional spectroscopy and functional imaging approaches to studying thalamostriatal and corticostriatal connectivity, and dorsal striatal cholinergic involvement in cognitive flexibility.

In chapter two, we demonstrated that nuclei forming part of either of the major subdivisions of the anterior, lateral, medial or posterior thalamus were clearly delineated from each other using the automated segmentation approach described by Iglesias et al. (2018), when compared with the Morel atlas of the thalamus (Krauth et al., 2010; Morel, 2007; Morel et al., 1997). We found mixed segmentation efficacy within each subdivision, with posterior thalamic nuclei generally less well defined according to the Morel atlas compared to anterior, lateral, or medial thalamic nuclei. Importantly, we found the centromedian nucleus was particularly well defined, and the parafascicular nucleus was defined to a lesser extent. The centromedian, part of the intralaminar nuclear group, had the highest overlap measure of all nuclei in the medial thalamus, and the second lowest dissimilarity measure of all thalamic nuclei. The parafascicular nucleus, which is also an intralaminar nucleus, had relatively less overlap and higher dissimilarity than the centromedian nucleus, but with a segmentation that was mostly self-contained and within the boundaries of the

centromedian nucleus in the Morel atlas. This is important because in chapter four we combined segmentations of the centromedian and parafascicular nuclei to generate seed timeseries for psychophysiological analysis, and we are confident that segmentations are likely to faithfully recapitulate the location and shape of these nuclei.

Chapter three assessed variability in choline containing compound concentrations measured at rest with magnetic resonance spectroscopy in the dorsal striatum and in the parieto-occipital cortex. Previous work has shown functionally relevant changes in choline in both regions and that this measure could be used as a proxy for studying acetylcholine dynamics (Bell et al., 2018; Lindner et al., 2017). Firstly, we find concentrations of choline containing compounds measured using separate peaks for choline and for glycerophosphocholine plus phosphocholine are highly correlated with the concentrations of a single peak modelled to contain all choline-containing metabolites. Choline concentrations estimated from spectra averaged from 128 and 256 transients were inconsistent in both the striatum and parieto-occipital cortex across two sessions one week apart. Glycerophosphocholine plus phosphocholine concentrations were consistent for the parieto-occipital cortex and striatum in only one of the sessions. There were no differences at the group level between concentrations averaged from 128 and 256 transients. Striatal glycerophosphocholine plus phosphocholine concentrations were consistent between sessions for spectra averaged 128 transients and spectra averaged from 256 transients. Glycerophosphocholine plus phosphocholine concentrations were inconsistent between sessions in the parieto-occipital cortex. Choline concentrations were inconsistent between sessions in both the parieto-occipital cortex and the striatum, and for metabolite averaged from 128 and from 256 transients. These findings suggest that concentrations of the choline containing compounds not associated with acetylcholine function remain relatively stable in the striatum over time. Additionally, increasing the number of transients during acquisition may improve quantitation estimates for choline.

Having demonstrated in chapter two that we can use the approach described by Iglesias et al. (2018) to individually parcellate the centromedian and parafascicular nuclei of the thalamus, in chapter four we used these parcellations to study thalamostriatal functional connectivity, as well as corticostriatal functional connectivity during serial reversal learning. Firstly, we found whole brain activation during reversal learning that was broadly in line with previous functional imaging studies of reversal learning. We also found that functional connectivity between the centromedian-parafascicular nuclei and the dorsal striatum and between the lateral orbitofrontal cortex and the dorsal striatum were significantly increased for negative outcomes versus positive outcomes during reversal learning. However, while no differences in thalamostriatal functional connectivity were found during specific phases of the task, corticostriatal functional connectivity was found to be

driven specifically by differences in activation during the stability phase, which follows the reversal of reward contingencies where an alternative response strategy is implemented. We also report exploratory findings suggesting the frontopolar cortex may track the relative advantage of the unused response strategy (the counterfactual), and that the anterior cingulate is responsive to outcomes that are incongruent with the currently expected context of the task.

These findings suggest thalamostriatal connectivity between the centromedian-parafascicular nuclei and the dorsal striatum during serial reversal learning may reflect a general error signal following negative outcomes which is used for guiding goal-directed behaviour by signalling a potential change in context and preparing for a possible change in response strategy. Conversely, corticostriatal connectivity between the lateral orbitofrontal cortex and the dorsal striatum was found to be specific to the stability phase of the task where participants are implementing a change in behavioural policy. This suggests these regions may be involved in the implementation of flexible changes in behaviour, as has been suggested by previous work (Hampshire et al., 2012; Rygula et al., 2010; Stalnaker et al., 2016). The roles these corticostriatal and thalamostriatal connections play in cognitive flexibility are likely to be supported by other brain regions, including the frontopolar and anterior cingulate cortices.

Lastly, we use magnetic resonance spectroscopy to investigate the relationship between the state of the dorsal striatal cholinergic system at rest with serial reversal learning performance in chapter five. Based on our findings in chapter three, we acquired spectroscopy data averaged from 256 transients. Computational modelling was used to derive latent measures of behaviour using a reinforcement learning model, while perseverative and regressive errors were used to describe behaviour. Choline levels were predicted by the number of perseverative and regressive errors, and by the learning rate for positive and negative prediction errors. More specifically, perseverative and regressive errors, and the learning rate for positive prediction errors were negatively associated with choline concentrations. The learning rate for negative prediction errors was positively associated with choline concentrations. These results suggest that the state of the striatal cholinergic system at rest is related to reversal learning performance, in line with the findings of Bell, Lindner, et al. (2019). However, unlike Bell, Lindner, et al. (2019) who find that choline concentrations at rest are positively correlated with perseverative errors, and that the learning rate for negative prediction errors is inversely correlated with dorsal striatal choline in uninstructed multi-alternative reversal learning, we find the opposite here in our serial reversal learning task. These opposing findings may be driven by differences in the task design and underlying neural computations required in uninstructed multi-alternative versus two-choice serial reversal learning. This possibility, in light also of the fMRI findings of chapter four, is discussed in the following section.

Striatal involvement in serial reversal learning

As demonstrated by a wealth of prior evidence from the human and animal literature, as well as the work presented here, the dorsal striatum has an important role in producing flexible, goal-directed behaviour. In the following section I shall propose a potential role for the striatum, its connectivity with the orbitofrontal cortex and centromedian-parafascicular nuclei of the thalamus, and its modulation by the striatal cholinergic system in serial reversal learning.

The striatum has a critical role in the production of flexible, goal directed behaviour. Its main inputs are glutamatergic afferents from the cortex and thalamus, and dopaminergic afferents from the ventral tegmental area and substantia nigra. Medium spiny neurons are the primary neuronal cell type in the striatum and form synaptic connections with both glutamatergic and dopaminergic projections. Cholinergic activity within the striatum has several direct and indirect effects on medium spiny neurons in the striatum. Acetylcholine can have excitatory effect on medium spiny neurons via the expression of the muscarinic M1 receptor on direct and indirect pathway medium spiny neurons (Abudukeyoumu et al., 2019; Assous, 2021), and via the M1 receptor expression on glutamatergic projections (Ding et al., 2010). Acetylcholine also has a direct inhibitory effect on medium spiny neurons via M4 muscarinic receptors (Assous, 2021; Kreitzer, 2009), and an indirect inhibitory effect through nicotinic acetylcholine receptors on GABAergic interneurons (English et al., 2012) and through M2 muscarinic receptors on glutamatergic projection neurons (Ding et al., 2010). Additionally, dopamine release, which is traditionally thought to act as a teaching signal in the striatum (Schultz et al., 1997), can be modulated or even induced by acetylcholine in the absence of an action potential in dopaminergic neurons (Threlfell et al., 2010, 2012). Cholinergic interneurons thus have a broad range of effects on the dynamics of striatal activity, with one proposed overarching role being the modulation of the rate of learning and plasticity in the striatum (Cox & Witten, 2019).

The serial reversal learning task used here has several distinct features compared to the multi-alternative reversal learning task previously used to demonstrate the importance of corticostriatal and thalamostriatal connections, and of cholinergic activity in human reversal learning (Bell et al., 2018; Bell, Langdon, et al., 2019; Bell, Lindner, et al., 2019). Firstly, the multi-alternative reversal learning task has a protracted period of initial and reversal learning, where participants discover stimulus-outcome contingencies. Successfully learning the initial and reversed contingencies in the multi-alternative is not trivial, with fewer than half the participants reaching the learning criterion during initial and reversal learning in previous work (Bell et al., 2018; Bell, Langdon, et al., 2019; Bell, Lindner, et al., 2019). Furthermore, participants in the multi-alternative task are not given

instruction about the reversal of contingencies. In this context, we describe participant's internal representation of task context as "unsaturated", since they only compile mature task representations following both the protracted initial and reversal learning periods. Conversely, these contingencies are simpler and more readily learned in the serial reversal learning task by virtue of the fact that only two response options are available, and that the occurrence of reversals is instructed. In this task, most participants reach criterion during both initial and reversal learning at similar rates. Therefore, task representation in serial reversal learning may be considered "saturated", as it is readily acquired and complete, because no additional information is relevant for representing task structure, once an "if not A, then B" heuristic has formed.

Previous work has demonstrated that multiple contexts are concurrently represented in the striatum following reversal learning training, and that these state representations may depend on cholinergic activity (Bradfield & Balleine, 2017). In a recent review paper Stayte et al. (2021) present converging evidence suggesting the orbitofrontal cortex, striatal cholinergic system, and centromedian-parafascicular nuclei of the thalamus work in concert to produce these internal representations, and that these representations are important for goal-directed behaviour. The orbitofrontal cortex is well positioned to support internal state representations as it receives inputs from multiple sensory domains, the hippocampus, and the amygdala. Sensory, memory, and affective information can then be integrated to infer the current state of the individual. Conversely, the centromedian-parafascicular nuclei do not receive direct sensory input, nor do they receive input from the hippocampus and amygdala. Instead, the centromedian-parafascicular nuclei receive input from regions associated with motor functioning and attention, such as the laterodorsal tegmental nucleus, pedunculopontine nucleus, primary motor cortex, and cerebellar nuclei (Cornwall & Phillipson, 1988). Orbitofrontal and centromedian-parafascicular regions thus provide separable information useful for inferring and generating an internal representation of the current state via their converging connectivity on the cholinergic interneurons in the striatum (Bradfield et al., 2013; Bradfield & Balleine, 2017; Stalnaker et al., 2016). These cholinergic interneurons can then modulate the activity of medium spiny neurons via the direct and indirect effects of acetylcholine receptor expression.

Due to the protracted period of learning in the multi-alternative reversal learning task, corticostriatal and thalamostriatal systems are involved in both the discovery and learning of the initial and reversal contexts. By contrast, in the serial reversal learning task these representations are "pre-loaded" through instruction and require only a short period of learning to be generated, with subsequent flexible behavioural output based on inferences about the current context. Lower choline concentrations at rest are associated with better performance during the multi-alternative

reversal learning task (Bell et al., 2018; Bell, Lindner, et al., 2019), and may facilitate internal representation formation by generating a greater contrast in acetylcholine concentrations between the initial and reversal learning periods. Conversely, in the work presented here we find that higher levels of choline are positively associated with serial reversal learning performance. Previous work has demonstrated that choline is the rate limiting factor in the synthesis of acetylcholine (Taylor & Brown, 1999), and has suggested choline levels are proportional to acetylcholine concentration (Koshimura et al., 1990; Wang et al., 2008). Therefore, higher levels of choline at rest may reflect greater potential to modulate internal representations by acetylcholine during serial reversal learning, influencing the activity of medium spiny neurons.

Corticostriatal and thalamostriatal connectivity also likely contribute to the modulation of internal representations by striatal cholinergic interneurons. Here, we show functional connectivity between the centromedian-parafascicular nuclei and dorsal striatum, and between the lateral orbitofrontal cortex and dorsal striatum is significantly greater when negative feedback is received. However, while thalamostriatal connectivity was relatively increased throughout the task, corticostriatal connectivity increase was specific to when participants changed to using an alternate response strategy. Connectivity between the centromedian-parafascicular nuclei and the striatum may therefore provide a generic signal for a potential need to change due to negative feedback. The effect of thalamostriatal connectivity on the output of the striatum may be gated by corticostriatal connectivity between the lateral orbitofrontal cortex and striatum, with the orbitofrontal cortex inferring the current state. In this way, the whole system can determine whether to switch to using an alternate internal representation of task context. This position is supported by previous evidence showing the orbitofrontal cortex generates internal state representations from its many inputs (Wilson et al., 2014), that the orbitofrontal cortex is necessary for dorsal striatal cholinergic interneurons internal state representations (Stalnaker et al., 2016), that the centromedian-parafascicular nuclei respond to salient events that are behaviourally relevant (Matsumoto et al., 2001), are important for reversal learning (Bradfield et al., 2013; Bradfield & Balleine, 2017; Brown et al., 2010), and that cortical and thalamic inputs equally influence the effect cholinergic interneurons have on medium spiny neurons (Mamaligas et al., 2019).

Strengths and limitations

Localising thalamic activation

One of the main methodological strengths of this work is that our automated segmentation approach to defining the location of the centromedian and parafascicular nuclei in subject space was faithful to the Morel thalamic atlas (Krauth et al., 2010; Morel, 2007; Morel et al., 1997). This is important because we can be confident that our thalamic seed used for our psychophysiological analysis was representative of BOLD activation in the centromedian-parafascicular during reversal learning. Furthermore, we used a functional imaging acquisition protocol optimised for studying small, subcortical structures. Here, the spatial resolution used ($1.6mm^3$) is relatively high compared to other studies using functional imaging studies at three tesla. Compromises when designing a functional imaging protocol and analysis pipeline include voxel size and the need to smooth the acquired signal to reduce noise. Here, we aimed to reduce partial volume effects in the thalamus by using a small voxel size and minimising the smoothing of our functional data by using a kernel that was only two times our voxel resolution. Both these decisions have the undesired effect of reducing our signal to noise ratio (Tabelow et al., 2009), but were important if we were to isolate our signal to specific nuclei in the thalamus. The decision to increase our spatial resolution also reduced the temporal resolution of our data. To circumvent this problem, we acquired functional data using multiband slice acceleration, reducing the time taken to acquire a single volume. Although multiband slice acceleration can sometimes cause spurious slice leakage artefacts in data due to eye movement (McNabb et al., 2020), we did not detect this artefact using our acquisition protocol.

The acquisition protocol used here for acquiring functional data pushes what is feasibly possible for imaging data acquisition using magnetic resonance imaging at three tesla. Ultra-high field magnetic resonance imaging at seven tesla and above would have several benefits for future studies aiming to address the functional role of thalamic nuclei in cognitive processes. The increased magnetic field strength increases the signal to noise ratio, relative to using equivalent acquisition parameters at three tesla. Additionally, ultra-high field work offers the opportunity to trade off some signal to noise in favour of increasing spatial or temporal resolution. Increased temporal resolution would benefit model fitting by increasing the number of datapoints available to estimate the response shape in different conditions, while increasing spatial resolution would further help in the isolation of activation to specific thalamic nuclei, reducing the blending of signals between regions due to partial volume effects.

Spectroscopy acquisition

Although the voxel size reported here (2.25cm^3) for our striatal spectroscopy acquisition is in line with our previous striatal spectroscopy work (Bell et al., 2018; Bell, Lindner, et al., 2019), it is smaller than the size used for striatal voxels in other studies[9], and aims to reduce partial volume effects during spectral acquisition. This may appear counter-productive given that increases in spectroscopy voxel size are associated with increases in signal to noise ratio in the acquired spectra (Gonen et al., 2001), but we aimed to prioritise anatomical inference. Acquisition of metabolite spectra in the striatum is associated with several issues. Firstly, while the use of surface coils improves the acquisition of metabolite spectra, the striatum is too deep for surface coil acquisition to be feasible (Gerard & Peterson, 2003). Secondly, the basal ganglia is an iron rich region of the brain (Schenck, 1995), and the presence of iron reduces the homogeneity of the magnetic field, causing a reduction of signal quality. These challenges, coupled with frequency drift due to gradient coil heating (El-Sharkawy et al., 2006; Harris et al., 2014; Lange et al., 2011) may explain why we had a higher rate of spectra that were not quantifiable in chapter five compared with chapter three. Therefore, although the result presented in chapter five suggest a relationship between dorsal striatal choline concentrations at rest and flexibility during serial reversal learning these findings should be treated with caution given the relatively small sample size presented in the study.

In chapter three, some of the variance in metabolite concentrations between sessions may be related to variability in voxel positioning from one session to another. Despite having relatively high overlap between sessions for both the striatum and parieto-occipital cortex at the group level, we had a relatively large distribution of overlap values across participants. The consistency of manual voxel positioning for magnetic resonance spectroscopy acquisitions can be problematic in multi-session studies even when anatomical markers are used to guide voxel positioning, because of individual differences in anatomy and variability in slice positioning and image contrast used when planning voxel location. One way to overcome this limitation is to use a functional localiser to identify regions with significant activation relating to the behaviour of interest (Lindner et al., 2017). Alternatively, an automated voxel positioning approach could be used. For instance the AVP software produced by Woodcock et al. (2018) contains a suite of functions that can be used to co-register a template voxel to a participant, and use these registration parameters to consistently place the voxel across sessions and participants. Automated voxel positioning is useful as it minimises nuisance variance due to variability in voxel positioning, and because it can be used to consistently

[9] For instance, Soreni et al. (2006) use a voxel size of 4cm^3

localise regions for which there may be no clear task that produces reliable activation, as is the case for many cognitive functions.

Another potential source of variability in metabolite quantitation is head motion during data acquisition. Correcting for motion artefacts during functional imaging data collection can be achieved by using image registration to re-align individual volumes with each other (Jenkinson et al., 2002). However, spectroscopy data cannot be retrospectively corrected for participant motion during data acquisition. This means that even if an automated approach is used for voxel positioning and the participant's head is partially restrained, spectra are likely to be distorted by motion. This includes micro-movements that are not perceivable by participants actively trying to keep their head still. To circumvent motion-related distortion of the metabolite spectra, prospective motion correction can be used (Zaitsev et al., 2010). Prospective motion correction involves the online tracing of participant head movement and adjustment of the field of view used for data acquisition. It improves the quality of acquired data, and minimises alterations to spectroscopy data (Andrews-Shigaki et al., 2011; Callaghan et al., 2015; Maclaren et al., 2012). The work presented here did not involve the use of prospective motion correction due to a lack of access to hardware, however its use would have been beneficial particularly for minimising variability in the data presented in chapter three. Nevertheless, in chapter three we did try to minimise possible external sources of variance that we were able to control. For instance, we scanned all participants at approximately the same time of day to reduce diurnal effects (Soreni et al., 2006), and ensured we acquired the first scan of the day to reduce the effects of gradient coil temperature on frequency drift (El-Sharkawy et al., 2006; Harris et al., 2014; Lange et al., 2011).

Multimodal imaging

Combining functional magnetic resonance imaging with magnetic resonance spectroscopy enabled us to probe the role of striatal connectivity and neurochemistry in cognitive flexibility. In isolation, both methods have their limitations but combining findings from both modalities enables us to paint a clearer picture of their functional relevance. For instance, although striatal cholinergic interneurons are likely to contribute to variability the BOLD signal detected using functional magnetic resonance imaging, they are suggested to account for 1-2% to 20% of the total neuronal cell population in the human striatum (Bernácer et al., 2007; Prado et al., 2017). Therefore, a portion of variance in the BOLD signal will be related to cholinergic interneuron activity indirectly.

Similarly, although spectroscopy can be used to infer how the state of the system at rest may influence subsequent flexibility, as shown here and in previous work (Bell, Lindner, et al., 2019),

we are nevertheless unable to explain functional changes in connectivity using magnetic spectroscopy. However, BOLD imaging allows us to study changes in functional connectivity over time during different phases of the task. In this way, we can use a combination of magnetic resonance imaging and spectroscopy to gain a more nuanced perspective on the potential role of the striatum in reversal learning. Future work could use functional magnetic resonance spectroscopy to investigate further the functional role of the striatal cholinergic system during reversal learning, as in previous work (Bell et al., 2018). Additionally, this approach could be improved by simultaneously acquiring spectroscopy data from two locations (Dehghani et al., 2020), and acquiring interleaved water suppressed and unsuppressed spectra, where the latter can be used to simultaneously infer BOLD activation based on its direct relationship with the amplitude and width of unsuppressed water spectrum (Apsvalka et al., 2015). Concurrently acquiring data in this way could directly measure changes in functional connectivity between two regions and functional changes in neurochemistry, alongside changes in task-related behaviour.

Reversal learning task

The simplicity of the serial reversal learning task used here means it is applicable in multiple settings. For instance, serial reversal learning has been used in studies of development, mental disorder, and neurodegeneration (e.g. Boehme et al., 2017; Cools et al., 2007; Wetterling et al., 2015), and could also be used for translational work across species. The serial reversal learning task could also be used to study the dynamics of how people flexibly adjust their use of prior knowledge across successive reversals. Across several reversals of reward contingencies participants may form better representations of the task structure and predict more reliably when feedback suggests reward contingencies have reversed. In this way the serial reversal learning task could be used to measure meta-flexibility, and study how people learn to regulate flexible and stable behaviour (see Geddert & Egner, 2021; Siqi-Liu & Egner, 2020). However, its simplicity means the serial reversal learning task is less appropriate than the multi-alternative task for studying the dynamics of how people form representations of different contexts, since participants are told of the existence of reversals before starting the task and because the two stimuli have a mutually exclusive relationship.

Future directions and conclusions

Here, we have shown that corticostriatal and thalamostriatal connectivity and the state of the striatal cholinergic system at rest are associated with performance during a serial reversal learning task. Furthermore, we have proposed dissociable roles for cortical, striatal, and thalamic regions during serial reversal learning and multi-alternative reversal learning, and that these roles are driven by differences in demands between the tasks. Future work should aim to disentangle further the separable contributions of connectivity and the striatal cholinergic system during the formation and utilisation of internal representations. Electrophysiological recordings in the cortex, striatum, and thalamus of animals that have previously learned initial and reversed task contexts could be used to determine how these regions interact to use prior knowledge to guide behaviour. This would provide further evidence of how information from the cortex and thalamus are integrated by the striatal cholinergic system, and how the system uses this information to produce flexible output.

Animal research can also be used to further our understanding of the relationship between concentrations of choline containing metabolites and acetylcholine. Techniques traditionally used in rodent and primate neuroscience to study neurochemistry, such as microdialysis, enable the direct measurement of neurotransmitter concentrations. This includes acetylcholine, and therefore most work interested in studying the functional relevance of the cholinergic system does so directly. Thus, though there is some evidence suggesting a causal relationship between choline and acetylcholine function, more work is needed to clearly define the parameters of this relationship. Moreover, by concurrently measuring acetylcholine dynamics and choline concentrations using magnetic resonance spectroscopy, inferences can be made about how changes in one modality and temporal dimension relate to the other. Future spectroscopy work would benefit from using file-types that enable us to separate individual transients during acquisition. In the work presented in chapter three, the dataset generated had spectra saved as an average of all the transients in each acquisition. This meant that we could not disentangle the effects of the number of transients on the reliability of quantitation. In future by running a single acquisition with many transients that are not averaged, we could sample from this acquisition to investigate whether the number of transients is related to the reliability of the averaged spectra, and what effect the number of transients has on the signal to noise ratio of the quantified spectra.

The use of ultra-high field magnetic resonance imaging will also have several benefits for future work in this area. Firstly, the increased signal to noise ratio should increase the contrast of the boundary between the mediodorsal and pulvinar nuclei that is used by the segmentation algorithm. This would improve the delineation of individual thalamic nuclei and may lead to more accurate

identification of individual thalamic nuclei than for data acquired at three tesla. Increased field strength could also improve the signal to noise ratio, the spatial or the temporal resolution of functional imaging data collected during reversal, and of metabolite spectra acquired using magnetic resonance spectroscopy. These improvements should help to further localise the signal to individual regions of the cortex, striatum, and thalamus, as well as de-noising acquired metabolite spectra. This latter effect may help in the separation of choline from glycerophosphocholine and phosphocholine and may improve the temporal resolution of future work investigating the functional dynamics of the choline containing compounds. Improved temporal resolution could thus allow us to study whether functional changes in choline concentrations are observed during serial reversal learning, and if so whether these differences are consistent or not with the dynamics observed during the multi-alternative task.

In summary, in the methodological aspects of this work, firstly we showed that automated segmentation can be used to faithfully delineate the major thalamic areas based on their constituent nuclei, and that segmentation accuracy was variable across individual nuclei. However, importantly we found that we were able to individually define the centromedian and parafascicular nuclei, and that the combination of these nuclei had little non-specificity. Secondly, we found that concentrations of glycerophosphocholine and phosphocholine remain relatively stable in the striatum over time, but that choline concentrations are not. Choline is associated with concentrations of acetylcholine and thus these results suggest that acetylcholine concentrations at rest may vary over time. We also show that quantifying separating peaks for the choline containing compounds produced concentration estimates that were positively associated with estimates generated using a single peak for the choline containing compounds.

In the functional aspects of the work, we show that functional connectivity between the lateral orbitofrontal cortex and dorsal striatum, and between the centromedian-parafascicular nuclei are associated with negative feedback during reversal learning. Furthermore, we show that while thalamostriatal connectivity is not associated with any specific phase of the task, corticostriatal connectivity is associated with the phase in the task where participants switch to using an alternate response strategy. Additionally, we show that the concentration of choline at rest is positively associated with reversal learning performance. We suggest that corticostriatal connectivity may modulate the influence of thalamostriatal connections on the representation of context by cholinergic interneurons, and that higher concentration of choline at rest is associated with more efficient use of internal representations of context during serial reversal learning.

We examined these findings in the context of prior work on the contributions of the striatal cholinergic system and it's input from the cortex and thalamus to cognitive flexibility, and discuss emerging methodological opportunities to drive further insight.

References:

Abudukeyoumu, N., Hernandez-Flores, T., Garcia-Munoz, M., & Arbuthnott, G. W. (2019). Cholinergic modulation of striatal microcircuits. *European Journal of Neuroscience*, *49*(5), 604–622. https://doi.org/10.1111/ejn.13949

Andrews-Shigaki, B. C., Armstrong, B. S. R., Zaitsev, M., & Ernst, T. (2011). Prospective motion correction for magnetic resonance spectroscopy using single camera retro-grate reflector optical tracking. *Journal of Magnetic Resonance Imaging*, *33*(2), 498–504. https://doi.org/10.1002/jmri.22467

Apsvalka, D., Gadie, A., & Mullins, P. G. (2015). Event-related dynamics of glutamate and BOLD signal at 3 T in a repetition suppression paradigm. *NeuroImage*, *118*, 292–300. https://doi.org/10.1016/j.neuroimage.2015.06.015

Assous, M. (2021). Striatal cholinergic transmission. Focus on nicotinic receptors' influence in striatal circuits. *European Journal of Neuroscience*, *53*(8), 2421–2442. https://doi.org/10.1111/ejn.15135

Bell, T., Langdon, A., Lindner, M., Lloyd, W., & Christakou, A. (2019). *Orbitofrontal and Thalamic Influences on Striatal Involvement in Human Reversal Learning* (p. 246371). https://doi.org/10.1101/246371

Bell, T., Lindner, M., Langdon, A., Mullins, P. G., & Christakou, A. (2019). Regional Striatal Cholinergic Involvement in Human Behavioral Flexibility. *Journal of Neuroscience*, *39*(29), 5740–5749. https://doi.org/10.1523/JNEUROSCI.2110-18.2019

Bell, T., Lindner, M., Mullins, P. G., & Christakou, A. (2018). Functional neurochemical imaging of the human striatal cholinergic system during reversal learning. *European Journal of Neuroscience*, *47*(10), 1184–1193. https://doi.org/10.1111/ejn.13803

Bernácer, J., Prensa, L., & Giménez-Amaya, J. M. (2007). Cholinergic Interneurons Are Differentially Distributed in the Human Striatum. *PLOS ONE*, *2*(11), e1174. https://doi.org/10.1371/journal.pone.0001174

Boehme, R., Lorenz, R. C., Gleich, T., Romund, L., Pelz, P., Golde, S., Flemming, E., Wold, A., Deserno, L., Behr, J., Raufelder, D., Heinz, A., & Beck, A. (2017). Reversal learning strategy in adolescence is associated with prefrontal cortex activation. *European Journal of Neuroscience*, *45*(1), 129–137. https://doi.org/10.1111/ejn.13401

Bradfield, L. A., & Balleine, B. W. (2017). Thalamic Control of Dorsomedial Striatum Regulates Internal State to Guide Goal-Directed Action Selection. *The Journal of Neuroscience*, *37*(13), 3721–3733. https://doi.org/10.1523/JNEUROSCI.3860-16.2017

Bradfield, L. A., Bertran-Gonzalez, J., Chieng, B., & Balleine, B. W. (2013). The thalamostriatal pathway and cholinergic control of goal-directed action: Interlacing new with existing learning in the striatum. *Neuron*, *79*(1), 153–166. https://doi.org/10.1016/j.neuron.2013.04.039

Brown, H. D., Baker, P. M., & Ragozzino, M. E. (2010). The Parafascicular Thalamic Nucleus Concomitantly Influences Behavioral Flexibility and Dorsomedial Striatal Acetylcholine

Output in Rats. *Journal of Neuroscience*, *30*(43), 14390–14398. https://doi.org/10.1523/JNEUROSCI.2167-10.2010

Callaghan, M. F., Josephs, O., Herbst, M., Zaitsev, M., Todd, N., & Weiskopf, N. (2015). An evaluation of prospective motion correction (PMC) for high resolution quantitative MRI. *Frontiers in Neuroscience*, *9*, 97. https://doi.org/10.3389/fnins.2015.00097

Cools, R., Lewis, S. J. G., Clark, L., Barker, R. A., & Robbins, T. W. (2007). L-DOPA disrupts activity in the nucleus accumbens during reversal learning in Parkinson's disease. *Neuropsychopharmacology: Official Publication of the American College of Neuropsychopharmacology*, *32*(1), 180–189. https://doi.org/10.1038/sj.npp.1301153

Cornwall, J., & Phillipson, O. T. (1988). Afferent projections to the parafascicular thalamic nucleus of the rat, as shown by the retrograde transport of wheat germ agglutinin. *Brain Research Bulletin*, *20*(2), 139–150. https://doi.org/10.1016/0361-9230(88)90171-2

Cox, J., & Witten, I. B. (2019). Striatal circuits for reward learning and decision-making. *Nature Reviews Neuroscience*, *20*(8), 482–494. https://doi.org/10.1038/s41583-019-0189-2

Dehghani, M., Edden, R. A. E., & Near, J. (2020). *Simultaneous ultra-short TE-MRS in two voxels using a SPECIAL sequence with Hadamard encoding*. ISMRM 2020. https://archive.ismrm.org/2020/0491.html

Ding, J. B., Guzman, J. N., Peterson, J. D., Goldberg, J. A., & Surmeier, D. J. (2010). Thalamic Gating of Corticostriatal Signaling by Cholinergic Interneurons. *Neuron*, *67*(2), 294–307. https://doi.org/10.1016/j.neuron.2010.06.017

El-Sharkawy, A. M., Schär, M., Bottomley, P. A., & Atalar, E. (2006). Monitoring and correcting spatio-temporal variations of the MR scanner's static magnetic field. *Magnetic Resonance Materials in Physics, Biology and Medicine*, *19*(5), 223–236. https://doi.org/10.1007/s10334-006-0050-2

English, D. F., Ibanez-Sandoval, O., Stark, E., Tecuapetla, F., Buzsáki, G., Deisseroth, K., Tepper, J. M., & Koos, T. (2012). GABAergic circuits mediate the reinforcement-related signals of striatal cholinergic interneurons. *Nature Neuroscience*, *15*(1), 123–130. https://doi.org/10.1038/nn.2984

Geddert, R., & Egner, T. (2021). *No need to choose: Independent regulation of cognitive stability and flexibility challenges the stability-flexibility tradeoff* (p. 2021.08.10.455850). https://doi.org/10.1101/2021.08.10.455850

Gerard, E., & Peterson, B. S. (2003). Developmental processes and brain imaging studies in Tourette syndrome. *Journal of Psychosomatic Research*, *55*(1), 13–22. https://doi.org/10.1016/S0022-3999(02)00581-0

Gonen, O., Gruber, S., Li, B. S. Y., Mlynárik, V., & Moser, E. (2001). Multivoxel 3D Proton Spectroscopy in the Brain at 1.5 Versus 3.0 T: Signal-to-Noise Ratio and Resolution Comparison. *American Journal of Neuroradiology*, *22*(9), 1727–1731.

Hampshire, A., Chaudhry, A. M., Owen, A. M., & Roberts, A. C. (2012). Dissociable roles for lateral orbitofrontal cortex and lateral prefrontal cortex during preference driven reversal learning. *NeuroImage*, *59*(4), 4102–4112. https://doi.org/10.1016/j.neuroimage.2011.10.072

Harris, A. D., Glaubitz, B., Near, J., Evans, C. J., Puts, N. A. J., Schmidt-Wilcke, T., Tegenthoff, M., Barker, P. B., & Edden, R. A. E. (2014). Impact of frequency drift on gamma-aminobutyric acid-edited MR spectroscopy. *Magnetic Resonance in Medicine*, *72*(4), 941–948. https://doi.org/10.1002/mrm.25009

Iglesias, J. E., Insausti, R., Lerma-Usabiaga, G., Bocchetta, M., Van Leemput, K., Greve, D. N., van der Kouwe, A., Fischl, B., Caballero-Gaudes, C., & Paz-Alonso, P. M. (2018). A probabilistic atlas of the human thalamic nuclei combining ex vivo MRI and histology. *NeuroImage*, *183*, 314–326. https://doi.org/10.1016/j.neuroimage.2018.08.012

Jenkinson, M., Bannister, P., Brady, M., & Smith, S. (2002). Improved Optimization for the Robust and Accurate Linear Registration and Motion Correction of Brain Images. *NeuroImage*, *17*(2), 825–841. https://doi.org/10.1016/S1053-8119(02)91132-8

Koshimura, K., Miwa, S., Lee, K., Hayashi, Y., Hasegawa, H., Hamahata, K., Fujiwara, M., Kimura, M., & Itokawa, Y. (1990). Effects of choline administration on in vivo release and biosynthesis of acetylcholine in the rat striatum as studied by in vivo brain microdialysis. *Journal of Neurochemistry*, *54*(2), 533–539.

Krauth, A., Blanc, R., Poveda, A., Jeanmonod, D., Morel, A., & Székely, G. (2010). A mean three-dimensional atlas of the human thalamus: Generation from multiple histological data. *NeuroImage*, *49*(3), 2053–2062. https://doi.org/10.1016/j.neuroimage.2009.10.042

Kreitzer, A. C. (2009). Physiology and Pharmacology of Striatal Neurons. *Annual Review of Neuroscience*, *32*(1), 127–147. https://doi.org/10.1146/annurev.neuro.051508.135422

Lange, T., Zaitsev, M., & Buechert, M. (2011). Correction of frequency drifts induced by gradient heating in 1H spectra using interleaved reference spectroscopy. *Journal of Magnetic Resonance Imaging: JMRI*, *33*(3), 748–754. https://doi.org/10.1002/jmri.22471

Lindner, M., Bell, T., Iqbal, S., Mullins, P. G., & Christakou, A. (2017). In vivo functional neurochemistry of human cortical cholinergic function during visuospatial attention. *PloS One*, *12*(2), e0171338. https://doi.org/10.1371/journal.pone.0171338

Maclaren, J., Armstrong, B. S. R., Barrows, R. T., Danishad, K. A., Ernst, T., Foster, C. L., Gumus, K., Herbst, M., Kadashevich, I. Y., Kusik, T. P., Li, Q., Lovell-Smith, C., Prieto, T., Schulze, P., Speck, O., Stucht, D., & Zaitsev, M. (2012). Measurement and Correction of Microscopic Head Motion during Magnetic Resonance Imaging of the Brain. *PLOS ONE*, *7*(11), e48088. https://doi.org/10.1371/journal.pone.0048088

Mamaligas, A. A., Barcomb, K., & Ford, C. P. (2019). Cholinergic Transmission at Muscarinic Synapses in the Striatum Is Driven Equally by Cortical and Thalamic Inputs. *Cell Reports*, *28*(4), 1003-1014.e3. https://doi.org/10.1016/j.celrep.2019.06.077

Matsumoto, N., Minamimoto, T., Graybiel, A. M., & Kimura, M. (2001). Neurons in the Thalamic CM-Pf Complex Supply Striatal Neurons With Information About Behaviorally Significant Sensory Events. *Journal of Neurophysiology*, *85*(2), 960–976. https://doi.org/10.1152/jn.2001.85.2.960

McCool, M. F., Patel, S., Talati, R., & Ragozzino, M. E. (2008). Differential involvement of M1-type and M4-type muscarinic cholinergic receptors in the dorsomedial striatum in task switching. *Neurobiology of Learning and Memory*, *89*(2), 114–124. https://doi.org/10.1016/j.nlm.2007.06.005

McNabb, C. B., Lindner, M., Shen, S., Burgess, L. G., Murayama, K., & Johnstone, T. (2020). Inter-slice leakage and intra-slice aliasing in simultaneous multi-slice echo-planar images. *Brain Structure and Function*, *225*(3), 1153–1158. https://doi.org/10.1007/s00429-020-02053-2

Morel, A. (2007). *Stereotactic Atlas of the Human Thalamus and Basal Ganglia*. CRC Press.

Morel, A., Magnin, M., & Jeanmonod, D. (1997). Multiarchitectonic and stereotactic atlas of the human thalamus. *Journal of Comparative Neurology*, *387*(4), 588–630. https://doi.org/10.1002/(SICI)1096-9861(19971103)387:4<588::AID-CNE8>3.0.CO;2-Z

Prado, V. F., Janickova, H., Al-Onaizi, M. A., & Prado, M. A. M. M. (2017). Cholinergic circuits in cognitive flexibility. *Neuroscience*, *345*, 130–141. https://doi.org/10.1016/j.neuroscience.2016.09.013

Ragozzino, M. E., & Choi, D. (2004). Dynamic Changes in Acetylcholine Output in the Medial Striatum During Place Reversal Learning. *Learning & Memory*, *11*(1), 70–77. https://doi.org/10.1101/lm.65404

Ragozzino, M. E., Jih, J., & Tzavos, A. (2002). Involvement of the dorsomedial striatum in behavioral flexibility: Role of muscarinic cholinergic receptors. *Brain Research*, *953*(1–2), 205–214. https://doi.org/10.1016/S0006-8993(02)03287-0

Ragozzino, M. E., Mohler, E. G., Prior, M., Palencia, C. A., & Rozman, S. (2009). Acetylcholine activity in selective striatal regions supports behavioral flexibility. *Neurobiology of Learning and Memory*, *91*(1), 13–22. https://doi.org/10.1016/j.nlm.2008.09.008

Rygula, R., Walker, S. C., Clarke, H. F., Robbins, T. W., & Roberts, A. C. (2010). Differential Contributions of the Primate Ventrolateral Prefrontal and Orbitofrontal Cortex to Serial Reversal Learning. *Journal of Neuroscience*, *30*(43), 14552–14559. https://doi.org/10.1523/JNEUROSCI.2631-10.2010

Schenck, J. F. (1995). Imaging of brain iron by magnetic resonance: T2 relaxation at different field strengths. *Journal of the Neurological Sciences*, *134*, 10–18. https://doi.org/10.1016/0022-510X(95)00203-E

Schultz, W., Dayan, P., & Montague, P. R. (1997). A Neural Substrate of Prediction and Reward. *Science*, *275*(5306), 1593–1599. https://doi.org/10.1126/science.275.5306.1593

Siqi-Liu, A., & Egner, T. (2020). Contextual Adaptation of Cognitive Flexibility is driven by Task- and Item-Level Learning. *Cognitive, Affective, & Behavioral Neuroscience*, *20*(4), 757–782. https://doi.org/10.3758/s13415-020-00801-9

Soreni, N., Noseworthy, M. D., Cormier, T., Oakden, W. K., Bells, S., & Schachar, R. (2006). Intraindividual variability of striatal 1H-MRS brain metabolite measurements at 3 T. *Magnetic Resonance Imaging*, *24*(2), 187–194. https://doi.org/10.1016/j.mri.2005.10.027

Stalnaker, T. A., Berg, B., Aujla, N., & Schoenbaum, G. (2016). Cholinergic Interneurons Use Orbitofrontal Input to Track Beliefs about Current State. *The Journal of Neuroscience : The Official Journal of the Society for Neuroscience*, *36*(23), 6242–6257. https://doi.org/10.1523/JNEUROSCI.0157-16.2016

Stayte, S., Dhungana, A., Vissel, B., & Bradfield, L. A. (2021). Parafascicular Thalamic and Orbitofrontal Cortical Inputs to Striatum Represent States for Goal-Directed Action Selection. *Frontiers in Behavioral Neuroscience*, *15*. https://doi.org/10.3389/fnbeh.2021.655029

Tabelow, K., Piëch, V., Polzehl, J., & Voss, H. U. (2009). High-resolution fMRI: Overcoming the signal-to-noise problem. *Journal of Neuroscience Methods*, *178*(2), 357–365. https://doi.org/10.1016/j.jneumeth.2008.12.011

Taylor, P., & Brown, J. H. (1999). Synthesis, Storage and Release of Acetylcholine. *Basic Neurochemistry: Molecular, Cellular and Medical Aspects. 6th Edition*. https://www.ncbi.nlm.nih.gov/books/NBK28051/

Threlfell, S., Clements, M. A., Khodai, T., Pienaar, I. S., Exley, R., Wess, J., & Cragg, S. J. (2010). Striatal Muscarinic Receptors Promote Activity Dependence of Dopamine Transmission via Distinct Receptor Subtypes on Cholinergic Interneurons in Ventral versus Dorsal Striatum. *Journal of Neuroscience*, *30*(9), 3398–3408. https://doi.org/10.1523/JNEUROSCI.5620-09.2010

Threlfell, S., Lalic, T., Platt, N. J., Jennings, K. A., Deisseroth, K., & Cragg, S. J. (2012). Striatal Dopamine Release Is Triggered by Synchronized Activity in Cholinergic Interneurons. *Neuron*, *75*(1), 58–64. https://doi.org/10.1016/j.neuron.2012.04.038

Wang, X.-C. C., Du, X.-X. X., Tian, Q., & Wang, J.-Z. Z. (2008). Correlation between choline signal intensity and acetylcholine level in different brain regions of rat. *Neurochemical Research*, *33*(5), 814–819. https://doi.org/10.1007/s11064-007-9509-4

Wetterling, F., McCarthy, H., Tozzi, L., Skokauskas, N., O'Doherty, J. P., Mulligan, A., Meaney, J., Fagan, A. J., Gill, M., & Frodl, T. (2015). Impaired reward processing in the human prefrontal cortex distinguishes between persistent and remittent attention deficit hyperactivity disorder. *Human Brain Mapping*, *36*(11), 4648–4663. https://doi.org/10.1002/hbm.22944

Wilson, R. C., Takahashi, Y. K., Schoenbaum, G., & Niv, Y. (2014). Orbitofrontal Cortex as a Cognitive Map of Task Space. *Neuron*, *81*(2), 267–279. https://doi.org/10.1016/j.neuron.2013.11.005

Woodcock, E. A., Arshad, M., Khatib, D., & Stanley, J. A. (2018). Automated Voxel Placement: A Linux-based Suite of Tools for Accurate and Reliable Single Voxel Coregistration. *Journal of Neuroimaging in Psychiatry & Neurology*, *3*(1), 1–8. https://doi.org/10.17756/jnpn.2018-020

Zaitsev, M., Speck, O., Hennig, J., & Büchert, M. (2010). Single-voxel MRS with prospective motion correction and retrospective frequency correction. *NMR in Biomedicine*, *23*(3), 325–332. https://doi.org/10.1002/nbm.1469